EMERGING FUNCTIONS OF SEPTINS - VOLUME II

EDITED BY: Manoj B. Menon and Matthias Gaestel
PUBLISHED IN: Frontiers in Cell and Developmental Biology

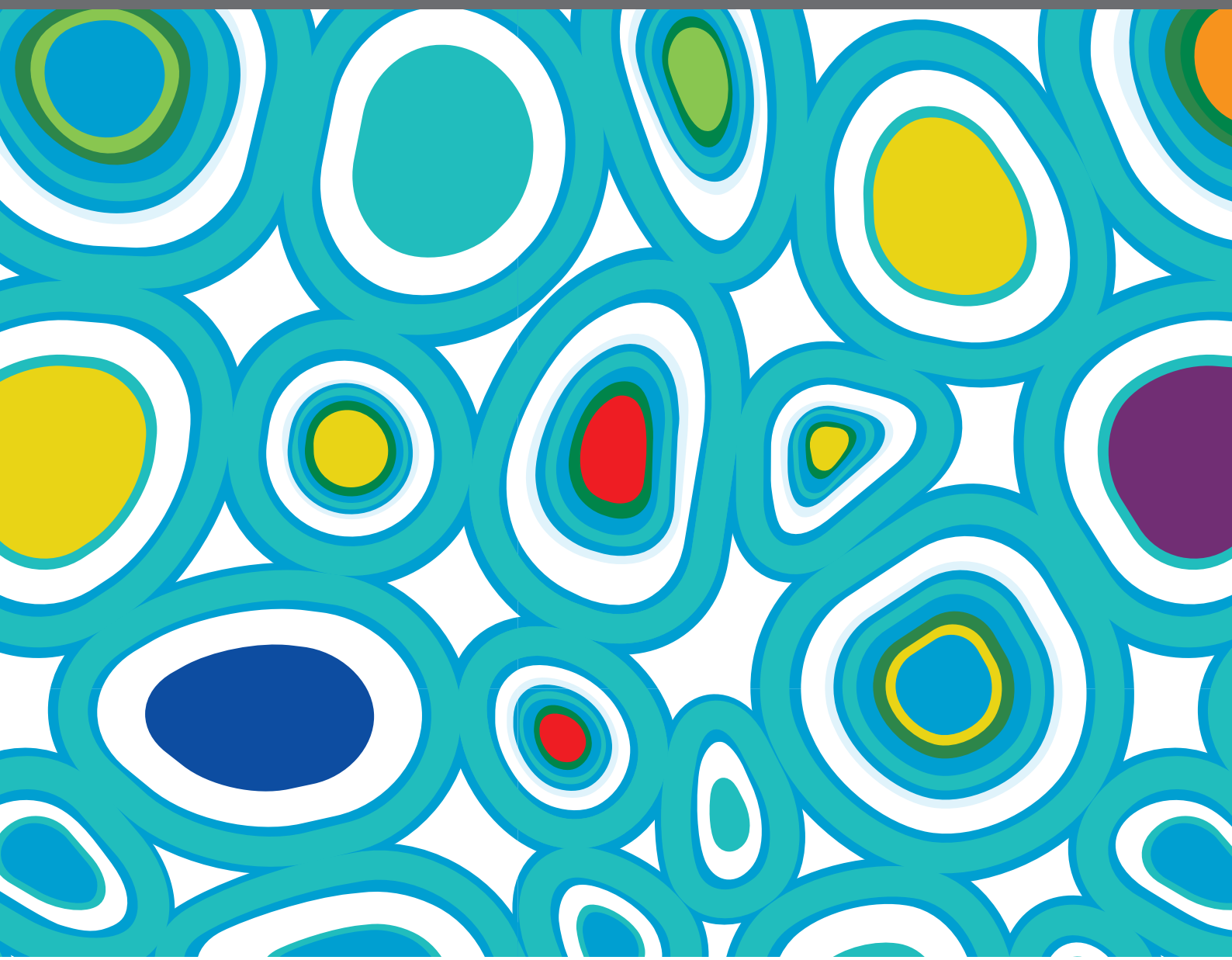

frontiers Research Topics

ISSN 1664-8714
ISBN 978-2-88976-542-3
DOI 10.3389/978-2-88976-542-3

About Frontiers

Frontiers is more than just an open-access publisher of scholarly articles: it is a pioneering approach to the world of academia, radically improving the way scholarly research is managed. The grand vision of Frontiers is a world where all people have an equal opportunity to seek, share and generate knowledge. Frontiers provides immediate and permanent online open access to all its publications, but this alone is not enough to realize our grand goals.

Frontiers Journal Series

The Frontiers Journal Series is a multi-tier and interdisciplinary set of open-access, online journals, promising a paradigm shift from the current review, selection and dissemination processes in academic publishing. All Frontiers journals are driven by researchers for researchers; therefore, they constitute a service to the scholarly community. At the same time, the Frontiers Journal Series operates on a revolutionary invention, the tiered publishing system, initially addressing specific communities of scholars, and gradually climbing up to broader public understanding, thus serving the interests of the lay society, too.

Dedication to Quality

Each Frontiers article is a landmark of the highest quality, thanks to genuinely collaborative interactions between authors and review editors, who include some of the world's best academicians. Research must be certified by peers before entering a stream of knowledge that may eventually reach the public - and shape society; therefore, Frontiers only applies the most rigorous and unbiased reviews.
Frontiers revolutionizes research publishing by freely delivering the most outstanding research, evaluated with no bias from both the academic and social point of view. By applying the most advanced information technologies, Frontiers is catapulting scholarly publishing into a new generation.

What are Frontiers Research Topics?

Frontiers Research Topics are very popular trademarks of the Frontiers Journals Series: they are collections of at least ten articles, all centered on a particular subject. With their unique mix of varied contributions from Original Research to Review Articles, Frontiers Research Topics unify the most influential researchers, the latest key findings and historical advances in a hot research area! Find out more on how to host your own Frontiers Research Topic or contribute to one as an author by contacting the Frontiers Editorial Office: frontiersin.org/about/contact

EMERGING FUNCTIONS OF SEPTINS - VOLUME II

Topic Editors:
Manoj B. Menon, Indian Institute of Technology Delhi, India
Matthias Gaestel, Hannover Medical School, Germany

Citation: Menon, M. B., Gaestel, M., eds. (2022). Emerging Functions of Septins - Volume II. Lausanne: Frontiers Media SA.
doi: 10.3389/978-2-88976-542-3

Table of Contents

frontiers | Frontiers in Cell and Developmental Biology

EDITORIAL
published: 16 June 2022
doi: 10.3389/fcell.2022.949824

Editorial: Emerging Functions of Septins—Volume II

Manoj B. Menon[1]* *and Matthias Gaestel*[2]*

[1]Kusuma School of Biological Sciences, Indian Institute of Technology Delhi, New Delhi, India, [2]Institute for Cell Biochemistry, Hannover Medical School, Hannover, Germany

Keywords: septins, cytokinesis, signaling, cytoskeleton, SEPT, GTPase

Editorial on the Research Topic

Emerging Functions of Septins—Volume II

The first identified members of the septin family of cytoskeletal GTPases were originally discovered in the budding yeast *Saccharomyces cerevisiae* as crucial regulators of mother-bud separation. They form a unique heteropolymeric cytoskeletal network and participate in diverse physiological functions [reviewed in (Mostowy and Cossart, 2012)]. Septin genes are conserved across eukaryotic genomes except in higher plants. In the initial decades of septin biology, research was focussed on their functions in yeast, while major breakthroughs have been achieved in the mammalian septin biology over the past two decades. Much like the intermediate filaments, the presence of heteropolymeric networks consisting of multiple septin isoforms with potential redundancy and the absence of specific inhibitors have hindered progress of septin research. In the present century, the use of mouse genetics, RNA-interference, and the advent of CRISPR/Cas9 technologies have aided in functional characterisation of septins and have uncovered isoform-specific physiological functions of septins. Septins have gained prominence as the distinct fourth component of mammalian cytoskeleton. In the first volume of the Frontiers Research topic on septins, we successfully presented contributions from across the septin field ranging from yeast cell division to human cancer and infections (Menon and Gaestel). In this second volume of the Frontiers Research topic on the emerging functions of septins, we have once again compiled a diverse collection of six reviews and four original research articles ranging from the changing models of septin oligomerisation and analyses of canonical septin functions to the cell-type specific non-canonical roles of septins in immune cells, stem cells, neurons and cancer.

The thirteen mammalian septins are classified into four groups (Septin2, Septin3, Septin6, and Septin7), named after the prominent member of the respective group. The basic repeating unit of the septin cytoskeleton is a hexamer consisting of Septin2, 6, and 7 and/or an octamer consisting of Septin2, 6, 7, and 3 group members. Until recently, the most acceptable model of the repeating unit was that of a palindromic S7-S6-S2-S2-S6-S7 hexamer and an octamer formed by addition of Septin3 group members at the termini (Sirajuddin et al., 2007; Kim et al., 2011). However, recent studies have provided evidence for revision of this model wherein the subunit organisation is inverted to give a S2-S6-S7-S7-S6-S2 core-septin hexamer (McMurray and Thorner, 2019; Mendonca et al., 2019; Soroor et al., 2021). In a thought-provoking review article, Cavini et al. provides an update on structural biology of septins with a focus on the domains and interfaces which stabilizes hexamers, octamers and the higher order filaments. While the vast majority of *in vitro*-polymerisation and GTP hydrolysis studies on mammalian septins have focussed on single septin subunits and hexamers, the focus has recently been shifted to octameric complexes (Iv et al., 2021; Soroor et al., 2021). The research article by Fischer et al. reports the biochemical characterisation of the septin octamer (S2-S6-S7-S9-S9-S7-S6-S2) and presents kinetic data on the nucleotide hydrolysis properties of human

OPEN ACCESS

Edited and reviewed by:
Ana Cuenda,
Spanish National Research Council (CSIC), Spain

***Correspondence:**
Manoj B. Menon
menon@bioschool.iitd.ac.in
Matthias Gaestel
gaestel.matthias@mh-hannover.de

Specialty section:
This article was submitted to Signaling, a section of the journal Frontiers in Cell and Developmental Biology

Received: *21 May 2022*
Accepted: *31 May 2022*
Published: *16 June 2022*

Citation:
Menon MB and Gaestel M (2022) Editorial: Emerging Functions of Septins—Volume II. Front. Cell Dev. Biol. 10:949824. doi: 10.3389/fcell.2022.949824

septin oligomers. Interestingly, based on the *in vitro*-polymerisation assays they propose a role for the Septin9 C-terminal region in septin filament assembly. Taking a slight deviation from the world of septin structures, Shuman and Momany review septin classification, conservation of sequence motifs in septins across kingdoms, positional orthology within heteropolymers and their evolutionary relationships. While the canonical core heteropolymers of septins are formed by the major four phylogenetic groups of septins, they present an interesting discussion on the group 5 septins, which only transiently associate with the core heteromers and are absent in the animal kingdom. Structural and functional analyses of more group 5 septins will be necessary to understand the origin and evolution of the septin family.

Septins were originally identified as proteins with role in yeast budding and the name "septin" originates from "septa" forming protein. Septins undergo cell cycle specific transitions in the budding yeast and one of the most fascinating structures formed by the septin cytoskeleton across the species is the hourglass-shaped collar formed at the mother bud-neck. In their focussed mini-review article, Marquardt et al. provide one of the best available and up-to-date summary of the molecular mechanisms driving the transition of a nascent septin ring at the bud-site to a stable hour-glass, followed by resolution into a double-ring structure facilitating budding yeast cytokinesis. Complementing this mechanistic take on the budding yeast cytokinesis is the article by Russo and Krauss which discusses the role of septins and septin remodelling in mammalian cell cytokinesis. While the central theme of septin functions in cytokinesis is established across genera and kingdoms, there are many unanswered questions regarding regulators of localized filament assembly, potential GEFs (guanine-nucleotide exchange factors), association with other cytoskeletal elements and membrane components in this process.

Despite their discovery as proteins with central role in cell division, non-dividing neuronal cells show strong expression of septins and a role for septins in neuronal morphogenesis is well established (Tada et al., 2007; Ageta-Ishihara et al., 2013). Recent work using the *Septin8* mutant mouse also indicates a role for septins in scaffolding the myelin sheath and accelerating nerve conduction (Patzig et al., 2016). One of the proposed mechanisms of septin-dependent regulation of neuronal morphogenesis is dependent on TAOK2-mediated phosphorylation of Septin7 at its C-terminal tail (Yadav et al., 2017). In their research article, Byeon et al. report the identification of phosphorylation-dependent interaction partners of Septin7 and propose a 14-3-3 dependent mechanism for septin-mediated dendritic spine maturation. This newly established link between septins and the 14-3-3 family of phosphorylation-dependent ubiquitous signalling adaptors is also expected to be relevant to other cell-types and models. Regulation of store-operated calcium signaling is another non-canonical function of the septin cytoskeleton discovered in the past decade (Sharma et al., 2013; Deb et al., 2016). In a contribution in this direction, Dhanya and Hasan investigates the role of septins in the neuronal pathogenesis associated with the deficiency of endoplasmic reticulum Ca^{2+} sensor STIM1 in mice. They report significant alleviation of the motor coordination defects in the *Stim1* knockout mouse upon the co-deletion of *Septin7* in purkinje neurons and propose septins as potential targets against neurodegenerative diseases caused by Ca^{2+} signaling defects.

Functions of septins in the cells of the hematopoietic lineages are also often linked to their membrane association and interplay with the cortical actin cytoskeleton (Gilden et al., 2012). Despite normal development of hematopoietic lineages upon pan-septin depletion in the *Septin7* knockout mice (Menon et al., 2014), septins regulate lymphocyte migration (Tooley et al., 2009) and were shown to associate with macrophage phagosomes (Huang et al., 2008), indicating clear roles in the hematopoietic system. Septins are key mediators of platelet degranulation and septin gene mutations have been associated with bleeding disorders. In an interesting mini review, Neubauer and Zieger compare septin expression and functions in platelets and endothelial cells. The recent findings from the *Septin8* knockout mice are being discussed in the context of platelet-endothelial cell interplay at the sites of vascular injury. The recent discovery from the *Septin7* knockout mice indicate a role for the Cdc42-Borg4-Septin7 axis in maintaining hematopoietic stem cell polarity and function (Kandi et al., 2021). The review by Schuster and Geiger summarises our current understanding on septin functions in stem cells and ageing. The role of septins as central mediators of asymmetric cell division from yeast to mammals is underscored in this unique review. Menon et al. reports a myeloid-specific *Septin7* conditional knockout mouse which displays the unique dichotomy of septin-dependence of cell division between monocytes and macrophages. While the development of monocytes is unaffected in the septin-deficient bone-marrow, the *in-vitro* cultivated bone-marrow derived macrophages display cytokinetic defects in the absence of Septin7. However, the multinucleated Septin7-deficient macrophages are functionally comparable to their wild-type counterparts.

Septins are crucial player in multiple stages of cell division and several studies have linked septins to cancer development (Cerveira et al., 2011; Pous et al.). However, a direct functional role for septins in tumorigenesis has not been established yet. Menon et al. describe the first *in vivo*-tumor model assessing the consequence of septin loss of function in lung cancer progression. The findings conclusively prove the role of septin-dependent proliferation in lung tumorigenesis and reconfirm the relevance of septins as targets against solid tumors.

Our understanding on the mechanisms of septin-dependent cytokinesis is constantly being revised based on findings from yeast to mammals, including the recent findings regarding the role of septins in asymmetric stem cell division. The revised order of septin subunits in the core hexamer and octamer units of mammalian septins have reignited research on redundancy and isoform-specificity of septin functions. In addition, the repertoire of cell-type specific functions of septins in neurons, hematopoietic lineages, and endothelial cells are also constantly growing. With the widespread use of CRISPR/Cas9 technology as well as septin-deficient mouse

models, further physiologically relevant functions of the septin family proteins are rapidly emerging. Collectively, the articles in the second volume of this research topic, which include four original research publications from diverse aspects of mammalian septin biology, exemplarily and comprehensively summarise these advances in the field.

AUTHOR CONTRIBUTIONS

MM and MG wrote the editorial.

FUNDING

This work for MM lab is supported by the DST-SERB start-up research grant #SRG/2020/001396. MG lab is supported by the Deutsche Forschungsgemeinschaft (GA 453/16-1).

ACKNOWLEDGMENTS

We thank all contributing authors, editors and reviewers for their support to the Research Topic.

REFERENCES

Ageta-Ishihara, N., Miyata, T., Ohshima, C., Watanabe, M., Sato, Y., Hamamura, Y., et al. (2013). Septins Promote Dendrite and Axon Development by Negatively Regulating Microtubule Stability via HDAC6-Mediated Deacetylation. *Nat. Commun.* 4, 2532. doi:10.1038/ncomms3532

Cerveira, N., Bizarro, S., and Teixeira, M. R. (2011). MLL-SEPTIN Gene Fusions in Hematological Malignancies. *Biol. Chem.* 392, 713–724. doi:10.1515/bc.2011.072

Deb, B. K., Pathak, T., and Hasan, G. (2016). Store-independent Modulation of Ca2+ Entry through Orai by Septin 7. *Nat. Commun.* 7, 11751. doi:10.1038/ncomms11751

Gilden, J. K., Peck, S., Chen, Y. C. M, and Krummel, M. F. (2012). The Septin Cytoskeleton Facilitates Membrane Retraction during Motility and Blebbing. *J. Cell Biol.* 196, 103–114. doi:10.1083/jcb.201105127

Huang, Y.-W., Yan, M., Collins, R. F., Diciccio, J. E., Grinstein, S., and Trimble, W. S. (2008). Mammalian Septins Are Required for Phagosome Formation. *MBoC* 19, 1717–1726. doi:10.1091/mbc.e07-07-0641

Iv, F., Martins, C. S., Castro-Linares, G., Taveneau, C., Barbier, P., Verdier-Pinard, P., et al. (2021). Insights into Animal Septins Using Recombinant Human Septin Octamers with Distinct SEPT9 Isoforms. *J. Cell Sci.* 134. doi:10.1242/jcs.258484

Kandi, R., Senger, K., Grigoryan, A., Soller, K., Sakk, V., Schuster, T., et al. (2021). Cdc42-Borg4-Septin7 axis Regulates HSC Polarity and Function. *EMBO Rep.* 22, e52931. doi:10.15252/embr.202152931

Kim, M. S., Froese, C. D., Estey, M. P., and Trimble, W. S. (2011). SEPT9 Occupies the Terminal Positions in Septin Octamers and Mediates Polymerization-dependent Functions in Abscission. *J. Cell Biol.* 195, 815–826. doi:10.1083/jcb.201106131

McMurray, M. A., and Thorner, J. (2019). Turning it inside Out: The Organization of Human Septin Heterooligomers. *Cytoskeleton* 76, 449–456. doi:10.1002/cm.21571

Mendonça, D. C., Macedo, J. N., Guimarães, S. L., Barroso Da Silva, F. L., Cassago, A., Garratt, R. C., et al. (2019). A Revised Order of Subunits in Mammalian Septin Complexes. *Cytoskeleton* 76, 457–466. doi:10.1002/cm.21569

Menon, M. B., Sawada, A., Chaturvedi, A., Mishra, P., Schuster-Gossler, K., Galla, M., et al. (2014). Genetic Deletion of SEPT7 Reveals a Cell Type-specific Role of Septins in Microtubule Destabilization for the Completion of Cytokinesis. *PLoS Genet.* 10, e1004558. doi:10.1371/journal.pgen.1004558

Mostowy, S., and Cossart, P. (2012). Septins: the Fourth Component of the Cytoskeleton. *Nat. Rev. Mol. Cell Biol.* 13, 183–194. doi:10.1038/nrm3284

Patzig, J., Erwig, M. S., Tenzer, S., Kusch, K., Dibaj, P., Möbius, W., et al. (2016). Septin/anillin Filaments Scaffold Central Nervous System Myelin to Accelerate Nerve Conduction. *Elife* 5. doi:10.7554/eLife.17119

Sharma, S., Quintana, A., Findlay, G. M., Mettlen, M., Baust, B., Jain, M., et al. (2013). An siRNA Screen for NFAT Activation Identifies Septins as Coordinators of Store-Operated Ca2+ Entry. *Nature* 499, 238–242. doi:10.1038/nature12229

Sirajuddin, M., Farkasovsky, M., Hauer, F., Kühlmann, D., Macara, I. G., Weyand, M., et al. (2007). Structural Insight into Filament Formation by Mammalian Septins. *Nature* 449, 311–315. doi:10.1038/nature06052

Soroor, F., Kim, M. S., Palander, O., Balachandran, Y., Collins, R. F., Benlekbir, S., et al. (2021). Revised Subunit Order of Mammalian Septin Complexes Explains Their *In Vitro* Polymerization Properties. *MBoC* 32, 289–300. doi:10.1091/mbc.e20-06-0398

Tada, T., Simonetta, A., Batterton, M., Kinoshita, M., Edbauer, D., and Sheng, M. (2007). Role of Septin Cytoskeleton in Spine Morphogenesis and Dendrite Development in Neurons. *Curr. Biol.* 17, 1752–1758. doi:10.1016/j.cub.2007.09.039

Tooley, A. J., Gilden, J., Jacobelli, J., Beemiller, P., Trimble, W. S., Kinoshita, M., et al. (2009). Amoeboid T Lymphocytes Require the Septin Cytoskeleton for Cortical Integrity and Persistent Motility. *Nat. Cell Biol.* 11, 17–26. doi:10.1038/ncb1808

Yadav, S., Oses-Prieto, J. A., Peters, C. J., Zhou, J., Pleasure, S. J., Burlingame, A. L., et al. (2017). TAOK2 Kinase Mediates PSD95 Stability and Dendritic Spine Maturation through Septin7 Phosphorylation. *Neuron* 93, 379–393. doi:10.1016/j.neuron.2016.12.006

Conflict of Interest: The authors declare that the research was conducted in the absence of any commercial or financial relationships that could be construed as a potential conflict of interest.

frontiers in Cell and Developmental Biology

MINI REVIEW
published: 04 November 2021
doi: 10.3389/fcell.2021.768309

Septin Remodeling During Mammalian Cytokinesis

*Giulia Russo and Michael Krauss**

Leibniz-Forschungsinstitut für Molekulare Pharmakologie (FMP), Berlin, Germany

Cytokinesis mediates the final separation of a mother cell into two daughter cells. Septins are recruited to the cleavage furrow at an early stage. During cytokinetic progression the septin cytoskeleton is constantly rearranged, ultimately leading to a concentration of septins within the intercellular bridge (ICB), and to the formation of two rings adjacent to the midbody that aid ESCRT-dependent abscission. The molecular mechanisms underlying this behavior are poorly understood. Based on observations that septins can associate with actin, microtubules and associated motors, we review here established roles of septins in mammalian cytokinesis, and discuss, how septins may support cytokinetic progression by exerting their functions at particular sites. Finally, we discuss how this might be assisted by phosphoinositide-metabolizing enzymes.

Keywords: septins, cytokinesis, actomyosin, microtubules, phosphoinositides

OPEN ACCESS

Edited by:
Matthias Gaestel,
Hannover Medical School, Germany

Reviewed by:
Elias T. Spiliotis,
Drexel University, United States
Aurélie Bertin,
UMR168 Unite physico-chimie Curie (PCC), France

****Correspondence:***
Michael Krauss
krauss@fmp-berlin.de

Specialty section:
This article was submitted to Signaling, a section of the journal Frontiers in Cell and Developmental Biology

Received: *31 August 2021*
Accepted: *18 October 2021*
Published: *04 November 2021*

Citation:
Russo G and Krauss M (2021) Septin Remodeling During Mammalian Cytokinesis. Front. Cell Dev. Biol. 9:768309. doi: 10.3389/fcell.2021.768309

INTRODUCTION

Cytokinesis starts when the centralspindlin complex activates Rho A at the equatorial plane of the cell cortex to initiate the formation of the contractile machinery (Glotzer, 2009; Zhang and Glotzer, 2015) (**Figure 1A**). GTP-loaded Rho A associates with anillin, a scaffolding protein that can roughly be divided into two functional halves (Carim et al., 2020): The N-terminus coordinates the recruitment of formins, actin, myosin II and Rho-dependent kinase to trigger actin polymerization and myosin II activation. Anillin thereby orchestrates the assembly of a stable contractile ring (Piekny and Maddox, 2010). Through its C-terminal domain anillin associates with Rho A, $PI(4,5)P_2$ and septins and drives the translocation of septins to the newly forming cleavage furrow (Oegema et al., 2000; Field C. M. et al., 2005; Liu et al., 2012; Sun et al., 2015).

Surprisingly, though present already at early stages of cytokinesis septins are dispensable for initial furrow ingression. Recent studies instead demonstrate key roles during the maturation of the cytokinetic bridge, and in the final step of abscission (see below). Here, we summarize our current knowledge of septin behavior and functions at different stages of cytokinesis, and discuss mechanisms underlying their redistribution during cytokinetic progression.

Septin Functions During Cleavage Furrow Initiation and Ingression

Several lines of evidence indicated that septins function already at early stages of cytokinesis. Septins associate with anillin, a master regulator of actomyosin ring assembly (Carim et al., 2020), through its C-terminal pleckstrin homology (PH) domain (Field C. M. et al., 2005; Liu et al., 2012). Septin recruitment to the forming cleavage furrow requires anillin, and might be reinforced by anillin-dependent F-actin crosslinking (Kinoshita et al., 1997; Kinoshita et al., 2002; Matsuda et al., 2020) (**Figure 1B**). Consistent with a role at the actomyosin ring Joo et al. demonstrated that SEPT2 directly interacts with myosin II, and scaffolds myosin II association with Citron kinase and Rock to support activation of this motor (Joo et al., 2007). Surprisingly, however, even when complex formation of septins with myosin II is inhibited, cells manage to assemble a contractile ring, and the

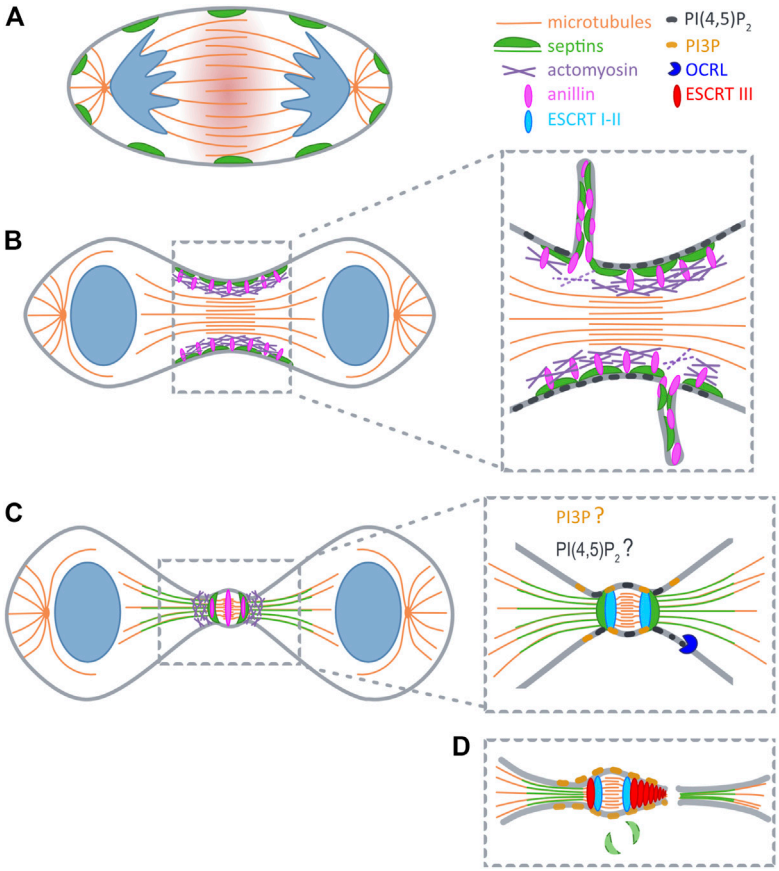

FIGURE 1 | Septins during cytokinesis. **(A)** At anaphase RhoA is activated at the midzone (red shadow). **(B)** At early telophase septins (green) are recruited to furrow by anillin (pink), and during furrow constriction promote extrusion of plasma membrane tubules. **(C)** After ingression septins reorganize into a double ring and support the formation of secondary ingression sites by dictating the relocalization of anillin and actomyosin (purple). At the same time SEPT9 locally activates Tsg101 (light blue). Initial recruitment of ESCRTI to the midbody is not depicted for clarity reasons. **(D)** Recruitment of ESCRTIII (red) occurs concomitantly with the disappearance of septin double rings. $PI(4,5)P_2$ (dark grey) builds up early at the cleavage furrow, and might also become concentrated at the midbody ring. $PI(4,5)P_2$ is hydrolyzed upon arrival of OCRL (blue) at the ICB. Prior to abscission a pool of PI(3)P (yellow) is generated at the midbody that likely supports ESCRT assembly.

cleavage furrow ingresses. Only as soon as the ICB is formed, the furrow becomes destabilized and retracts (Joo et al., 2007). Similar observations were made in HeLa cells expressing an anillin chimera, in which the C-terminal $PI(4,5)P_2$- and septin-binding PH domain is replaced by a PH domain that retains affinity for $(PI4,5)P_2$, but cannot associate with septins (Renshaw et al., 2014). Together, these studies indicate that septins are not required for the assembly of the contractile ring itself, but rather contribute to its shrinkage, or promote its tethering to the midzone.

In line with this interpretation live cell imaging in HeLa cells, as well as in *Drosophila* S2 cells revealed internalization of packages of anillin and a subset of associated cytokinetic proteins, including septins, during maturation of the midbody ring (El Amine et al., 2013; Renshaw et al., 2014) (**Figure 1B**). In both systems this phenomenon depends on anillin's capability to associate with septins. Based on their findings in *Drosophila* Carim et al. suggested that an anilloseptin subnetwork supports the reduction of circumference of the contractile ring (Carim et al., 2020). According to their model closure of the contractile ring builds tension that disengages anillin from the actomyosin network to induce extrusion of anilloseptin-containing plasma membrane tubules.

Septins Prime the Abscission Machinery at Late Stages of Cytokinesis

Superresolution imaging revealed that during elongation of the ICB anillin and septins form a collar-like structure, that gradually elongates through the assembly of an array of circular (or helical) filaments oriented parallel to the plane of cell division (Renshaw et al., 2014). Subsequently, anillin translocates to the midbody, and – dependent on its interaction with septins – to two flanking rings (**Figure 1C**). Septins, on the other hand, are excluded from the midbody, but colocalize with anillin at the flanking rings (Karasmanis et al., 2019). Thus, septins and anillin appear to switch roles at this stage, with septins dictating the localization of anillin. At the double ring two secondary actomyosin rings are formed, which serve to further constrict the bridge to a diameter of 100–300 nm (Wang et al., 2019). These constriction sites might

explain why septins serve a barrier function to prevent premature loss of cytokinetic proteins from the ICB by diffusional spread (Estey et al., 2010).

One of the secondary ingression sites will eventually evolve into the site of abscission. Abscission relys on the ESCRT machinery (Mierzwa and Gerlich, 2014; Addi et al., 2018), the recruitment of which occurs sequentially. First, ALIX and TSG101 associate with the midbody through their association with CEP55 (Lee et al., 2008). Both proteins subsequently support the recruitment of the ESCRTIII component CHMP4B in two parallel acting pathways (Christ et al., 2016). CHMP4B then translocates to the secondary ingression sites, in a step that depends on anillin, anillin's interaction with septins, and, consequently, also septins themselves (Renshaw et al., 2014) (**Figures 1C,D**).

A recent study by Karasmanis et al. (2019) provided more detailed mechanistic insight into the impact of SEPT9 on ESCRT rearrangements within the ICB. As expected, loss of SEPT9 does not affect the enrichment of ALIX and TSG101 at the midbody, but severely impairs the assembly of ESCRTIII into symmetric rings flanking the midbody. As the authors found SEPT9 to associate directly with Tsg101, they hypothesized that SEPT9 locally activates Tsg101 to facilitate complex formation with downstream ESCRTs and to coordinate their stepwise assembly. Indeed, in absence of SEPT9 ESCRTIII fails to reassemble into the characteristic cone-shaped structures that promote abscission. Intriguingly, both septins organized in rings, and ESCRT-III are comprised of arrays of regularly spaced, 10–20 nm wide filaments (Guizetti et al., 2011; Ong et al., 2014). These similarities in dimension and arrangement raise the possibility that septin rings act as a template for the formation of higher-order assemblies of ESCRT-III.

Roles of Septin Association With Microtubules During Cytokinesis

Septins are found associated with microtubules in several cell types, to regulate their nucleation, organization, dynamics, posttranslational modification, the capture of their plus-ends at the cell cortex, and microtubule-dependent transport events (Spiliotis and Nakos, 2021). Here, we will summarize roles of microtubule-associated septins during chromosome alignment and segregation, and discuss how they may assist abscission at late stages of cytokinesis.

Chromosomes that fail to align at metaphase are captured by centromere-associated protein E (CENP-E), which has been shown to be a binding partner of SEPT7 (Zhu et al., 2008). The maintenance of CENP-E at kinetochore microtubules also requires the presence of SEPT2 that partially colocalizes with those microtubules in a network of short SEPT2-containing filaments found juxtaposed with kinetochores (Spiliotis et al., 2005). In line with a function of septins in chromosome segregation, loss of SEPT7, as of SEPT2, causes the mis-localization of CENP-E to the spindle poles, and results in defects in chromosome alignment at the metaphase plate (Spiliotis et al., 2005; Zhu et al., 2008).

Super-resolution imaging of MDCK cells, for instance, revealed that septins localize on microtubule portions distal to the midbody, but are excluded from the midbody itself (Karasmanis et al., 2019). The latter finding could reflect a competition by microtubule-associated proteins enriched at the midbody, including PRC1 and centralspindlin (Glotzer, 2009).

The molecular mechanisms underlying the redistribution of septins from the cortex to microtubules remain largely elusive, but some evidence suggests a regulatory role of Cdc42, and a modulatory function of posttranslational modifications. In interphase the maintenance of septins on actin stress fibers relies on active Cdc42 and Cdc42 effector proteins (Borgs). Cdc42 inactivation, or depletion of Borgs triggers septin redistribution onto microtubules (Salameh et al., 2021). During mitosis Cdc42 localizes to the central spindle at metaphase, to concentrate at the ICB at telophase (Oceguera-Yanez et al., 2005). Moreover, Cdc42 activity peaks at metaphase, and drops during telophase (Oceguera-Yanez et al., 2005). This suggests that local inactivation of Cdc42 at the ICB might release septins from cortical actin at late stages of cytokinesis. The subsequent translocation to microtubules might by driven by their preference for arrays of parallel, or stabilized microtubules (Spiliotis and Nakos, 2021). Further, the association of septins with microtubules appears to be modulated by posttranslational modifications, such as sumoylation (Ribet et al., 2017). Ribet et al. identified sumoylation sites in several human septins, and demonstrated that non-sumoylatable septin variants form aberrant bundles in interphase. During cytokinesis such bundles accumulate along the ICB during cytokinesis, where they probably align with microtubules, and cause late cytokinetic defects (Ribet et al., 2017).

The roles that septins play on bridging microtubules are gradually emerging. Given that SEPT9 promotes microtubule bundling *in vitro* (Bai et al., 2013), septins might facilitate bundling of microtubules at constriction sites, and – due to their interaction with $PI(4,5)P2_2$ (see below) – aid microtubule attachment to the plasma membrane. Further, septins support microtubule severing that precedes abscission, as indicated by findings in fibroblasts derived from SEPT7 knockout mice (Menon et al., 2014). These fibroblasts display hyperacetylated microtubules, and show abscission defects. Importantly, the cytokinesis block can be bypassed by expression of stathmin, suggesting that SEPT7 facilitates the destabilization of microtubules within the ICB to prime them for severing.

Another level of regulation is suggested by the interplay between septins and kinesins (Spiliotis and Nakos, 2021). A recent study demonstrates that SEPT7 colocalizes and interacts with MKLP2/KIF20A (Qiu et al., 2020), a kinesin required for cleavage furrow stability at late stages of cytokinesis (Wu et al., 2019). Loss of SEPT7 depletes MKLP2 from the ICB in neural progenitor cells and leads to cell division defects (Qiu et al., 2020). It is, thus, not unlikely that septins similarly affect the localization and/or activity of other kinesin motors functioning at other stages of cytokinesis. For instance, septins could serve to locally concentrate the centralspindlin complex through associating with its motor component MKLP1/KIF23 (Mishima, 2016).

Phosphoinositides Guide Cytokinetic Factors to the Plasma Membrane

Phosphoinositides (PIs) are differentially phosphorylated derivatives of the membrane phospholipid phosphatidylinositol (Krauss and Haucke, 2007). PI(4,5)P_2 is prevalently present at the plasma membrane and builds up early at the newly forming cleavage furrow, leading to an about 4,5 fold increase in concentration at the ingressed cleavage furrow (Field S. J. et al., 2005) (**Figure 1B**). Conclusively, PI(4,5)P_2 has been implicated in the recruitment of numerous cytokinetic factors, including centralspindlin (Lekomtsev et al., 2012), anillin (Liu et al., 2012; Sun et al., 2015) and septins (Zhang et al., 1999; Tanaka-Takiguchi et al., 2009).

To date, surprisingly little is known about the PI-kinases that generate pools of PI(4,5)P_2 during cytokinesis, in particular of the ones that underlie the *de novo* formation of higher-ordered septin structures, or that promote their attachment at the cell cortex. In mammalian cells overexpressed PIPKIβ, a PI(4,5)P_2-synthesizing enzyme, is found enriched at the cleavage furrow (Emoto et al., 2005), but it remains unclear, whether PIPK1β affects the distribution of cytokinetic factors.

At late stages of cytokinesis centralspindlin accumulates at the midbody (Hutterer et al., 2009). Its motor subunit MKLP1 forms complex with Arf6, and promotes its recruitment of this small GTPase to the midbody (Boman et al., 1999; Makyio et al., 2012). Of note, Arf6 associates with, and activates PIPKI enzymes (Honda et al., 1999; Krauss et al., 2003). This suggests that the MKLP1-Arf6 complex initiates the generation of a PI(4,5)P_2 pool at the midbody to assist the concentration of PI(4,5)P_2-binding, cytokinetic proteins at this locale.

Prior to abscission, PI(4,5)P_2 at the ICB is hydrolyzed by Oculo-cerebro-renal syndrome of Lowe (OCRL) (Dambournet et al., 2011), a 5-phosphatase, that is recruited by endosomal Rab35, and delivered to the ICB to dephosphorylate PI(4,5)P_2. Cells lacking expression of Rab35, or of OCRL, display defects in abscission, exhibit increased local levels of PI(4,5)P_2 and accumulate F-actin at the ICB. By contrast, overexpression of dominant-negative Rab35 triggers accumulation of PI(4,5)P_2, but also of septins on abnormal intracellular vacuoles formed before entry into mitosis (Kouranti et al., 2006). Taken together, these observations emphasize the key role of PI(4,5)P_2 in guiding the subcellular distribution of septins, and suggest that the delivery of OCRL promotes the release of septins (and probably of anillin) from the cell cortex within the ICB. Likely, this also facilitates their association with microtubules (see above).

The final abscission reaction requires the stepwise assembly of the ESCRT machinery, some components of which depend on PI(3) for their association with at endosomal membranes (Yorikawa et al., 2005; Teo et al., 2006). PI(3)P also accumulates at the midbody during cytokinesis, where it recruits the centrosomal protein and PI(3)P-binding protein FYVE-CENT and its binding partner TTC19 (Sagona et al., 2010). TTC19 in turn interacts with CHMP4B, and accordingly, loss of TTC19 or of FYVE-CENT triggers late cytokinetic defects (Sagona et al., 2010). Based on their observations the authors of this study hypothesized that midbody-associated PI(3)P is delivered by fusion of endosomes with the plasma membrane at the ICB. Alternatively, and based on analogy (Posor et al., 2013), one might speculate that a plasma membrane-based PI conversion mechanism could involve the stepwise hydrolysis of PI(4,5)P_2 into PI(4)P (through OCRL), towards the generation of PI(3)P, for instance through the synthesis of a PI(3,4)P_2 intermediate.

Future Directions

Although roles of septins during cytokinesis are firmly established, several aspects remain unclear. What are the molecular mechanisms underlying extrusion of anillin, septin and select cytokinetic proteins in tubules? Why do septins translocate to ICB microtubules, what is the functional relevance of this "hopping" behaviour, and why is it not observed in all cell types? How exactly is the translocation to microtubules modulated by posttranslational modifications, in particular by phosphorylation through mitotic kinases? Which motors, other than MKLP2/KIF20A, are retained at the ICB by septins? Which enzymes promote changes in phosphoinositide identity at the ICB? In particular, how are pools of PI(3)P and its derivatives generated, that appear at the ICB and support ESCRT-dependent abscission, and where exactly are these pools localized (Gulluni et al., 2017) (**Figure 1D**)? Given the dimensions of the ICB, answers to these questions will clearly rely on the application of super-resolution microscopy techniques.

AUTHOR CONTRIBUTIONS

GR and MK wrote the Mini-Review.

FUNDING

This work was supported by a grant from the German research funding agency Deutsche Forschungsgemeinschaft (grant number SFB958/A11).

REFERENCES

Addi, C., Bai, J., and Echard, A. (2018). Actin, Microtubule, Septin and ESCRT Filament Remodeling during Late Steps of Cytokinesis. *Curr. Opin. Cel Biol.* 50, 27–34. doi:10.1016/j.ceb.2018.01.007

Bai, X., Bowen, J. R., Knox, T. K., Zhou, K., Pendziwiat, M., Kuhlenbäumer, G., et al. (2013). Novel Septin 9 Repeat Motifs Altered in Neuralgic Amyotrophy Bind and Bundle Microtubules. *J. Cel Biol* 203, 895–905. doi:10.1083/jcb.201308068

Boman, A. L., Kuai, J., Zhu, X., Chen, J., Kuriyama, R., and Kahn, R. A. (1999). Arf Proteins Bind to Mitotic Kinesin-like Protein 1 (MKLP1) in a GTP-dependent Fashion. *Cell Motil. Cytoskeleton* 44, 119–132. doi:10.1002/(sici)1097-0169(199910)44:2<119::aid-cm4>3.0.co;2-c

Carim, S. C., Kechad, A., and Hickson, G. R. X. (2020). Animal Cell Cytokinesis: The Rho-dependent Actomyosin-Anilloseptin Contractile Ring as a Membrane Microdomain Gathering, Compressing, and Sorting Machine. *Front. Cel Dev. Biol.* 8, 575226. doi:10.3389/fcell.2020.575226

Christ, L., Wenzel, E. M., Liestøl, K., Raiborg, C., Campsteijn, C., and Stenmark, H. (2016). ALIX and ESCRT-I/II Function as Parallel ESCRT-III Recruiters in Cytokinetic Abscission. *J. Cel Biol* 212, 499–513. doi:10.1083/jcb.201507009

Dambournet, D., Machicoane, M., Chesneau, L., Sachse, M., Rocancourt, M., El Marjou, A., et al. (2011). Rab35 GTPase and OCRL Phosphatase Remodel Lipids and F-Actin for Successful Cytokinesis. *Nat. Cel Biol* 13, 981–988. doi:10.1038/ncb2279

El Amine, N., Kechad, A., Jananji, S., and Hickson, G. R. X. (2013). Opposing Actions of Septins and Sticky on Anillin Promote the Transition from Contractile to Midbody Ring. *J. Cel Biol* 203, 487–504. doi:10.1083/jcb.201305053

Emoto, K., Inadome, H., Kanaho, Y., Narumiya, S., and Umeda, M. (2005). Local Change in Phospholipid Composition at the Cleavage Furrow Is Essential for Completion of Cytokinesis. *J. Biol. Chem.* 280, 37901–37907. doi:10.1074/jbc.m504282200

Estey, M. P., Di Ciano-Oliveira, C., Froese, C. D., Bejide, M. T., and Trimble, W. S. (2010). Distinct Roles of Septins in Cytokinesis: SEPT9 Mediates Midbody Abscission. *J. Cel Biol* 191, 741–749. doi:10.1083/jcb.201006031

Field, C. M., Coughlin, M., Doberstein, S., Marty, T., and Sullivan, W. (2005a). Characterization Ofanillinmutants Reveals Essential Roles in Septin Localization and Plasma Membrane Integrity. *Development* 132, 2849–2860. doi:10.1242/dev.01843

Field, S. J., Madson, N., Kerr, M. L., Galbraith, K. A. A., Kennedy, C. E., Tahiliani, M., et al. (2005b). PtdIns(4,5)P2 Functions at the Cleavage Furrow during Cytokinesis. *Curr. Biol.* 15, 1407–1412. doi:10.1016/j.cub.2005.06.059

Glotzer, M. (2009). The 3Ms of central Spindle Assembly: Microtubules, Motors and MAPs. *Nat. Rev. Mol. Cel Biol* 10, 9–20. doi:10.1038/nrm2609

Guizetti, J., Schermelleh, L., Mäntler, J., Maar, S., Poser, I., Leonhardt, H., et al. (2011). Cortical Constriction during Abscission Involves Helices of ESCRT-III-dependent Filaments. *Science* 331, 1616–1620. doi:10.1126/science.1201847

Gulluni, F., Martini, M., and Hirsch, E. (2017). Cytokinetic Abscission: Phosphoinositides and ESCRT S Direct the Final Cut. *J. Cel. Biochem.* 118, 3561–3568. doi:10.1002/jcb.26066

Honda, A., Nogami, M., Yokozeki, T., Yamazaki, M., Nakamura, H., Watanabe, H., et al. (1999). Phosphatidylinositol 4-Phosphate 5-Kinase α Is a Downstream Effector of the Small G Protein ARF6 in Membrane Ruffle Formation. *Cell* 99, 521–532. doi:10.1016/s0092-8674(00)81540-8

Hutterer, A., Glotzer, M., and Mishima, M. (2009). Clustering of Centralspindlin Is Essential for its Accumulation to the central Spindle and the Midbody. *Curr. Biol.* 19, 2043–2049. doi:10.1016/j.cub.2009.10.050

Joo, E., Surka, M. C., and Trimble, W. S. (2007). Mammalian SEPT2 Is Required for Scaffolding Nonmuscle Myosin II and its Kinases. *Develop. Cel* 13, 677–690. doi:10.1016/j.devcel.2007.09.001

Karasmanis, E. P., Hwang, D., Nakos, K., Bowen, J. R., Angelis, D., and Spiliotis, E. T. (2019). A Septin Double Ring Controls the Spatiotemporal Organization of the ESCRT Machinery in Cytokinetic Abscission. *Curr. Biol.* 29, 2174–2182.e7. doi:10.1016/j.cub.2019.05.050

Kinoshita, M., Field, C. M., Coughlin, M. L., Straight, A. F., and Mitchison, T. J. (2002). Self- and Actin-Templated Assembly of Mammalian Septins. *Develop. Cel* 3, 791–802. doi:10.1016/s1534-5807(02)00366-0

Kinoshita, M., Kumar, S., Mizoguchi, A., Ide, C., Kinoshita, A., Haraguchi, T., et al. (1997). Nedd5, a Mammalian Septin, Is a Novel Cytoskeletal Component Interacting with Actin-Based Structures. *Genes Dev.* 11, 1535–1547. doi:10.1101/gad.11.12.1535

Kouranti, I., Sachse, M., Arouche, N., Goud, B., and Echard, A. (2006). Rab35 Regulates an Endocytic Recycling Pathway Essential for the Terminal Steps of Cytokinesis. *Curr. Biol.* 16, 1719–1725. doi:10.1016/j.cub.2006.07.020

Krauss, M., and Haucke, V. (2007). Phosphoinositides: Regulators of Membrane Traffic and Protein Function. *FEBS Lett.* 581, 2105–2111. doi:10.1016/j.febslet.2007.01.089

Krauss, M., Kinuta, M., Wenk, M. R., De Camilli, P., Takei, K., and Haucke, V. (2003). ARF6 Stimulates clathrin/AP-2 Recruitment to Synaptic Membranes by Activating Phosphatidylinositol Phosphate Kinase Type Iγ. *J. Cel Biol* 162, 113–124. doi:10.1083/jcb.200301006

Lee, H. H., Elia, N., Ghirlando, R., Lippincott-Schwartz, J., and Hurley, J. H. (2008). Midbody Targeting of the ESCRT Machinery by a Noncanonical Coiled Coil in CEP55. *Science* 322, 576–580. doi:10.1126/science.1162042

Lekomtsev, S., Su, K.-C., Pye, V. E., Blight, K., Sundaramoorthy, S., Takaki, T., et al. (2012). Centralspindlin Links the Mitotic Spindle to the Plasma Membrane during Cytokinesis. *Nature* 492, 276–279. doi:10.1038/nature11773

Liu, J., Fairn, G. D., Ceccarelli, D. F., Sicheri, F., and Wilde, A. (2012). Cleavage Furrow Organization Requires PIP2-Mediated Recruitment of Anillin. *Curr. Biol.* 22, 64–69. doi:10.1016/j.cub.2011.11.040

Makyio, H., Ohgi, M., Takei, T., Takahashi, S., Takatsu, H., Katoh, Y., et al. (2012). Structural Basis for Arf6-MKLP1 Complex Formation on the Flemming Body Responsible for Cytokinesis. *EMBO J.* 31, 2590–2603. doi:10.1038/emboj.2012.89

Matsuda, K., Sugawa, M., Yamagishi, M., Kodera, N., and Yajima, J. (2020). Visualizing Dynamic Actin Cross-linking Processes Driven by the Actin-binding Protein Anillin. *FEBS Lett.* 594, 1237–1247. doi:10.1002/1873-3468.13720

Menon, M. B., Sawada, A., Chaturvedi, A., Mishra, P., Schuster-Gossler, K., Galla, M., et al. (2014). Genetic Deletion of SEPT7 Reveals a Cell Type-specific Role of Septins in Microtubule Destabilization for the Completion of Cytokinesis. *Plos Genet.* 10, e1004558. doi:10.1371/journal.pgen.1004558

Mierzwa, B., and Gerlich, D. W. (2014). Cytokinetic Abscission: Molecular Mechanisms and Temporal Control. *Develop. Cel* 31, 525–538. doi:10.1016/j.devcel.2014.11.006

Mishima, M. (2016). Centralspindlin in Rappaport's Cleavage Signaling. *Semin. Cel Develop. Biol.* 53, 45–56. doi:10.1016/j.semcdb.2016.03.006

Oceguera-Yanez, F., Kimura, K., Yasuda, S., Higashida, C., Kitamura, T., Hiraoka, Y., et al. (2005). Ect2 and MgcRacGAP Regulate the Activation and Function of Cdc42 in Mitosis. *J. Cel Biol* 168, 221–232. doi:10.1083/jcb.200408085

Oegema, K., Savoian, M. S., Mitchison, T. J., and Field, C. M. (2000). Functional Analysis of a Human Homologue of the Drosophila Actin Binding Protein Anillin Suggests a Role in Cytokinesis. *J. Cel Biol* 150, 539–552. doi:10.1083/jcb.150.3.539

Ong, K., Wloka, C., Okada, S., Svitkina, T., and Bi, E. (2014). Architecture and Dynamic Remodelling of the Septin Cytoskeleton during the Cell Cycle. *Nat. Commun.* 5, 5698. doi:10.1038/ncomms6698

Piekny, A. J., and Maddox, A. S. (2010). The Myriad Roles of Anillin during Cytokinesis. *Semin. Cel Develop. Biol.* 21, 881–891. doi:10.1016/j.semcdb.2010.08.002

Posor, Y., Eichhorn-Gruenig, M., Puchkov, D., Schöneberg, J., Ullrich, A., Lampe, A., et al. (2013). Spatiotemporal Control of Endocytosis by Phosphatidylinositol-3,4-Bisphosphate. *Nature* 499, 233–237. doi:10.1038/nature12360

Qiu, R., Runxiang, Q., Geng, A., Liu, J., Xu, C. W., Menon, M. B., et al. (2020). SEPT7 Interacts with KIF20A and Regulates the Proliferative State of Neural Progenitor Cells during Cortical Development. *Cereb. Cortex* 30, 3030–3043. doi:10.1093/cercor/bhz292

Renshaw, M. J., Liu, J., Lavoie, B. D., and Wilde, A. (2014). Anillin-dependent Organization of Septin Filaments Promotes Intercellular Bridge Elongation and Chmp4B Targeting to the Abscission Site. *Open Biol.* 4, 130190. doi:10.1098/rsob.130190

Ribet, D., Boscaini, S., Cauvin, C., Siguier, M., Mostowy, S., Echard, A., et al. (2017). SUMOylation of Human Septins Is Critical for Septin Filament Bundling and Cytokinesis. *J. Cel Biol* 216, 4041–4052. doi:10.1083/jcb.201703096

Sagona, A. P., Nezis, I. P., Pedersen, N. M., Liestøl, K., Poulton, J., Rusten, T. E., et al. (2010). PtdIns(3)P Controls Cytokinesis through KIF13A-Mediated Recruitment of FYVE-CENT to the Midbody. *Nat. Cel Biol* 12, 362–371. doi:10.1038/ncb2036

Salameh, J., Cantaloube, I., Benoit, B., Pous, C., and Baillet, A. (2021). Cdc42 and its BORG2 and BORG3 Effectors Control the Subcellular Localization of Septins between Actin Stress Fibers and Microtubules. *Curr. Biol.* 31, 4088–4103.e5. doi:10.1016/j.cub.2021.07.004

Spiliotis, E. T., Kinoshita, M., and Nelson, W. J. (2005). A Mitotic Septin Scaffold Required for Mammalian Chromosome Congression and Segregation. *Science* 307, 1781–1785. doi:10.1126/science.1106823

Spiliotis, E. T., and Nakos, K. (2021). Cellular Functions of Actin- and Microtubule-Associated Septins. *Curr. Biol.* 31, R651–R666. doi:10.1016/j.cub.2021.03.064

Sun, L., Guan, R., Lee, I.-J., Liu, Y., Chen, M., Wang, J., et al. (2015). Mechanistic Insights into the anchorage of the Contractile Ring by Anillin and Mid1. *Develop. Cel* 33, 413–426. doi:10.1016/j.devcel.2015.03.003

Tanaka-Takiguchi, Y., Kinoshita, M., and Takiguchi, K. (2009). Septin-mediated Uniform Bracing of Phospholipid Membranes. *Curr. Biol.* 19, 140–145. doi:10.1016/j.cub.2008.12.030

Teo, H., Gill, D. J., Sun, J., Perisic, O., Veprintsev, D. B., Vallis, Y., et al. (2006). ESCRT-I Core and ESCRT-II GLUE Domain Structures Reveal Role for GLUE in Linking to ESCRT-I and Membranes. *Cell* 125, 99–111. doi:10.1016/j.cell.2006.01.047

Wang, K., Wloka, C., and Bi, E. (2019). Non-muscle Myosin-II Is Required for the Generation of a Constriction Site for Subsequent Abscission. *iScience* 13, 69–81. doi:10.1016/j.isci.2019.02.010

Wu, W.-D., Yu, K.-W., Zhong, N., Xiao, Y., and She, Z.-Y. (2019). Roles and Mechanisms of Kinesin-6 KIF20A in Spindle Organization during Cell Division. *Eur. J. Cel Biol.* 98, 74–80. doi:10.1016/j.ejcb.2018.12.002

Yorikawa, C., Shibata, H., Waguri, S., Hatta, K., Horii, M., Katoh, K., et al. (2005). Human CHMP6, a Myristoylated ESCRT-III Protein, Interacts Directly with an ESCRT-II Component EAP20 and Regulates Endosomal Cargo Sorting. *Biochem. J.* 387, 17–26. doi:10.1042/bj20041227

Zhang, D., and Glotzer, M. (2015). The RhoGAP Activity of CYK-4/MgcRacGAP Functions Non-canonically by Promoting RhoA Activation during Cytokinesis. *Elife* 4, e08898. doi:10.7554/eLife.08898

Zhang, J., Kong, C., Xie, H., Mcpherson, P. S., Grinstein, S., and Trimble, W. S. (1999). Phosphatidylinositol Polyphosphate Binding to the Mammalian Septin H5 Is Modulated by GTP. *Curr. Biol.* 9, 1458–1467. doi:10.1016/s0960-9822(00)80115-3

Zhu, M., Wang, F., Yan, F., Yao, P. Y., Du, J., Gao, X., et al. (2008). Septin 7 Interacts with Centromere-Associated Protein E and Is Required for its Kinetochore Localization. *J. Biol. Chem.* 283, 18916–18925. doi:10.1074/jbc.m710591200

Conflict of Interest: The authors declare that the research was conducted in the absence of any commercial or financial relationships that could be construed as a potential conflict of interest.

Publisher's Note: All claims expressed in this article are solely those of the authors and do not necessarily represent those of their affiliated organizations, or those of the publisher, the editors and the reviewers. Any product that may be evaluated in this article, or claim that may be made by its manufacturer, is not guaranteed or endorsed by the publisher.

frontiers in Cell and Developmental Biology

MINI REVIEW
published: 11 November 2021
doi: 10.3389/fcell.2021.768409

Role of Septins in Endothelial Cells and Platelets

*Katharina Neubauer and Barbara Zieger**

Department of Pediatrics and Adolescent Medicine, Division of Pediatric Hematology and Oncology, Medical Center, Faculty of Medicine, University of Freiburg, Freiburg, Germany

Septins are conserved cytoskeletal GTP-binding proteins identified in almost all eukaryotes except higher plants. Mammalian septins comprise 13 family members with either ubiquitous or organ- and tissue-specific expression patterns. They form filamentous oligomers and complexes with other proteins to serve as diffusions barrier and/or multi-molecular scaffolds to function in a physiologically regulated manner. Diverse septins are highly expressed in endothelial cells and platelets, which play an important role in hemostasis, a process to prevent blood loss after vascular injury. Endothelial septins are involved in cellular processes such as exocytosis and in processes concerning organismal level, like angiogenesis. Septins are additionally found in endothelial cell-cell junctions where their presence is required to maintain the integrity of the barrier function of vascular endothelial monolayers. In platelets, septins are important for activation, degranulation, adhesion, and aggregation. They have been identified as mediators of distinct platelet functions and being essential in primary and secondary hemostatic processes. Septin-knockout mouse studies show the relevance of septins in several aspects of hemostasis. This is in line with reports that dysregulation of septins is clinically relevant in human bleeding disorders. The precise function of septins in the biology of endothelial cells and platelets remains poorly understood. The following mini-review highlights the current knowledge about the role of septin cytoskeleton in regulating critical functions in these two cell types.

Keywords: septins, platelets, endothelial cells, angiogenesis, cell-cell junction, exocytosis, hemostasis

OPEN ACCESS

Edited by:
Manoj B. Menon,
Indian Institute of Technology Delhi, India

Reviewed by:
Olga Vagin,
UCLA David Geffen School of Medicine, United States
Andrei Karginov,
University of Illinois at Chicago, United States
Michael Krauß,
Leibniz-Institut für Molekulare Pharmakologie (FMP), Germany

****Correspondence:***
Barbara Zieger
barbara.zieger@uniklinik-freiburg.de

Specialty section:
This article was submitted to Signaling, a section of the journal Frontiers in Cell and Developmental Biology

Received: *31 August 2021*
Accepted: *25 October 2021*
Published: *11 November 2021*

Citation:
Neubauer K and Zieger B (2021) Role of Septins in Endothelial Cells and Platelets. Front. Cell Dev. Biol. 9:768409. doi: 10.3389/fcell.2021.768409

INTRODUCTION

Endothelial cells (ECs) form a continuous thin layer (endothelium), which lines the interior surface of blood and lymphatic vessels separating the lumen from the surrounding tissue (Baldwin and Thurston 2001). The structure of ECs varies depending on the tissue (Gomez-Salinero and Rafii 2018). Vascular endothelium was originally considered a simple passive barrier and is meanwhile known to be crucial to maintain vessel integrity. Thereby, endothelial cell functions are versatile and comprise mediating vascular tone, hemostasis, regulating transport from the blood to underlying cells and tissues, permeability, cellular adhesion, smooth muscle cell proliferation, angiogenesis, and vessel wall inflammation (Kruger-Genge et al., 2019). Crucial communication partners of the ECs are platelets, small anuclear cells. ECs and platelets interact and regulate their activities mutually via direct and indirect signaling (Ruggeri 2003). One of the platelet's key functions is to support hemostasis, a process of plug formation at the site of vascular injury to stop excessive bleeding. As a result of exposure to physical or biochemical stimuli, the initial activation step is the adhesion of platelets to the subendothelial matrix via collagen-bound von Willebrand Factor (vWF) and platelet

glycoprotein (GP)Ib-V-IX complex. The vWF in plasma is released from ECs and platelets. Consequently, platelets come into close proximity of the injured vessel allowing the interaction of glycoprotein (GP)VI, the major collagen receptor on platelet membranes, with collagen. GPVI binding to collagen leads to platelet activation including the secretion of their intracellular granules and activation of the fibrinogen receptor integrin $\alpha_{IIb}\beta_{3.}$ Fibrinogen binding to integrin $\alpha_{IIb}\beta_3$ in turn induces platelet aggregation with each other to form a hemostatic plug resulting in vascular occlusion. In this process, the platelet cytoskeleton reorganizes to undergo a change in shape from disc-shaped into spheres with protruding filopodia and lamellipodia (Jurk and Kehrel 2005). Although endothelial cells and platelets are different cell types, they share several properties. Both cell types derive from a common bone marrow-derived progenitor cell (Choi 2002). Not only platelets but also ECs circulate to a small amount in peripheral blood (Lin et al., 2000). ECs and platelets rearrange their cytoskeleton to promote changes in cell shape. They have the ability to store bioactive substances in cytoplasmic granules and release their cargo by exocytosis. Some endothelial and platelet proteins are identical, such as vWF or the cell adhesion molecule P-selectin (Denis 2002) Septins are also highly expressed in both ECs and platelets.

Mammalian septins comprise 13 family members which are either ubiquitously expressed or restricted to specific tissues or cell types (Dolat et al., 2014). All known septins are composed of a highly conserved central GTP-binding region flanked by N- and C-terminal with variable length. Most septins exhibit a C-terminal coiled-coil region, which may be necessary for interactions with other septins or proteins (Fung et al., 2014). Septins display the capability to form heterocomplexes *in vivo* and *in vitro*. The first characterized complex was the hexamer SEPT7-6-2-2-6-7 (Sirajuddin et al., 2007), which can become an octamer by the inclusion of two Septin 9 molecules (Sandrock et al., 2011). These polymers form further nonpolar filaments (Bridges and Gladfelter 2015) that can assemble in various higher-order structures, such as rings and gauzes by lateral stacking and tandem annealing (Kinoshita 2003; Valadares et al., 2017). Moreover, they can bind to phosphoinositides of cell membranes via a N-terminal polybasic domain (Zhang et al., 1999). Septin filaments thus represent an important component of the cytoskeleton, among actin, microtubules, and intermediate filaments (Mostowy and Cossart 2012). Septin-based structures may rearrange and disassemble in cells under the control of diverse factors and covalent modifications; however, the exact mechanisms of assembly and disassembly remain elusive (Kinoshita 2003). Septins participate in a spectrum of cellular processes involving the rearrangement of cytoskeletal elements or the motility of cellular membranes, for instance cytokinesis, cell polarity, endo- and exocytosis, or apoptosis (Hall and Russell 2004). Septin cytoskeleton is known to interact with actin filaments and microtubules in different contexts (Mostowy and Cossart 2012; Mavrakis et al., 2014; Bezanilla et al., 2015) and to contribute to intracellular membrane-associated processes, such as endomembrane fusion or mitochondrial fission (Mostowy and Cossart 2012; Dolat and Spiliotis 2016; Pagliuso et al., 2016). The cytoskeleton is a dynamic network and maintains cell morphology and movement, but it also enables rapid signaling events (Janmey 1998). Cytoskeletal remodeling is an important event in both ECs and platelets. The role of actin and microtubules in this process is well-established, whereas the septin network's involvement is less clear. This mini-review focuses on the impact of septins in ECs and platelets summarizing the current knowledge in this field.

SEPTINS IN ENDOTHELIAL CELLS

Endothelial Septin Expression

Diverse reports show that septins are expressed in ECs in a distinct tissue-dependent expression pattern. In the human eye, SEPT4, SEPT5, and SEPT8 have been detected in corneal ECs (Pache et al., 2005). In human umbical vein ECs (HUVECs), SEPT2, SEPT4, SEPT5, SEPT7, and SEPT11 have been shown to be expressed (Blaser et al., 2006; Bartsch et al., 2010). Colocalization with the cytoskeletal protein α-tubulin was detected for SEPT2, SEPT4, SEPT7, and SEPT11 *in vitro* but only SEPT2 and SEPT7 colocalize with actin filaments (Bartsch et al., 2010).

Septins Involved in Endothelial Endo- and Exocytosis

In HUVECs, SEPT4 and SEPT11 have been shown to be colocalized with the vesicle-associated protein synaptobrevin 1 (VAMP1), which belongs to the SNARE (soluble *N*-ethylmaleimide-sensitive factor attachment protein receptor) protein family (Bartsch et al., 2010). Since exocytosis is mediated by SNAREs (Chen and Scheller 2001) some researchers hypothesize that septins may be involved in exocytotic processes. Furthermore, SEPT2, SEPT4, SEPT7, and SEPT11 colocalize with the endocytosis marker transferrin receptor seemingly in the plasma membrane and in endosomes suggesting that these septins play a role in endocytotic processes. However, the impact of septins in these mechanisms in ECs remains unexplored (Bartsch et al., 2010).

SEPT7 is known to be involved in the endocytosis of microbial pathogens. Infection with Candida albicans leads to rearranged endothelial actin filaments forming pseudopods to pull the organism into the EC. In response to the infection, SEPT7 interacts with the endothelial adhesion protein N-cadherin. This SEPT7/N-cadherin complex accumulates around C. albicans hyphae and is necessary for the maximum endocytosis of C. albicans (Phan et al., 2013).

Role of Septins in Angiogenesis

SEPT7 is reportedly involved in angiogenesis in microvascular cardiac ECs (Liu et al., 2014). ECs are the main players in angiogenesis, forming new blood vessels from preexisting ones. The major driver of this process is the arrangement of ECs in tip and stalk cells. Tip cells form filopodia that invade the surrounding tissue, leading the path toward neo-vessel formation (Eilken and Adams 2010). Angiogenesis requires cell polarity and the highly coordinated morphogenesis of ECs,

which involves the accurate coupling of different cytoskeletal networks within the EC. In this process, SEPT7 has been shown to form a complex with Borg5 (Binder of the Rho GTPase 5) and to colocalize with actomyosin fibers (Liu et al., 2014). In general, Borg proteins have been shown to interact directly with septins and thereby influence actin and septin cytoskeleton (Sheffield et al., 2003). Liu et al. discovered that SEPT7/Borg5 facilitate the positioning and organization of contractile actomyosin fibers above the nucleus of primary mouse cardiac ECs. Genetic deletion of Borg5 as well as SEPT7 knockdown resulted in the disruption of perinuclear actomyosin and diminished persistent directional migration. The authors suggest that the SEPT7/Borg5 complex controls actomyosin activity to ensure persistent directional migration and efficient microvascular angiogenesis. Borgs are effectors of the Rho family GTPase Cdc42. Septin/Borg interactions have been found to be inhibited by constitutively active Cdc42. Overexpression of Cdc42 cause a loss of septin filaments (Joberty et al., 2001). A recent study shows that Cdc42 controls the subcellular localization of septins between actin stress fibers and microtubules (Salameh et al., 2021).

Vessel branching and angiogenesis is facilitated by the presence of podosomes. These are specialized compartmentalized actin-rich cell-matrix contacts able to locally secrete proteases and remodel the extracellular matrix (Gimona et al., 2008). A recent study showed that some septins (SEPT2, SEPT6, SEPT7, and SEPT9) are expressed in podosomes and identified the septin cytoskeleton as a novel component of endothelial podosomes (Collins et al., 2020). Collins et al. reported that SEPT2 in ECs is required for podosomal matrix remodeling and EC invasion, suggesting SEPT2 mediates the formation of functional podosomes, thereby facilitating the initial step of angiogenic invasion. The authors demonstrated that also SEPT6 and SEPT7 are necessary for regulation of matrix degeneration by ECs, but not SEPT9 despite all these septins were found in endothelial podosomes. This highlights the different roles for individual septins in this process.

There is also evidence that septins play a role in oxidative stress, a process caused by an imbalance of nitric oxide (NO) and reactive oxygen species (ROS). Oxidative stress induces vascular endothelial injury and is a mediator and modulator of angiogenesis (Kim and Byzova 2014). SEPT4 has been identified as an oxidative stress factor, which can promote oxidative vascular endothelial damage by interacting with apoptosis-related protein $PARP_1$. This has been shown by knock-down and over-expression of SEPT4 (Zhang et al., 2018). Furthermore, SEPT4 is a physiological substrate of the ubiquitin ligase WWP2 involved in oxidative stress vascular endothelial injury. WWP2 mediates the degeneration of SEPT4, which inhibits formation of the SEPT4/$PARP_1$ complex to suppress endothelial damage and vascular remodeling (Zhang et al., 2020).

Septins Required for Cell-Cell Junction Integrity

The endothelial barrier function relies on cell-cell junctions that comprise tight junctions, adherens junctions, desmosomes, and gap junctions. Kim and Cooper characterized septin filaments in ECs using a monolayer system of primary human dermal microvascular ECs (Kim and Cooper 2018). They found SEPT2 located at cell-junction membranes and forming curved structures. SEPT2 was enriched especially in regions of positive membrane curvature associated with actin-rich membrane protrusions. Loss of SEPT2 led to a disrupted VE-cadherin structure and membrane dynamics, assuming that septins promote cadherin-based cell junctions and regulate the integrity of the barrier function formed by endothelial monolayers. SEPT2 may function as mechanical support for the actin-rich protrusions known to be essential for the assembly and stability of cadherin-based cell junctions.

In another study, Kim and Cooper extended their analysis by questioning whether SEPT2 is required to regulate the organization of other cell-adhesion proteins, focusing on PECAM-1 (platelet endothelial cell adhesion molecule-1), nectin-2, afadin, TJP (the tight junction protein), and ZO-1 (zonula occludens-1) (Kim and Cooper 2021). SEPT2 filaments are normally localized at junctions and are linked to the membrane by direct interaction with PIP_2 (phosphatidylinositol 4,5-bisphosphate). Indeed, the loss of SEPT2 at cell junctions leads to striking spatial disorganization of all these junctional proteins: thereby, the expression levels of these proteins were unaffected by the loss of SEPT2 except for nectin-2, whose expression was greatly increased. These results suggest that the junctional location of SEPT2 is required for the sound organization of junctional proteins (Kim and Cooper 2021).

SEPTINS IN PLATELETS

Septin Expression in Platelets

In platelets, SEPT2, SEPT4, SEPT5, SEPT6, SEPT7, SEPT8, SEPT9, and SEPT11 are expressed as indicated *via* immunofluorescent staining, Western Blot analysis, or immunogold staining (Yagi et al., 1998; Zieger et al., 2000; Blaser et al., 2003; Blaser et al., 2004; Bartsch et al., 2010; Sandrock et al., 2011). There is no evidence to date for the expression of other septins. Platelet septins tend to form ring-shaped filaments (Martinez et al., 2006), which have been observed for SEPT5 and SEPT6 in suspensions of fixed human platelets. SEPT5 rings have also been detected in human fibrinogen-adhered platelets (Martinez et al., 2006). Sept8 displays rings in fibrinogen- and in collagen-adhered mouse platelets (Neubauer et al., 2021). Rings are the most often observed higher-order structure of septins in various organisms and cell-types. Such ring-shaped structures are often associated with other cytoskeletal networks, like actin and tubulin, or are located in discrete regions in the plasma membrane acting as diffusion barrier (Ewers et al., 2014) and/or cellular scaffold affecting various cellular functions, including cytokinesis (Gupta et al., 2018). In human platelets, SEPT5 and SEPT6 are located near the α-tubulin-rich platelet microtubule ring (Martinez et al., 2006). There is ample evidence that microtubules form a closed circular bundle running near the cell periphery, known as marginal band, which maintains the characteristic discoid shape of resting platelets (Kowit et al., 1988)

TABLE 1 | Summary table of known septin localization and functions in endothelial cells and platelets.

	Endothelial cells			Platelets		
	Subcellular localization and colocalization	**Functions**	**References**	**Subcellular localization and colocalization**	**Functions**	**References**
Septin 2	Actin filaments		Bartsch et al. (2010)			
	α-Tubulin		Bartsch et al. (2010)			
	Cell-junction membranes; PIP_2	Assembly and stability of cadherin-based cell junctions	Kim and Cooper (2018)			
		Organization of junctional proteins	Kim and Cooper (2021)			
	Podosomes	Matrix degeneration/Angiogenesis	Collins et al. (2020)			
Septin 4	α-Tubulin		Bartsch et al. (2010)	Surrounding α-granules		Blaser et al. (2004)
	$PARP_1$	Apoptosis	Zhang et al. (2018)			
	Transferrin receptor	Endocytosis	Bartsch et al. (2010)			
	VAMP1	Exocytosis	Bartsch et al. (2010)			
	WWP2	Oxidative stress	Zhang et al. (2020)			
Septin 5				Ring near marginal band		Martinez et al. (2006)
				Surrounding α-granules	Exocytosis (δ-granule secretion)	Dent et al. (2002)
				Syntaxin 4		Dent et al. (2002)
Septin 6	Actin filaments		Bartsch et al. (2010)	Ring near marginal band		Martinez et al. (2006)
	α-Tubulin		Bartsch et al. (2010)			
	Podosomes	Matrix degeneration/Angiogenesis	Collins et al. (2020)			
Septin 7	Actomyosin fibers	Angiogenesis	Liu et al. (2014)			
	Borg5	Angiogenesis	Liu et al. (2014)			
	N-cadherin	Endocytosis	Phan et al. (2013)			
	Podosomes	Matrix degeneration and angiogenic invasion	Collins et al. (2020)			
	Transferrin receptor	Endocytosis	Bartsch et al. (2010)			
Septin 8				Ring	Platelet activation Exocytosis (α-granule secretion) Aggregation Spreading PS exposure Thrombin generation	Neubauer et al. (2021)
				Surrounding α-granules		Blaser et al. (2004)
Septin 9	Podosomes		Collins et al. (2020)		Exocytosis (δ-granule secretion)	Neubauer et al. (2019)
Septin 11	α-Tubulin		Bartsch et al. (2010)			
	Tansferrin receptor	Endocytosis	Bartsch et al. (2010)			
	VAMP1	Exocytosis	Bartsch et al. (2010)			

Abbreviations: PIP_2, phosphatidylinositol 4,5-bisphosphate; VAMP1, vesicle-associated protein synaptobrevin 1; Borg5, Binder of the Rho GTPase 5; $PARP_1$, apoptosis-related protein; PS, phosphatidylserine.

suggesting that septin-rings may play a role in ensuring shape stability of resting platelets. Furthermore, SEPT5, SEPT6, and Sept8 display a punctate localization in the cytoplasm (Martinez et al., 2006; Neubauer et al., 2021). In platelets, septins demonstrate strong affinity to each other in forming complexes composed of multiple septin proteins (Sandrock et al., 2011).

Platelet Septins Involved in Exocytosis

Platelet secretion of intracellular α-, δ-, and lysosomal granules is a form of regulated exocytosis, which is crucial for hemostasis, thrombosis, and inflammatory processes. In human platelets, SEPT4 and SEPT8 tend to be localized surrounding α-granules (Blaser et al., 2004) as well as SEPT5 (Dent et al., 2002). After platelet activation, SEPT4 and SEPT8 move to the platelet surface, suggesting a direct role in exocytosis (Blaser et al., 2004). Indeed, Sept8-deficient mouse platelets exhibit remarkably reduced α-granule secretion, but not of δ- or lysosomal granules (Neubauer et al., 2021). Transgenic overexpression of Sept5 in mice is associated with fewer and larger α-granules, indicating that Sept5 supports normally sized α-granules (Kato et al., 2004). In contrast, loss of Sept5 in mouse platelets leads to an enhanced release of δ-granules (serotonin) in response to subthreshold levels of agonists (Dent et al., 2002). A patient with homozygous co-deletion of SEPT5 and GPIbβ, a subunit of the platelet adhesion receptor (GP)Ib-V-IX, presented dramatically reduced platelet α-granule and slightly reduced δ-granule secretion, evidence not observed in patients with only a GPIbβ deletion but normal SEPT5 expression (Bartsch et al., 2011). Family members having a congenital pathogenic variant in the N-terminal region of the *SEPT9*-gene suffer from a mild δ-granule secretion defect (Neubauer et al., 2019). Bai et al. demonstrated that the N-terminal domain of SEPT9 binds and bundles microtubules by interacting with β-tubulin. In a cell line, a mutation in this region caused diminished intracellular microtubule bundling and impaired asymmetric neurite growth (Bai et al., 2013). During platelet activation, the marginal band needs to be re-arranged to ensure degranulation. The granules are concentrated in the platelet center and are surrounded by a smaller microtubule ring (White and Burris 1984). This close packaging is required for the fusion of granules not only with the plasma membrane but also between individual granules to guarantee a rapid secretion of the whole cargo. It had been hypothesized that the coiling of the marginal band, its compression through actomyosin contraction and the formation of a smaller microtubule ring leads to an accumulation of granules in the center of activated platelets (Sadoul 2015). Interestingly, Sept5 and Sept8 appear to have opposing roles, maybe because these two septins have been found to interact to individual factors of the exocytosis machinery. Platelets use soluble N-ethylmaleimide sensitive factor attachment protein receptor (SNARE)-mediated fusion of granules with the plasma membrane. Vesicular (v)-SNAREs and target (t)-SNAREs on the cell membrane form a protein complex to release granular cargo. The membrane fusion of α-granules and δ-granules requires different sets of SNAREs (Flaumenhaft 2003). SEPT5 has been hypothesized to inhibit the degranulation of δ-granules by binding the t-SNARE protein syntaxin 4 (Dent et al., 2002). In neurons, which share similarities with platelets in the control of neurotransmitter release and platelet granule secretion, respectively, Sept8 has been suggested to control the formation of the v-SNARE-complex at the synapse and subsequent exocytosis via dynamic interactions with VAMP2 (vesicle-associated membrane protein 2) (Ito et al., 2009).

Sept8 is Involved in Primary and Secondary Hemostasis

In addition to the degranulation described above, Sept8 is known to be involved in platelet functions in primary hemostasis through comprehensive analyses using a Sept8-knockout mouse model (Neubauer et al., 2021). Loss of Sept8 in mouse platelets caused a pronounced defect in activation, adherence, and aggregation. In detail: Sept8-deficient platelets displayed a reduction in activated integrin $\alpha_{IIb}\beta_3$. Platelet activation is associated with the binding of fibrinogen to the major receptor integrin $\alpha_{IIb}\beta_3$ at the platelet surface, which is crucial for platelet bridging and subsequent aggregation. In contrast to the reduced aggregation caused by the loss of Sept8, a Sept5 deletion leads to an enhanced aggregation with an agonist requiring a platelet-secretory response (Dent et al., 2002). Sept8-deficient platelets exhibited delayed spreading on fibrinogen, a process by which adherent platelets flatten at sites of vascular damage and expand their contact area by deforming of the plasma membrane (Neubauer et al., 2021). Reorganization of the cytoskeleton network is essential for all these processes and for degranulation. This entails disrupting cell-cell adhesions, cell scattering, and enhanced cell motility. Sept8 could thus contribute to this process by interacting with actin filaments, microtubules, and intermediate filaments (Mostowy and Cossart 2012). In addition to primary hemostasis, Sept8 is known to be involved in secondary hemostasis (coagulation) (Neubauer et al., 2021). This is a process that leads to the formation of a stable platelet plug by activated coagulation factors, specifically thrombin, which converts fibrinogen to fibrin. A Sept8-deletion in mouse platelets leads to reduced thrombin generation. Furthermore, Sept8-deficient platelets exhibit reduced exposure of the membrane phospholipid phosphatidylserine (PS), which is provided physiologically by activated platelets on their cell surface and is incorporated into the developing clot demonstrating disturbed procoagulant activity of Sept8-deficient platelets. These findings revealed Sept8 as a modulator of distinct platelet functions associated with primary and secondary hemostatic processes.

Regulation of Septins in Stored Platelets

A proteome analysis of platelet concentrates, which are essential in transfusion therapy, found that SEPT2 was quantitatively altered during platelets storage; the researchers hypothesize that septins may play a dynamic role during storage (Thiele et al., 2007). In a further study, microRNA-223 was found to regulate SEPT2 and SEPT6 in stored platelets (Chattopadhyay et al., 2018). Since platelets are anucleated cells, downregulation via microRNAs is one of the possible posttranscriptional mechanisms acting in platelets. MicroRNA-223 forms a complex with Argonaute 2 (AGO2) protein, the catalytic component of RISC (RNA Induced Silencing Complex).

CONCLUSION

Eight out of 13 septins are highly expressed in both ECs and platelets and are known to play important roles (**Table 1**). Many of their functions are associated with reorganizing the cytoskeleton network, such as angiogenesis in ECs, or degranulation and spreading during platelet hemostasis. In addition, septins can also be a part of structures like cell-cell junctions where they are essential for the integrity of endothelial monolayers. However, the molecular mechanisms of septin-function in both cell types require further investigation in the future.

AUTHOR CONTRIBUTIONS

KN and BZ drafted the manuscript.

FUNDING

The authors' research work is supported by the grants from the Deutsche Forschungsgemeinschaft (DFG/ZI 486/4-1 and DFG/ZI 486/8-1).

REFERENCES

Bai, X., Bowen, J. R., Knox, T. K., Zhou, K., Pendziwiat, M., Kuhlenbäumer, G., et al. (2013). Novel Septin 9 Repeat Motifs Altered in Neuralgic Amyotrophy Bind and Bundle Microtubules. *J. Cel. Biol.* 203 (6), 895–905. doi:10.1083/jcb.201308068

Baldwin, A. L., and Thurston, G. (2001). Mechanics of Endothelial Cell Architecture and Vascular Permeability. *Crit. Rev. Biomed. Eng.* 29 (2), 247–278. doi:10.1615/critrevbiomedeng.v29.i2.20

Bartsch, I., Bläser, S., Röseler, S., Sandrock, K., Busse, A., Huber, M., et al. (2010). Human Endothelial and Platelet Septin SEPT11: Cloning of Novel Variants and Characterisation of Interaction Partners. *Thromb. Haemost.* 104 (6), 1201–1210. doi:10.1160/TH10-07-0472

Bartsch, I., Sandrock, K., Lanza, F., Nurden, P., Hainmann, I., Pavlova, A., et al. (2011). Deletion of Human GP1BB and SEPT5 Is Associated with Bernard-Soulier Syndrome, Platelet Secretion Defect, Polymicrogyria, and Developmental Delay. *Thromb. Haemost.* 106 (3), 475–483. doi:10.1160/TH11-05-0305

Bezanilla, M., Gladfelter, A. S., Kovar, D. R., and Lee, W.-L. (2015). Cytoskeletal Dynamics: a View from the Membrane. *J. Cel. Biol.* 209 (3), 329–337. doi:10.1083/jcb.201502062

Bläser, S., Horn, J., Würmell, P., Bauer, H., Strümpell, S., Nurden, P., et al. (2004). The Novel Human Platelet Septin SEPT8 Is an Interaction Partner of SEPT4. *Thromb. Haemost.* 91 (5), 959–966. 04050959 [pii]. doi:10.1160/TH03-09-0578

Bläser, S., Jersch, K., Hainmann, I., Zieger, W., Wunderle, D., Busse, A., et al. (2003). Isolation of New Splice Isoforms, Characterization and Expression Analysis of the Human Septin SEPT8 (KIAA0202). *Gene* 312, 313–320. S0378111903006358 [pii]. doi:10.1016/s0378-1119(03)00635-8

Bläser, S., Röseler, S., Rempp, H., Bartsch, I., Bauer, H., Lieber, M., et al. (2006). Human Endothelial Cell Septins: SEPT11 Is an Interaction Partner of SEPT5. *J. Pathol.* 210 (1), 103–110. doi:10.1002/path.2013

Bridges, A. A., and Gladfelter, A. S. (2015). Septin Form and Function at the Cell Cortex. *J. Biol. Chem.* 290 (28), 17173–17180. doi:10.1074/jbc.R114.634444

Chattopadhyay, M., Dahiya, N., and Atreya, C. (2018). MicroRNA-223 Regulates Septin-2 and Septin-6 in Stored Platelets. *Mirna* 7 (3), 223–228. doi:10.2174/2211536607666180626122750

Chen, Y. A., and Scheller, R. H. (2001). SNARE-mediated Membrane Fusion. *Nat. Rev. Mol. Cel Biol.* 2 (2), 98–106. doi:10.1038/35052017

Choi, K. (2002). The Hemangioblast: a Common Progenitor of Hematopoietic and Endothelial Cells. *J. Hematotherapy Stem Cel Res.* 11 (1), 91–101. doi:10.1089/152581602753448568

Collins, K. B., Kang, H., Matsche, J., Klomp, J. E., Rehman, J., Malik, A. B., et al. (2020). Septin2 Mediates Podosome Maturation and Endothelial Cell Invasion Associated with Angiogenesis. *J. Cel. Biol.* 219 (2). doi:10.1083/jcb.201903023

Denis, C. V. (2002). Molecular and cellular biology of von Willebrand factor. *Int. J. Hematol.* 75 (1), 3–8. doi:10.1007/BF02981972

Dent, J., Kato, K., Peng, X.-R., Martinez, C., Cattaneo, M., Poujol, C., et al. (2002). A Prototypic Platelet Septin and its Participation in Secretion. *Proc. Natl. Acad. Sci.* 99 (5), 3064–3069. doi:10.1073/pnas.052715199

Dolat, L., Hu, Q., and Spiliotis, E. T. (2014). Septin Functions in Organ System Physiology and Pathology. *Biol. Chem.* 395 (2), 123–141. doi:10.1515/hsz-2013-0233

Dolat, L., and Spiliotis, E. T. (2016). Septins Promote Macropinosome Maturation and Traffic to the Lysosome by Facilitating Membrane Fusion. *J. Cel. Biol.* 214 (5), 517–527. doi:10.1083/jcb.201603030

Eilken, H. M., and Adams, R. H. (2010). Dynamics of Endothelial Cell Behavior in Sprouting Angiogenesis. *Curr. Opin. Cel Biol.* 22 (5), 617–625. doi:10.1016/j.ceb.2010.08.010

Ewers, H., Tada, T., Petersen, J. D., Racz, B., Sheng, M., and Choquet, D. (2014). A Septin-dependent Diffusion Barrier at Dendritic Spine Necks. *PloS one* 9 (12), e113916. doi:10.1371/journal.pone.0113916

Flaumenhaft, R. (2003). Molecular Basis of Platelet Granule Secretion. *Arterioscler. Thromb. Vasc. Biol.* 23 (7), 1152–1160. doi:10.1161/01.ATV.0000075965.88456.48

Fung, K. Y. Y., Dai, L., and Trimble, W. S. (2014). Cell and Molecular Biology of Septins. *Int. Rev. Cel Mol Biol.* 310, 289–339. doi:10.1016/B978-0-12-800180-6.00007-4

Gimona, M., Buccione, R., Courtneidge, S. A., and Linder, S. (2008). Assembly and Biological Role of Podosomes and Invadopodia. *Curr. Opin. Cel Biol.* 20 (2), 235–241. doi:10.1016/j.ceb.2008.01.005

Gomez-Salinero, J. M., and Rafii, S. (2018). Endothelial Cell Adaptation in Regeneration. *Science* 362 (6419), 1116–1117. doi:10.1126/science.aar4800

Gupta, D. K., Du, J., Kamranvar, S. A., and Johansson, S. (2018). Tension-induced Cytokinetic Abscission in Human Fibroblasts. *Oncotarget* 9 (10), 8999–9009. doi:10.18632/oncotarget.24016

Hall, P. A., and Russell, S. H. (2004). The Pathobiology of the Septin Gene Family. *J. Pathol.* 204 (4), 489–505. doi:10.1002/path.1654

Ito, H., Atsuzawa, K., Morishita, R., Usuda, N., Sudo, K., Iwamoto, I., et al. (2009). Sept8 Controls the Binding of Vesicle-Associated Membrane Protein 2 to Synaptophysin. *J. Neurochem.* 108 (4), 867–880. doi:10.1111/j.1471-4159.2008.05849.x

Janmey, P. A. (1998). The Cytoskeleton and Cell Signaling: Component Localization and Mechanical Coupling. *Physiol. Rev.* 78 (3), 763–781. doi:10.1152/physrev.1998.78.3.763

Joberty, G., Perlungher, R. R., Sheffield, P. J., Kinoshita, M., Noda, M., Haystead, T., et al. (2001). Borg Proteins Control Septin Organization and Are Negatively Regulated by Cdc42. *Nat. Cel Biol.* 3 (10), 861–866. doi:10.1038/ncb1001-861

Jurk, K., and Kehrel, B. E. (2005). Platelets: Physiology and Biochemistry. *Semin. Thromb. Hemost.* 31 (4), 381–392. doi:10.1055/s-2005-916671

Jurk, K., Neubauer, K., Petermann, V., Kumm, E., and Zieger, B. (2021). Impaired Platelet Function in Sept8-Deficient Mice *In Vitro*. *Thromb. Haemost.* 121 (4), 484–494. doi:10.1055/s-0040-1718733

Kato, K., Martinez, C., Russell, S., Nurden, P., Nurden, A., Fiering, S., et al. (2004). Genetic Deletion of Mouse Platelet Glycoprotein Ibβ Produces a Bernard-Soulier Phenotype with Increased α-granule Size. *Blood* 104 (8), 2339–2344. doi:10.1182/blood-2004-03-1127

Kim, J., and Cooper, J. A. (2021). Junctional Localization of Septin 2 Is Required for Organization of Junctional Proteins in Static Endothelial Monolayers. *Atvb* 41 (1), 346–359. doi:10.1161/ATVBAHA.120.315472

Kim, J., and Cooper, J. A. (2018). Septins Regulate Junctional Integrity of Endothelial Monolayers. *MBoC* 29 (13), 1693–1703. doi:10.1091/mbc.E18-02-0136

Kim, Y.-W., and Byzova, T. V. (2014). Oxidative Stress in Angiogenesis and Vascular Disease. *Blood* 123 (5), 625–631. doi:10.1182/blood-2013-09-512749

Kinoshita, M. (2003). Assembly of Mammalian Septins. *J. Biochem.* 134 (4), 491–496. doi:10.1093/jb/mvg182

Kowit, J. D., Linck, R. W., and Kenney, D. M. (1988). Isolated Cytoskeletons of Human Blood Platelets: Dark-Field Imaging of Coiled and Uncoiled Microtubules. *Biol. Cel* 64 (3), 283–291. doi:10.1016/0248-4900(88)90002-0

Krüger-Genge, A., Blocki, A., Franke, R. P., and Jung, F. (2019). Vascular Endothelial Cell Biology: An Update. *Ijms* 20 (18), 4411. doi:10.3390/ijms20184411

Lin, Y., Weisdorf, D. J., Solovey, A., and Hebbel, R. P. (2000). Origins of Circulating Endothelial Cells and Endothelial Outgrowth from Blood. *J. Clin. Invest.* 105 (1), 71–77. doi:10.1172/JCI8071

Liu, Z., Vong, Q. P., Liu, C., and Zheng, Y. (2014). Borg5 Is Required for Angiogenesis by Regulating Persistent Directional Migration of the Cardiac Microvascular Endothelial Cells. *Mol. Biol. Cel* 25 (6), 841–851. doi:10.1091/mbc.E13-09-0543

Martinez, C., Corral, J., Dent, J. A., Sesma, L., Vicente, V., and Ware, J. (2006). Platelet Septin Complexes Form Rings and Associate with the Microtubular Network. *J. Thromb. Haemost.* 4 (6), 1388–1395. JTH1952 [pii]. doi:10.1111/j.1538-7836.2006.01952.x

Mavrakis, M., Azou-Gros, Y., Tsai, F.-C., Alvarado, J., Bertin, A., Iv, F., et al. (2014). Septins Promote F-Actin Ring Formation by Crosslinking Actin Filaments into Curved Bundles. *Nat. Cel Biol.* 16 (4), 322–334. doi:10.1038/ncb2921

Mostowy, S., and Cossart, P. (2012). Septins: the Fourth Component of the Cytoskeleton. *Nat. Rev. Mol. Cel Biol.* 13 (3), 183–194. doi:10.1038/nrm3284

Neubauer, K., Boeckelmann, D., Koehler, U., Kracht, J., Kirschner, J., Pendziwiat, M., et al. (2019). Hereditary Neuralgic Amyotrophy in Childhood Caused by Duplication within the SEPT9 Gene: A Family Study. *Cytoskeleton* 76 (1), 131–136. doi:10.1002/cm.21479

Pache, M., Zieger, B., Bläser, S., and Meyer, P. (20052005). Immunoreactivity of the Septins SEPT4, SEPT5, and SEPT8 in the Human Eye. *J. Histochem. Cytochem.* 53 (9), 1139–1147. [pii]. doi:10.1369/jhc.4A6588.2005

Pagliuso, A., Tham, T. N., Stevens, J. K., Lagache, T., Persson, R., Salles, A., et al. (2016). A Role for Septin 2 in Drp1-mediated Mitochondrial Fission. *EMBO Rep.* 17 (6), 858–873. doi:10.15252/embr.201541612

Phan, Q. T., Eng, D. K., Mostowy, S., Park, H., Cossart, P., and Filler, S. G. (2013). Role of Endothelial Cell Septin 7 in the Endocytosis of Candida Albicans. *mBio* 4 (6), e00542–13. doi:10.1128/mBio.00542-13

Ruggeri, Z. M. (2003). Von Willebrand Factor, Platelets and Endothelial Cell Interactions. *J. Thromb. Haemost.* 1 (7), 1335–1342. doi:10.1046/j.1538-7836.2003.00260.x

Sadoul, K. (2015). New Explanations for Old Observations: Marginal Band Coiling during Platelet Activation. *J. Thromb. Haemost.* 13 (3), 333–346. doi:10.1111/jth.12819

Salameh, J., Cantaloube, I., Benoit, B., Poüs, C., and Baillet, A. (2021). Cdc42 and its BORG2 and BORG3 Effectors Control the Subcellular Localization of Septins between Actin Stress Fibers and Microtubules. *Curr. Biol.* 31 (18), 4088–4103. e5. doi:10.1016/j.cub.2021.07.004

Sandrock, K., Bartsch, I., Bläser, S., Busse, A., Busse, E., and Zieger, B. (2011). Characterization of Human Septin Interactions. *BiolChem* 392 (8-9), 751–761. doi:10.1515/BC.2011.081

Sheffield, P. J., Oliver, C. J., Kremer, B. E., Sheng, S., Shao, Z., and Macara, I. G. (2003). Borg/septin Interactions and the Assembly of Mammalian Septin Heterodimers, Trimers, and Filaments. *J. Biol. Chem.* 278 (5), 3483–3488. doi:10.1074/jbc.M209701200

Sirajuddin, M., Farkasovsky, M., Hauer, F., Kühlmann, D., Macara, I. G., Weyand, M., et al. (2007). Structural Insight into Filament Formation by Mammalian Septins. *Nature* 449 (7160), 311–315. nature06052 [pii]. doi:10.1038/nature06052

Thiele, T., Steil, L., Gebhard, S., Scharf, C., Hammer, E., Brigulla, M., et al. (2007). Profiling of Alterations in Platelet Proteins during Storage of Platelet Concentrates. *Transfusion* 47 (7), 1221–1233. doi:10.1111/j.1537-2995.2007.01255.x

Valadares, N. F., d' Muniz Pereira, H., Ulian Araujo, A. P., and Garratt, R. C. (2017). Septin Structure and Filament Assembly. *Biophys. Rev.* 9 (5), 481–500. doi:10.1007/s12551-017-0320-4

White, J. G., and Burris, S. M. (1984). Morphometry of Platelet Internal Contraction. *Am. J. Pathol.* 115 (3), 412–417.

Yagi, M., Zieger, B., Roth, G. J., and Ware, J. (1998). Structure and Expression of the Human Septin Gene HCDCREL-1. *Gene* 212 (2), 229–236. doi:10.1016/s0378-1119(98)00146-2

Zhang, J., Kong, C., Xie, H., McPherson, P. S., Grinstein, S., and Trimble, W. S. (1999). Phosphatidylinositol Polyphosphate Binding to the Mammalian Septin H5 Is Modulated by GTP. *Curr. Biol.* 9 (24), 1458–1467. doi:10.1016/s0960-9822(00)80115-3

Zhang, N., Zhang, Y., Wu, B., You, S., and Sun, Y. (2020). Role of WW Domain E3 Ubiquitin Protein Ligase 2 in Modulating Ubiquitination and Degradation of Septin4 in Oxidative Stress Endothelial Injury. *Redox Biol.* 30, 101419. doi:10.1016/j.redox.2019.101419

Zhang, N., Zhang, Y., Zhao, S., and Sun, Y. (2018). Septin4 as a Novel Binding Partner of PARP1 Contributes to Oxidative Stress Induced Human Umbilical Vein Endothelial Cells Injure. *Biochem. biophysical Res. Commun.* 496 (2), 621–627. doi:10.1016/j.bbrc.2018.01.105

Zieger, B. B., Tran, I., Hainmann, A., Wunderle, J., Zgaga-Griesz, A., Blaser, S., et al. (2000). Characterization and Expression Analysis of Two Human Septin Genes, PNUTL1 and PNUTL2. *Gene* 261 (2), 197–203. S0378111900005278 [pii]. doi:10.1016/s0378-1119(00)00527-8

Conflict of Interest: The authors declare that the research was conducted in the absence of any commercial or financial relationships that could be construed as a potential conflict of interest.

Publisher's Note: All claims expressed in this article are solely those of the authors and do not necessarily represent those of their affiliated organizations, or those of the publisher, the editors and the reviewers. Any product that may be evaluated in this article, or claim that may be made by its manufacturer, is not guaranteed or endorsed by the publisher.

frontiers in Cell and Developmental Biology

REVIEW
published: 19 November 2021
doi: 10.3389/fcell.2021.765085

The Structural Biology of Septins and Their Filaments: An Update

*Italo A. Cavini[1], Diego A. Leonardo[1], Higor V. D. Rosa[1], Danielle K. S. V. Castro[1,2], Humberto D'Muniz Pereira[1], Napoleão F. Valadares[3], Ana P. U. Araujo[1] and Richard C. Garratt[1]**

[1]São Carlos Institute of Physics, University of São Paulo, São Carlos, Brazil, [2]São Carlos Institute of Chemistry, University of São Paulo, São Carlos, Brazil, [3]Department of Cellular Biology, University of Brasília, Brasília, Brazil

In order to fully understand any complex biochemical system from a mechanistic point of view, it is necessary to have access to the three-dimensional structures of the molecular components involved. Septins and their oligomers, filaments and higher-order complexes are no exception. Indeed, the spontaneous recruitment of different septin monomers to specific positions along a filament represents a fascinating example of subtle molecular recognition. Over the last few years, the amount of structural information available about these important cytoskeletal proteins has increased dramatically. This has allowed for a more detailed description of their individual domains and the different interfaces formed between them, which are the basis for stabilizing higher-order structures such as hexamers, octamers and fully formed filaments. The flexibility of these structures and the plasticity of the individual interfaces have also begun to be understood. Furthermore, recently, light has been shed on how filaments may bundle into higher-order structures by the formation of antiparallel coiled coils involving the C-terminal domains. Nevertheless, even with these advances, there is still some way to go before we fully understand how the structure and dynamics of septin assemblies are related to their physiological roles, including their interactions with biological membranes and other cytoskeletal components. In this review, we aim to bring together the various strands of structural evidence currently available into a more coherent picture. Although it would be an exaggeration to say that this is complete, recent progress seems to suggest that headway is being made in that direction.

Keywords: septin, structural biology, cytoskeletal protein, protein filament, hetero-oligomeric complex, GTP-binding domain, coiled coil

OPEN ACCESS

Edited by:
Matthias Gaestel,
Hannover Medical School, Germany

Reviewed by:
Helge Ewers,
Freie Universität Berlin, Germany
Thomas Gronemeyer,
University of Ulm, Germany

****Correspondence:***
Richard C. Garratt
richard@ifsc.usp.br

Specialty section:
This article was submitted to Signaling, a section of the journal Frontiers in Cell and Developmental Biology

Received: *26 August 2021*
Accepted: *27 October 2021*
Published: *19 November 2021*

Citation:
Cavini IA, Leonardo DA, Rosa HVD, Castro DKSV, D'Muniz Pereira H, Valadares NF, Araujo APU and Garratt RC (2021) The Structural Biology of Septins and Their Filaments: An Update. Front. Cell Dev. Biol. 9:765085. doi: 10.3389/fcell.2021.765085

1 INTRODUCTION

Since the first identification of septins in *Saccharomyces cerevisiae*, more than 50 years ago by Hartwell (Hartwell, 1971), studies regarding the role they play in the cell have contributed to highlighting their fascinating properties. The initial studies in yeast cells showed that septins appeared to be membrane associated and formed a collar at the budding neck, important for recruiting proteins for cell division (Byers and Goetsch, 1976; Longtine et al., 2000; Finnigan et al., 2016; Tamborrini et al., 2018). Nowadays, it is known that in animal cells, septins may be found at a variety of locations, depending on the type and stage of cell development and may also act to restrict the diffusion of membrane components and rigidify the cell cortex at specific sites (Barral et al., 2000; Spiliotis and Gladfelter, 2012; Palander et al., 2017; Spiliotis, 2018; Spiliotis and McMurray, 2020). It

is therefore not surprising that septins are involved in many important cellular processes, such as cytokinesis, phagocytosis, ciliogenesis, cytoskeletal dynamics during bacterial entrapment, barrier formation, cellular polarization and morphogenesis, besides several others that demand membrane remodeling and/or scaffolding capabilities (Longtine et al., 2000; Hu et al., 2010; Mostowy et al., 2010; Mostowy and Cossart, 2012; Ewers et al., 2014; Beber et al., 2019; Falk et al., 2019; Robertin and Mostowy, 2020; Szuba et al., 2021).

In order to remodel cell morphology, septins interact with other cytoskeletal elements, for example in the nucleation and branching of actin filaments (Hu et al., 2012; Mavrakis et al., 2014). However, although there are several reports in the literature of co-localization of septins with actin and microtubules, it is not yet fully understood how these interactions occur, whether they are direct or indirect and whether they depend on the polymerization of septins or not (Mavrakis et al., 2014; Spiliotis, 2018; Spiliotis and Nakos, 2021). A recent report assessing the self-oligomerization of budding yeast septins on biomimetic membranes showed that octamers (rather than full filaments) were able to reshape membranes (Vial et al., 2021).

As a cytoskeleton component, septins are proteins with the inherent ability to self-assemble into filaments (Byers and Goetsch, 1976; Field et al., 1996; Frazier et al., 1998; Sirajuddin et al., 2007), and subsequently into more sophisticated architectures, as reviewed by Marquardt et al. (2019). The molecular basis for this is still an outstanding research question. Of note is that many post-translational modifications such as phosphorylation, acetylation, ubiquitination and sumoylation have already been observed modulating septin filament dynamics (Johnson and Blobel, 1999; Takahashi et al., 1999; Zhang et al., 2000; Hernández-Rodríguez and Momany, 2012; Ribet et al., 2017). Additionally, septins bind (and often hydrolyse) GTP, justifying their inclusion as members of the diverse family of P-loop GTPases (Leipe et al., 2002; Weirich et al., 2008; Sirajuddin et al., 2009). At least in yeast, GTP hydrolysis appears to be involved in the assembly of specific heterocomplexes (Weems and McMurray, 2017), and evidence also suggests that the nature of the bound nucleotide may play a role in membrane association by higher-order septin assemblies (Bertin et al., 2010; Bridges et al., 2014). However, tracing a correspondence between yeast and mammalian septins is not trivial and hampered by the significant phylogenetic differences between the heterocomplexes observed in fungi and animals. Thus, the relationship between filament assembly and GTP hydrolysis requires further work in order to be fully understood.

Septins are ubiquitous in opisthokonts, but orthologous septin families are also present in a broader range of other eukaryotes (Nishihama et al., 2011). The number of genes coding for septins in different organisms is quite variable. For example, there are species with only one or two genes, such as *Chlamydomonas* and *Caenorhabditis elegans*, respectively. Conversely, extensive gene amplification in vertebrates has led to 13 septins genes in humans and mice. In more extreme cases, gene duplication has resulted in further paralogues for many septins, culminating in a set of at least 17 in *Danio rerio,* for example (Willis et al., 2016). In view of such expansion, mammalian septins (Kinoshita, 2003), and later metazoans (Cao et al., 2007), have been classified into four groups, based on sequence similarities: SEPT2 group (SEPT1, SEPT2, SEPT4 and SEPT5), SEPT3 group (SEPT3, SEPT9 and SEPT12), SEPT6 group (SEPT6, SEPT8, SEPT10, SEPT11 and SEPT14) and SEPT7 group (SEPT7 alone) (Pan et al., 2007; Hilary Russell and Hall, 2011).

The dynamics of septin filament assembly changes radically during the cell cycle, albeit in a highly regulated way, both in time and space (Marquardt et al., 2020). Several binding partners could be key players in this process in which they may act by regulating septin remodeling (Nakahira et al., 2010; Sandrock et al., 2011). Some of the regulatory proteins of the cytoskeleton which show direct or indirect association with septins in different organisms include anillin (Kinoshita et al., 2002), CDC42 effector proteins (CDC42EP or Borg's) (Sheffield et al., 2003), end-binding protein 1 (EB1) (Nölke et al., 2016; Nakos et al., 2019a) along with many others. An exhaustive review of septin binding partners can be found in Neubauer and Zieger (2017).

Due to their wide-ranging roles in fundamental cellular processes, septin dysfunction has been implicated in a series of pathologies, including (but not limited to) male infertility, neurodegenerative diseases and cancer (Peterson and Petty, 2010; Angelis and Spiliotis, 2016; Palander et al., 2017). The regulation of septin expression is crucial for orchestrating cell homeostasis and thus it is not uncommon for pathologies, such as certain types of cancer, to be associated with changes in the levels of protein expression or mutations in a particular septin gene (Angelis and Spiliotis, 2016). The SEPT9_i1 isoform, for instance, was found to be overexpressed in breast tumors and linked to many other types of cancer (Gonzalez et al., 2009). Additionally, several neuropathies, such as Parkinson's and Alzheimer's diseases, have also been associated with septin accumulation (Kinoshita et al., 1998; Ageta-Ishihara et al., 2013; Tokhtaeva et al., 2015) and biophysical studies have demonstrated that *in vitro* individual septin subunits are unstable and tend to aggregate into amyloid-like structures (Garcia et al., 2007; Pissuti Damalio et al., 2012; Kumagai et al., 2019). This seems to imply that, under physiological conditions, heterocomplexes would be expected to be the predominant intracellular species, underlining their natural tendency to self-organize.

Although more than 50 years have passed since the discovery of septins, much remains to be learned about the potential roles of monomers, oligomers, filaments and higher-order structures. Taken together, data from structural studies of septins have brought important contributions to clarify these issues. In this review, it is not our intention to overload the reader with excessive structural detail. Instead, we aim to collate the major structural discoveries described over recent years, bring them together into a single document and relate them, where possible, to septin function. In so doing, we hope to stimulate the appearance of new hypotheses which will throw light on structure-function relationships at all levels of septin organization.

2 THE SEPTIN DOMAIN ARCHITECTURE

Septins belong to the family of small GTPases and are characterized by possessing a GTP-binding (G-) domain. This

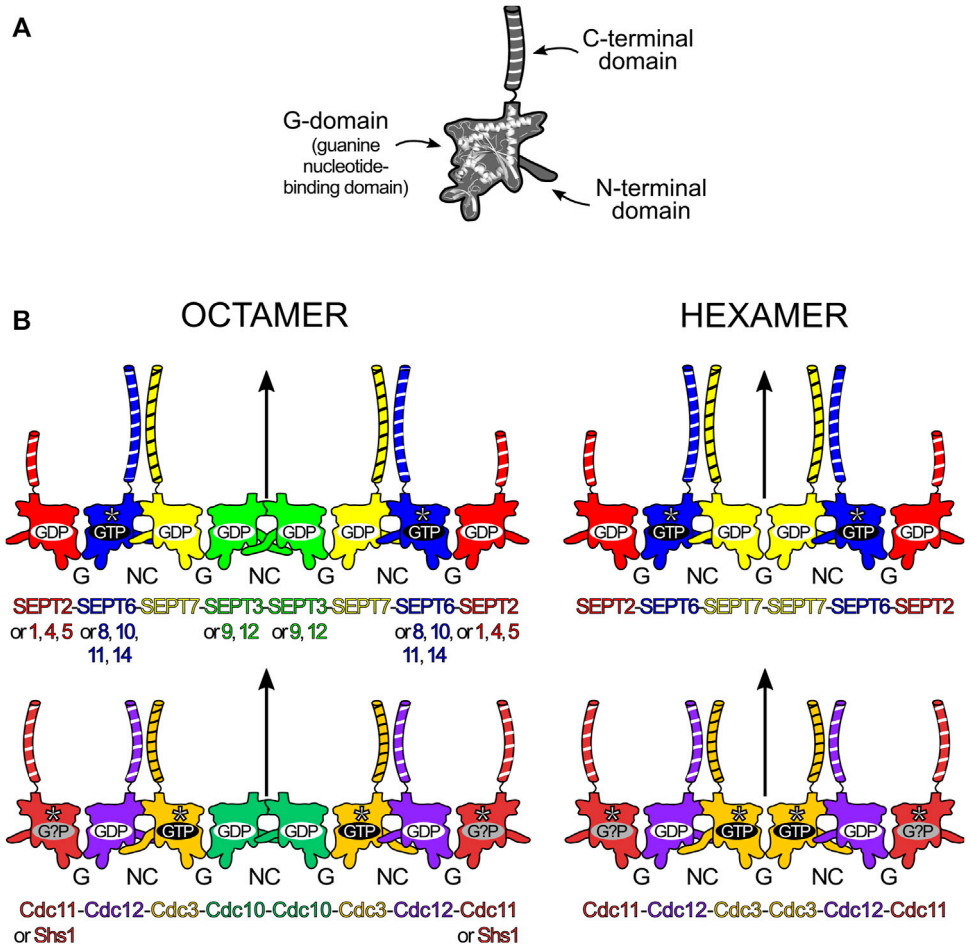

FIGURE 1 | Structural elements and core particle composition of septin filaments. **(A)** The septin structure is divided into three main domains: the N-terminal domain, the guanine nucleotide-binding domain (or G-domain) and the C-terminal domain (depicted with black and white stripes). **(B)** Octameric **(left)** and hexameric **(right)** core particles in human **(top)** and baker's yeast (*Saccharomyces cerevisiae*, **bottom**). In human septins, replacements according to "Kinoshita's rule" are depicted on the octamer. Straight arrows represent the twofold rotational symmetry (diad) axis at the center of the core particle. The yeast hexameric oligomer presented is that formed in the absence of Cdc10 (Cdc10-less oligomer). SEPT6-group members (blue), Cdc3 and Cdc11 are catalytically inactive and do not hydrolyse GTP (asterisks). Cdc11 seems to bind only cytosolic GDP (although speculatively) and Shs1 can also cap octamers, replacing Cdc11. The long N-domains in SEPT3 and Cdc3 are also represented.

was identified in the first amino acid sequences of septins by the presence of the P-loop motif, characteristic of GTP/ATP binding proteins (Longtine et al., 1996). The GTPase activity itself was later demonstrated by *in vitro* assays (Field et al., 1996). Different from other small GTPases, septins possess variable N- and C-terminal extensions or domains (or simply N- and C-domains) (**Figure 1A**; Field and Kellogg, 1999). Although there is no exact definition (in terms of residue position) for the limits of each domain, the overall consensus is to accept that the N-domain lies upstream of the first β-strand of the characteristic G-domain fold, prior to the P-loop, and the C-domain lies downstream to the final α-helix (α6).

The N-domain is highly variable in both length and amino acid sequence and is predominantly unstructured, being classified as an IUD (intrinsically unstructured domain) (Garcia et al., 2006; Pan et al., 2007). At its C-terminus, the N-domain has a region which forms an α-helix, dubbed α0, which includes a polybasic sequence (PB1) associated with membrane phospholipid interaction (Zhang et al., 1999; Bertin et al., 2010). The G-domain is highly conserved and has all the necessary motifs for binding GTP. Among the motifs shared with small GTPases are the P-loop or Walker A box (Walker et al., 1982) (also called G1) which oversees coordinating the phosphate moieties of the nucleotide, the switches I and II (G2 and G3 respectively) which are related to the hydrolytic mechanism itself and the G4 motif that confers specificity for GTP over other nucleotide triphosphates (Pan et al., 2007). Four septin-specific motifs have been identified in the G-domain (Sep1-4) as well as six specific residues which are conserved in 86–94% of all septin sequences (Pan et al., 2007). The G-domain terminates in a characteristic sequence known as the septin unique element (SUE), important for filament formation (Versele et al., 2004). The C-domain is variable but typically includes a region compatible with the formation of coiled coils

(Versele et al., 2004; Pan et al., 2007), although this is absent from some septins, including the SEPT3 group in humans and Cdc10 in yeast.

3 THE SEPTIN HETERO-OLIGOMER: THE BUILDING BLOCK FOR POLYMERIZATION

All of the many important functions that septins perform in the cell are related to their ability to assemble into highly organized filaments. Although filaments can subsequently generate many kinds of higher-order structures (bundles, rings, gauzes, etc.), all are comprised of filaments, which are built by end-to-end association of core particles (also known as protofilaments or simply oligomers). A core particle is a nonpolar, linear hetero-oligomeric complex of septin subunits, interacting side-by-side, like beads on a string (**Figure 1B**). Septins use different domains for hetero-oligomerization: with each monomer interacting with its neighbors by alternate interfaces, named NC (from the N- and C-terminal domains) and G (from the G-domain) (**Figure 1B**). Each domain and interface will be discussed in further detail later in this review.

In mammals, both *in vitro* and *in vivo*, septins from the different groups assemble to form the core particles. These are symmetric and have 2*n* subunits forming a palindromic arrangement, with *n* being the number of different septins in its composition. This results in a diad axis (C_2) at its centre, lying perpendicular to the main axis of the oligomer (**Figure 1B**). A septin filament is then likely assembled *in vivo* by the end-to-end annealing/collision of these core particles on the plasma membrane (Bridges et al., 2014). The core particle is, therefore, the building block of the filament and is usually defined as the oligomer which persists in high ionic strength solution *in vitro*, as several studies have shown how salt concentration modulates filament polymerization (Frazier et al., 1998; Versele et al., 2004; Bertin et al., 2008).

The number of septin monomers in the core particle can be variable and is species-dependent. For example, *C. elegans* has only two septins (Unc-59 and Unc-61) which form tetramers and polymerize to play roles in cytokinesis, migration and cell polarity (Nguyen et al., 2000; John et al., 2007). In *S. cerevisiae*, baker's yeast, four septins (Cdc3, Cdc10, Cdc11/Shs1 and Cdc12) generate octamers (Bertin et al., 2008; Garcia et al., 2011). In mammalian cells, septins from three or four different groups can be incorporated into the core particle, leading to the formation of hetero-oligomeric hexamers or octamers, respectively (Kim et al., 2011; Sellin et al., 2011). A noteworthy feature, usually referred to as "Kinoshita's rule" (Valadares et al., 2017; Spiliotis and McMurray, 2020), is that within the core particle, each septin is predicted to be interchangeable with another from the same group, thereby generating diversity (Kinoshita, 2003). On the other hand, as far as is known, the position of each septin group within the particle is fixed (Mendonça et al., 2019). Kinoshita's rule predicts 20 and 60 different combinations for hexamers and octamers respectively. How many of these are physiologically relevant and how their properties and functions may vary represent important outstanding questions.

In humans, the difference between the hexamer and the octamer is the incorporation of a SEPT3-group member in the latter which is absent from the former (Füchtbauer et al., 2011; Kim et al., 2011; Sellin et al., 2011; Sellin et al., 2014; Abbey et al., 2016). For many years, the subunit order of the human hexamer (and therefore that implied for the octamer) was erroneously considered to be SEPT7-6-2-2-6-7. New studies have shown the correct order to be SEPT2-6-7-7-6-2 (Mendonça et al., 2019; Mendonça et al., 2021) or SEPT2-6-7-3-3-7-6-2 in the case of octamers (**Figure 1B**; DeRose et al., 2020; Soroor et al., 2021; Iv et al., 2021).

Recent publications from *in vitro* experiments using mammalian septins bring fresh data to support the idea of hexamers and octamers coexisting within a single filament (DeRose et al., 2020; Soroor et al., 2021). This appears completely plausible in the light of the corrected subunit order since both hexamers and octamers have an exposed SEPT2 NC-interface at their termini (DeRose et al., 2020; Soroor et al., 2021), raising the possibility of a wide range of filaments differing in their hexamer-to-octamer ratio. There is also evidence pointing towards specific cellular functions that only arrangements including SEPT3-group members could perform (Estey et al., 2010; Bai et al., 2013; Kuo et al., 2015; Karasmanis et al., 2018).

In mitotic yeast cells, the octameric core particle is Cdc11-12-3-10-10-3-12-11 (**Figure 1B**; Versele et al., 2004; Bertin et al., 2008). Shs1, a non-essential septin in *S. cerevisiae*, can substitute for Cdc11, usually giving rise to ring-like arrangements (Garcia et al., 2011). Octamers polymerize through the NC-interface of Cdc11 (or Shs1), matching that which occurs in human septins; but in *C. elegans*, the Unc septin oligomers (Unc-59-61-61-59) seem to polymerize through an exposed G-interface (John et al., 2007). Yeast septins can also form hexamers when specific subunits are absent (Cdc10-less oligomers, Cdc11-12-3-3-12-11 and Cdc11/Shs1-less oligomers, Cdc12-3-10-10-3-12), but these are unable to form long filaments (Frazier et al., 1998; Versele et al., 2004; McMurray et al., 2011; Johnson et al., 2020). Albeit considered rare in fungi, naturally-occurring septin hexamers have been found in *Aspergillus nidulans* (oligomers lacking AspD, a Cdc10 homologue), where they coexisted with octamers (Hernández-Rodríguez et al., 2014).

The GTP binding and hydrolytic ability of each septin are likely related to the order and overall composition of the assembly (Sirajuddin et al., 2009; Weems and McMurray, 2017; Abbey et al., 2019). Some septins display no (or very little) GTPase activity as they lack the catalytic threonine from the G2 motif in switch I. This is the case for all SEPT6-group septins (Sirajuddin et al., 2007; Zent and Wittinghofer, 2014) and both Cdc3 and Cdc11 in yeast (Versele and Thorner, 2004). It is intriguing, however, that the non-catalytic septins in mammals and yeast do not map to equivalent positions within the core particles (**Figure 1B**). Furthermore, in yeast, one of the catalytically inactive subunits (Cdc3) is bound to GTP, as anticipated,

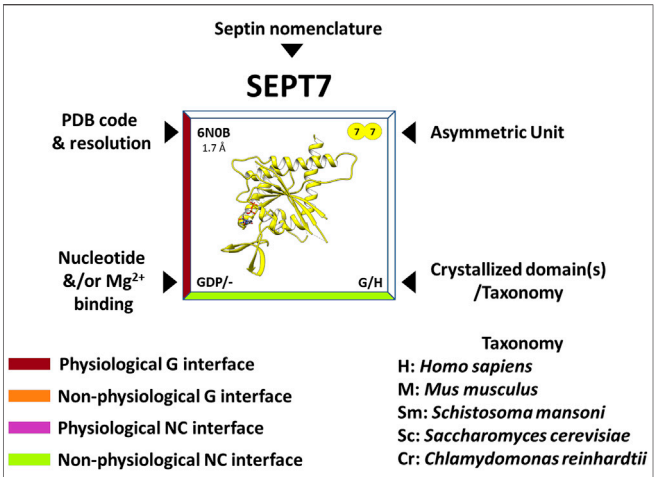

FIGURE 2 | Features of the "Septin Chart" (see complete figure in **Supplementary Figure S1**). The PDB code and resolution are shown in the upper left corner, the contents of the asymmetric unit in the upper right, the presence and nature of the bound nucleotide/magnesium in the lower left corner and finally, in the lower right, the purified and crystallized domain(s) as well as the acronym of the organism to which it belongs (e.g., H = *Homo sapiens*). In addition, the edges of the box surrounding the structure are color-coded and refer to the contact interfaces observed in the crystal: burgundy for a physiological G-interface, orange for a non-physiological G-interface, purple for a physiological NC-interface and lime for a non-physiological NC-interface. In some cases, in order to observe some of the interfaces, it is necessary to apply crystallographic symmetry operations to the asymmetric unit.

while the other (Cdc11) is hypothetically bound to GDP, presumably acquired from the cytosol (Farkasovsky et al., 2005; Weems and McMurray, 2017). However, another model claims that Cdc3 and Cdc11 are apoproteins even when incorporated into octamers (Baur et al., 2019). This conundrum is expected to be resolved once more structural information on yeast septins becomes available.

4 THE CURRENT COMPLETENESS OF THE STRUCTURAL INFORMATION AVAILABLE

Back in 2007, the first hetero-oligomeric septin structure was reported. This was the mammalian SEPT2-6-7 hexamer and was solved by X-ray diffraction at 4.0 Å resolution (Sirajuddin et al., 2007). For many years, this was the only structural model available for a hetero-oligomeric complex and due to its low resolution, many questions were left unanswered. Some of these were clarified by employing a "divide-and-conquer" strategy, first by the structure determination of single septin G-domains (Sirajuddin et al., 2007; Sirajuddin et al., 2009; Serrão et al., 2011; Zent et al., 2011; Macedo et al., 2013; Zeraik et al., 2014; Brognara et al., 2019) and later by better understanding the interfaces formed between them by solving the structures of both homo- and heterodimeric complexes (Brognara et al., 2019; Castro et al., 2020; Rosa et al., 2020). Recently, the original hexameric complex, SEPT2-6-7, has been solved by cryo-EM at 3.6 Å resolution, providing important additional information (Mendonça et al., 2021).

Nowadays, the richness of the structural information available (mainly from human septins) has made it possible to rationalize many functional aspects of the individual domains and the structural motifs they contain. At the time of writing, there are 32 septin structures available in the PDB, representing different domains and oligomeric states. In the "Septin Chart" (**Supplementary Figure S1**), we present this structural diversity, in a format inspired by the periodic table, to facilitate access to basic structural information (the asymmetric unit, PDB code, resolution, bound nucleotides, etc.). As a representative example, **Figure 2** shows the septin structure with the highest resolution currently available (SEPT7, PDB:6N0B). Each cell in the table explicitly indicates if the interfaces observed in the crystal structure are expected to be physiological (based on the canonical model of **Figure 1B**) or non-physiological (*promiscuous*). The latter are frequently observed in crystal structures and raise the intriguing question of why they apparently do not form physiologically.

5 THE G-DOMAINS

In the following section, we describe the "anatomy" of the G-domain, and its structural components (motifs), principally those for which it has been possible to ascribe a specific function. **Figure 3** depicts their spatial disposition and also establishes the standard nomenclature employed for the elements of secondary structure which characterize the septin fold (Valadares et al., 2017). However, in this review, whilst we preserve the standard names of the six strands which comprise the main β-sheet (β1-β6), we propose that those of the three-stranded β-meander should be renamed βa, βb and βc, rather than β9, β10/7, and β8, for the sake of simplicity. Additionally, we make use of a new nomenclature to refer to particularly important positions/residues employing the following format: "residue(motif)". For example, Thr(Sw1) refers to the catalytic threonine from switch I. This nomenclature eliminates the need for quoting specific residue positions, which vary from septin to septin. The nomenclature can be extended to the use of "residue (motif/group)" in order to indicate a specific septin group. This is particularly useful when referring to the so called *characteristic* residues (amino acid residues present essentially in a unique septin group and absent from all others) (Rosa et al., 2020). The new labels can be readily converted to the numerical format by using **Supplementary Table S1** (human septins) and **Supplementary Table S2** (septins from other organisms).

The G-domain is the most highly conserved among septins and is also generally the longest, although the longest isoform of SEPT9 has an N-domain of comparable size. Its fold resembles that of Ras GTP-binding proteins (Pai et al., 1989; Pai et al., 1990), displaying a central six-stranded β-sheet enclosed by α-helices in an αβα sandwich. However, when compared to Ras, septins display three additional exclusive features that are linked to their functions (highlighted in red on **Figure 3B**).

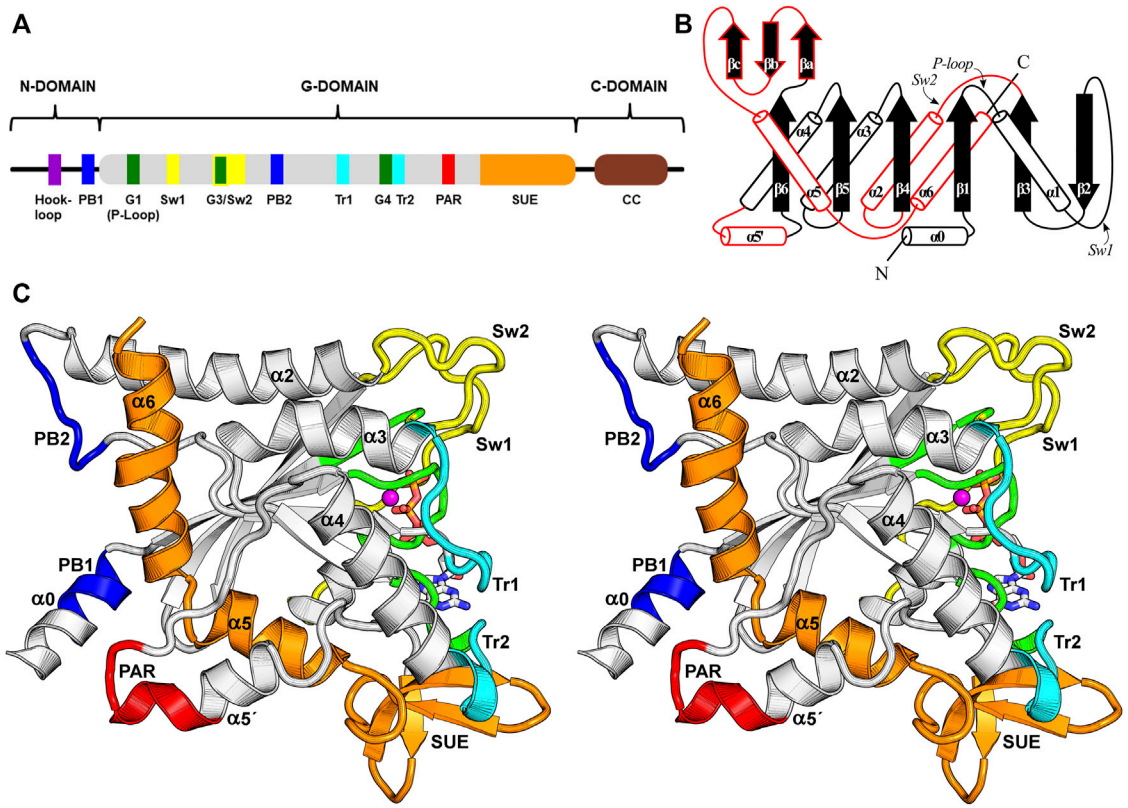

FIGURE 3 | The septin G-domain. **(A)** Schematic representation of the septin domains and their hallmark features. The N-domain presents variable length and encompasses the α0 helix, which contains the polybasic region 1 (PB1). The G-domain contains all the essential nucleotide-binding motifs (G1, G3, G4) and the switches important for catalysis. Other functional elements related to interface formation, such as a second polybasic region (PB2), a polyacidic region (PAR), the *trans*-loops 1 and 2 (Tr1 and Tr2) and the septin unique element (SUE) are also indicated. The C-domain often contains heptad repeats that form coiled coils (CC). **(B)** A schematic topology diagram for the septin G-domain fold. Three unique features observed in septins are highlighted in red. **(C)** Stereo representation of the G-domain highlighting some of its features employing the same color code used in panel **(A)**. Several of these features and secondary structure elements are labeled. The PB1, PB2 and PAR are close to the NC-interface, while the switch I (Sw1), switch II (Sw2), Tr1 and Tr2 participate in the G-interface. The SUE is an exclusive feature of septins and participates in both interfaces. The Mg^{2+} ion is coloured in magenta.

The first septin exclusive feature encompasses the longer switch II region (which participates in G-interface dimerization, **Figure 4**), an elongated α2 helix spanning the G- and NC-interfaces, and a lengthy loop containing the second polybasic region (PB2) that plays a critical role at the NC-interface (see **Section 9**). This long loop connects α2 to β4 and contains part of the highly conserved septin-specific motifs, Sep1 (ExxxxR) and Sep2 (DxRV/IHxxxY/FFI/LxP) (Pan et al., 2007). The loop runs underneath α2, preventing it from making direct contact with the underlying β-sheet and giving it structural autonomy (Castro et al., 2020). In total, this first feature adds 28 residues to human septins when compared to the equivalent region in H-Ras p21 (Pai et al., 1989; Pai et al., 1990).

A second feature unique to septins is an extended loop followed by an additional helix, termed α5′. These elements connect the α4 helix to the β6 strand, and correspond to at least 20 additional residues when compared to Ras. This region, and markedly the α5′ helix, displays low sequence conservation, except for a polyacidic region (PAR) located at the end of the loop and the beginning of α5′. The PAR participates in the NC-interface as a multipurpose element: in some structures it is observed interacting with the PB1 of the α0 helix (**Figure 3C**), and in others, it interacts with the PB2 that succeeds the α2 helix (see **Section 9** and **Section 10.1**).

The final distinct feature is the septin unique element (SUE) (Versele et al., 2004), which also spans from the G-to the NC-interface and enables filament formation. The SUE is roughly 60 residues in length and may be divided into two portions. The first half comprises three small β-strands that form a very twisted β-meander (βa-βc). This region is an integral part of the G-interface, contacts the nucleotide and has a significant role in G-interface dimerization. A single mutation T282Y in the SEPT3 β-meander favors the formation of homodimeric G-interfaces in solution, in contrast to monomers formed by the wild type (Macedo et al., 2013). This mutation was also necessary to stabilize the SEPT7-SEPT3 heterodimeric complex for crystallographic studies (Rosa et al., 2020). The second part of the SUE begins with two consecutive turns formed mostly by conserved residues, and continues through helices α5 and α6, the latter being the second longest helix in the G-domain, forming

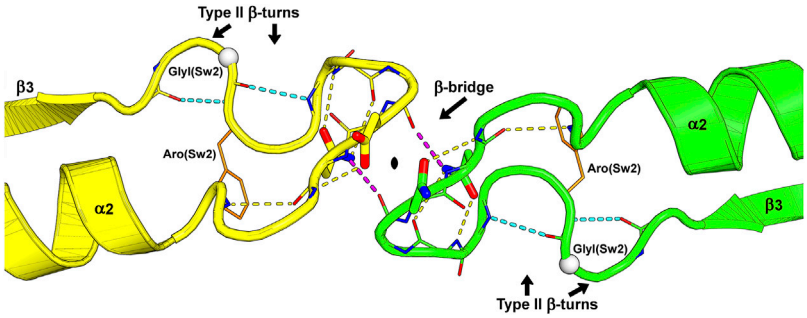

FIGURE 4 | The switch II region at the G-interface of the SEPT7-SEPT3 heterodimer (PDB:6UQQ). An essentially identical arrangement is observed at all physiological G-interfaces. The wide-type β-bridge, which lies on the pseudo-twofold symmetry axis relating the two monomers, is labeled, and its two hydrogen bonds are colored in purple. Over the β-bridge, an aspartic acid in SEPT7 (yellow) and an asparagine in SEPT3 (green), i.e., the positions Asx(Sw2), are represented as sticks and positioned on opposite sides of the symmetry axis (black lozenge at the center). Under the β-bridge, each subunit presents an asparagine residue, Asn(Sw2), whose side chain is represented as sticks, forming hydrogen bonds to both the main chain nitrogen and oxygen atoms of the residue three positions prior in the sequence. In each subunit, two consecutive type II β-turns forming an "S" shape are labeled, and their hydrogen bonds are colored in cyan. Some side chains and main chain atoms were removed for clarity. Aro(Sw2) is indicated as it may play a role in communication between adjacent interfaces and Glyl(Sw2) is represented as a white sphere.

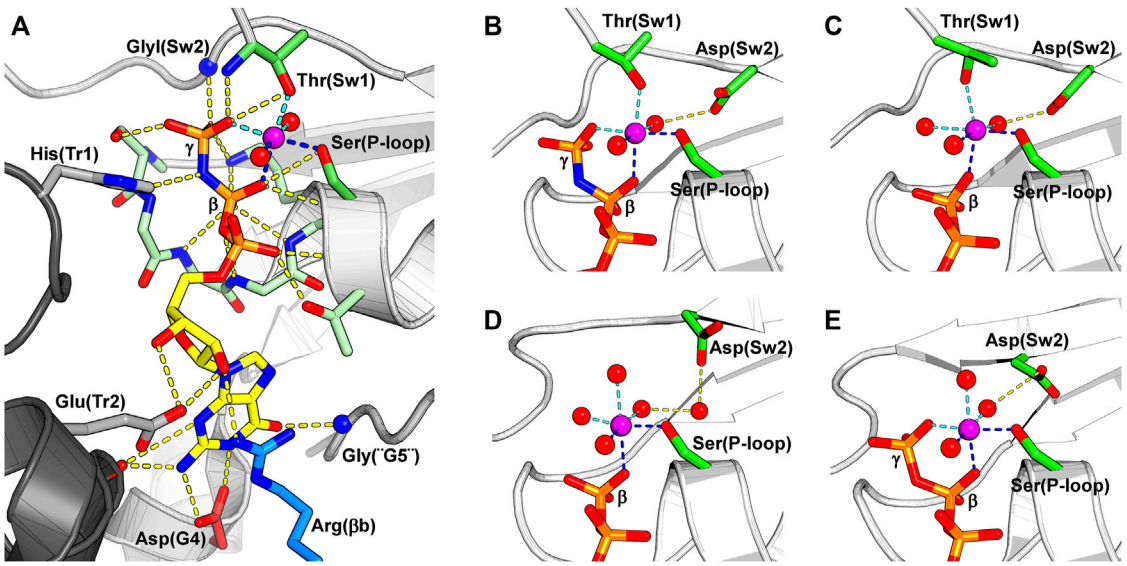

FIGURE 5 | The nucleotide-binding pocket and the different modes of magnesium coordination. The β-phosphate, Ser(P-loop) and a water molecule participate in all depicted Mg^{2+} coordination schemes, and their coordination to the Mg^{2+} is shown by dark blue dotted lines. The magnesium ion is colored in purple. **(A)** A GTP analogue (GMPPNP) bound to SEPT12 (PDB:6MQ9). The nucleotide and the residues interacting with it are represented as sticks. Key residues from the septin versions of the five classical nucleotide-binding elements found in small GTPases are labeled: G1 is represented by Ser(P-loop), G2 by Thr(Sw1), G3 by Glyl(Sw2), G4 by Asp(G4) and G5 by Gly("G5"). Often septins are said not to possess G2 and G5, but here we describe their remnants explicitly as such. The conserved arginine from the SUE, Arg(βb), is colored in blue. On the left side of the figure, two residues from the other subunit of the G-interface (dark grey) are represented; a histidine from the *trans*-loop 1, His(Tr1), that binds to the β-phosphate, and a glutamate from the *trans*-loop 2, Glu(Tr2), that forms a hydrogen bond to the ribose ring. **(B)** Magnesium coordination in a catalytically active septin bound to the non-hydrolysable GTP analogue, GMPPNP (PDB:6MQ9). **(C)** A *tightly* bound Mg^{2+} in a catalytically active septin bound to GDP. Thr(Sw1) remains as a ligand in this case, and Asp(Sw2) continues to coordinate the metal via a water molecule (PDB:6MQK). **(D)** In a *weakly* bound Mg^{2+} ion, also in the presence of GDP, Thr(Sw1) has now been replaced by a water molecule, and the participation of Asp(Sw2) is mediated by two waters rather than one (PDB:6N12). **(E)** Magnesium coordination in a non-catalytic septin bound to GTP. The Mg^{2+} coordination sphere is formed by the β- and γ- phosphates, Ser(P-loop) and three water molecules, one of which is held by the side chain of Asp(Sw2) (PDB:6UPQ).

part of the NC-interface. Helices α5 and α6 together form an elbow-like structure which has recently been shown to be important for stabilizing helix α0 from the neighboring subunit within the interface (see **Section 9**). The SUE is, therefore, an integral part of both interfaces and explains why septins, unlike other small GTPases, are able to polymerize.

5.1 The Fundamental Elements of the G-Domain

5.1.1 Switch I

The switch I is a long solvent-exposed loop connecting helix α1 to strand β2. It inherits its name from the small GTPases, in which switch I is part of the universal loaded spring mechanism that promotes GTP hydrolysis conformation (Vetter and Wittinghofer, 2001). A threonine residue from switch I, Thr(Sw1), is essential for the hydrolytic mechanism (Sirajuddin et al., 2009), and its main chain nitrogen atom is observed interacting with the γ-phosphate in structures of catalytic septins bound to GTP analogues, while its side chain coordinates the Mg^{2+} ion and its main chain carbonyl, the catalytic water (**Figure 5A**).

Switch I is arguably the least conserved region of the G-domain in human septins. The region is longer than in H-Ras, and is incomplete in many crystal structures. Its conformation depends on the septin group, the bound nucleotide, crystal packing and whether it forms a G-interface with a physiological partner or not. This conformational flexibility is physiologically relevant because in septins switch I has an additional role in the formation of the G-interface and may hold the key to selecting the correct G-interface partner (see **Section 6.2**) (Rosa et al., 2020).

5.1.2 Switch II

Switch II both participates in the hydrolytic mechanism and contributes to G-interface stability. It contains the G3 motif, an integral part of the universal switch mechanism. This conserved motif contains a glycine residue, GlyI(Sw2) in **Figure 5A**, that binds to the γ-phosphate and an aspartic acid residue, Asp(Sw2) in **Figures 5B–E**, that coordinates the Mg^{2+} ion via a water molecule. After hydrolysis, this region adopts a slightly different conformation, positioning GlyI(Sw2) at the centre of a planar S-shaped structure formed by two consecutive type II β-turns (**Figure 4**). Following GlyI(Sw2) is an aromatic residue, Aro(Sw2), that is able to adopt different rotamers and it has been suggested that this may play a role in communication between adjacent G- and NC-interfaces (see **Section 10.2**).

5.1.3 Helix α2

In septins, helix α2 is twice the size of its equivalent in small GTPases and extends from the G-to the NC-interface. It connects switch II at the G-interface to PB2 at the NC-interface, two regions that display a degree of conformational plasticity. These traits flag α2 as a candidate to act as a conduit for information transfer between the G and NC-interfaces (see **Section 10.2**).

5.1.4 The Polyacidic Region and Alpha Helix 5′

All septins present a polyacidic region (PAR) at the beginning of helix α5′ and the loop preceding it. The angle of helix α5′ in relation to the G-domain varies which may influence the position of the PAR with respect to the PB1 of helix α0 from the neighboring subunit when the NC-interface is in its canonical (open) conformation (see **Section 9** and **Section 10.1**). Indeed, the cryo-EM structure of the SEPT2/6/7 complex confirms a direct interaction between the PAR and PB1, when α0 is stored within the interface (**Figure 3C**).

5.1.5 The Septin Unique Element and Alpha Helix 6

The septin unique element (SUE) (Versele et al., 2004) is a continuous sequence which forms the C-terminal region of the G-domain and, as its name implies, is conserved, essential and exclusive to septins. It contributes to both interfaces as described above.

Helix α6 is the final element of secondary structure to form part of the G-domain and lies perpendicular to the main filament axis at the NC-interface. It also lies perpendicular to helix α2, and together these long helices stand out as a distinctive feature of the G-domain. A characteristic feature of α6 is a visible unwinding of the helix at its center, generating an α-aneurism (Keefe et al., 1993). The conserved nature of the aneurism and its conspicuous location at the NC-interface suggests that it may have a functional role. However, this has yet to be elucidated. Intriguingly, due to a residue deletion, the single septin from *Chlamydomonas reinhardtii* does not present the α-aneurism resulting in significant topographic alterations to the NC-interface which is not observed in the crystal structure thereby impeding the *in crystallo* formation of filaments (Pinto et al., 2017). It is, therefore, unclear if this single septin is able to form homofilaments *in vivo*.

Helix α6 presents two conserved charged residues, glutamic acid Glu(α6) and arginine Arg(α6), that take part in an extensive hydrogen-bonding network which forms the upper part of the NC-interface. The pattern of salt bridges depends on the conformation of the NC-interface (see **Section 9.1**).

5.2 The GTP-Binding Site and the Magnesium Coordination States

5.2.1 Classic Nucleotide-Binding Motifs

All currently deposited structural data on septins (with the exception of Cdc11, PDB:5AR1) exhibit a bound guanine nucleotide as an integral part of the G-domain, where it participates in the G-interface. Small GTPases employ five classic motifs (G1-G5) in nucleotide binding, and septins use their versions of these motifs to maintain the nucleotide tightly bound and to perform catalysis.

The G1 motif presents the consensus GxxGxGKS/T and forms the P-loop. Several main chain nitrogen atoms of this motif interact with the β-phosphate, while the side chain of Ser(P-loop) coordinates the Mg^{2+} ion. This region is followed by a threonine residue in helix α1 that binds the α-phosphate. Switch I (Sw1) includes the septin version of the G2 motif, which contributes a threonine residue, Thr(Sw1), that binds both the γ-phosphate and the Mg^{2+} ion and is essential for catalysis (Sirajuddin et al., 2009). The G3 motif is part of switch II (Sw2) where, in catalytic septins, the glycine residue GlyI(Sw2) binds the γ-phosphate (**Figure 5A**). Moreover, this region bears an aspartic acid residue, Asp(Sw2), that binds and orients a water molecule to coordinate the Mg^{2+} ion (**Figures 5B–E**). Oddly, in catalytically inactive septins, Asp(Sw2) may be replaced by a serine, an asparagine or a glutamate, the latter being able to coordinate

the Mg^{2+} ion directly. In the G4 motif (A/GK/RAD in human septins), the lysine (or arginine) interacts with the ribose, while the aspartate (Asp(G4)) forms two hydrogen bonds to the guanine base. In septins, a single glycine, Gly("G5"), represents the remnants of the G5 motif. Finally, human septins boast a conserved arginine residue in the septin unique element, Arg(βb) in **Figure 5A**, that is part of the nucleotide-binding pocket.

In addition to the residues from the G-domain to which the nucleotide is bound, two residues from the neighboring subunit reach across the G-interface and assist in nucleotide binding: a histidine from the *trans*-loop 1 (His(Tr1)) interacts with the β-phosphate and a glutamate from the *trans*-loop 2 (Glu(Tr2)) forms a hydrogen bond to the ribose (**Figure 5A**). Exclusive to algal septins, an arginine residue from the Sep3 motif interacts directly with the γ-phosphate of the neighboring subunit, acting like a catalytic "arginine finger" and accelerating GTP hydrolysis (Pinto et al., 2017).

5.2.2 Magnesium Coordination States

Several coordination states for Mg^{2+} have been observed in different crystal structures (**Figures 5B–E**), and in approximately half the cases, the Mg^{2+} ion is either absent or cannot be modeled. A common feature of all such coordination schemes is the participation of Ser(P-loop), the β-phosphate and a water molecule.

In catalytically active septins, prior to catalysis, the Mg^{2+} ion is hexa-coordinated by a water molecule, Ser(P-loop), Thr(Sw1), the β- and γ- phosphates and Asp(Sw2) via a second water. After catalysis, however, GDP-bound septins display two possible magnesium coordination schemes. The first presents a *tightly* bound Mg^{2+}, quite similar to that observed for GTP, but with a third water molecule replacing the γ-phosphate (**Figure 5C**). The second possibility is a *weakly* bound Mg^{2+} ion where a fourth water molecule replaces Thr(Sw1) and there are now two intervening waters between Asp(Sw2) and the metal. The transition from *tight* to *weak* binding may represent snapshots of different steps in the process of metal release upon catalysis.

In catalytic septins, switch II and particularly switch I are observed in very different conformations depending on the nucleotide bound, indicating that catalysis triggers major conformational changes at the G-interface. It would seem that the Mg^{2+} ion and its ligands are essential components of this mechanism. However, the full details of the role which Mg^{2+} plays during GTP binding and hydrolysis in the case of septins has yet to be fully elucidated.

6 THE G-INTERFACE

6.1 G-Interface Components and the Basis for Kinoshita's Rule

With the first description of a septin structure (Sirajuddin et al., 2007), the critical role of the G-interface for the molecular assembly of the core particle became evident. As a result of the dozens of structures determined subsequently, the nature of the interactions involved at the interface has become clear and the exquisite manner by which stability, specificity and exchangeability arise have begun to be understood (Brognara et al., 2019; Rosa et al., 2020). In general, the G-interface is extremely well conserved in different structures, preserving almost perfectly the relative positions of the two monomers involved. Furthermore, no crystal structure presenting an intact G-interface has been observed in the absence of bound nucleotide. This suggests the ligand to be an integral component of the interface and/or that substrate hydrolysis through a GAP-like mechanism depends on dimer formation (Gasper et al., 2009; Sirajuddin et al., 2009; Zent and Wittinghofer, 2014). This section will describe the surface regions on the monomers which participate in the G-interface, highlighting the structural differences between groups and specifying the details which contribute to correct filament assembly.

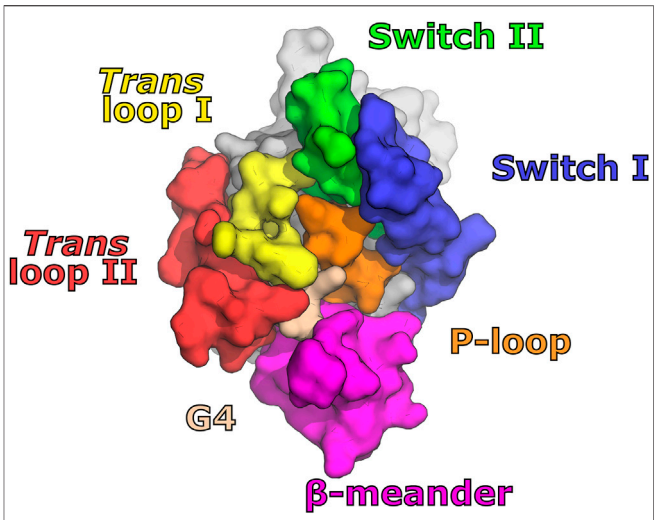

FIGURE 6 | Motifs interacting at septin G-interfaces. Seven main contact regions are indicated on the G-side of the monomer. They are distributed in a diamond-like shape with switch II at the top; switch I, *trans*-loops 1 and 2, the P-loop and G4 at the center; and the β-meander at the bottom.

The standard model for the human hexamer implies the existence of G-interfaces between SEPT2 and SEPT6 and between two copies of SEPT7 (**Figure 1B**). In the octamer, the latter is replaced by a SEPT7-SEPT3 interface. At these interfaces, up to seven contact regions within the G-domain of each monomer form a diamond-like shape (**Figure 6**). At the top of the diamond, the two switch II regions interact, as shown in **Figure 4**. The central region, where the contact surface is widest, involves Tr1, the P-loop and G4. This also includes the switch I region in the case of SEPT2-and SEPT6-group member interfaces. At the bottom, the β-meander participates in interactions with Tr2 of the corresponding partner. Even at *promiscuous* interfaces, many of these features are preserved, including those involved in nucleotide binding. Although some subtle variation has been observed within the interface core (e.g., mutation to Glu(P-loop) in the SEPT3 group and in *Drosophila* Pnut/SEPT7 or to the β-meander in the SEPT3 group), it is the

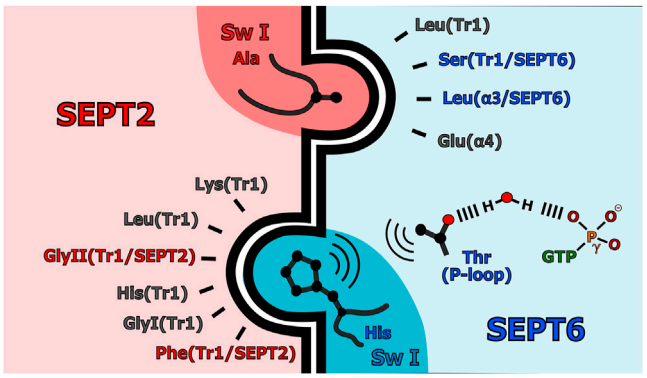

FIGURE 7 | Interaction specificities in the SEPT2-SEPT6 G-interface. Simplified scheme for the heterotypic interface highlighting the importance of residues coming from switch I on both sides of the interface. Group-specific (*characteristic*) residues are shown colored, in red for SEPT2 and in blue for SEPT6. The network of interactions leading from the interface to the γ-phosphate of the GTP is shown.

region at the rim of the interface, particularly switch I, which presents the greatest variability between septin groups (Rosa et al., 2020).

6.2 Switch I Determines the Selectivity at the G-Interface Formed Between Septins of the SEPT2 and SEPT6 Groups

How do the correct pairings of septins arise at the different G-interfaces of the core particle during spontaneous assembly? This is a question relating to the interactions involved in molecular recognition. Switch I makes a significant contribution to the contact area at the G-interface between septins of the SEPT2 and SEPT6 groups (but not those between SEPT7 and SEPT3) (Rosa et al., 2020). This raises the possibility that the selectivity that drives members of these two groups together may be related to selective interactions involving group-specific residues found within the switch I regions. Such interactions are shown in **Figure 7** and **Supplementary Figure S2**.

An interaction network involving group-specific (or *characteristic*) residues is observed between the Tr1 of SEPT2 and the P-loop/Switch I of SEPT6/8/11 (**Figure 7**). The hydroxyl of a *characteristic* threonine residue in the SEPT6 group, Thr(P-loop/SEPT6), interacts with the γ-phosphate of GTP via a water molecule, thereby orienting its methyl group towards His(Sw1/SEPT6). This allows the correct orientation of the imidazole ring of His(Sw1/SEPT6) to accept a hydrogen bond from the main chain of SEPT2. His(Sw1/SEPT6) fits snugly into a pocket formed by Tr1 of SEPT2, whose conformation is determined by the *characteristic* residues Phe(Tr1/SEPT2) and GlyII(Tr1/SEPT2). Compared with septins from other groups, the *trans*-loop 1 of SEPT2 adopts a more extended conformation (**Supplementary Figure S2A**; Rosa et al., 2020). Both the ordering of switch I in SEPT6/8/11 and the conformation of *trans*-loop 1 in SEPT2 are necessary for correct partner pairing at the interface. No other group combination would provide the appropriate structural features for the fit schematically represented in **Figure 7**. This can be verified by observing the disordered and/or incomplete switch I regions, present at *promiscuous* G-interfaces such as the homodimer of SEPT2, *Sm*SEPT10 and SEPT3 (Sirajuddin et al., 2007; Zent et al., 2011; Macedo et al., 2013; Zeraik et al., 2014).

The involvement of GTP in the interaction network (**Figure 7**) suggests a functional significance for the lack of catalytic activity in the SEPT6 group. The persisting γ-phosphate should be considered a characteristic feature of the SEPT6 group as it aids in correctly orienting Thr(P-loop/SEPT6) towards His(Sw1/SEPT6). In the remaining groups of septins, this threonine is replaced by a serine, incapable of forming the hydrophobic contact with His(Sw1/SEPT6).

On the other side of the G-interface, in the switch I region of SEPT2, a *characteristic* amino acid Ala(Sw1/SEPT2), fits into a cavity in SEPT6/8/11 (**Figure 7** and **Supplementary Figure S2B**). The presence of amino acids with longer side chains at this position in the SEPT3 group, or a proline in SEPT7 or even its absence altogether in the SEPT6 group (**Supplementary Table S1**) suggests that this interaction would only be viable in the case of the SEPT2 group (Rosa et al., 2020). Ala(Sw1/SEPT2) interacts via Van der Waals contacts with Ser(Tr1/SEPT6) which forms a hydrogen bond with the main chain of an aspartic acid in SEPT2. This interaction is only possible for the SEPT6 group where Ser(Tr1/SEPT6) is always either serine or threonine. This allows for the correct orientation of switch I of SEPT2, permitting Ala(Sw1/SEPT2) to fit into its complementary pocket in SEPT6.

In summary, the presence of *characteristic* residues converges on the correct structural organization of switch I and the *trans*-loop 1 of the SEPT6 and SEPT2 groups, favoring the formation of the specific G-interface. Since the interactions involved, by definition, can be generated by any member of the groups involved, this provides a molecular basis for the understanding of Kinoshita's rule (substitutability between members within a group). As a "side effect", we begin to understand the reason why the SEPT6 group lacks catalytic activity. By retaining the γ-phosphate, a network of interactions can form, guaranteeing the correct pairing of members of these two groups at the G-interface.

6.3 Switch II Interaction at Physiological G-Interfaces

The crystal structures of homodimers and heterodimers have made it possible to demonstrate that the complete ordering of switch II is related to the formation of physiological G-interfaces (Zent et al., 2011; Zeraik et al., 2014; Brognara et al., 2019; Castro et al., 2020; Rosa et al., 2020). The structure which results from the pairing of the two switch II regions is shown in **Figure 4**. In general, this pairing does not arise at *promiscuous* G-interfaces, which frequently appear in crystal structures of isolated G-domains of a single septin (**Supplementary Figure S3**).

By comparing the GTP- and GDP-bound forms of the *Schistosoma* septin, *Sm*SEPT10, a mechanism, controlled by

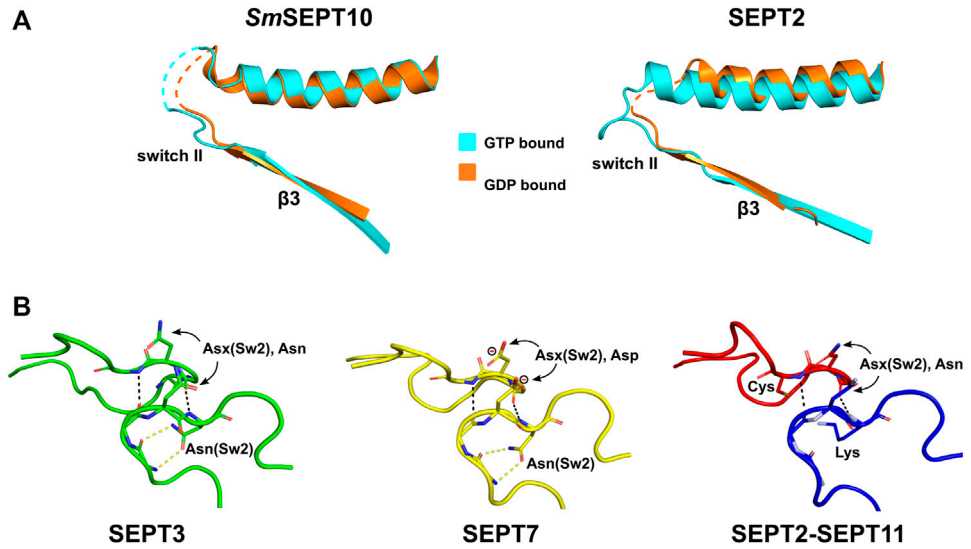

FIGURE 8 | Switch II diversity at the G-interface. **(A)** β-slippage of the β3-strand in *Sm*SEPT10 and SEPT2. After GTP hydrolysis, the β3-strand slides in the direction of the G-interface, which prevents the formation of the correct contacts between the two copies of switch II (the β-bridge). PDB:4KVA (left; GTP, cyan), PDB: 4KV9 (left; GDP, orange), PDB:3FTQ (right; GMPPNP, cyan), PDB:2QNR (right; GDP, orange). **(B)** The β-bridge (characterized by the hydrogen bonds shown as black dashed lines) in homotypic and heterotypic G-interfaces. Asx(Sw2) residues, conserved in septins, are paired across the interface. In SEPT7, this position is an aspartic acid (formal charge displayed). An asparagine residue, Asn(Sw2), conserved in the SEPT3 and SEPT7 groups, forms hydrogen bonds (yellow dashed lines) with the main chain, helping to stabilize the β-bridge. A lysine substitutes this aspargine in the SEPT6 group and cysteines appear in this position in SEPT1 and SEPT2, suggesting a new mechanism to stabilize the β-bridge in these cases. SEPT3, PDB:4Z54; SEPT7, PDB: 6N0B; SEPT2-11, PDB:6UPQ.

nucleotide hydrolysis, was described for β-strand slippage (Zeraik et al., 2014). When bound to GTP, the β3-strand is in the "non-slipped" state and switch II is partially ordered (forming the type II β-turns described in **Section 5.1.2**). However, in the GDP-bound state, β3 is slipped towards the G-interface by two residues causing a dramatic rearrangement of the hydrogen bonding within the sheet. As a consequence of slippage, switch II becomes disordered and the G-interface is partially destroyed (**Figure 8A**). This phenomenon was also described for SEPT2 (Valadares et al., 2017) and, in both septins, the homotypic G-interfaces are *promiscuous* (i.e., not predicted by the canonical model shown in **Figure 1B**). β-strand slippage was initially proposed as a mechanism for transmitting information from the G-interface to the NC-interface, forcing the α0 helix to change conformation (see **Section 9** and **Section 10.1**) (Valadares et al., 2017).

The accumulation of many high-resolution structures for known physiological G-interfaces, including SEPT2-SEPT6/8/11, SEPT7-SEPT3$_{T282Y}$ and SEPT7 alone (Brognara et al., 2019; Rosa et al., 2020), has forced this idea to be revised. In all these cases (as well as the homotypic interfaces formed by SEPT3-group members) the two switches are very well ordered (**Supplementary Figure S3**), forming a conserved wide-type β-bridge (**Figure 4**, **Figure 8B**) and the β3-strand remains unslipped. The available data suggests that the presence of the β-bridge is a consistent and necessary feature of a physiological G-interface and that slippage only occurs at *promiscuous* interfaces. Indeed, it has been suggested that slippage may be the result of "negative design" during evolution to disfavour *promiscuous* interfaces from forming *in vivo* (Brognara et al., 2019). In this sense, it is interesting that the SEPT3 group also presents a well ordered β-bridge and may be indicative of alternative subunit arrangements including homopolymers (Nakos et al., 2019b). On the other hand, the absence of β-strand slippage in septins of the SEPT3 group may instead be an artefact related to the presence of Mg^{2+} in the structure bound to GDP, which may aid in holding the strand in the non-slipped position (Castro et al., 2020).

The intermolecular β-bridge is stabilized by main chain hydrogen bonds, which place asparagine or aspartic acid residues (Asx(Sw2)) paired across the interface (**Figure 8B**). The main chain torsion angles observed for Asx(Sw2) are unusual and rarely adopted by other amino acids (Hovmöller et al., 2002), which suggests the β-bridge to be a unique structural motif in septins, differentiating them from other small GTPases. β-turns before and after the β-bridge aid in its correct orientation (Brognara et al., 2019; Rosa et al., 2020). SEPT3 and SEPT7 have an asparagine (Asn(Sw2)) immediately after Asx(Sw2), whose side chain forms hydrogen bonds in the homo- (SEPT3-3, SEPT7-7) and heterodimers (SEPT3-7), further stabilizing the structure (**Figure 8B**). Heterodimers of SEPT2 with SEPT6/8/11, on the other hand, present a cysteine (partially conserved for the SEPT2 group) or a lysine (conserved in the SEPT6 group) at this position (**Figure 8B**). This consequently eliminates the interactions made by the asparagines and suggests an alternative mechanism for stabilizing the structure in these cases. Rosa et al. (2020) have speculated that the side chains of the lysine and the cysteine, which face one another under the β-bridge, could potentially form a rare Lys-Cys covalent bond described for the first time only recently (Ruszkowski and Dauter,

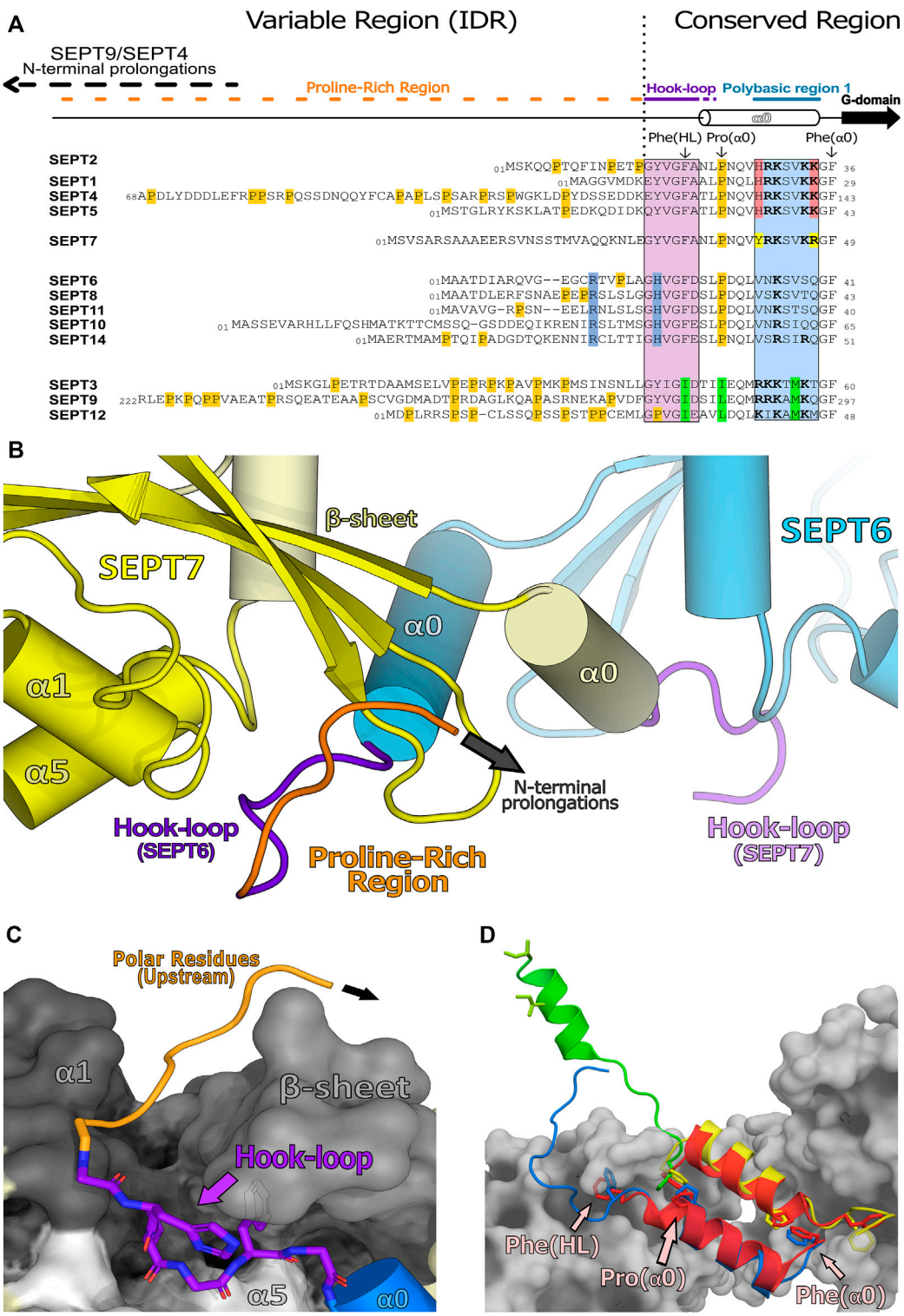

FIGURE 9 | Human septin N-domains and their structured regions. **(A)** Alignment of all human N-terminal sequences showing the unstructured region (variable region or intrinsically disordered region, IDR) and the structured region (conserved region). This alignment also highlights the conserved residues within a septin group (also known as *characteristic* residues, in their respective colors) as well as proline residues (in orange). **(B)** Domain-swapped "hook-loop" highlighting the unstructured proline region (orange) and the hook-loop (purple) (PDB:7M6J). **(C)** Elements of SEPT7 (in greyscale) which accommodate the hook-loop of SEPT6 into a cleft. Residues with small side chains from the "hook-loop" are important for these interactions. **(D)** Helix α0 and its orientations within available septin structures (SEPT3 in green, PDB:4Z54; SEPT6 in blue-SEPT7 in yellow, PDB:7M6J; SEPT2 in red, PDB:2QA5). Also highlighted, as sticks, are residues which are essential for the NC-interface and/or the conformation of α0 (Phe(HL), Phe(α0) and Pro(α0); indicated in only one chain for clarity). These phenylalanines act as anchors and are conserved in SEPT2, SEPT6 and SEPT7 groups but are mutated to isoleucines in the SEPT3 group which may be related to additional α0 mobility in the latter.

2016; Wang, 2019; Wensien et al., 2021). Further investigation of such a bond forming *in vivo* and its potential relevance in stabilizing septin core particles is clearly necessary. Particularly interesting is the fact that the cysteine residue is not conserved in all human SEPT2-group members (only in SEPT2 itself and SEPT1) and this may provide a means to fine-tune inter-subunit affinities even within the paradigm imposed by Kinoshita's rule.

7 THE N-TERMINAL DOMAINS

7.1 The Septin N-Terminal Domain and its Modular Features

The septin N-terminal domain is the least studied in terms of structure and the most variable region amongst all septins. This domain contains a structured α-helix (α0, preceding the G-domain), which often contains a polybasic basic region (PB1) believed to be crucial for membrane interaction (Zhang et al., 1999). However, the greater part of the septin N-domain, upstream to this helix, is intrinsically unstructured (Garcia et al., 2006). Some septins with long N-terminal prolongations (such as human SEPT4 and SEPT9) can be expressed as numerous alternatively spliced isoforms, giving rise to multiple possibilities and functional variation in the different tissues where they are present. Amongst mammalian septins, for example, SEPT9 possesses more than 30 different isoforms (Connolly et al., 2014; Zuvanov et al., 2019), and many functions have been shown to be isoform-specific (Estey et al., 2010; Connolly et al., 2011; Kim et al., 2011).

A description of the N-domain can be made with reference to the characteristics of the conserved regions observed in mammalian septin sequences and highlighted in the alignment given in **Figure 9A**. Conveniently, this can be divided into two modules. Firstly, the unstructured (variable) region (IDR), including the prolongations observed for some SEPT4 and SEPT9 isoforms, whose long N-termini may have analogues in other species (Cdc3 in yeast or Pnut in *Drosophila*), along with some modulatory motifs within the downstream proline-rich region. Secondly, the structured (conserved) region consists of two components: 1) a domain-swapped loop (the "hook-loop") important for NC-interface stabilization and 2) the α0 helix including PB1, the most conserved, structured and functionally characterized region of the N-domain.

7.2 The Extended SEPT9/SEPT4 N-Domains: Specificity for Protein-Protein Interactions

The N-domains observed in the longest isoforms of SEPT9 and SEPT4 possess specific motifs attributed to interacting with cytoskeletal proteins such as actin and microtubules (Bai et al., 2013; Smith et al., 2015; Verdier-Pinard et al., 2017). In particular, attempts have been made to divide the long domain found in SEPT9 into two distinct regions based on amino acid content. The first half is a basic domain containing a cytoskeletal binding region (CBR) involved in cytoskeletal protein recognition. The second half is more acidic and includes a proline-rich motif together with the structured (conserved) region (**Supplementary Figure S4**). The prolongations observed in these septins have also been shown to directly mediate interactions with proteins associated with other functions, such as vesicle trafficing (dynactin) (Kesisova et al., 2021) and signalling pathways (CIF15, SA-RhoGEF) (Nagata and Inagaki, 2005; Diesenberg et al., 2015). For a more detailed review on interactions involving the N-domain see Spiliotis and Nakos (2021).

7.3 Proline-Rich Motifs: Tuning Interactions and Functions

The proline-rich region, which follows the basic CBR, has also been credited with binding to different protein partners, thereby modulating protein interactions and functions. Some septin isoforms lacking the CBR present enhanced affinity towards signaling factors containing SH3 domains known to recognize proline-rich motifs. Many modulatory motifs and PTM sites have also been described within this region (such as acetylation, phosphorylation and SUMOylation motifs) (Van Damme et al., 2012; Zhou et al., 2013; Ribet et al., 2017). These modules could act as switches controlling and altering the effects of their flanking regions such as the CBR itself.

Shorter isoforms lacking the unstructured region were also shown to lose interaction specificities, and to increase binding to non-canonical paralogs and/or *promiscuous* partners, thereby, expanding their ordinary interactome (Devlin et al., 2021). It has been suggested that the presence of these proline-rich motifs (together with charged residues) (**Supplementary Figure S4**) might fine-tune NC-interface interactions and further restrict abnormal contacts and unusual filament assembly (Kim et al., 2012; Weems and McMurray, 2017; Jiao et al., 2020; Soroor et al., 2021).

7.4 Structured Regions Within the N-Domain

7.4.1 The Domain-Swapped "Hook-Loop"

At the start of the structured region, there is a largely conserved motif (V/IGF/I), part of the "hook-loop" (HL, for short), connecting the unstructured proline-rich motif to the α0 helix. The hook-loop participates in domain-swapping, where it is buried in a groove formed by its NC-interface partner (**Figure 9B**). This cleft lies under the central β-sheet (β1, β2, β3) and is flanked by part of α1 and by one side of the C-terminal region of α5′ (Sirajuddin et al., 2007; Sirajuddin et al., 2009; Mendonça et al., 2021), stabilizing the interaction between NC partners (**Figure 9C**). Of particular note is the final hydrophobic residue of the motif, Phe(HL). In known structures, this phenylalanine, prior to α0, is buried in a hydrophobic pocket which aids in anchoring the helix within the NC-interface (**Figure 9D**; Sirajuddin et al., 2007). The preceding conserved glycine (Gly(HL)) may be necessary to give sufficient flexibility to allow the phenylalanine to uncouple from the pocket and release α0 from the interface when it closes (see **Section 9** and **Section 10.1**). It seems likely that this motif emerged early in evolutionary history, since it is conserved to some extent even in paraseptins

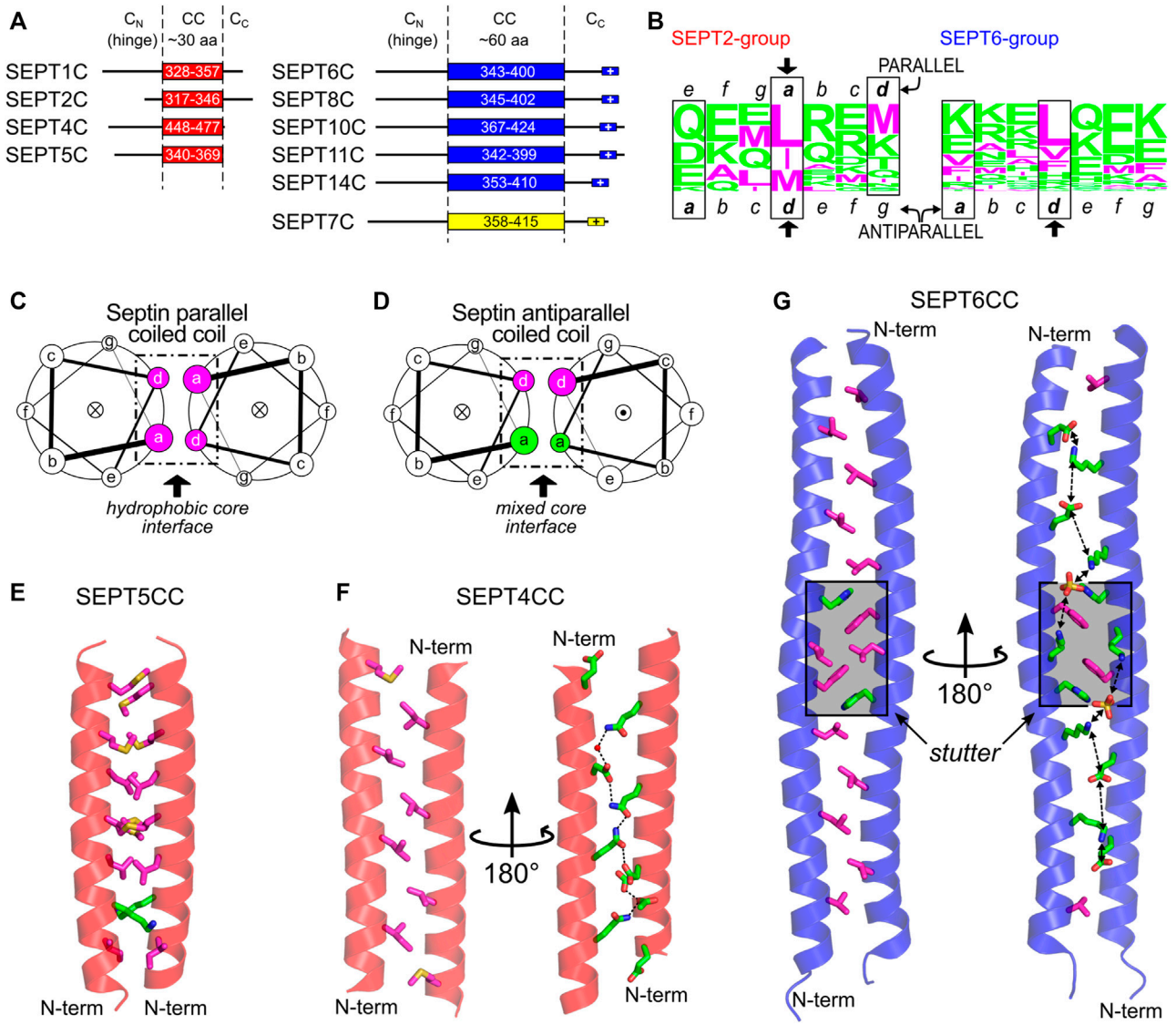

FIGURE 10 | The C-domain and the septin coiled coils. **(A)** C-domain elements in SEPT2- (red), SEPT6- (blue) and SEPT7-group members (yellow) as reported by Leonardo et al. (Leonardo et al., 2021). The following Uniprot entries were used for residue numbering: SEPT1, Q8WYJ6; SEPT2, Q15019; SEPT4, O43236; SEPT5, Q99719; SEPT6, Q14141-2; SEPT7, Q16181; SEPT8, Q92599-2; SEPT11, Q9NVA2; SEPT14, Q6ZU15. **(B)** CC heptad motifs in members of human SEPT2 **(left)** and SEPT6 group **(right)** represented using a residue frequency sequence logo. Identified core positions are highlighted in boxes and register assignment is shown as seen in the X-ray structures. General helical wheel schemes for **(C)** parallel and **(D)** antiparallel human septin coiled coils, showing the different chemical composition of residues in the core (*a* and *d* positions). The dot (●) or cross (×) inside the circles represent the helix direction, outward- and inward-pointing, respectively. **(E)** The parallel septin coiled coil of SEPT5 from the SEPT2 group (PDB:6WCU) showing mainly hydrophobic *a* and *d* side chain residues as sticks. **(F)** The antiparallel septin coiled coil of SEPT4 from the SEPT2 group (PDB:6WB3) showing the two sides of the interface (*d*-side, left; *a*-side, right) and the chain of hydrogen bonds seen on the hydrophilic side. **(G)** Antiparallel septin coiled coil of SEPT6 (PDB:6WBP) showing the two sides of the interface (as in panel **(F)**, but including the aromatic residue of the stutter, in both views) and the chain of favorable salt bridges seen on the hydrophilic *a* side. The stutter region is highlighted in grey. Throughout the figure, magenta and green colors represent hydrophobic and hydrophilic residues, respectively.

and probably existed in their common ancestor. However, in paraseptins, the motif is not used to accomplish domain swapping (Sun et al., 2002; Koenig et al., 2008).

7.4.2 Alpha Zero and Polybasic Region 1

The α0 helix is sometimes considered to be part of the G-domain but here we include it in the N-domain, as both the helix itself and the G-domain lacking it, are able to fold independently. The α0 helix is an integral part of the NC-interface (see **Section 9**), where its structure has been best defined in the recent cryo-EM study of the SEPT2/6/7 hexamer (PDB:7M6J). The PB1 of α0, a stretch of seven residues, can be divided into two basic elements: proximal and distal. Four basic residues comprise PB1 in the SEPT2, SEPT3 and SEPT7 groups, but only one in the SEPT6 group, which

therefore lacks a genuine polybasic region. In the SEPT2 and SEPT7 groups the four basic residues are divided equally between the proximal and distal regions and are distributed in an asymmetric fashion around the helix such that they are buried within the NC-interface, interacting with different components of the neighboring subunit (Mendonça et al., 2021). Furthermore, truncations within this region revealed its essential role not only for correct heterocomplex assembly and polymerization events but also for PIP selection during membrane association (Zhang et al., 1999; Casamayor and Snyder, 2003; Omrane et al., 2019; Taveneau et al., 2020).

The hook-loop, the α0 helix and the PB1 motif of the SEPT3 group present some unique properties when compared with their paralogues. The anchor Phe(HL) is replaced by an isoleucine, there is no proline in the first helical turn of α0 (**Figure 9D**) and the distribution of basic residues about the α0 helix is different from SEPT2 and SEPT7. These variations suggest that the N-terminal region of the SEPT3 group members may behave differently to other septins (see **Section 9.3** and **Section 10**).

8 THE C-TERMINAL DOMAINS

The C-terminal domains of septins have long been associated with filament bundling. Models have been suggested in which these domains may form cross-bridges between neighboring filaments leading to higher-order complexes. It is often assumed that the coiled-coil regions within the domain have a major role in this process. However, it is only very recently that detailed structural information has become available for these domains and this is beginning to shed light on the organization of filaments and bundles.

8.1 Components Within the C-Terminal Domains

Coiled-coil (CC) sequences are found in the C-terminal domain of most septins, with some exceptions (e.g., members of the human SEPT3 group and the yeast septin Cdc10). In humans, the length of the coiled coils varies among the different groups: in the SEPT2 group, it comprises around 30 residues, whilst in the SEPT6 and SEPT7 groups, it is approximately twice as long (**Figure 10A**; Leonardo et al., 2021). In yeast, there is a lack of direct structural information available and the output from prediction tools together with the information/assumptions adopted by different authors (Versele et al., 2004; Barth et al., 2008; Meseroll et al., 2013; Finnigan et al., 2015; Mela and Momany, 2019; Taveneau et al., 2020) means that it is unclear whether yeast septins share similar coiled-coil lengths or not (**Supplementary Figure S5**).

Apart from the coiled coil itself, there are potentially two flanking regions in the C-domain: C_N, the region between the final helix of the G-domain (α6) and the coiled coil, and C_C, the region subsequent to the coiled coil (**Figure 10A**). The C_N region is highly variable and believed to be quite flexible. It appears to act as a hinge, allowing the coiled coil to move with respect to the G-domain (Sirajuddin et al., 2007; Mendonça et al., 2021). This region in Shs1 (more specifically residues 350–445, **Supplementary Figure S5**) has been implicated in stabilizing octamers (Taveneau et al., 2020). Similarly, the region flanking the C-terminus of the coiled-coil (C_C) is believed to be mostly unstructured. In the SEPT6 and SEPT7 groups, at the very end of the C-terminal domain, a polybasic sequence is present (K/RK/RDKxK/RKN/K and EKNKKKGK, respectively). This motif, together with other polybasic domains in septins (PB1 and PB2), could assist in membrane interaction. Although still under debate, some studies indicate that specific C-domains (or parts of them) do indeed have a role in membrane association (Zeraik et al., 2016; Cannon et al., 2019; Jiao et al., 2020; Woods et al., 2021).

8.2 The Coiled-Coil Motif in General

Coiled coils are present in a wide variety of proteins and can be described as super-helical assemblies of two or more α-helices coiled together (Lupas and Bassler, 2017; Woolfson, 2017). One of the main roles of coiled coils is to promote protein oligomerization. The hallmark of dimeric coiled-coil sequences is the presence of heptads, repetitions of seven amino acid residues dubbed *a-b-c-d-e-f-g*. Positions *a* and *d* are occupied mostly by hydrophobic residues, frequently leucine or isoleucine. These two positions form the hydrophobic core at the interface of the coiled coil and they interact with neighboring residues by "knobs-into-holes" contacts (Crick, 1953). In parallel dimeric coiled coils, the core interactions are *a-a* and *d-d*, creating mixed strips including both *a* and *d* side chains on both sides of the coiled-coil interface (**Figure 10C** and **Supplementary Figure S6A**). In antiparallel dimeric coiled coils, however, the contacts are *a-d* (i.e., an *a* residue from one helix paired with a *d* residue from the other). This places all side chains from the *a* residues on one side of the coiled-coil interface (and therefore the side chains from *d* residues on the other) (**Figure 10D** and **Supplementary Figure S6B**).

Other positions (*b*, *c*, *e*, *f*, *g*) are more exposed and are usually occupied by hydrophilic residues. Since two turns of a standard helix do not exactly match the heptad length, the helices pack into a left-handed super-coiled structure. However, insertion of non-canonical repeats with lengths other than seven may modify the packing angle between the helices (Brown et al., 1996; Gruber and Lupas, 2003). An insertion of four residues (called a stutter), for example, creates a block of 11 residues (7 + 4) and leads to the unwinding of the left-handed supercoil (Brown et al., 1996; Gruber and Lupas, 2003).

8.3 Coiled Coils in Septins

Not visible in the structures of human septin oligomers due to the flexibility of C_N (Sirajuddin et al., 2007; Mendonça et al., 2021), the C-domains are expected to participate in two different types of coiled coil along the filament: the SEPT2 homodimer and the SEPT6-SEPT7 heterodimer (in yeast, the Cdc11 homodimer and the Cdc12-Cdc3 heterodimer, **Figure 1B**), both at NC-interfaces. Given the directions of the final helices (α6) of the respective G-domains, and how they project perpendicular to the main filament axis, septin coiled coils were inferred to be parallel. FRET experiments show that the C-domains of SEPT6 and SEPT7 do

indeed form heterodimeric parallel coiled coils (Low and Macara, 2006), even though they are capable of also assembling into homodimers (Almeida Marques et al., 2012; Sala et al., 2016). Circular dichroism data showed that the heterodimer is more stable than the homodimers (Almeida Marques et al., 2012; Sala et al., 2016), presumably due to unfavorable like-charge repulsion at *a* positions in the latter (Sala et al., 2016). No detailed structural evidence is currently available for the heterodimeric coiled coil, but it is expected that it would aid in guiding the correct assembly of the core particles (Almeida Marques et al., 2012; Meseroll et al., 2013; Sala et al., 2016). Concerning the C-terminal domain of SEPT2, it has been shown that its cleavage by Zika virus NS2B-NS3 protease is associated with mitotic defects in neural progenitor cells (Li et al., 2019), emphasizing the importance of the domain presumably in correct filament assembly.

Recently, the first structures of septin coiled coils were solved by X-ray diffraction. These were five homodimeric coiled coils of human SEPT1, SEPT4, SEPT5 (from the SEPT2 group), and SEPT6 and SEPT8 (from the SEPT6 group) (Leonardo et al., 2021). In the SEPT2-group structures, while SEPT5CC is a conventional parallel coiled coil with hydrophobic residues in *a* and *d* (**Figures 10C,E**), SEPT1CC and SEPT4CC (**Figure 10F**) are antiparallel (**Figure 10D**) and use a different contact interface which only partially overlaps with that observed for SEPT5CC. It has been suggested that this implies that the sequences are orientationally ambiguous (Leonardo et al., 2021). The residues which are common to the interface in both arrangements are shown by an arrow in **Figure 10B** and a similar pattern appears to be present in yeast septins. Additionally, the residues in *a*, which occupy *e* positions in the parallel form, are all hydrophilic (**Figure 10B**, note that the sequence register must be altered in order to preserve the standard definitions for the heptad positions). These establish hydrophilic contacts down the *a*-side of the interface, forming a chain of hydrogen bonds which interleaves acidic residues with glutamines thereby avoiding like-charge repulsion (**Figure 10F**) (Leonardo et al., 2021).

The two coiled-coil structures of the SEPT6 group (SEPT6, **Figure 10G**, and SEPT8) are also antiparallel. Both structures are very similar and, essentially, the same region forms the coiled coil, which confirms the intrinsic disorder of the flanking C_N and C_C regions since, for the SEPT8 construct, the entire C-domain was crystallized (Leonardo et al., 2021). Here, *a* positions are populated by lysines and glutamates. Since these residues form a strip down the *a*-side of the interface, this results in a chain of potential inter-helical salt bridges which would stabilize the dimer (**Figure 10G**). One particularity of these two structures (compared to the antiparallel structures of SEPT1CC and SEPT4CC) is the presence of a conserved stutter in the sequences of all SEPT6-group members (FE/DxL↓KxxH/Q, where the arrow indicates the break in the heptad register). The stutter decreases the supercoiling, leading to a structure in which the helices effectively lie side-by-side. This lack of supercoiling effectively maintains the side chains of equivalent register positions (*a* or *d*) on the same side of the interface along the entire length of the coiled coil (**Figure 10G**).

It has been suggested that the two orientations for the coiled coils could be metastable structures (Leonardo et al., 2021) and

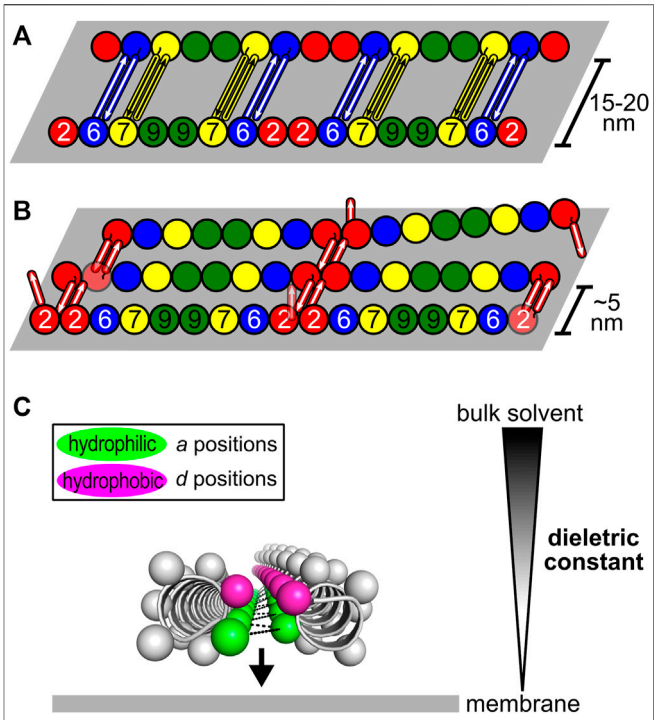

FIGURE 11 | Model for how antiparallel coiled coils could mediate septin filament interconnections (Leonardo et al., 2021). The G- and the C-domains are represented as spheres and rods, respectively. **(A)** Loosely-paired filaments (or a "railroad-track") separated by 15–20 nm are likely to be connected by antiparallel homodimers formed by the coiled coils of SEPT6 and SEPT7. **(B)** Tightly-paired sheets of filaments interconnected by antiparallel homodimers of SEPT2 coiled coils. **(C)** Solvent-protection of the hydrophilic side of the interface (*a* positions, green) in the antiparallel coiled coils. By facing the membrane, where the dielectric constant is lower than in bulk solvent, the formation of polar interactions is favored (black dashes).

modulated by the chemical microenvironment in which the coiled coil is embedded. NMR studies with coiled-coil peptides from the SEPT2 group in aqueous solution show that they have a tendency to be parallel with a conventional hydrophobic interface (Leonardo et al., 2021). On the other hand, when antiparallel, the septin coiled coil buries hydrophilic residues inside the interface. This would only be expected to happen in an environment of low dielectric constant where solvent has been largely excluded, similar to that found inside crystals.

8.4 Coiled Coils and Filament Pairing/ Bundling

Although apparently important for the stabilization of the NC-interface in the parallel orientation, the C-domains are not required for polymerization (Sirajuddin et al., 2007; Szuba et al., 2021), indicative of an additional role. They have also been associated with the formation of paired filaments, gauzes and stacked filament structures (Bertin et al., 2008; Bertin et al., 2010; Jiao et al., 2020; Szuba et al., 2021). Two kinds of spacing between filaments have been reported *in vitro* both in yeast and in mammalian septins: tight (~5 nm) (Bertin et al., 2010; Jiao et al.,

2020; Leonardo et al., 2021; Szuba et al., 2021) and loose (15–20 nm) (Frazier et al., 1998; Versele et al., 2004; Bertin et al., 2008, 2010; Leonardo et al., 2021). The former resembles the lengths of the coiled coils of the SEPT2-group members (4–5 nm). The wider spacing is compatible with the coiled coils of the SEPT6-and SEPT7-group members (8–11 nm) when taking into account contributions from unstructured parts of the C-domain (C_N and C_C) (Leonardo et al., 2021). The former has also been proposed to arise from lateral contacts between G-domains (Szuba et al., 2021). However, in yeast, deleting the C-domain of Cdc11 or Cdc3/Cdc12 eliminated tighly- and loosely-paired filaments, respectively, supporting the involvement of specific C-domains in maintaining each type of spacing (Bertin et al., 2010).

A recent model attempts to relate the structural data on the predominantly antiparallel coiled coils to their potential role in mediating filament cross-bridging (**Figures 11A,B**; Leonardo et al., 2021). Previously, based on experiments with yeast septins, the formation of four-helix-bundles interconnecting filaments had been proposed (Bertin et al., 2008). However, evidence for tetrameric coiled coils has not been forthcoming (Almeida Marques et al., 2012; Leonardo et al., 2021). Additionally, the use of equimolar mixtures of the coiled-coil peptides from SEPT6 and SEPT7 in crystallization assays—expecting the crystallization of the heterodimer—yielded only antiparallel SEPT6 homodimers (Leonardo et al., 2021). The model shown in **Figure 11** is a proposal for how both tight and loose spacings could arise by simple antiparallel pairings, which does not require the appearance of four-helix bundles. Although the details remain unknown, it is likely that the hydrophilic face (*a* positions) of these coiled coils would have to be solvent-protected to be stable, for instance by facing the membrane, where the dielectric constant is known to be lower (**Figure 11C**).

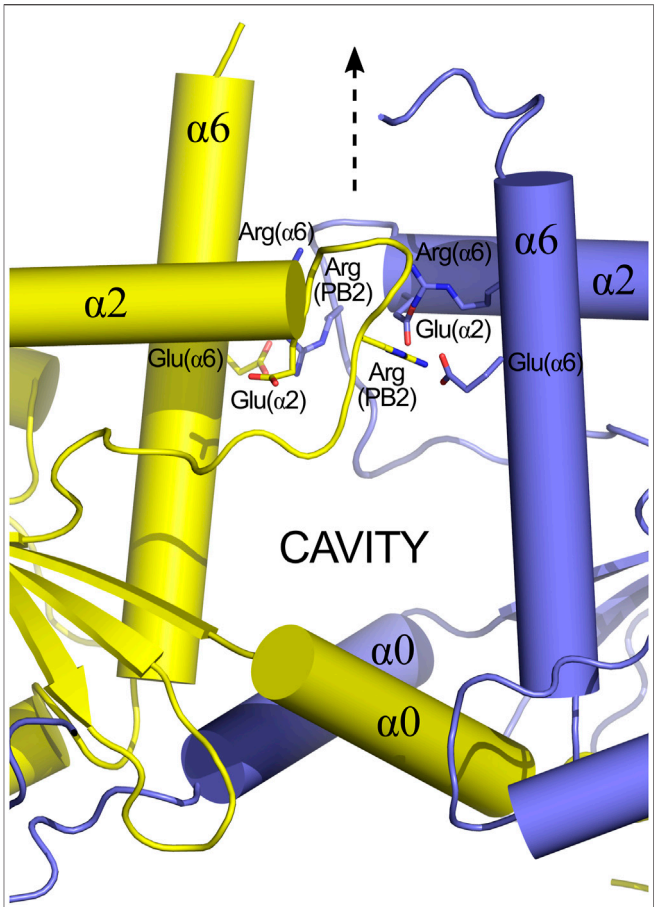

FIGURE 12 | The NC-interface and its cavity (PDB:7M6J, chains D and E). SEPT6 and SEPT7 are coloured in blue and yellow, respectively. The pseudo symmetry diad is displayed (dashed arrow). The NC-interface has an upper part (indicated by residues around the C-terminus of helices α2) and the lower part (α0). In the upper part, four residues conserved in most septins are indicated on both subunits: Glu(α2), Arg(PB2), Glu(α6) and Arg(α6). The inter-subunit electrostatic interactions are made between Glu(α2) and Arg(PB2), Glu(α6) and Arg(PB2) and Arg(α6) with the helical dipole of helix α2.

9 THE NC-INTERFACES

The polymerization of septin core particles in accordance with the canonical model generates either two or three chemically distinct NC-interfaces (**Figure 1B**). The SEPT6-SEPT7 NC-interface is common to both oligomers and has been most fully characterized in the cryo-EM structure of the SEPT2/6/7 complex (PDB:7M6J; Mendonça et al., 2021). The SEPT2-SEPT2 NC-interface is also common to both hexamers and octamers and is responsible for end-to-end polymerization. The SEPT3-SEPT3 NC-interface, unique to octamers, varies in terms of inter-subunit contacts and has been only partially described due to the lack of the α0 helix in most crystallized constructs.

9.1 SEPT6-SEPT7

Although the NC-interface between SEPT6-7 was originally reported in the crystal structure deposited in 2007 (PDB: 2QAG; Sirajuddin et al., 2007), the low resolution of the data at the time precluded its full description. The cryo-EM structure (PDB:7M6J; Mendonça et al., 2021), taken together with high-resolution crystal structures of its components, reveals that the NC-interface can be divided into two regions: the upper part, where salt bridges are formed by residues from the α6 helix and the loop following α2, and the lower part, formed mainly by contacts made by helix α0. The two regions are connected by one face of helix α6 (**Figure 12**). The upper part of the interface has been extensively described previously (Valadares et al., 2017; Castro et al., 2020). It involves inter-subunit electrostatic interactions made between, Glu(α2) and Arg(PB2), Glu(α6) and Arg(PB2) and Arg(α6) with the helical dipole of helix α2, according to our simplified nomenclature (**Figure 12**; Sirajuddin et al., 2007; Macedo et al., 2013; Valadares et al., 2017).

Helix α0 of SEPT7 contains a genuine polybasic region (PB1), composed of seven residues, including four positive charges. The same region in SEPT6 contains only one (**Figure 9A**). In SEPT7, PB1 can conveniently be divided into a proximal region and a distal region, each containing two basic residues. Both regions

form contacts with SEPT6 across the interface; the proximal region with helices α5 and α6 (including the elbow which connects them) and the distal region with the PAR.

One feature revealed by the cryo-EM structure is a large cavity at the SEPT6-7 NC-interface (**Figure 12**), whose perimeter is defined by the upper and lower contact regions together with α6. The bottom of the cavity is limited by a platform formed by the two α0 helices, held in place by the interactions described above, together with a phenylalanine anchor (Phe(α0)) at the boundary between α0 and the G-domain. It is interesting to note that the α0 helix is therefore anchored by two well-conserved phenylalanines at either end; Phe(HL) from the hook-loop (**Section 7.4.1**) and Phe(α0) at the interface with the G-domain. The cavity has no known function but is necessary for the monomers to be able to slide with respect to one another, although it is still unknown if this shifting is a general phenomenon which applies to all NC-interfaces or if it is restricted to the SEPT3 group alone (see **Section 9.3** and **Section 10.3**). Other possible roles for the cavity cannot be eliminated, for example, in lipid binding during membrane association.

9.2 SEPT2-SEPT2

The homotypic SEPT2-SEPT2 NC-interface was partially described by the 3.4 Å structure of SEPT2 lacking the C-domain, reported in 2007 (PDB:2QA5; Sirajuddin et al., 2007). It is the main determinant of septin filament polymerization and its exposure at the ends of the oligomers permits the formation of filaments including a mixture of octameric and hexameric core particles. In this crystal structure, the upper part of the interface is similar to that described above. Indeed, the network of salt bridges involving charged residues from the α6 helix and the loop following α2 is a general feature of homologues in general, suggesting this to be a constant feature of all NC-interfaces.

In order to better understand the totality of the interface, we generated a SEPT2α0 model based on the highest resolution structure available (PDB:6UPQ) to which the α0 helix from PDB: 2QA5 had been grafted. The SEPT2α0 NC-interface is in the open conformation in this model with α0 buried, as described for the case of SEPT6-7.

Like SEPT7, SEPT2 possesses a genuine PB1 with four positively charged residues divided into proximal and distal parts. Based on these observations, it has been suggested that similar interactions to those described for SEPT6-7 would be expected to participate across the interface (Mendonça et al., 2021). It appears clear from the model that interactions between PB1 and the PAR are to be anticipated. However, the SEPT2 NC-interface is now known to be the weakest link along the filament (at least in terms of its susceptibility to salt concentration) and molecular simulations appear to justify its fragility (Mendonça et al., 2019). In contrast, in terms of contact area and estimated free energy, the SEPT6-7 NC-interface (PDB: 7M6J) is estimated by PISA (Krissinel and Henrick, 2007) to be more stable than the SEPT2-2 NC-interface (2,149.8 $Å^2$ and -16.6 kcal/mol, respectively, compared to 1,636.3 $Å^2$ and −6.5 kcal/mol). Taken together, it is therefore possible to rationalize the rupture of filaments preferentially at homotypic SEPT2 interfaces at high ionic strength.

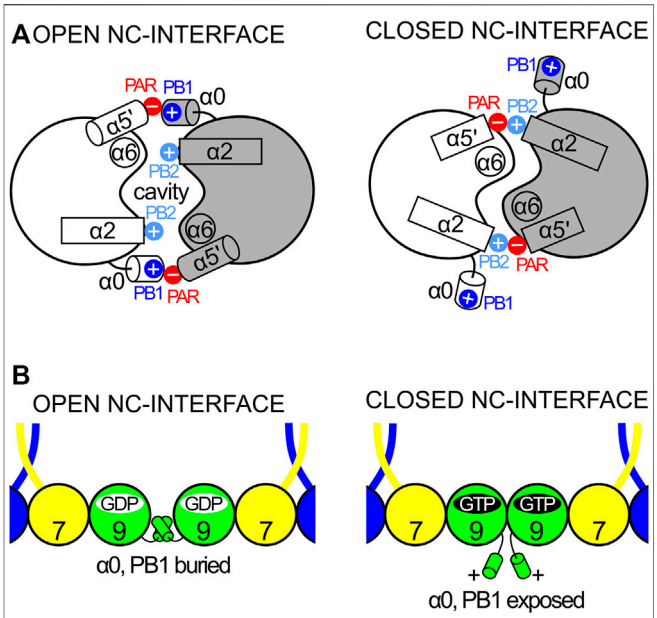

FIGURE 13 | The dual role of the PAR, the exposure of PB1 and the concertina movement at the NC-interface. **(A)** When the interface is open, the PAR interacts with PB1 (left) but when closed with PB2 (right). **(B)** The closure of the interface results in exposing α0 and its associated PB1, releasing it from its buried (inactive) state in the NC-interface and enabling it for membrane association.

9.3 SEPT3-SEPT3

In all crystal structures presenting an NC-interface, the same canonical "open" conformation is observed, except for the SEPT3 group (Sirajuddin et al., 2007; Macedo et al., 2013; Castro et al., 2020). In these, the homotypic NC-interface is physiological and occupies the center of the octamer (Mendonça et al., 2019; Soroor et al., 2021). Its plasticity results in at least three different conformations: open, closed, and shifted (Macedo et al., 2013; Castro et al., 2020). The crystal structures of the SEPT3 G-domain (PDB:4Z51 and PDB: 4Z54) complexed to either nucleotide are found to be in the closed form. For the G-domain of SEPT12 (PDB:6MQ9 and PDB:6MQK), both types of interface (open and closed) are found within the same filament, independent of the nucleotide, and the closed interface presents a displacement that breaks the twofold symmetry (the "shifted" conformation). In the case of SEPT9 (PDB:5CYP and PDB:5CYO), the conformation depends on the bound nucleotide, being open when bound to GDP and closed when bound to GTPγS (Macedo et al., 2013; Castro et al., 2020).

Since the closed conformation has thus far only been observed for SEPT3/9/12, it is tempting to believe that this is a unique property of the group. As mentioned above (**Section 7.4**), the N-terminal region in these septins presents some unique properties, including the charge distribution along α0 and the

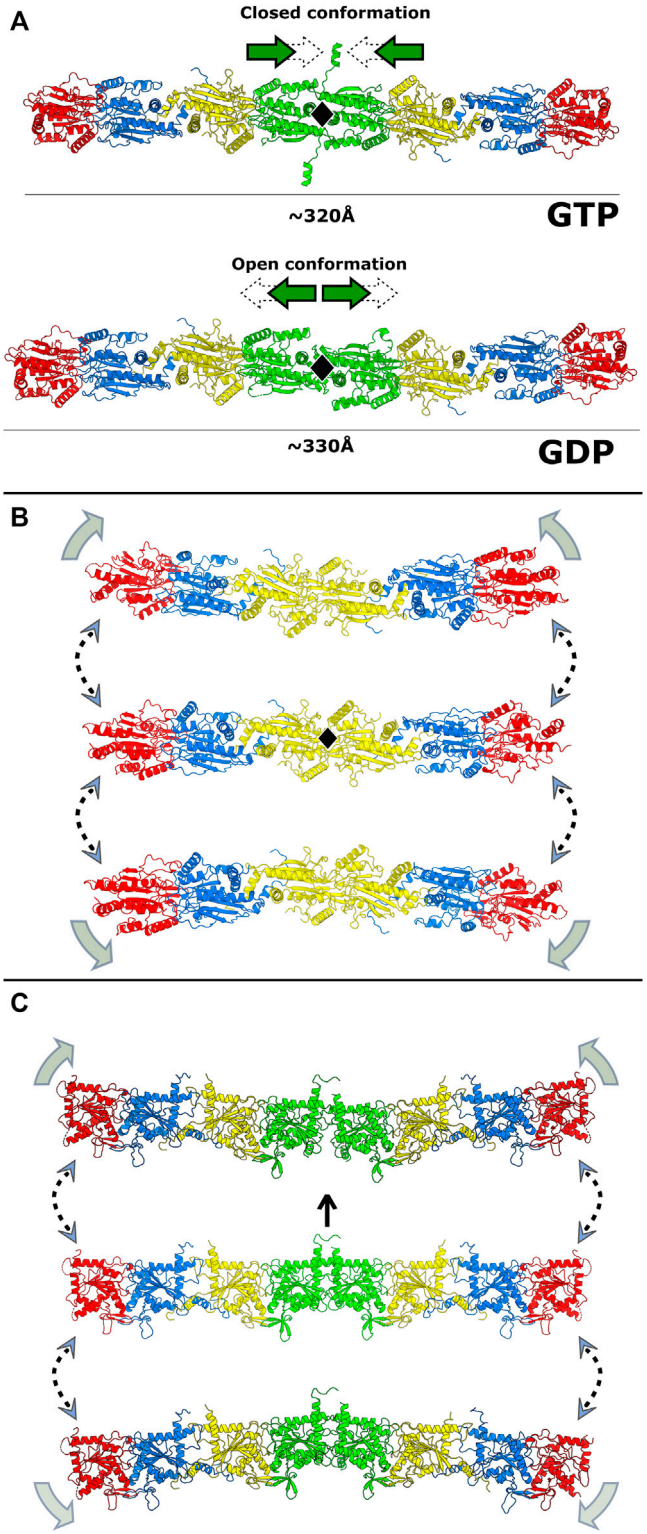

FIGURE 14 | Intrinsic flexibility of the filament. **(A)** The proposed concertina movement of the octamer due to the opening and closing of the central SEPT3-group NC-interface. In this case, the twofold symmetry is preserved. **(B)** Flexion of the hexamer around the twofold axis between the two copies of SEPT7 at the center (yellow) present in the cryo-EM model (*Continued*)

FIGURE 14 | (PDB:7M6J). The centre figure shows a linear particle which has a strict twofold axis perpendicular to the page (black lozenge). Above and below are shown bent particles. **(C)** Proposed flexion of the octamer, based on variations to the central NC-interface observed in crystal structures involving SEPT3-group members. In the central figure, the twofold axis is vertical (arrow). The upper complex is based on a central closed and shifted interface (PDB:6MQK) and the lower complex on the heterodimeric structure of SEPT7-SEPT3$_{T282Y}$ (PDB:6UQQ).

absence of one of the anchoring phenylalanines (Phe(HL)). These features could facilitate its exit from the cavity, allowing for the closure of the NC-interface, which would otherwise be impossible due to steric hindrance.

10 DOMAIN MOVEMENTS WITHIN A FILAMENT AND INSIGHTS INTO MEMBRANE INTERACTION

10.1 Squeezing of the Central NC-Interface

The canonical open conformation of the NC-interface is characterized by a ~20 Å separation between the two α6 helices, which is reduced to approximately 12 Å in the SEPT3 group when the interface closes. This conformational change results from a rearrangement of the salt bridges at the upper part of the interface (Macedo et al., 2013; Castro et al., 2020). With the closure of the interface, the PB2 region, which follow α2, wraps around α6 of its neighbor and approaches the polyacidic region (PAR). Specifically, Arg(PB2) dips down into the interface forming a new salt bridge with a glutamic acid from the PAR (Macedo et al., 2013; Castro et al., 2020). In this new conformation, Glu(α2) interacts directly with Arg(α6), which no longer interacts with the α2 helix dipole (Macedo et al., 2013; Castro et al., 2020). As a consequence, the α6 helices approach one another while the α2 helices move apart.

With the closure of the interface, the α0 helix is displaced out of the NC-interface, thereby gaining conformational freedom (Castro et al., 2020). This is not only suggested by the steric hindrance, which would result if α0 were to remain within the interface but has actually been observed experimentally in one of the crystal structures of SEPT3 (PDB:4Z54). Different to when hidden within the interface, where its positive charges are inward-pointing and occupied in stabilizing the interface itself, once liberated, PB1 would be free to interact with membranes (Zhang et al., 1999; Bertin et al., 2010).

Figure 13 schematizes the differences between the open and closed states. Under this proposal, the PAR plays two important roles: 1) harboring α0 and its PB1 when buried in the open state and 2) stabilizing the closed conformation by interacting with PB2. As such, the open conformation appears incompatible with membrane association by PB1, but rather is necessary for its safe storage when this is not required (Castro et al., 2020). This mechanism is also compatible with a role for PB2 in membrane association on interface closure. As this occurs, and PB2 wraps around helix α6 of the neighboring subunit to interact with the PAR, it becomes more exposed on the filament side

where it could act in concert with PB1 in membrane association. Indeed, its role as such has already been proposed (Omrane et al., 2019) and is compatible with the sense of bending of the hexamer observed by cryo-EM (PDB:7M6J) (see **Section 10.3**).

In all protein structures from the SEPT3 group, the α5′ helix is oriented differently from that observed for other septins, lying roughly parallel to the filament axis. This is due to the presence of *characteristic* residues such as *cis*Pro(α4-α5′/SEPT3), which result in the N-terminus of α5′ coming closer to α6 (Castro et al., 2020). This displaces the PAR upwards in a way which would favor interacting with PB2 in the closed conformation. The combined differences observed in the SEPT3 group, including those associated with α0, α5′ and the lack of a C-terminal coiled coil, may sum to give this NC-interface its apparently unique plasticity.

10.2 Communication Between Adjacent Interfaces and Information Transfer

The closed structure of the G-domain of SEPT9 (PDB:5CYP) was obtained by soaking a GDP-bound crystal (in the open conformation) with the GTP analogue, GTPγS, suggesting that the occurrence of nucleotide hydrolysis in the G-interface could result in conformational changes to the adjacent NC-interface. How might this occur now that β-strand slippage appears to have been eliminated as a potential conduit at physiological interfaces (see **Section 6.3**)? One possibility is helix α2, which runs from the switch II region of the G-interface at its N-terminus to the PB2 region of the NC-interface at its C-terminus. The septin specific sequence Sep2 (Pan et al., 2007) runs underneath this helix such that it is unable to pack against the central β-sheet (see **Section 5.1.3**). This unusual arrangement (Chothia et al., 1981) may free up α2 and allow it to move with respect to the rest of the structure, potentially as a rigid body or rod. As such, the conformational changes which occur to switch II on GTP hydrolysis could be more readily transmitted via α2 to the neighboring NC-interface. Although speculative, this mechanism would provide a functional role for the Sep2 motif, justifying its strict conservation in septins during evolution (Pan et al., 2007).

Nothing is known about the mechanism of information transfer itself. However, a specific aromatic residue of the switch II region, Aro(Sw2), appears to be a potential candidate. The SEPT3 septins bound to non-hydrolyzable GTP analogues currently represent the best model available for the pre-hydrolysis state. In all such structures, this aromatic residue lies such that the plane of the aromatic ring is parallel to the surface of helix α2. However, structures in the presence of GDP suggest that nucleotide hydrolysis perturbs the switch II region, causing Aro(Sw2) to assume an alternative conformation in which the ring lies approximately perpendicular to the helix surface (**Supplementary Figure S7**; Rosa et al., 2020). The change to the Aro(Sw2) rotamer appears to be directly coupled to a second aromatic residue, Phe(α3), on the inner surface of helix α3. This aromatic cluster rearrangement lifts α2 further from the underlying β-sheet, potentially giving it the necessary freedom to move and thus perturb the neighbouring NC-interface towards which it is slightly shifted (**Supplementary Figure S7**). The notion that this aromatic cluster could be essential for communication gains support from the fact that Phe(α3) is lacking in the catalytically inactive septins where, by definition, such a mechanism would be inoperative anyway. It is interesting to note that the information transfer may be due to a transitory perturbation to α2 rather than a switch between two well-defined states, an idea supported by the fact that the shifts described above are rather subtle. Clearly, more work is necessary on this point.

10.3 Transverse Modes of Filament Flexibility

The concertina movement due to opening and closing of the NC-interface of the SEPT3-group septins (**Figure 14A**) is not the only structural flexibility of the core particles for which there is experimental evidence. Although the flexibility of the hexamer had been noted previously (Sirajuddin et al., 2007), the study of Mendonça et al. (2021) was able to attribute this principally to movement at the central G-interface (SEPT7-SEPT7) (**Figure 14B**). The direction of greatest bending corresponded to flexion of the particle around the twofold axis which relates the two trimers (**Figure 14B**, center). Interestingly, this bending may be related to the recognition and/or interaction of the filaments with membranes. If the curvature of the oligomer were coincident with that of the membrane, it would lie laterally such that the main aperture to the cavity at the NC-interface would face the membrane. This raises intriguing possibilities, including, for example, that both PB1 and PB2 could interact simultaneously with negatively charged membrane lipids and that the cavity may play a role in this process. Obviously, the current scarcity of structural data only allows for speculation at this point and any attempt to draw a definitive conclusion would be premature.

Membrane recognition by septins can also be curvature-dependent, as has been shown for both yeast and animal septin complexes (Palander et al., 2017; Beber et al., 2019; Cannon et al., 2019; Woods et al., 2021). *In vitro* studies have shown that septin filaments preferentially bind to regions of curvature on the scale of microns (Bridges et al., 2016). Although the bending observed in the cryo-EM study only gives an indication of the direction of flexion and not its extent, nevertheless this would appear to be compatible with micron-scale recognition. Propagating the flexion observed at the central interface to all oligomers along a filament would easily produce ring-like structures with diameters compatible with the preferential curvatures already observed (Kinoshita et al., 2002; Tanaka-Takiguchi et al., 2009; Bridges et al., 2016; Beber et al., 2019).

Since the exposure of PB1 due to NC-interface closure is potentially a unique property of the SEPT3 group, this makes the conformational properties of the octameric particle of particular interest. At present, there are no experimental structures available for an octamer from any species. Nevertheless, the accumulation of partial structures of single septins and heterodimers, when taken together with that for the hexamer, mean that reliable models for the human octamer can be computationally generated. **Figure 14C** shows examples of how the variation observed at the central interface in the different crystal structures involving

SEPT3-group members leads to full particles which present considerable structural diversity.

Clearly, structural studies of octameric particles with a view to determining the extent and direction of bending will be essential to understanding the physical properties of filaments. How these properties may depend on the ratio of hexamers to octamers is an intriguing question to be answered. More important still is how these relate to septin association with membranes and the cytoskeleton and thereby impact on septin function.

11 FUTURE DIRECTIONS

In a review article published in 2017 (Valadares et al., 2017) it was suggested that single-particle cryo-electron microscopy would inevitably play a significant role in the future of the structural biology of septins. With the recent publication of the first structure of a hexameric particle at 3.6 Å, it would seem that this is already coming true. Undoubtedly, in the near future, cryo-electron tomography and subtomogram averaging of *in situ* samples will be able to provide a more realistic view of intracellular septin localization, function and dynamics and it is exciting to look forward to the future, knowing that these technologies are both powerful and robust.

As this review is being written, free worldwide access to the AI structure predictor, AlphaFold2 (Jumper et al., 2021), is already a reality and it stands to revolutionize the way we think about structural biology and the information it carries about complex biological systems, septins included. Overnight, structures with accuracies which are likely to be close to experimental have been made available for all septins from humans, yeast, *Drosophila* and *C. elegans*. Whereas structural information has been largely restricted to human septins up until now, this will no longer be the case in the future. What is needed, more than ever, is the ability to interrogate these structures in order to glean relevant biological insight. The challenge will be to understand how septins associate, how they are regulated and modulated, how they respond to their microenvironment and how the dynamics of monomers, oligomers, filaments and bundles is associated with their interactions with membranes, the cytoskeleton and their other binding partners. Much progress has been made in understanding the structure-function relationships of septins over recent years, but there is still plenty to be done. Rather than further dissecting septin filaments into their component parts, it is now incumbent on those active in the field to integrate current and future information into a more complete picture of the complex biological systems in which septins participate.

AUTHOR CONTRIBUTIONS

IAC: writing, figure preparation, and construction of the final version; DAL, HVDR, DKSVC, HDMP, and NFV: writing and figure preparation; APUA: writing; RCG: conceptualization, writing, and construction of the final version. All authors contributed to the review and approved its final version.

FUNDING

Brazilian funding agencies FAPESP (grants 2020/02897-1 and 2014/15546-1 and associated programs; scholarship grants 2018/19992-7 to IAC, 2016/04658-9 to DAL and 2019/22000-9 to HVDR) and CNPq (scholarship grant 142394/2018-1 to DKSVC).

SUPPLEMENTARY MATERIAL

The Supplementary Material for this article can be found online at: https://www.frontiersin.org/articles/10.3389/fcell.2021.765085/full#supplementary-material

REFERENCES

Abbey, M., Hakim, C., Anand, R., Lafera, J., Schambach, A., Kispert, A., et al. (2016). GTPase Domain Driven Dimerization of SEPT7 Is Dispensable for the Critical Role of Septins in Fibroblast Cytokinesis. *Sci. Rep.* 6, 20007–20015. doi:10.1038/srep20007

Abbey, M., Gaestel, M., and Menon, M. B. (2019). Septins: Active GTPases or Just GTP-binding Proteins? *Cytoskeleton* 76, 55–62. doi:10.1002/cm.21451

Ageta-Ishihara, N., Miyata, T., Ohshima, C., Watanabe, M., Sato, Y., Hamamura, Y., et al. (2013). Septins Promote Dendrite and Axon Development by Negatively Regulating Microtubule Stability via HDAC6-Mediated Deacetylation. *Nat. Commun.* 4, 2532–2611. doi:10.1038/ncomms3532

Almeida Marques, I., Valadares, N. F., Garcia, W., Damalio, J. C. P., Macedo, J. N. A., Araújo, A. P. U., et al. (2012). Septin C-Terminal Domain Interactions: Implications for Filament Stability and Assembly. *Cell Biochem. Biophys.* 62, 317–328. doi:10.1007/s12013-011-9307-0

Angelis, D., and Spiliotis, E. T. (2016). Septin Mutations in Human Cancers. *Front. Cell Dev. Biol.* 4, 122. doi:10.3389/fcell.2016.00122

Bai, X., Bowen, J. R., Knox, T. K., Zhou, K., Pendziwiat, M., Kuhlenbäumer, G., et al. (2013). Novel Septin 9 Repeat Motifs Altered in Neuralgic Amyotrophy Bind and Bundle Microtubules. *J. Cel Biol.* 203, 895–905. doi:10.1083/jcb.201308068

Barral, Y., Mermall, V., Mooseker, M. S., and Snyder, M. (2000). Compartmentalization of the Cell Cortex by Septins Is Required for Maintenance of Cell Polarity in Yeast. *Mol. Cel* 5, 841–851. doi:10.1016/s1097-2765(00)80324-x

Barth, P., Schoeffler, A., and Alber, T. (2008). Targeting Metastable Coiled-Coil Domains by Computational Design. *J. Am. Chem. Soc.* 130, 12038–12044. doi:10.1021/ja802447e

Baur, J. D., Rösler, R., Wiese, S., Johnsson, N., and Gronemeyer, T. (2019). Dissecting the Nucleotide Binding Properties of the Septins from *S. cerevisiae*. *Cytoskeleton* 76, 45–54. doi:10.1002/cm.21484

Beber, A., Alqabandi, M., Prévost, C., Viars, F., Lévy, D., Bassereau, P., et al. (2019). Septin-based Readout of PI(4,5)P2 Incorporation into Membranes of Giant Unilamellar Vesicles. *Cytoskeleton* 76, 92–103. doi:10.1002/cm.21480

Bertin, A., McMurray, M. A., Grob, P., Park, S.-S., Garcia, G., Patanwala, I., et al. (2008). Saccharomyces cerevisiae Septins: Supramolecular Organization of Heterooligomers and the Mechanism of Filament Assembly. *Proc. Natl. Acad. Sci.* 105, 8274–8279. doi:10.1073/pnas.0803330105

Bertin, A., McMurray, M. A., Thai, L., Garcia, G., III, Votin, V., Grob, P., et al. (2010). Phosphatidylinositol-4,5-bisphosphate Promotes Budding Yeast Septin Filament Assembly and Organization. *J. Mol. Biol.* 404, 711–731. doi:10.1016/j.jmb.2010.10.002

Bridges, A. A., Jentzsch, M. S., Oakes, P. W., Occhipinti, P., and Gladfelter, A. S. (2016). Micron-scale Plasma Membrane Curvature Is Recognized by the Septin Cytoskeleton. *J. Cel Biol.* 213, 23–32. doi:10.1083/jcb.201512029

Bridges, A. A., Zhang, H., Mehta, S. B., Occhipinti, P., Tani, T., and Gladfelter, A. S. (2014). Septin Assemblies Form by Diffusion-Driven Annealing on Membranes. *Proc. Natl. Acad. Sci. USA* 111, 2146–2151. doi:10.1073/pnas.1314138111

Brognara, G., Pereira, H. D. M., Brandão-Neto, J., Araujo, A. P. U., and Garratt, R. C. (2019). Revisiting SEPT7 and the Slippage of β-strands in the Septin Family. *J. Struct. Biol.* 207, 67–73. doi:10.1016/j.jsb.2019.04.015

Brown, J. H., Cohen, C., and Parry, D. A. D. (1996). Heptad Breaks in α-helical Coiled Coils: Stutters and Stammers. *Proteins* 26, 134–145. doi:10.1002/(SICI)1097-0134(199610)26:2<134::AID-PROT3>3.0.CO;2-G

Byers, B., and Goetsch, L. (1976). A Highly Ordered Ring of Membrane-Associated Filaments in Budding Yeast. *J. Cel Biol.* 69, 717–721. doi:10.1083/jcb.69.3.717

Cannon, K. S., Woods, B. L., Crutchley, J. M., and Gladfelter, A. S. (2019). An Amphipathic helix Enables Septins to Sense Micrometer-Scale Membrane Curvature. *J. Cel Biol.* 218, 1128–1137. doi:10.1083/jcb.201807211

Cao, L., Ding, X., Yu, W., Yang, X., Shen, S., and Yu, L. (2007). Phylogenetic and Evolutionary Analysis of the Septin Protein Family in Metazoan. *FEBS Lett.* 581, 5526–5532. doi:10.1016/j.febslet.2007.10.032

Casamayor, A., and Snyder, M. (2003). Molecular Dissection of a Yeast Septin: Distinct Domains Are Required for Septin Interaction, Localization, and Function. *Mol. Cel. Biol.* 23, 2762–2777. doi:10.1128/mcb.23.8.2762-2777.2003

Castro, D. K. S. d. V., da Silva, S. M. d. O., Pereira, H. D. M., MacEdo, J. N. A., Leonardo, D. A., Valadares, N. F., et al. (2020). A Complete Compendium of crystal Structures for the Human SEPT3 Subgroup Reveals Functional Plasticity at a Specific Septin Interface. *Int. Union Crystallogr. J.* 7, 462–479. doi:10.1107/S2052252520002973

Chothia, C., Levitt, M., and Richardson, D. (1981). Helix to helix Packing in Proteins. *J. Mol. Biol.* 145, 215–250. doi:10.1016/0022-2836(81)90341-7

Connolly, D., Hoang, H. G., Adler, E., Tazearslan, C., Simmons, N., Bernard, V. V., et al. (2014). Septin 9 Amplification and Isoform-specific Expression in Peritumoral and Tumor Breast Tissue. *Biol. Chem.* 395, 157–167. doi:10.1515/hsz-2013-0247

Connolly, D., Yang, Z., Castaldi, M., Simmons, N., Oktay, M. H., Coniglio, S., et al. (2011). Septin 9 Isoform Expression, Localization and Epigenetic Changes during Human and Mouse Breast Cancer Progression. *Breast Cancer Res.* 13, 76. doi:10.1186/bcr2924

Crick, F. H. C. (1953). The Packing of α-helices: Simple Coiled-Coils. *Acta Crystallogr.* 6, 689–697. Available at: http://scripts.iucr.org/cgi-bin/paper?S0365110X53001964. doi:10.1107/s0365110x53001964

DeRose, B. T., Kelley, R. S., Ravi, R., Kokona, B., Beld, J., Spiliotis, E. T., et al. (2020). Production and Analysis of a Mammalian Septin Hetero-octamer Complex. *Cytoskeleton* 77, 485–499. doi:10.1002/cm.21643

Devlin, L., Okletey, J., Perkins, G., Bowen, J. R., Nakos, K., Montagna, C., et al. (2021). Proteomic Profiling of the Oncogenic Septin 9 Reveals Isoform-specific Interactions in Breast Cancer Cells. *Proteomics* 21, 2100155. doi:10.1002/pmic.202100155

Diesenberg, K., Beerbaum, M., Fink, U., Schmieder, P., and Krauss, M. (2015). Septin 9 Negatively Regulates Ubiquitin-dependent Downregulation of Epidermal Growth Factor Receptor. *J. Cel Sci.* 128, 397–407. doi:10.1242/jcs.162206

Estey, M. P., Di Ciano-Oliveira, C., Froese, C. D., Bejide, M. T., and Trimble, W. S. (2010). Distinct Roles of Septins in Cytokinesis: SEPT9 Mediates Midbody Abscission. *J. Cel Biol.* 191, 741–749. doi:10.1083/jcb.201006031

Ewers, H., Tada, T., Petersen, J. D., Racz, B., Sheng, M., and Choquet, D. (2014). A Septin-dependent Diffusion Barrier at Dendritic Spine Necks. *PLoS One* 9, e113916. doi:10.1371/journal.pone.0113916

Falk, J., Boubakar, L., and Castellani, V. (2019). Septin Functions during Neuro-Development, a Yeast Perspective. *Curr. Opin. Neurobiol.* 57, 102–109. doi:10.1016/j.conb.2019.01.012

Farkasovsky, M., Herter, P., Voß, B., and Wittinghofer, A. (2005). Nucleotide Binding and Filament Assembly of Recombinant Yeast Septin Complexes. *Biol. Chem.* 386, 643–656. doi:10.1515/BC.2005.075

Field, C. M., Al-Awar, O., Rosenblatt, J., Wong, M. L., Alberts, B., and Mitchison, T. J. (1996). A Purified Drosophila Septin Complex Forms Filaments and Exhibits GTPase Activity. *J. Cel Biol.* 133, 605–616. doi:10.1083/jcb.133.3.605

Field, C. M., and Kellogg, D. (1999). Septins: Cytoskeletal Polymers or Signalling GTPases? *Trends Cel Biol.* 9, 387–394. doi:10.1016/s0962-8924(99)01632-3

Finnigan, G. C., Duvalyan, A., Liao, E. N., Sargsyan, A., and Thorner, J. (2016). Detection of Protein-Protein Interactions at the Septin Collar inSaccharomyces Cerevisiaeusing a Tripartite Split-GFP System. *MBoC* 27, 2708–2725. doi:10.1091/mbc.e16-05-0337

Finnigan, G. C., Takagi, J., Cho, C., and Thorner, J. (2015). Comprehensive Genetic Analysis of Paralogous Terminal Septin Subunits Shs1 and Cdc11 in Saccharomyces cerevisiae. *Genetics* 200, 821–841. doi:10.1534/genetics.115.176495

Frazier, J. A., Wong, M. L., Longtine, M. S., Pringle, J. R., Mann, M., Mitchison, T. J., et al. (1998). Polymerization of Purified Yeast Septins: Evidence that Organized Filament Arrays May Not Be Required for Septin Function. *J. Cel Biol.* 143, 737–749. doi:10.1083/jcb.143.3.737

Füchtbauer, A., Lassen, L. B., Jensen, A. B., Howard, J., Quiroga, A. d. S., Warming, S., et al. (2011). Septin9 Is Involved in Septin Filament Formation and Cellular Stability. *Biol. Chem.* 392, 769–777. doi:10.1515/BC.2011.088

Garcia, G., III, Bertin, A., Li, Z., Song, Y., McMurray, M. A., Thorner, J., et al. (2011). Subunit-dependent Modulation of Septin Assembly: Budding Yeast Septin Shs1 Promotes Ring and Gauze Formation. *J. Cel Biol.* 195, 993–1004. doi:10.1083/jcb.201107123

Garcia, W., de Araújo, A. P. U., de Oliveira Neto, M., Ballestero, M. R. M., Polikarpov, I., Tanaka, M., et al. (2006). Dissection of a Human Septin: Definition and Characterization of Distinct Domains within Human SEPT4. *Biochemistry* 45, 13918–13931. doi:10.1021/bi061549z

Garcia, W., de Araújo, A. P. U., Lara, F., Foguel, D., Tanaka, M., Tanaka, T., et al. (2007). An Intermediate Structure in the Thermal Unfolding of the GTPase Domain of Human Septin 4 (SEPT4/Bradeion-β) Forms Amyloid-like Filaments *In Vitro*. *Biochemistry* 46, 11101–11109. doi:10.1021/bi700702w

Gasper, R., Meyer, S., Gotthardt, K., Sirajuddin, M., and Wittinghofer, A. (2009). It Takes Two to Tango: Regulation of G Proteins by Dimerization. *Nat. Rev. Mol. Cell Biol.* 10, 423–429. doi:10.1038/nrm2689

Gonzalez, M. E., Makarova, O., Peterson, E. A., Privette, L. M., and Petty, E. M. (2009). Up-regulation of SEPT9_v1 Stabilizes C-Jun-N-Terminal Kinase and Contributes to its Pro-proliferative Activity in Mammary Epithelial Cells. *Cell Signal.* 21, 477–487. doi:10.1016/j.cellsig.2008.11.007

Gruber, M., and Lupas, A. N. (2003). Historical Review: Another 50th Anniversary - New Periodicities in Coiled Coils. *Trends Biochem. Sci.* 28, 679–685. doi:10.1016/j.tibs.2003.10.008

Hartwell, L. (1971). Genetic Control of the Cell Division Cycle in Yeast *1IV. Genes Controlling Bud Emergence and Cytokinesis. *Exp. Cel Res.* 69, 265–276. doi:10.1016/0014-4827(71)90223-0

Hernández-Rodríguez, Y., Masuo, S., Johnson, D., Orlando, R., Smith, A., Couto-Rodriguez, M., et al. (2014). Distinct Septin Heteropolymers Co-exist during Multicellular Development in the Filamentous Fungus Aspergillus nidulans. *PLoS One* 9, e92819. doi:10.1371/journal.pone.0092819

Hernández-Rodríguez, Y., and Momany, M. (2012). Posttranslational Modifications and Assembly of Septin Heteropolymers and Higher-Order Structures. *Curr. Opin. Microbiol.* 15, 660–668. doi:10.1016/j.mib.2012.09.007

Hovmöller, S., Zhou, T., and Ohlson, T. (2002). Conformations of Amino Acids in Proteins. *Acta Crystallogr. D Biol. Cryst.* 58, 768–776. doi:10.1107/s0907444902003359

Hu, J., Bai, X., Bowen, J. R., Dolat, L., Korobova, F., Yu, W., et al. (2012). Septin-driven Coordination of Actin and Microtubule Remodeling Regulates the Collateral Branching of Axons. *Curr. Biol.* 22, 1109–1115. doi:10.1016/j.cub.2012.04.019

Hu, Q., Milenkovic, L., Jin, H., Scott, M. P., Nachury, M. V., Spiliotis, E. T., et al. (2010). A Septin Diffusion Barrier at the Base of the Primary Cilium Maintains Ciliary Membrane Protein Distribution. *Science* 329, 436–439. doi:10.1126/science.1191054

Iv, F., Martins, C. S., Castro-Linares, G., Taveneau, C., Barbier, P., Verdier-Pinard, P., et al. (2021). Insights into Animal Septins Using Recombinant Human Septin Octamers with Distinct SEPT9 Isoforms. *J. Cel Sci.* 134, jcs258484. doi:10.1242/jcs.258484

Jiao, F., Cannon, K. S., Lin, Y. C., Gladfelter, A. S., and Scheuring, S. (2020). The Hierarchical Assembly of Septins Revealed by High-Speed AFM. *Nat. Commun.* 11, 5062–5113. doi:10.1038/s41467-020-18778-x

John, C. M., Hite, R. K., Weirich, C. S., Fitzgerald, D. J., Jawhari, H., Faty, M., et al. (2007). The Caenorhabditis elegans Septin Complex Is Nonpolar. *EMBO J.* 26, 3296–3307. doi:10.1038/sj.emboj.7601775

Johnson, C. R., Steingesser, M. G., Weems, A. D., Khan, A., Gladfelter, A., Bertin, A., et al. (2020). Guanidine Hydrochloride Reactivates an Ancient Septin Hetero-Oligomer Assembly Pathway in Budding Yeast. *Elife* 9, e54355. doi:10.7554/eLife.54355

Johnson, E. S., and Blobel, G. (1999). Cell Cycle-Regulated Attachment of the Ubiquitin-Related Protein SUMO to the Yeast Septins. *J. Cel Biol.* 147, 981–994. doi:10.1083/jcb.147.5.981

Jumper, J., Evans, R., Pritzel, A., Green, T., Figurnov, M., Ronneberger, O., et al. (2021). Highly Accurate Protein Structure Prediction with AlphaFold. *Nature*, 583–589, 596. doi:10.1038/s41586-021-03819-2

Karasmanis, E. P., Phan, C.-T., Angelis, D., Kesisova, I. A., Hoogenraad, C. C., McKenney, R. J., et al. (2018). Polarity of Neuronal Membrane Traffic Requires Sorting of Kinesin Motor Cargo during Entry into Dendrites by a Microtubule-Associated Septin. *Develop. Cel* 46, 204–218. doi:10.1016/j.devcel.2018.06.013

Keefe, L. J., Sondek, J., Shortle, D., and Lattman, E. E. (1993). The Alpha Aneurism: a Structural Motif Revealed in an Insertion Mutant of Staphylococcal Nuclease. *Proc. Natl. Acad. Sci.* 90, 3275–3279. doi:10.1073/pnas.90.8.3275

Kesisova, I. A., Robinson, B. P., and Spiliotis, E. T. (2021). A Septin GTPase Scaffold of Dynein-Dynactin Motors Triggers Retrograde Lysosome Transport. *J. Cel Biol.* 220, e202005219. doi:10.1083/JCB.202005219

Kim, M. S., Froese, C. D., Estey, M. P., and Trimble, W. S. (2011). SEPT9 Occupies the Terminal Positions in Septin Octamers and Mediates Polymerization-dependent Functions in Abscission. *J. Cel Biol.* 195, 815–826. doi:10.1083/jcb.201106131

Kim, M. S., Froese, C. D., Xie, H., and Trimble, W. S. (2012). Uncovering Principles that Control Septin-Septin Interactions. *J. Biol. Chem.* 287, 30406–30413. doi:10.1074/jbc.M112.387464

Kinoshita, A., Kinoshita, M., Akiyama, H., Tomimoto, H., Akiguchi, I., Kumar, S., et al. (1998). Identification of Septins in Neurofibrillary Tangles in Alzheimer's Disease. *Am. J. Pathol.* 153, 1551–1560. doi:10.1016/s0002-9440(10)65743-4

Kinoshita, M. (2003). Assembly of Mammalian Septins. *J. Biochem.* 134, 491–496. doi:10.1093/jb/mvg182

Kinoshita, M., Field, C. M., Coughlin, M. L., Straight, A. F., and Mitchison, T. J. (2002). Self- and Actin-Templated Assembly of Mammalian Septins. *Develop. Cel* 3, 791–802. doi:10.1016/s1534-5807(02)00366-0

Koenig, P., Oreb, M., Höfle, A., Kaltofen, S., Rippe, K., Sinning, I., et al. (2008). The GTPase Cycle of the Chloroplast Import Receptors Toc33/Toc34: Implications from Monomeric and Dimeric Structures. *Structure* 16, 585–596. doi:10.1016/j.str.2008.01.008

Krissinel, E., and Henrick, K. (2007). Inference of Macromolecular Assemblies from Crystalline State. *J. Mol. Biol.* 372, 774–797. doi:10.1016/j.jmb.2007.05.022

Kumagai, P. S., Martins, C. S., Sales, E. M., Rosa, H. V. D., Mendonça, D. C., Damalio, J. C. P., et al. (2019). Correct Partner Makes the Difference: Septin G-Interface Plays a Critical Role in Amyloid Formation. *Int. J. Biol. Macromolecules* 133, 428–435. doi:10.1016/j.ijbiomac.2019.04.105

Kuo, Y. C., Shen, Y. R., Chen, H. I., Lin, Y. H., Wang, Y. Y., Chen, Y. R., et al. (2015). SEPT12 Orchestrates the Formation of Mammalian Sperm Annulus by Organizing Core Octameric Complexes with Other SEPT Proteins. *J. Cel Sci.* 128, 923–934. doi:10.1242/jcs.158998

Leipe, D. D., Wolf, Y. I., Koonin, E. V., and Aravind, L. (2002). Classification and Evolution of P-Loop GTPases and Related ATPases. *J. Mol. Biol.* 317, 41–72. doi:10.1006/jmbi.2001.5378

Leonardo, D. A., Cavini, I. A., Sala, F. A., Mendonça, D. C., Rosa, H. V. D., Kumagai, P. S., et al. (2021). Orientational Ambiguity in Septin Coiled Coils and its Structural Basis. *J. Mol. Biol.* 433, 166889. doi:10.1016/j.jmb.2021.166889

Li, H., Saucedo-Cuevas, L., Yuan, L., Ross, D., Johansen, A., Sands, D., et al. (2019). Zika Virus Protease Cleavage of Host Protein Septin-2 Mediates Mitotic Defects in Neural Progenitors. *Neuron* 101, 1089–1098. doi:10.1016/j.neuron.2019.01.010

Longtine, M. S., DeMarini, D. J., Valencik, M. L., Al-Awar, O. S., Fares, H., De Virgilio, C., et al. (1996). The Septins: Roles in Cytokinesis and Other Processes. *Curr. Opin. Cel Biol.* 8, 106–119. doi:10.1016/s0955-0674(96)80054-8

Longtine, M. S., Theesfeld, C. L., McMillan, J. N., Weaver, E., Pringle, J. R., and Lew, D. J. (2000). Septin-dependent Assembly of a Cell Cycle-Regulatory Module in Saccharomyces cerevisiae. *Mol. Cel. Biol.* 20, 4049–4061. doi:10.1128/mcb.20.11.4049-4061.2000

Low, C., and Macara, I. G. (2006). Structural Analysis of Septin 2, 6, and 7 Complexes. *J. Biol. Chem.* 281, 30697–30706. doi:10.1074/jbc.M605179200

Lupas, A. N., and Bassler, J. (2017). Coiled Coils - A Model System for the 21st Century. *Trends Biochem. Sci.* 42, 130–140. doi:10.1016/j.tibs.2016.10.007

Macedo, J. N. A., Valadares, N. F., Marques, I. A., Ferreira, F. M., Damalio, J. C. P., Pereira, H. M., et al. (2013). The Structure and Properties of Septin 3: a Possible Missing Link in Septin Filament Formation. *Biochem. J.* 450, 95–105. doi:10.1042/bj20120851

Marquardt, J., Chen, X., and Bi, E. (2019). Architecture, Remodeling, and Functions of the Septin Cytoskeleton. *Cytoskeleton* 76, 7–14. doi:10.1002/cm.21475

Marquardt, J., Yao, L.-L., Okada, H., Svitkina, T., and Bi, E. (2020). The LKB1-like Kinase Elm1 Controls Septin Hourglass Assembly and Stability by Regulating Filament Pairing. *Curr. Biol.* 30, 2386–2394. doi:10.1016/j.cub.2020.04.035

Mavrakis, M., Azou-Gros, Y., Tsai, F.-C., Alvarado, J., Bertin, A., Iv, F., et al. (2014). Septins Promote F-Actin Ring Formation by Crosslinking Actin Filaments into Curved Bundles. *Nat. Cel Biol.* 16, 322–334. doi:10.1038/ncb2921

McMurray, M. A., Bertin, A., Garcia, G., III, Lam, L., Nogales, E., and Thorner, J. (2011). Septin Filament Formation Is Essential in Budding Yeast. *Develop. Cel* 20, 540–549. doi:10.1016/j.devcel.2011.02.004

Mela, A., and Momany, M. (2019). Septin Mutations and Phenotypes in S. cerevisiae. *Cytoskeleton* 76, 33–44. doi:10.1002/cm.21492

Mendonça, D. C., Guimarães, S. L., Pereira, H. D. M., Pinto, A. A., de Farias, M. A., de Godoy, A. S., et al. (2021). An Atomic Model for the Human Septin Hexamer by Cryo-EM. *J. Mol. Biol.* 433, 167096. doi:10.1016/j.jmb.2021.167096

Mendonça, D. C., Macedo, J. N., Guimarães, S. L., Barroso da Silva, F. L., Cassago, A., Garratt, R. C., et al. (2019). A Revised Order of Subunits in Mammalian Septin Complexes. *Cytoskeleton* 76, 457–466. doi:10.1002/cm.21569

Meseroll, R. A., Occhipinti, P., and Gladfelter, A. S. (2013). Septin Phosphorylation and Coiled-Coil Domains Function in Cell and Septin Ring Morphology in the Filamentous Fungus Ashbya Gossypii. *Eukaryot. Cel.* 12, 182–193. doi:10.1128/ec.00251-12

Mostowy, S., Bonazzi, M., Hamon, M. A., Tham, T. N., Mallet, A., Lelek, M., et al. (2010). Entrapment of Intracytosolic Bacteria by Septin Cage-like Structures. *Cell Host & Microbe* 8, 433–444. doi:10.1016/j.chom.2010.10.009

Mostowy, S., and Cossart, P. (2012). Septins: the Fourth Component of the Cytoskeleton. *Nat. Rev. Mol. Cell Biol.* 13, 183–194. doi:10.1038/nrm3284

Nagata, K.-I., and Inagaki, M. (2005). Cytoskeletal Modification of Rho Guanine Nucleotide Exchange Factor Activity: Identification of a Rho Guanine Nucleotide Exchange Factor as a Binding Partner for Sept9b, a Mammalian Septin. *Oncogene* 24, 65–76. doi:10.1038/sj.onc.1208101

Nakahira, M., Macedo, J. N. A., Seraphim, T. V., Cavalcante, N., Souza, T. A. C. B., Damalio, J. C. P., et al. (2010). A Draft of the Human Septin Interactome. *PLoS One* 5, e13799. doi:10.1371/journal.pone.0013799

Nakos, K., Radler, M. R., and Spiliotis, E. T. (2019a). Septin 2/6/7 Complexes Tune Microtubule Plus-End Growth and EB1 Binding in a Concentration- and Filament-dependent Manner. *MBoC* 30, 2913–2928. doi:10.1091/mbc.e19-07-0362

Nakos, K., Rosenberg, M., and Spiliotis, E. T. (2019b). Regulation of Microtubule Plus End Dynamics by Septin 9. *Cytoskeleton* 76, 83–91. doi:10.1002/cm.21488

Neubauer, K., and Zieger, B. (2017). The Mammalian Septin Interactome. *Front. Cell Dev. Biol.* 5, 3. doi:10.3389/fcell.2017.00003

Nguyen, T. Q., Sawa, H., Okano, H., and White, J. G. (2000). The C. elegans Septin Genes, Unc-59 and Unc-61, Are Required for normal Postembryonic Cytokineses and Morphogenesis but Have No Essential Function in Embryogenesis. *J. Cel Sci.* 113, 3825–3837. doi:10.1242/jcs.113.21.3825

Nishihama, R., Onishi, M., and Pringle, J. R. (2011). New Insights into the Phylogenetic Distribution and Evolutionary Origins of the Septins. *Biol. Chem.* 392, 681–687. doi:10.1515/BC.2011.086

Nölke, T., Schwan, C., Lehmann, F., Østevold, K., Pertz, O., and Aktories, K. (2016). Septins Guide Microtubule Protrusions Induced by Actin-Depolymerizing Toxins likeClostridium Difficiletransferase (CDT). *Proc. Natl. Acad. Sci. USA* 113, 7870–7875. doi:10.1073/pnas.1522717113

Omrane, M., Camara, A. S., Taveneau, C., Benzoubir, N., Tubiana, T., Yu, J., et al. (2019). Septin 9 Has Two Polybasic Domains Critical to Septin Filament Assembly and Golgi Integrity. *iScience* 13, 138–153. doi:10.1016/j.isci.2019.02.015

Pai, E. F., Kabsch, W., Krengel, U., Holmes, K. C., John, J., and Wittinghofer, A. (1989). Structure of the Guanine-Nucleotide-Binding Domain of the Ha-Ras Oncogene Product P21 in the Triphosphate Conformation. *Nature* 341, 209–214. doi:10.1038/341209a0

Pai, E. F., Krengel, U., Petsko, G. A., Goody, R. S., Kabsch, W., and Wittinghofer, A. (1990). Refined crystal Structure of the Triphosphate Conformation of H-Ras P21 at 1.35 A Resolution: Implications for the Mechanism of GTP Hydrolysis. *EMBO J.* 9, 2351–2359. doi:10.1002/j.1460-2075.1990.tb07409.x

Palander, O., El-Zeiry, M., and Trimble, W. S. (2017). Uncovering the Roles of Septins in Cilia. *Front. Cell Dev. Biol.* 5, 36. doi:10.3389/fcell.2017.00036

Pan, F., Malmberg, R. L., and Momany, M. (2007). Analysis of Septins across Kingdoms Reveals Orthology and New Motifs. *BMC Evol. Biol.* 7, 103. doi:10.1186/1471-2148-7-103

Peterson, E., and Petty, E. (2010). Conquering the Complex World of Human Septins: Implications for Health and Disease. *Clin. Genet.* 77, 511–524. doi:10.1111/j.1399-0004.2010.01392.x

Pinto, A. P. A., Pereira, H. M., Zeraik, A. E., Ciol, H., Ferreira, F. M., Brandão-Neto, J., et al. (2017). Filaments and Fingers: Novel Structural Aspects of the Single Septin from Chlamydomonas Reinhardtii. *J. Biol. Chem.* 292, 10899–10911. doi:10.1074/jbc.m116.762229

Pissuti Damalio, J. C., Garcia, W., Alves Macêdo, J. N., de Almeida Marques, I., Andreu, J. M., Giraldo, R., et al. (2012). Self Assembly of Human Septin 2 into Amyloid Filaments. *Biochimie* 94, 628–636. doi:10.1016/j.biochi.2011.09.014

Ribet, D., Boscaini, S., Cauvin, C., Siguier, M., Mostowy, S., Echard, A., et al. (2017). SUMOylation of Human Septins Is Critical for Septin Filament Bundling and Cytokinesis. *J. Cel Biol.* 216, 4041–4052. doi:10.1083/jcb.201703096

Robertin, S., and Mostowy, S. (2020). The History of Septin Biology and Bacterial Infection. *Cell. Microbiol.* 22, e13173. doi:10.1111/cmi.13173

Rosa, H. V. D., Leonardo, D. A., Brognara, G., Brandão-Neto, J., D'Muniz Pereira, H., Araújo, A. P. U., et al. (2020). Molecular Recognition at Septin Interfaces: the Switches Hold the Key. *J. Mol. Biol.* 432, 5784–5801. doi:10.1016/j.jmb.2020.09.001

Russell, S. E. H., and Hall, P. A. (2011). Septin Genomics: A Road Less Travelled. *Biol. Chem.* 392, 763–767. doi:10.1515/BC.2011.079

Ruszkowski, M., and Dauter, Z. (2016). On Methylene-Bridged Cysteine and Lysine Residues in Proteins. *Protein Sci.* 25, 1734–1736. doi:10.1002/pro.2958

Sala, F. A., Valadares, N. F., Macedo, J. N. A., Borges, J. C., and Garratt, R. C. (2016). Heterotypic Coiled-Coil Formation Is Essential for the Correct Assembly of the Septin Heterofilament. *Biophysical J.* 111, 2608–2619. doi:10.1016/j.bpj.2016.10.032

Sandrock, K., Bartsch, I., Bläser, S., Busse, A., Busse, E., and Zieger, B. (2011). Characterization of Human Septin Interactions. *Biol. Chem.* 392, 751–761. doi:10.1515/BC.2011.081

Sellin, M. E., Sandblad, L., Stenmark, S., and Gullberg, M. (2011). Deciphering the Rules Governing Assembly Order of Mammalian Septin Complexes. *MBoC* 22, 3152–3164. doi:10.1091/mbc.e11-03-0253

Sellin, M. E., Stenmark, S., and Gullberg, M. (2014). Cell Type-specific Expression of SEPT3-Homology Subgroup Members Controls the Subunit Number of Heteromeric Septin Complexes. *MBoC* 25, 1594–1607. doi:10.1091/mbc.e13-09-0553

Serrão, V. H. B., Alessandro, F., Caldas, V. E. A., Marçal, R. L., D'Muniz Pereira, H., Thiemann, O. H., et al. (2011). Promiscuous Interactions of Human Septins: the GTP Binding Domain of SEPT7 Forms Filaments within the crystal. *Febs Lett.* 585, 3868–3873. doi:10.1016/j.febslet.2011.10.043

Sheffield, P. J., Oliver, C. J., Kremer, B. E., Sheng, S., Shao, Z., and Macara, I. G. (2003). Borg/septin Interactions and the Assembly of Mammalian Septin Heterodimers, Trimers, and Filaments. *J. Biol. Chem.* 278, 3483–3488. doi:10.1074/jbc.m209701200

Sirajuddin, M., Farkasovsky, M., Hauer, F., Kühlmann, D., Macara, I. G., Weyand, M., et al. (2007). Structural Insight into Filament Formation by Mammalian Septins. *Nature* 449, 311–315. doi:10.1038/nature06052

Sirajuddin, M., Farkasovsky, M., Zent, E., Wittinghofer, A., and Fersht, A. (2009). GTP-induced Conformational Changes in Septins and Implications for Function. *Proc. Natl. Acad. Sci.* 106, 16592–16597. doi:10.1073/pnas.0902858106

Smith, C., Dolat, L., Angelis, D., Forgacs, E., Spiliotis, E. T., and Galkin, V. E. (2015). Septin 9 Exhibits Polymorphic Binding to F-Actin and Inhibits Myosin and Cofilin Activity. *J. Mol. Biol.* 427, 3273–3284. doi:10.1016/j.jmb.2015.07.026

Soroor, F., Kim, M. S., Palander, O., Balachandran, Y., Collins, R. F., Benlekbir, S., et al. (2021). Revised Subunit Order of Mammalian Septin Complexes Explains Their *In-Vitro* Polymerization Properties. *Mol. Biol. Cel* 32, 289–300. doi:10.1091/mbc.e20-06-0398

Spiliotis, E. T. (2018). Spatial Effects - site-specific Regulation of Actin and Microtubule Organization by Septin GTPases. *J. Cel Sci.* 131, jcs207555. doi:10.1242/jcs.207555

Spiliotis, E. T., and Gladfelter, A. S. (2012). Spatial Guidance of Cell Asymmetry: Septin GTPases Show the Way. *Traffic* 13, 195–203. doi:10.1111/j.1600-0854.2011.01268.x

Spiliotis, E. T., and McMurray, M. A. (2020). Masters of Asymmetry - Lessons and Perspectives from 50 Years of Septins. *MBoC* 31, 2289–2297. doi:10.1091/mbc.e19-11-0648

Spiliotis, E. T., and Nakos, K. (2021). Cellular Functions of Actin- and Microtubule-Associated Septins. *Curr. Biol.* 31, R651–R666. doi:10.1016/j.cub.2021.03.064

Sun, Y.-J., Forouhar, F., Li, H.-m., Tu, S.-L., Yeh, Y.-H., Kao, S., et al. (2002). Crystal Structure of Pea Toc34, a Novel Gtpase of the Chloroplast Protein Translocon. *Nat. Struct. Biol.* 9, 95–100. doi:10.1038/nsb744

Szuba, A., Bano, F., Castro-Linares, G., Iv, F., Mavrakis, M., Richter, R. P., et al. (2021). Membrane Binding Controls Ordered Self-Assembly of Animal Septins. *Elife* 10, e63349. doi:10.7554/eLife.63349

Takahashi, Y., Iwase, M., Konishi, M., Tanaka, M., Toh-e, A., and Kikuchi, Y. (1999). Smt3, a SUMO-1 Homolog, Is Conjugated to Cdc3, a Component of Septin Rings at the Mother-Bud Neck in Budding Yeast. *Biochem. Biophysical Res. Commun.* 259, 582–587. doi:10.1006/bbrc.1999.0821

Tamborrini, D., Juanes, M. A., Ibanes, S., Rancati, G., and Piatti, S. (2018). Recruitment of the Mitotic Exit Network to Yeast Centrosomes Couples Septin Displacement to Actomyosin Constriction. *Nat. Commun.* 9, 4308–4315. doi:10.1038/s41467-018-06767-0

Tanaka-Takiguchi, Y., Kinoshita, M., and Takiguchi, K. (2009). Septin-mediated Uniform Bracing of Phospholipid Membranes. *Curr. Biol.* 19, 140–145. doi:10.1016/j.cub.2008.12.030

Taveneau, C., Blanc, R., Péhau-Arnaudet, G., Di Cicco, A., and Bertin, A. (2020). Synergistic Role of Nucleotides and Lipids for the Self-Assembly of Shs1 Septin Oligomers. *Biochem. J.* 477, 2697–2714. doi:10.1042/bcj20200199

Tokhtaeva, E., Capri, J., Marcus, E. A., Whitelegge, J. P., Khuzakhmetova, V., Bukharaeva, E., et al. (2015). Septin Dynamics Are Essential for Exocytosis. *J. Biol. Chem.* 290, 5280–5297. doi:10.1074/jbc.m114.616201

Valadares, N. F., d' Muniz Pereira, H., Ulian Araujo, A. P., and Garratt, R. C. (2017). Septin Structure and Filament Assembly. *Biophys. Rev.* 9, 481–500. doi:10.1007/s12551-017-0320-4

Van Damme, P., Lasa, M., Polevoda, B., Gazquez, C., Elosegui-Artola, A., Kim, D. S., et al. (2012). N-terminal Acetylome Analyses and Functional Insights of the N-Terminal Acetyltransferase NatB. *Proc. Natl. Acad. Sci.* 109, 12449–12454. doi:10.1073/pnas.1210303109

Verdier-Pinard, P., Salaun, D., Bouguenina, H., Shimada, S., Pophillat, M., Audebert, S., et al. (2017). Septin 9_i2 Is Downregulated in Tumors, Impairs Cancer Cell Migration and Alters Subnuclear Actin Filaments. *Sci. Rep.* 7. doi:10.1038/srep44976

Versele, M., Gullbrand, B., Shulewitz, M. J., Cid, V. J., Bahmanyar, S., Chen, R. E., et al. (2004). Protein-Protein Interactions Governing Septin Heteropentamer Assembly and Septin Filament Organization inSaccharomyces Cerevisiae. *MBoC* 15, 4568–4583. doi:10.1091/mbc.e04-04-0330

Versele, M., and Thorner, J. (2004). Septin Collar Formation in Budding Yeast Requires GTP Binding and Direct Phosphorylation by the PAK, Cla4. *J. Cel Biol.* 164, 701–715. doi:10.1083/jcb.200312070

Vetter, I. R., and Wittinghofer, A. (2001). The Guanine Nucleotide-Binding Switch in Three Dimensions. *Science* 294, 1299–1304. doi:10.1126/science.1062023

Vial, A., Taveneau, C., Costa, L., Chauvin, B., Nasrallah, H., Godefroy, C., et al. (2021). Correlative AFM and Fluorescence Imaging Demonstrate Nanoscale Membrane Remodeling and Ring-like and Tubular Structure Formation by Septins. *Nanoscale* 13, 12484–12493. doi:10.1039/d1nr01978c

Walker, J. E., Saraste, M., Runswick, M. J., and Gay, N. J. (1982). Distantly Related Sequences in the Alpha- and Beta-Subunits of ATP Synthase, Myosin, Kinases and Other ATP-Requiring Enzymes and a Common Nucleotide Binding Fold. *EMBO J.* 1, 945–951. doi:10.1002/j.1460-2075.1982.tb01276.x

Wang, J. (2019). Crystallographic Identification of Spontaneous Oxidation Intermediates and Products of Protein Sulfhydryl Groups. *Protein Sci.* 28, 472–477. doi:10.1002/pro.3568

Weems, A., and McMurray, M. (2017). The Step-wise Pathway of Septin Hetero-Octamer Assembly in Budding Yeast. *Elife* 6, e23689. doi:10.7554/eLife.23689

Weirich, C. S., Erzberger, J. P., and Barral, Y. (2008). The Septin Family of GTPases: Architecture and Dynamics. *Nat. Rev. Mol. Cell Biol.* 9, 478–489. doi:10.1038/nrm2407

Wensien, M., von Pappenheim, F. R., Funk, L.-M., Kloskowski, P., Curth, U., Diederichsen, U., et al. (2021). A Lysine-Cysteine Redox Switch with an NOS Bridge Regulates Enzyme Function. *Nature* 593, 460–464. doi:10.1038/s41586-021-03513-3

Willis, A., Mazon-Moya, M., and Mostowy, S. (2016). Investigation of Septin Biology *In Vivo* Using Zebrafish. *Methods Cel Biol.* 136, 221–241. doi:10.1016/bs.mcb.2016.03.019

Woods, B. L., Cannon, K. S., Vogt, E. J. D., Crutchley, J. M., and Gladfelter, A. S. (2021). Interplay of Septin Amphipathic Helices in Sensing Membrane-Curvature and Filament Bundling. *Mol. Biol. Cel.* 32, br5. doi:10.1091/mbc.e20-05-0303

Woolfson, D. N. (2017). Coiled-Coil Design: Updated and Upgraded. *Subcell Biochem.*, 35–61. doi:10.1007/978-3-319-49674-0_2

Zent, E., Vetter, I., and Wittinghofer, A. (2011). Structural and Biochemical Properties of Sept7, a Unique Septin Required for Filament Formation. *Biol. Chem.* 392, 791–797. doi:10.1515/BC.2011.082

Zent, E., and Wittinghofer, A. (2014). Human Septin Isoforms and the GDP-GTP Cycle. *Biol. Chem.* 395, 169–180. doi:10.1515/hsz-2013-0268

Zeraik, A. E., Pereira, H. M., Santos, Y. V., Brandão-Neto, J., Spoerner, M., Santos, M. S., et al. (2014). Crystal Structure of a Schistosoma Mansoni Septin Reveals the Phenomenon of Strand Slippage in Septins Dependent on the Nature of the Bound Nucleotide. *J. Biol. Chem.* 289, 7799–7811. doi:10.1074/jbc.m113.525352

Zeraik, A. E., Staykova, M., Fontes, M. G., Nemuraitė, I., Quinlan, R., Araújo, A. P. U., et al. (2016). Biophysical Dissection of Schistosome Septins: Insights into Oligomerization and Membrane Binding. *Biochimie* 131, 96–105. doi:10.1016/j.biochi.2016.09.014

Zhang, J., Kong, C., Xie, H., McPherson, P. S., Grinstein, S., and Trimble, W. S. (1999). Phosphatidylinositol Polyphosphate Binding to the Mammalian Septin H5 Is Modulated by GTP. *Curr. Biol.* 9, 1458–1467. doi:10.1016/S0960-9822(00)80115-3

Zhang, Y., Gao, J., Chung, K. K. K., Huang, H., Dawson, V. L., and Dawson, T. M. (2000). Parkin Functions as an E2-dependent Ubiquitin- Protein Ligase and Promotes the Degradation of the Synaptic Vesicle-Associated Protein, CDCrel-1. *Proc. Natl. Acad. Sci.* 97, 13354–13359. doi:10.1073/pnas.240347797

Zhou, H., Di Palma, S., Preisinger, C., Peng, M., Polat, A. N., Heck, A. J. R., et al. (2013). Toward a Comprehensive Characterization of a Human Cancer Cell Phosphoproteome. *J. Proteome Res.* 12, 260–271. doi:10.1021/pr300630k

Zuvanov, L., Mota, D. M. D., Araujo, A. P. U., and DeMarco, R. (2019). A Blueprint of Septin Expression in Human Tissues. *Funct. Integr. Genomics* 19, 787–797. doi:10.1007/s10142-019-00690-3

Conflict of Interest: The authors declare that the research was conducted in the absence of any commercial or financial relationships that could be construed as a potential conflict of interest.

Publisher's Note: All claims expressed in this article are solely those of the authors and do not necessarily represent those of their affiliated organizations, or those of the publisher, the editors and the reviewers. Any product that may be evaluated in this article, or claim that may be made by its manufacturer, is not guaranteed or endorsed by the publisher.

frontiers in Cell and Developmental Biology

MINI REVIEW
published: 25 November 2021
doi: 10.3389/fcell.2021.793920

Septin Assembly and Remodeling at the Cell Division Site During the Cell Cycle

Joseph Marquardt[†], *Xi Chen*[†] *and Erfei Bi* *

Department of Cell and Developmental Biology, Perelman School of Medicine, University of Pennsylvania, Philadelphia, PA, United States

The septin family of proteins can assemble into filaments that further organize into different higher order structures to perform a variety of different functions in different cell types and organisms. In the budding yeast *Saccharomyces cerevisiae*, the septins localize to the presumptive bud site as a cortical ring prior to bud emergence, expand into an hourglass at the bud neck (cell division site) during bud growth, and finally "split" into a double ring sandwiching the cell division machinery during cytokinesis. While much work has been done to understand the functions and molecular makeups of these structures, the mechanisms underlying the transitions from one structure to another have largely remained elusive. Recent studies involving advanced imaging and *in vitro* reconstitution have begun to reveal the vast complexity involved in the regulation of these structural transitions, which defines the focus of discussion in this mini-review.

Keywords: septins, septin-associated proteins, RhoGEF, anillin, Elm1, Bud3, Bud4

OPEN ACCESS

Edited by:
Matthias Gaestel,
Hannover Medical School, Germany

Reviewed by:
Michael McMurray,
University of Colorado Denver, United States
Simonetta Piatti,
Délégation Languedoc Roussillon (CNRS), France

***Correspondence:**
Erfei Bi
ebi@pennmedicine.upenn.edu

[†]*These authors have contributed equally to this work*

Specialty section:
This article was submitted to Signaling, a section of the journal Frontiers in Cell and Developmental Biology

Received: *12 October 2021*
Accepted: *08 November 2021*
Published: *25 November 2021*

Citation:
Marquardt J, Chen X and Bi E (2021) Septin Assembly and Remodeling at the Cell Division Site During the Cell Cycle. Front. Cell Dev. Biol. 9:793920. doi: 10.3389/fcell.2021.793920

INTRODUCTION

Septins are GTP-binding proteins that assemble into heteropolymers that can organize into various filament-containing structures such as rings, hourglasses, and gauzes in different cell types (Byers and Goetsch, 1976a; Kim et al., 1991; Frazier et al., 1998; Lippincott et al., 2001; Ihara et al., 2005; Kissel et al., 2005; Rodal et al., 2005; John et al., 2007; Sirajuddin et al., 2007; Tada et al., 2007; Xie et al., 2007; Bertin et al., 2008; Ong et al., 2014; Renshaw et al., 2014; Karasmanis et al., 2019; Wang et al., 2019). As such, they are considered the fourth cytoskeletal component along with microfilaments, intermediate filaments, and microtubules (Mostowy and Cossart, 2012). Septins play critical roles in cytokinesis, exocytosis, mitosis, ciliogenesis, and cell morphogenesis by acting as a cellular scaffold and/or diffusion barrier (Longtine et al., 1996; Gladfelter et al., 2001; Weirich et al., 2008; McMurray and Thorner, 2009; Oh and Bi, 2011; Mostowy and Cossart, 2012; Dolat et al., 2014). Not surprisingly, mutations in human septin genes have been linked to several diseases including male infertility, cancer, and neurodegenerative diseases (Hall and Russell, 2004; Roeseler et al., 2009; Lin et al., 2011; Dolat et al., 2014; Ageta-Ishihara and Kinoshita, 2021).

Septins are conserved in eukaryotes except higher land plants (Pan et al., 2007). In humans, there are 13 septin genes whose products can form several different combinations of heterooligomers (usually octamers) depending on the tissue type in which they are expressed (Kinoshita, 2003; Pan et al., 2007; Estey et al., 2010; Sellin et al., 2011; Mendonca et al., 2019; Soroor et al., 2021). Additionally, many septin genes, especially *SEPT9*, code for multiple isoform variants (Robertson et al., 2004; Hall et al., 2005; Estey et al., 2010; Connolly et al., 2011a; Connolly et al., 2011b; Sellin et al., 2012). Such a complexity in septin expression and assembly has hampered the rapid progress in the analysis of human septins. Model organisms have had a major impact on our understanding of

septin biology with much of the emphasis placed on the budding yeast *Saccharomyces cerevisiae*. There are a total of seven septin genes in *S. cerevisiae*, five of which (*CDC3, CDC10, CDC11, CDC12,* and *SHS1*) are expressed in mitotically active cells (Hartwell, 1971; Byers and Goetsch, 1976b; Carroll et al., 1998; Mino et al., 1998) and the other two (*SPR3* and *SPR28*) are expressed during meiosis (Ozsarac et al., 1995; De Virgilio et al., 1996; Fares et al., 1996). The limited number of septin genes, coupled with the ease of genetic manipulation and easily scored phenotypes associated with septin malfunction, make budding yeast an excellent model organism for studying the regulation of septin organization.

To understand how septin high order structures are regulated, the precise organization of their building blocks must be known. In *S. cerevisiae*, the mitotic septins oligomerize into hetero-octamers comprised of a core Cdc12-Cdc3-Cdc10-Cdc10-Cdc3-Cdc12 hexamer with either Cdc11 or Shs1 at the terminal ends (Bertin et al., 2008; Garcia et al., 2011; Khan et al., 2018). The presence of Cdc11 or Shs1 can influence what higher order structures form *in vitro*, with Cdc11-capped octamers more likely to form paired filaments from end-on-end Cdc11 interactions (Frazier et al., 1998; Bertin et al., 2008) and Shs1-capped octamers to laterally associate into curved bundles and rings (Garcia et al., 2011). With Cdc11 and Shs1 both expressed in mitotic cells, it is possible that the regulated combination of differentially capped octamers could produce the distinct structures *in vivo*, from the nascent ring at the presumptive bud site, to the hourglass at the bud neck, and finally the double ring surrounding the cytokinesis machinery during cell division (Bertin et al., 2012; Ong et al., 2014; Mcquilken et al., 2017; Weems and McMurray, 2017; Marquardt et al., 2019).

The septin architecture is dynamically remodeled at the division site during the cell cycle, and this involves the regulation by post-translational modifications (PTMs) and septin-associated proteins (SAPs) (Gladfelter et al., 2001; McMurray and Thorner, 2009; Hernández-Rodríguez and Momany, 2012; Alonso et al., 2015; Perez et al., 2016). Many yeast septins have PTMs such as phosphorylation, acetylation, and sumoylation added or removed at precise times, which may change their architectural organization [for full reviews on these modifications see (Hernández-Rodríguez and Momany, 2012; Perez et al., 2016; Marquardt et al., 2019)]. In fact, several protein kinases such as the LKB1-like Elm1 and the MARK/PAR1-related Gin4 not only depend on septins for their localization to the bud neck, but also influence the stability or functionality of the septin structures present there (Longtine et al., 1998; Bouquin et al., 2000; Mortensen et al., 2002; Asano et al., 2006). Besides the PTMs, different SAPs are also involved in the regulation of septin organization during the cell cycle. For example, Bni5 is associated with the septin hourglass before cytokinesis (Lee et al., 2002; Fang et al., 2010) and can bundle septin filaments *in vitro* (Patasi et al., 2015; Booth et al., 2016). The Rho guanine nucleotide-exchange factor (RhoGEF) Bud3 and the anillin-like protein Bud4 can stabilize the double ring structure during cytokinesis (Wloka et al., 2011; Eluere et al., 2012; Mcquilken et al., 2017).

In this review, we will summarize and draw conclusions from recent work that has begun to illustrate the regulation that occurs at the transition times between both the nascent ring to hourglass (Marquardt et al., 2020) and the hourglass to double ring structures (Chen et al., 2020). These different structures each have specific functions at their respective stages during the cell cycle and the precise transformations over a relatively short time ensure that these functions are ordered appropriately. While we are beginning to elucidate the pathways involved in the regulation of these structural transitions, much work remains to fully comprehend the mechanisms of septin assembly and remodeling in yeast and beyond.

TRANSFORMING THE NASCENT SEPTIN RING INTO A SEPTIN HOURGLASS

Upon starting a new cell cycle, haploid cells develop a new bud site axial to the previous division site (Chant and Pringle, 1995; Pringle et al., 1995). Through a series of feedback loops involving the Rho-like small GTPase Cdc42, its GEFs, and GTPase-activating proteins, septin recruitment, and targeted exocytosis, a nascent ring is formed at the new budding site, and the growth of the bud begins (Gladfelter et al., 2002; Caviston et al., 2003; Iwase et al., 2006; Okada et al., 2013). The septin ring then expands into an hourglass spanning the bud-neck region. This septin hourglass serves as both a scaffold for the assembly of cytokinesis machinery such as the actomyosin ring (AMR) (Bi et al., 1998; Lippincott and Li, 1998; Fang et al., 2010; Schneider et al., 2013; Finnigan et al., 2015) and numerous other protein complexes such as the morphogenesis checkpoint cascade (Barral et al., 1999; Shulewitz et al., 1999; Longtine et al., 2000; Cid et al., 2001b) and as a membrane diffusion barrier to compartmentalize the mother and bud plasma membranes (Barral et al., 2000; Luedeke et al., 2005; Shcheprova et al., 2008). As a cellular scaffold, it is not surprising that the septin hourglass is highly stable when analyzed by fluorescence recovery after photo bleaching (FRAP), which is in stark contrast to the relatively mobile nature of the nascent ring during its initial assembly process (Caviston et al., 2003; Dobbelaere et al., 2003). It remains unclear whether an altered self-assembly state of septins and/or the addition of new SAPs during hourglass expansion accounts for this increased stability.

Understanding Paired and Unpaired Septin Filament Assembly and Organization *in vitro*

To understand how a stable hourglass can form from a relatively dynamic septin ring (**Figure 1A**), one must first understand how septins are assembled into filaments, which are further organized into higher-order structures such as rings and hourglasses. Yeast septins were first seen at the bud neck as a membrane-associated structure made from filaments with a 10 nm width (Byers and Goetsch, 1976a). However, when expressed and purified *in vitro* from *E. coli* or budding yeast in the presence of high salt (>300 mM KCl or NaCl) only septin rods of the approximate length of an octamer were formed

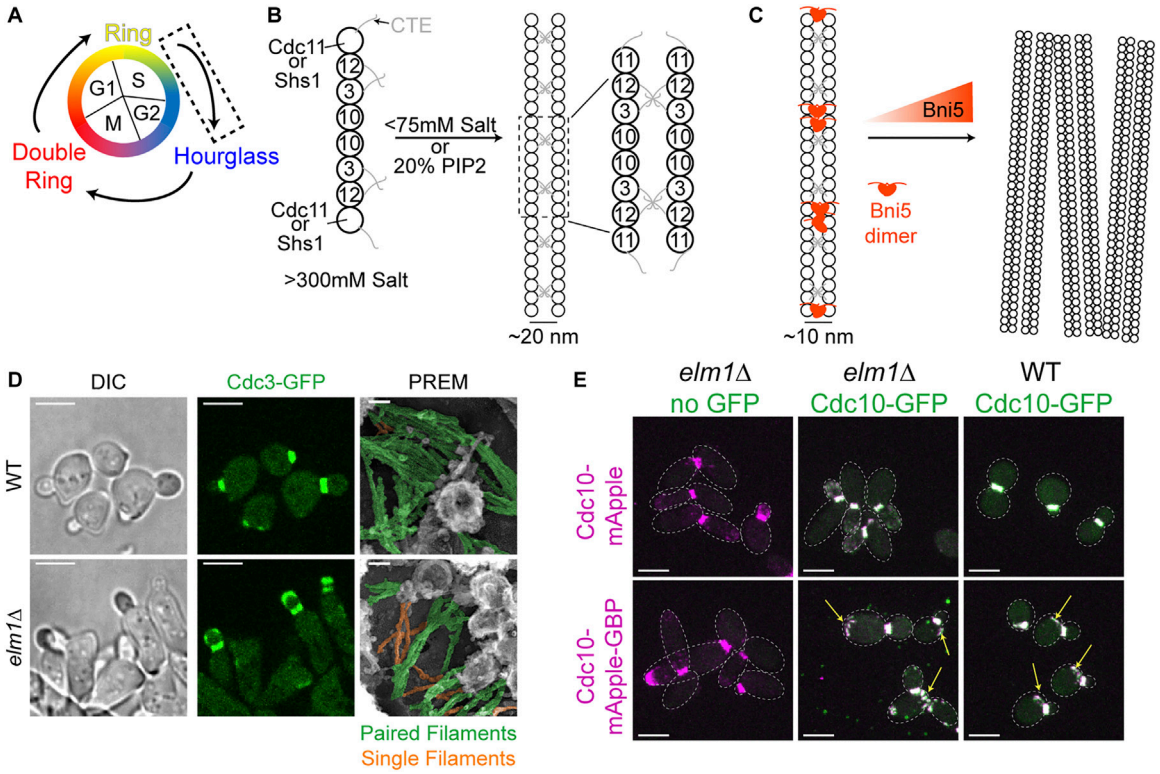

FIGURE 1 | Transitioning from a dynamic ring to a stable hourglass. **(A)** Depiction of different septin structures visualized during the yeast cell cycle. Arrows indicate transitions occurring between two structures. Dashed box indicates that the focus of this figure is on the nascent ring-to-hourglass transition that occurs during bud emergence and expansion. **(B) Left**, depiction of septin rod assembly in high salt (>300 mM KCl or NaCl) *in vitro* (Frazier et al., 1998; Bertin et al., 2008). **Right**, depiction of Cdc11-capped rods forming paired filaments in either low salt (<75 mM) (Bertin et al., 2008) or on the surface of PIP2-containing lipid monolayers (Bertin et al., 2010; Bridges et al., 2014); dashed box indicates zoomed in inset shown to the right. **(C) Left**, depiction of two Bni5 proteins (red molecules) interacting with Cdc11-CTEs found in paired septin filaments to lower the average interfilament distance to 10 nm (Finnigan et al., 2015; Booth et al., 2016). **Right**, depiction of Bni5 bundling septin filaments into large clusters *in vitro* in a dose-dependent manner (Patasi et al., 2015). **(D)** Representative images of WT **(top)** or *elm1Δ* **(bottom)** cells synchronized in G1 by α-factor arrest and released for 1.5 h to obtain small-to medium-sized buds. **Left** and **middle panels** show DIC and fluorescence imaging of Cdc3 (green), respectively; scale bars = 5 μm. **Right panels** show PREM images of samples with paired filaments pseudo-colored green and single filaments pseudo-colored orange; scale bars = 50 nm. Images taken from (Marquardt et al., 2020). **(E)** Representative images of indicated strains with Cdc10-mApple **(top row)** or Cdc10-mApple-GBP **(bottom row)** in magenta and Cdc10-GFP, which is expressed exogenously from a *CEN* plasmid, in green. Images are maximum projections. Yellow arrow indicates septin ring from previous cell cycle. Dotted line is cell periphery. Scale bars = 5 μm. Images taken from (Marquardt et al., 2020).

(**Figure 1B**, left) (Frazier et al., 1998; Bertin et al., 2008). When the ionic strength was lowered (50–75 mM salt) and with Cdc11 serving as the terminal septin subunit were filaments visualized (Frazier et al., 1998; Bertin et al., 2008), with the C-terminal extensions (CTEs) of Cdc3 and Cdc12 interacting on neighboring filaments to form the paired filaments (**Figure 1B**, right) (Bertin et al., 2008; Bertin et al., 2010). In contrast, the Shs1-capped septin rods associate laterally into curved bundles and rings *in vitro* under low salt condition (Garcia et al., 2011). While data from this study concerning the ability for Shs1-capped septin rods to assemble end-on-end into filaments is not as clear as that of Cdc11-capped septin rods, additional analysis by Förster Resonance Energy Transfer has more conclusively negated the possibility that two Shs1-capped rods can polymerize end-on-end (Booth et al., 2015). Given that the budding yeast cytoplasm has potassium and sodium concentrations of 200–300 and 20 mM, respectively (van Eunen et al., 2010; Cyert and Philpott, 2013), the ability of yeast septins to spontaneously generate filaments in the cytoplasm should be quite low.

Strikingly, in the presence of lipid monolayers containing 20% phosphatidylinositol-4,5-bisphosphate (PIP2), purified Cdc11-capped septin rods could form long paired septin filaments even at higher salt concentrations (**Figure 1B**, right) (Bertin et al., 2010; Bridges et al., 2014). This implies that septin octamers probably exist in the cytoplasm and are assembled into paired filaments once bound to the plasma membrane at the presumptive bud site or the bud neck. This indeed appears to be the case, as it was found by fluorescence correlation spectroscopy that septins in the cytoplasm exist as complexes and not as monomers or filaments (Bridges et al., 2014). The septin complexes appear to "sense" and favor the membrane curvature found at the bud neck, as the purified septin complexes preferentially engaged with lipid-coated beads of diameters producing a similar positive curvature as that found at the bud neck (Bridges et al., 2016; Cannon et al., 2019). The

organization of the septin filaments into higher-order structures may also be governed by the changes in membrane curvature during bud growth and cytokinesis, as suggested by a recent study that examined and modeled the impact of varying degrees of positive and negative curvature on septin filament assembly and organization on lipid-covered surfaces *in vitro* (Beber et al., 2019).

Higher-order assemblies of septins are likely regulated by PTMs as well as SAPs (Gladfelter et al., 2001; Mcmurray and Thorner, 2009; Hernández-Rodríguez and Momany, 2012; Alonso et al., 2015; Perez et al., 2016). One such SAP, Bni5, localizes to the bud neck in a septin-dependent manner (Lee et al., 2002). Bni5 appears to interact with the CTEs of the terminal subunits Cdc11 and Shs1 *in vitro* and *in vivo* (**Figure 1C**) (Finnigan et al., 2015; Booth et al., 2016). Recombinant Bni5 can reduce the distance between individual filaments of a paired filament and can also bundle septin filaments, thereby contributing to a higher-order organization (**Figures 1B,C**) (Patasi et al., 2015; Booth et al., 2016). It is possible that a combination of phospholipid composition, PTMs, and SAPs is able to bypass the need for positive curvature during the nascent septin ring formation, as there is no discernable bud neck at this point and the membrane topology at the presumptive bud site does not match the curvature preference of the septins. Taken together, the *in vitro* analysis of the ability of septins to interact with membranes, recognize membrane curvature, and recruit SAPs for higher-order organization will undoubtedly help understand the mechanisms for the assembly and regulation of the plethora of septin structures *in vivo*.

A LKB1-Like Kinase Acts as a Regulator of Septin Filament Pairing to Control Hourglass Assembly and Stabilization

Upon bud emergence or shortly after, the septins transition from a dynamic nascent ring at the presumptive bud site to a stable septin hourglass at the bud neck (Caviston et al., 2003; Dobbelaere et al., 2003). This stabilization could be caused by filament pairing as observed by thin-section EM and EM tomography (Byers and Goetsch, 1976a; Bertin et al., 2012; Bertin and Nogales, 2012) and by polarized fluorescence microscopy (Vrabioiu and Mitchison, 2006; Demay et al., 2011). These studies are not in agreement as to the orientation of the paired filaments in relation to the mother-bud axis, but are all in agreement that the hourglass seems to be made up of mainly paired filaments. This was further confirmed by our group in cell cortices visualized by platinum-replica electron microscopy (PREM) (Ong et al., 2014). The PREM data favors the orientation of radial paired filaments (about 300–400 nm in length) in an "early hourglass" being parallel to the mother-bud axis as postulated by the groups using polarized fluorescence microscopy (Vrabioiu and Mitchison, 2006; Demay et al., 2011), because the presumed same paired filaments in a "late or transitional hourglass" lie perpendicular to the visualized AMR that runs circumferentially at the bud neck (Ong et al., 2014). Despite the consensus on the paired filaments making up the septin hourglass, whether and how filament pairing is regulated *in vivo* has remained elusive.

We recently provided the first evidence of such regulation using genetic perturbations and PREM analyses of the septin hourglass *in vivo* (Marquardt et al., 2020). The protein kinase Elm1 localizes to the bud neck from bud emergence to the onset of cytokinesis in a septin dependent manner (Bouquin et al., 2000; Kang et al., 2016; Marquardt et al., 2020). This localization pattern matches perfectly with the timing of septin hourglass assembly and maintenance at the bud neck. Elm1 had already been implicated in maintaining the stability of septin structures at the bud neck (Bouquin et al., 2000; Asano et al., 2006), but the underlying mechanism had remained unknown at the time. We discovered that the septin hourglass was selectively destabilized with mostly the daughter half of the hourglass mislocalized to the growing bud cortex in *elm1Δ* mutants in both a kinase-dependent and -independent manner (**Figure 1D**, left and center panels) and that these phenotypes are at least partially mediated through Bni5 (Marquardt et al., 2020). This destabilization appears to be largely due to an increase in single septin filaments comprising the septin hourglass-like structure when visualized by PREM (**Figure 1D**, right panels) (Marquardt et al., 2020). This was confirmed by artificially pairing septin filaments using the GFP-nanobody/binding protein (GBP) system (Rothbauer et al., 2006; Kubala et al., 2010) and witnessing a significant rescue of the septin phenotype at the hourglass stage in *elm1Δ* cells (**Figure 1E**) (Marquardt et al., 2020). The same experiment also provided evidence that septin filament pairing and unpairing are likely regulated throughout the cell cycle, because aberrant septin structures at the old division site remained even in otherwise wild-type (WT) cells when the septins were forced to stay paired (**Figure 1E**, arrows) (Marquardt et al., 2020). Thus, to understand the structural transitions or architectural remodeling, one must understand the mechanisms of septin filament pairing and unpairing during the cell cycle.

TRANSFORMING THE SEPTIN HOURGLASS INTO A DOUBLE RING

At the onset of cytokinesis in *S. cerevisiae*, the septin hourglass undergoes a dramatic architectural remodeling by "splitting" into two separate rings (**Figure 2A**), which allows the AMR to access the plasma membrane and initiate its constriction (Kim et al., 1991; Cid et al., 2001a; Lippincott et al., 2001; Tamborrini et al., 2018). A similar transition occurs in the fission yeast *Schizosaccharomyces pombe* (Berlin et al., 2003; Tasto et al., 2003) as well as the filamentous fungus *Aspergillus nidulans* (Westfall and Momany, 2002). In mammalian cells (Renshaw et al., 2014; Karasmanis et al., 2019; Wang et al., 2019), septins also undergo reorganization from an hourglass-like structure during cleavage furrow ingression to a double ring during abscission. Despite the striking similarity of septin architectural remodeling at the division site across species, the molecular mechanisms underlying this process remain largely unknown in any system.

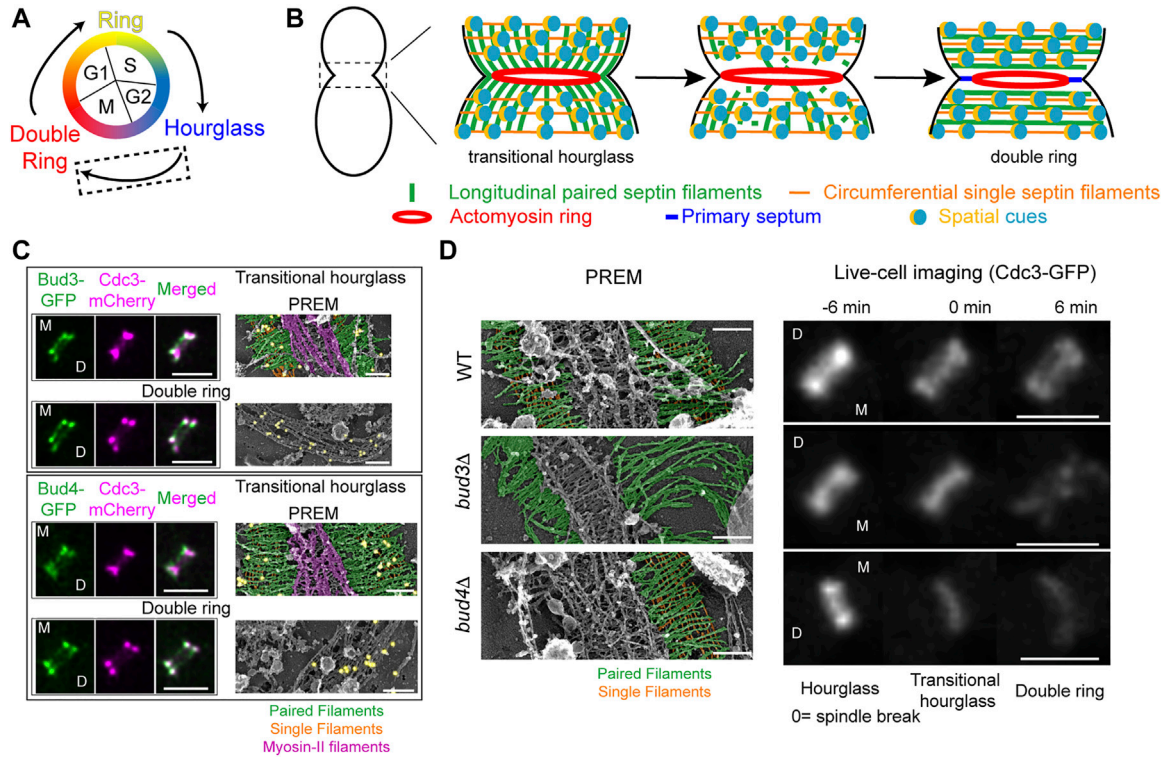

FIGURE 2 | Transitioning from an hourglass to a double ring. **(A)** Depiction of different septin structures visualized during the yeast cell cycle. Arrows indicate transitions occurring between two structures. Dashed box indicates that the focus of this figure is on the hourglass-to-double ring transition that occurs at the onset of cytokinesis. **(B)** A model of septin architectural remodeling at the division site. **(C)** Bud3 **(green, top)** and Bud4 **(green, bottom)** localization in relation to the septin hourglass and double ring (magenta) at the bud neck by iSIM. Scale bars = 2 μm. Immunogold labeling PREM analysis of Bud3 **(yellow, top)** and Bud4 **(yellow, bottom)** localization in relation to the septin transitional hourglass and double ring **(right panels)**. Scale bar = 200 nm. Paired filaments (green), single filaments (orange), and myosin-II filaments (purple). Images taken from (Chen et al., 2020). **(D)** PREM analysis of the transitional hourglass **(left panels)** with paired filaments pseudo-colored green and single filaments pseudo-colored orange; scale bars = 200 nm. Images taken from (Chen et al., 2020). Representative images of septin organization (Cdc3-GFP) at the bud neck during the HDR transition in WT **(top)**, *bud3Δ* **(middle)**, and *bud4Δ* **(bottom)** cells **(right panels)**. Scale bars = 2 μm. Images taken from (Chen et al., 2020).

Spatially Controlled Septin Filament Disassembly and Reorganization During the Hourglass-to-Double Ring Transition

Two major events are associated with the septin hourglass-to-double ring (HDR) transition: septin filament disassembly and reorganization. FRAP analysis indicates that septins become more dynamic during the HDR transition (Caviston et al., 2003; Dobbelaere et al., 2003). This dynamic change is accompanied by the net loss of septins at the division site by 20–30%, implicating septin filament disassembly in the process (Caviston et al., 2003; Dobbelaere et al., 2003; Demay et al., 2011; Wloka et al., 2011). Analysis by polarized fluorescence microscopy suggests that paired septin filaments reorganize from a radial arrangement in the hourglass to a circumferential arrangement in the double ring, a 90° change in filament orientation (Vrabioiu and Mitchison, 2006; Demay et al., 2011). Despite these insights, the detailed architectures of the septin hourglass and double ring at the filament level and the molecular mechanisms controlling the HDR transition remained unknown.

By combining cell synchronization with PREM, we have determined the architecture of different septin assemblies at the division site during the cell cycle (Ong et al., 2014; Chen et al., 2020; Marquardt et al., 2020). The "early hourglass" from pre-anaphase cells contains exclusively paired filaments arranged radially and parallel to the mother-bud axis (Ong et al., 2014). This structure is converted into a "transitional hourglass" before cytokinesis, in which the paired filaments are connected perpendicularly by periodic circumferential single septin filaments on the membrane-proximal side (Ong et al., 2014). Strikingly, these intersecting septin filaments, which define a septin gauze, are located exclusively at the outer zones of the transitional hourglass whereas myosin-II filaments occupy the middle zone but exclusively on the cytoplasmic side of the hourglass (**Figure 2B**, left) (Ong et al., 2014; Chen et al., 2020). At the onset of cytokinesis and under the control of the mitotic exit network (Cid et al., 2001a; Lippincott et al., 2001; Ong et al., 2014; Tamborrini et al., 2018; Chen et al., 2020), this "zonal" transitional hourglass is remodeled into a double ring that consists of exclusively circumferential paired and single septin filaments (**Figure 2B**, right) (Ong et al., 2014; Chen et al., 2020).

These distinct architectures revealed by PREM analysis provide a foundational blueprint for mechanistic analysis of septin high-order assembly and remodeling.

In addition to septin filament disassembly (**Figure 2B**, center) (Caviston et al., 2003; Dobbelaere et al., 2003; Demay et al., 2011; Wloka et al., 2011), careful analysis of septin behavior during the HDR transition by FRAP, photo-activation, photoconversion, and super-resolution microscopy suggests that there must be "spatial cues" present at the ends of the septin hourglass that controls septin filament reassembly and reorganization into a double ring (**Figure 2B**) (Ong et al., 2014). What are the spatial cues? How do they control the HDR transition? These questions remained unanswered.

A RhoGEF and an Anillin Act Together as the Spatial Cues to Drive the Septin Hourglass-to-Double Ring Transition

Our recent work suggests that the RhoGEF Bud3 and the anillin-like protein Bud4 function as the spatial cues to drive the HDR transition (Chen et al., 2020). Bud3 and Bud4 were initially identified as factors essential for axial budding in *S. cerevisiae* (Chant et al., 1995; Sanders and Herskowitz, 1996). Bud3 also acts as a GEF for Cdc42 in early G1 phase to spatially link successive polarization or budding events in haploid cells (Kang et al., 2014). Bud3 and Bud4 interact with each other (Kang et al., 2012; Kang et al., 2013; Wu et al., 2015) and associate with the septin hourglass after S/G2 and with the septin double ring after the HDR transition in a nearly identical pattern (**Figure 2C**, left) (Chant et al., 1995; Sanders and Herskowitz, 1996; Wloka et al., 2011; Kang et al., 2013; Chen et al., 2020). PREM coupled with immunogold labeling indicates that Bud3 and Bud4 specifically associate with the septin gauze at the outer zones of the transitional hourglass (**Figure 2C**, right) (Chen et al., 2020). Both proteins have been implicated in septin organization, likely at the stage of double ring formation (Lord et al., 2000; Gladfelter et al., 2005; Guo et al., 2011; Wloka et al., 2011; Eluere et al., 2012; Kang et al., 2013; Wu et al., 2015; Mcquilken et al., 2017). Taken together, these observations suggest that Bud3 and Bud4 likely define the spatial cues that act in the right place at the right time to drive the HDR transition, but how?

Live-cell imaging and PREM analyses demonstrate that Bud3 and Bud4 play distinct and essential roles in controlling the septin HDR transition (Chen et al., 2020). As indicated above, the transitional hourglass in WT cells possesses a zonal architecture where the myosin-II filaments are sandwiched by Bud3 and Bud4-decorated septin gauze (**Figure 2C**; **Figure 2D**, top row, left). During the HDR transition, the septins in the middle of the hourglass are preferentially lost whereas those at the ends of the hourglass are preferentially stabilized (**Figure 2D**, top row, right), leading to the double ring formation. In the absence of Bud3, however, the circumferential single filaments at the ends of the transitional hourglass are completely lost, with many of the structures displaying elongated paired filaments at one side of the hourglass (**Figure 2D**, middle row, left) (Chen et al., 2020). This filament-level observation may explain the phenotype of *bud3Δ* cells detected by live-cell imaging that, during the HDR transition, the septin hourglass was first thinned at its edges, followed by the disintegration or fragmentation of the remaining structure in the middle (**Figure 2D**, middle row, right) (Chen et al., 2020). These observations suggest that Bud3 is specifically required for the stabilization of the transitional hourglass at its edges, and, furthermore, this selective stabilization mechanism must act before the cell cycle-triggered disassembly of the septin filaments in the middle of the hourglass (located between the PM and the myosin-II filaments). In the absence of Bud4, the entire transitional hourglass became destabilized, often in an asymmetric manner where one side of the structure was affected more than the other (**Figure 2D**, bottom row, left) (Chen et al., 2020). This is consistent with live-cell imaging analysis showing that the mother side of the septin double ring is preferentially lost during the HDR transition (Wloka et al., 2011; Chen et al., 2020). In the absence of both Bud3 and Bud4, the transitional hourglass was severely compromised and, consequently, was hardly detectable by PREM and the double ring was essentially abolished (Chen et al., 2020). Taken together, these data suggest that Bud3 and Bud4 function as the spatial cues by exclusively localizing to the outer zones of the transitional hourglass and instructing the double ring formation at the ends of the hourglass. Bud3 is essential for the circumferential single filament assembly whereas Bud4 is likely required for the stability of both paired and single filaments in the transitional hourglass, especially at the mother side of the bud neck.

DISCUSSION

How a cell assembles a septin structure at a discrete membrane site and how the structure is remodeled *in situ* into a distinct architecture to perform specific functions are central questions in the septin field that remain largely unanswered. Based on the collective data presented above, it is safe to say that the transitions from the nascent ring to the hourglass and the hourglass to double ring require precise regulation by specific SAPs. Recent works have placed Elm1 as a regulator of septin filament pairing to stabilize the early septin hourglass at the onset of bud formation (Marquardt et al., 2020) and Bud3 and Bud4 as the spatial cues at the ends of a late hourglass to reorganize and stabilize both single and paired filaments during the HDR transition (Chen et al., 2020). By utilizing genetic perturbations and following septin kinetics via confocal microscopy and septin filament architecture *via* PREM, these studies have begun to elucidate the mechanisms of septin organization *in vivo* at an unprecedented resolution.

While Elm1 is known to regulate septin filament pairing during hourglass formation (Marquardt et al., 2020), the underlying mechanism remains unknown. Could Elm1 directly phosphorylate the septins or another SAP to induce the change from single to paired filaments, or does Elm1 oppose an unknown molecule that destabilizes septin filament pairing? As septins tend to form paired filaments *in vitro* either in solution under low-salt condition or on lipid monolayer even under high-salt condition (Frazier et al., 1998; Bertin et al., 2008; Bertin et al., 2010; Bridges

et al., 2014), we favor the latter possibility of an indirect regulation by antagonizing a destabilization factor. However, other studies have shown that Elm1 can phosphorylate SAPs with known roles in septin stability including Bni5 (Patasi et al., 2015), Gin4 (Asano et al., 2006), and the morphogenetic checkpoint kinase Hsl1 (Szkotnicki et al., 2008), leaving the possibility open for non-mutually exclusive pathways of action.

Protein kinases have been found to regulate septin structural stability in other systems including at the annulus of spermatozoa and at the base of dendritic spines (Brand et al., 2012; Shen et al., 2017; Yadav et al., 2017; Lin et al., 2019). Similar to the LKB1-like kinase Elm1, LKB1 regulates glucose metabolism by phosphorylating AMP-activated protein kinase (AMPK) (Hawley et al., 2003; Hong et al., 2003; Woods et al., 2003; Shaw et al., 2004; Rubenstein et al., 2006; Mccartney et al., 2016), and has a conserved function in polarity (Watts et al., 2000; Nakano and Takashima, 2012). However, there is no evidence thus far that LKB1 or other Elm1 "homologues" regulate septin architecture in other systems.

Bud3 and Bud4 are known to localize exclusively to the gauze-like structure at the outer zones of the transitional hourglass (Chen et al., 2020). However, it remains a mystery how this unique localization is achieved and how it facilitates the HDR transition. Does the Bud3 and Bud4 complex function as the membrane anchor to stabilize the single filaments at the ends of the transitional hourglass during the paired filament disassembly, and, at the same time, also function as the spatial landmark to recruit septin complexes and/or short filaments from the disassembled paired filaments and reassemble and reorganize them into a double ring? How Bud3 and Bud4 interact with each other and with the septins also remains unknown.

The HDR transition is triggered by the activation of the mitotic exit network (Cid et al., 2001a; Lippincott et al., 2001; Tamborrini et al., 2018) and is accompanied by 90° change in the orientation of the paired filaments (Vrabioiu and Mitchison, 2006; Demay et al., 2011; Ong et al., 2014). Whether and how Bud3 and Bud4 are involved in this process remains unknown. All these questions must be addressed in order to achieve a mechanistic understanding of the HDR transition.

Like the Bud3-Bud4 module in budding yeast, a RhoGEF-anillin module appears to be involved in the coordination of septin remodeling and cytokinesis in many organisms including fission yeast (Berlin et al., 2003; Tasto et al., 2003; Munoz et al., 2014; Wang et al., 2015), *Drosophila* (Hickson and O'Farrell, 2008), and mammalian cells (Frenette et al., 2012; Renshaw et al., 2014; Karasmanis et al., 2019; Wang et al., 2019). Whether this module represents a conserved core mechanism for septin remodeling during cytokinesis across model systems requires further investigation.

AUTHOR CONTRIBUTIONS

JM and XC wrote the initial draft. EB revised the manuscript. All authors read and approved the final manuscript.

FUNDING

This work was supported by the NIH grant GM116876.

ACKNOWLEDGMENTS

We thank the members of the Bi laboratory, especially Hiroki Okada, for stimulating discussions and critically reading the manuscript.

REFERENCES

Ageta-Ishihara, N., and Kinoshita, M. (2021). Developmental and Postdevelopmental Roles of Septins in the Brain. *Neurosci. Res.* 170, 6–12. doi:10.1016/j.neures.2020.08.006

Alonso, A., Greenlee, M., Matts, J., Kline, J., Davis, K. J., and Miller, R. K. (2015). Emerging Roles of Sumoylation in the Regulation of Actin, Microtubules, Intermediate Filaments, and Septins. *Cytoskeleton.* 72, 305–339. doi:10.1002/cm.21226

Asano, S., Park, J.-E., Yu, L.-R., Zhou, M., Sakchaisri, K., Park, C. J., et al. (2006). Direct Phosphorylation and Activation of a Nim1-Related Kinase Gin4 by Elm1 in Budding Yeast. *J. Biol. Chem.* 281, 27090–27098. doi:10.1074/jbc.m601483200

Barral, Y., Mermall, V., Mooseker, M. S., and Snyder, M. (2000). Compartmentalization of the Cell Cortex by Septins Is Required for Maintenance of Cell Polarity in Yeast. *Mol. Cell.* 5, 841–851. doi:10.1016/s1097-2765(00)80324-x

Barral, Y., Parra, M., Bidlingmaier, S., and Snyder, M. (1999). Nim1-Related Kinases Coordinate Cell Cycle Progression With the Organization of the Peripheral Cytoskeleton in Yeast. *Genes Development.* 13, 176–187. doi:10.1101/gad.13.2.176

Beber, A., Taveneau, C., Nania, M., Tsai, F.-C., Di Cicco, A., Bassereau, P., et al. (2019). Membrane Reshaping by Micrometric Curvature Sensitive Septin Filaments. *Nat. Commun.* 10, 420. doi:10.1038/s41467-019-08344-5

Berlin, A., Paoletti, A., and Chang, F. (2003). Mid2p Stabilizes Septin Rings During Cytokinesis in Fission Yeast. *J. Cell Biol.* 160, 1083–1092. doi:10.1083/jcb.200212016

Bertin, A., Mcmurray, M. A., Grob, P., Park, S.-S., Garcia, G., 3rd, Patanwala, I., et al. (2008). *Saccharomyces cerevisiae* Septins: Supramolecular Organization of Heterooligomers and the Mechanism of Filament Assembly. *Proc. Natl. Acad. Sci.* 105, 8274–8279. doi:10.1073/pnas.0803330105

Bertin, A., Mcmurray, M. A., Pierson, J., Thai, L., Mcdonald, K. L., Zehr, E. A., et al. (2012). Three-Dimensional Ultrastructure of the Septin Filament Network in Saccharomyces Cerevisiae. *MBoC.* 23, 423–432. doi:10.1091/mbc.e11-10-0850

Bertin, A., Mcmurray, M. A., Thai, L., Garcia, G., 3rd, Votin, V., Grob, P., et al. (2010). Phosphatidylinositol-4,5-Bisphosphate Promotes Budding Yeast Septin Filament Assembly and Organization. *J. Mol. Biol.* 404, 711–731. doi:10.1016/j.jmb.2010.10.002

Bertin, A., and Nogales, E. (2012). Septin Filament Organization in *Saccharomyces cerevisiae*. *Communicative Integr. Biol.* 5, 503–505. doi:10.4161/cib.21125

Bi, E., Maddox, P., Lew, D. J., Salmon, E. D., Mcmillan, J. N., Yeh, E., et al. (1998). Involvement of an Actomyosin Contractile Ring in *Saccharomyces cerevisiae* Cytokinesis. *J. Cell Biol.* 142, 1301–1312. doi:10.1083/jcb.142.5.1301

Booth, E. A., Sterling, S. M., Dovala, D., Nogales, E., and Thorner, J. (2016). Effects of Bni5 Binding on Septin Filament Organization. *J. Mol. Biol.* 428, 4962–4980. doi:10.1016/j.jmb.2016.10.024

Booth, E. A., Vane, E. W., Dovala, D., and Thorner, J. (2015). A Förster Resonance Energy Transfer (FRET)-Based System Provides Insight Into the Ordered

Assembly of Yeast Septin Hetero-Octamers. *J. Biol. Chem.* 290, 28388–28401. doi:10.1074/jbc.m115.683128

Bouquin, N., Barral, Y., Courbeyrette, R., Blondel, M., Snyder, M., and Mann, C. (2000). Regulation of Cytokinesis by the Elm1 Protein Kinase in *Saccharomyces cerevisiae*. *J. Cell Sci.* 113, 1435–1445. doi:10.1242/jcs.113.8.1435

Brand, F., Schumacher, S., Kant, S., Menon, M. B., Simon, R., Turgeon, B., et al. (2012). The Extracellular Signal-Regulated Kinase 3 (Mitogen-Activated Protein Kinase 6 [MAPK6])-MAPK-Activated Protein Kinase 5 Signaling Complex Regulates Septin Function and Dendrite Morphology. *Mol. Cell. Biol.* 32, 2467–2478. doi:10.1128/mcb.06633-11

Bridges, A. A., Jentzsch, M. S., Oakes, P. W., Occhipinti, P., and Gladfelter, A. S. (2016). Micron-Scale Plasma Membrane Curvature Is Recognized by the Septin Cytoskeleton. *J. Cell Biol.* 213, 23–32. doi:10.1083/jcb.201512029

Bridges, A. A., Zhang, H., Mehta, S. B., Occhipinti, P., Tani, T., and Gladfelter, A. S. (2014). Septin Assemblies Form by Diffusion-Driven Annealing on Membranes. *Proc. Natl. Acad. Sci. USA.* 111, 2146–2151. doi:10.1073/pnas.1314138111

Byers, B., and Goetsch, L. (1976a). A Highly Ordered Ring of Membrane-Associated Filaments in Budding Yeast. *J. Cell Biol.* 69, 717–721. doi:10.1083/jcb.69.3.717

Byers, B., and Goetsch, L. (1976b). Loss of the Filamentous Ring in Cytokinesis-Defective Mutants of Budding Yeast. *Abstr. First Internat. Congr. Cell Biol.* 70, 35a.

Cannon, K. S., Woods, B. L., Crutchley, J. M., and Gladfelter, A. S. (2019). An Amphipathic Helix Enables Septins to Sense Micrometer-Scale Membrane Curvature. *J. Cell Biol.* 218, 1128–1137. doi:10.1083/jcb.201807211

Carroll, C. W., Altman, R., Schieltz, D., Yates, J. R., and Kellogg, D. (1998). The Septins Are Required for the Mitosis-Specific Activation of the Gin4 Kinase. *J. Cell Biol.* 143, 709–717. doi:10.1083/jcb.143.3.709

Caviston, J. P., Longtine, M., Pringle, J. R., and Bi, E. (2003). The Role of Cdc42p GTPase-Activating Proteins in Assembly of the Septin Ring in Yeast. *MBoC.* 14, 4051–4066. doi:10.1091/mbc.e03-04-0247

Chant, J., Mischke, M., Mitchell, E., Herskowitz, I., and Pringle, J. R. (1995). Role of Bud3p in Producing the Axial Budding Pattern of Yeast. *J. Cell Biol.* 129, 767–778. doi:10.1083/jcb.129.3.767

Chant, J., and Pringle, J. R. (1995). Patterns of Bud-Site Selection in the Yeast *Saccharomyces cerevisiae*. *J. Cell Biol.* 129, 751–765. doi:10.1083/jcb.129.3.751

Chen, X., Wang, K., Svitkina, T., and Bi, E. (2020). Critical Roles of a RhoGEF-Anillin Module in Septin Architectural Remodeling During Cytokinesis. *Curr. Biol.* 30, 1477–1490. e1473. doi:10.1016/j.cub.2020.02.023

Cid, V. J., Adamiková, L., Sánchez, M., Molina, M., and Nombela, C. (2001a). Cell Cycle Control of Septin Ring Dynamics in the Budding Yeast. *Microbiology.* 147, 1437–1450. doi:10.1099/00221287-147-6-1437

Cid, V. J., Shulewitz, M. J., Mcdonald, K. L., and Thorner, J. (2001b). Dynamic Localization of the Swe1 Regulator Hsl7 During the Saccharomyces Cerevisiae Cell Cycle. *MBoC.* 12, 1645–1669. doi:10.1091/mbc.12.6.1645

Connolly, D., Abdesselam, I., Verdier-Pinard, P., and Montagna, C. (2011a). Septin Roles in Tumorigenesis. *Biol. Chem.* 392, 725–738. doi:10.1515/bc.2011.073

Connolly, D., Yang, Z., Castaldi, M., Simmons, N., Oktay, M. H., Coniglio, S., et al. (2011b). Septin 9 Isoform Expression, Localization and Epigenetic Changes during Human and Mouse Breast Cancer Progression. *Breast Cancer Res.* 13, R76. doi:10.1186/bcr2924

Cyert, M. S., and Philpott, C. C. (2013). Regulation of Cation Balance in *Saccharomyces cerevisiae*. *Genetics.* 193, 677–713. doi:10.1534/genetics.112.147207

De Virgilio, C., Demarini, D. J., and Pringle, J. R. (1996). *SPR28*, a Sixth Member of the Septin Gene Family in *Saccharomyces cerevisiae* that Is Expressed Specifically in Sporulating Cells. *Microbiology.* 142, 2897–2905. doi:10.1099/13500872-142-10-2897

Demay, B. S., Bai, X., Howard, L., Occhipinti, P., Meseroll, R. A., Spiliotis, E. T., et al. (2011). Septin Filaments Exhibit a Dynamic, Paired Organization That Is Conserved From Yeast to Mammals. *J. Cell Biol.* 193, 1065–1081. doi:10.1083/jcb.201012143

Dobbelaere, J., Gentry, M. S., Hallberg, R. L., and Barral, Y. (2003). Phosphorylation-Dependent Regulation of Septin Dynamics During the Cell Cycle. *Developmental Cell.* 4, 345–357. doi:10.1016/s1534-5807(03)00061-3

Dolat, L., Hu, Q., and Spiliotis, E. T. (2014). Septin Functions in Organ System Physiology and Pathology. *Biol. Chem.* 395, 123–141. doi:10.1515/hsz-2013-0233

Eluère, R., Varlet, I., Bernadac, A., and Simon, M.-N. (2012). Cdk and the Anillin Homolog Bud4 Define a New Pathway Regulating Septin Organization in Yeast. *Cell Cycle.* 11, 151–158. doi:10.4161/cc.11.1.18542

Estey, M. P., Di Ciano-Oliveira, C., Froese, C. D., Bejide, M. T., and Trimble, W. S. (2010). Distinct Roles of Septins in Cytokinesis: SEPT9 Mediates Midbody Abscission. *J. Cell Biol.* 191, 741–749. doi:10.1083/jcb.201006031

Fang, X., Luo, J., Nishihama, R., Wloka, C., Dravis, C., Travaglia, M., et al. (2010). Biphasic Targeting and Cleavage Furrow Ingression Directed by the Tail of a Myosin II. *J. Cell Biol.* 191, 1333–1350. doi:10.1083/jcb.201005134

Fares, H., Goetsch, L., and Pringle, J. R. (1996). Identification of a Developmentally Regulated Septin and Involvement of the Septins in Spore Formation in *Saccharomyces cerevisiae*. *J. Cell Biol.* 132, 399–411. doi:10.1083/jcb.132.3.399

Finnigan, G. C., Booth, E. A., Duvalyan, A., Liao, E. N., and Thorner, J. (2015). The Carboxy-Terminal Tails of Septins Cdc11 and Shs1 Recruit Myosin-II Binding Factor Bni5 to the Bud Neck in *Saccharomyces cerevisiae*. *Genetics.* 200, 843–862. doi:10.1534/genetics.115.176503

Frazier, J. A., Wong, M. L., Longtine, M. S., Pringle, J. R., Mann, M., Mitchison, T. J., et al. (1998). Polymerization of Purified Yeast Septins: Evidence That Organized Filament Arrays May Not Be Required for Septin Function. *J. Cell Biol.* 143, 737–749. doi:10.1083/jcb.143.3.737

Frenette, P., Haines, E., Loloyan, M., Kinal, M., Pakarian, P., and Piekny, A. (2012). An Anillin-Ect2 Complex Stabilizes central Spindle Microtubules at the Cortex During Cytokinesis. *PLoS One.* 7, e34888. doi:10.1371/journal.pone.0034888

Garcia, G., 3rd, Bertin, A., Li, Z., Song, Y., Mcmurray, M. A., Thorner, J., et al. (2011). Subunit-Dependent Modulation of Septin Assembly: Budding Yeast Septin Shs1 Promotes Ring and Gauze Formation. *J. Cell Biol.* 195, 993–1004. doi:10.1083/jcb.201107123

Gladfelter, A., Pringle, J. R., and Lew, D. J. (2001). The Septin Cortex at the Yeast Motherâ€"bud Neck. *Curr. Opin. Microbiol.* 4, 681–689. doi:10.1016/s1369-5274(01)00269-7

Gladfelter, A. S., Bose, I., Zyla, T. R., Bardes, E. S. G., and Lew, D. J. (2002). Septin Ring Assembly Involves Cycles of GTP Loading and Hydrolysis by Cdc42p. *J. Cell Biol.* 156, 315–326. doi:10.1083/jcb.200109062

Gladfelter, A. S., Kozubowski, L., Zyla, T. R., and Lew, D. J. (2005). Interplay Between Septin Organization, Cell Cycle and Cell Shape in Yeast. *J. Cell Sci.* 118, 1617–1628. doi:10.1242/jcs.02286

Guo, J., Gong, T., and Gao, X.-D. (2011). Identification of an Amphipathic Helix Important for the Formation of Ectopic Septin Spirals and Axial Budding in Yeast Axial Landmark Protein Bud3p. *PLoS One.* 6, e16744. doi:10.1371/journal.pone.0016744

Hall, P. A., Jung, K., Hillan, K. J., and Russell, S. H. (2005). Expression Profiling the Human Septin Gene Family. *J. Pathol.* 206, 269–278. doi:10.1002/path.1789

Hall, P. A., and Russell, S. H. (2004). The Pathobiology of the Septin Gene Family. *J. Pathol.* 204, 489–505. doi:10.1002/path.1654

Hartwell, L. (1971). Genetic Control of the Cell Division Cycle in Yeast *1IV. Genes Controlling Bud Emergence and Cytokinesis. *Exp. Cell Res.* 69, 265–276. doi:10.1016/0014-4827(71)90223-0

Hawley, S. A., Boudeau, J., Reid, J. L., Mustard, K. J., Udd, L., Mäkelä, T. P., et al. (2003). Complexes Between the LKB1 Tumor Suppressor, STRAD Alpha/Beta and MO25 Alpha/Beta Are Upstream Kinases in the AMP-Activated Protein Kinase Cascade. *J. Biol.* 2, 28. doi:10.1186/1475-4924-2-28

Hernández-Rodríguez, Y., and Momany, M. (2012). Posttranslational Modifications and Assembly of Septin Heteropolymers and Higher-Order Structures. *Curr. Opin. Microbiol.* 15, 660–668. doi:10.1016/j.mib.2012.09.007

Hickson, G. R., and O'farrell, P. H. (2008). Rho-Dependent Control of Anillin Behavior During Cytokinesis. *J. Cell Biol.* 180, 285–294.

Hong, S.-P., Leiper, F. C., Woods, A., Carling, D., and Carlson, M. (2003). Activation of Yeast Snf1 and Mammalian AMP-Activated Protein Kinase by Upstream Kinases. *Proc. Natl. Acad. Sci.* 100, 8839–8843. doi:10.1073/pnas.1533136100

Ihara, M., Kinoshita, A., Yamada, S., Tanaka, H., Tanigaki, A., Kitano, A., et al. (2005). Cortical Organization by the Septin Cytoskeleton Is Essential for Structural and Mechanical Integrity of Mammalian Spermatozoa. *Developmental Cell.* 8, 343–352. doi:10.1016/j.devcel.2004.12.005

Iwase, M., Luo, J., Nagaraj, S., Longtine, M., Kim, H. B., Haarer, B. K., et al. (2006). Role of a Cdc42p Effector Pathway in Recruitment of the Yeast Septins to the Presumptive Bud Site. *MBoC.* 17, 1110–1125. doi:10.1091/mbc.e05-08-0793

John, C. M., Hite, R. K., Weirich, C. S., Fitzgerald, D. J., Jawhari, H., Faty, M., et al. (2007). The *Caenorhabditis elegans* Septin Complex Is Nonpolar. *EMBO J.* 26, 3296–3307. doi:10.1038/sj.emboj.7601775

Kang, H., Tsygankov, D., and Lew, D. J. (2016). Sensing a Bud in the Yeast Morphogenesis Checkpoint: a Role for Elm1. *MBoC.* 27, 1764–1775. doi:10.1091/mbc.e16-01-0014

Kang, P. J., Angerman, E., Jung, C. H., and Park, H. O. (2012). Bud4 Mediates the Cell-Type-Specific Assembly of the Axial Landmark in Budding Yeast. *J. Cell Sci.* 125, 3840–3849. doi:10.1242/jcs.103697

Kang, P. J., Hood-Degrenier, J. K., and Park, H. O. (2013). Coupling of Septins to the Axial Landmark by Bud4 in Budding Yeast. *J. Cell Sci.* 126, 1218–1226. doi:10.1242/jcs.118521

Kang, P. J., Lee, M. E., and Park, H.-O. (2014). Bud3 Activates Cdc42 to Establish a Proper Growth Site in Budding Yeast. *J. Cell Biol.* 206, 19–28. doi:10.1083/jcb.201402040

Karasmanis, E. P., Hwang, D., Nakos, K., Bowen, J. R., Angelis, D., and Spiliotis, E. T. (2019). A Septin Double Ring Controls the Spatiotemporal Organization of the ESCRT Machinery in Cytokinetic Abscission. *Curr. Biol.* 29, 2174–2182. doi:10.1016/j.cub.2019.05.050

Khan, A., Newby, J., and Gladfelter, A. S. (2018). Control of Septin Filament Flexibility and Bundling by Subunit Composition and Nucleotide Interactions. *MBoC.* 29, 702–712. doi:10.1091/mbc.e17-10-0608

Kim, H. B., Haarer, B. K., and Pringle, J. R. (1991). Cellular Morphogenesis in the *Saccharomyces cerevisiae* Cell Cycle: Localization of the *CDC3* Gene Product and the Timing of Events at the Budding Site. *J. Cell Biol.* 112, 535–544. doi:10.1083/jcb.112.4.535

Kinoshita, M. (2003). Assembly of Mammalian Septins. *J. Biochem.* 134, 491–496. doi:10.1093/jb/mvg182

Kissel, H., Georgescu, M.-M., Larisch, S., Manova, K., Hunnicutt, G. R., and Steller, H. (2005). The Sept4 Septin Locus Is Required for Sperm Terminal Differentiation in Mice. *Developmental Cell.* 8, 353–364. doi:10.1016/j.devcel.2005.01.021

Kubala, M. H., Kovtun, O., Alexandrov, K., and Collins, B. M. (2010). Structural and Thermodynamic Analysis of the GFP:GFP-nanobody Complex. *Protein Sci.* 19, 2389–2401. doi:10.1002/pro.519

Lee, P. R., Song, S., Ro, H.-S., Park, C. J., Lippincott, J., Li, R., et al. (2002). Bni5p, a Septin-Interacting Protein, Is Required for normal Septin Function and Cytokinesis in *Saccharomyces cerevisiae*. *Mol. Cell. Biol.* 22, 6906–6920. doi:10.1128/mcb.22.19.6906-6920.2002

Lin, C. H., Shen, Y. R., Wang, H. Y., Chiang, C. W., Wang, C. Y., and Kuo, P. L. (2019). Regulation of Septin Phosphorylation: SEPT12 Phosphorylation in Sperm Septin Assembly. *Cytoskeleton.* 76, 137–142. doi:10.1002/cm.21491

Lin, Y.-H., Kuo, Y.-C., Chiang, H.-S., and Kuo, P.-L. (2011). The Role of the Septin Family in Spermiogenesis. *Spermatogenesis.* 1, 298–302. doi:10.4161/spmg.1.4.18326

Lippincott, J., and Li, R. (1998). Sequential Assembly of Myosin II, an IQGAP-Like Protein, and Filamentous Actin to a Ring Structure Involved in Budding Yeast Cytokinesis. *J. Cell Biol.* 140, 355–366. doi:10.1083/jcb.140.2.355

Lippincott, J., Shannon, K. B., Shou, W., Deshaies, R. J., and Li, R. (2001). The Tem1 Small GTPase Controls Actomyosin and Septin Dynamics During Cytokinesis. *J. Cell Sci.* 114, 1379–1386. doi:10.1242/jcs.114.7.1379

Longtine, M. S., Demarini, D. J., Valencik, M. L., Al-Awar, O. S., Fares, H., De Virgilio, C., et al. (1996). The Septins: Roles in Cytokinesis and Other Processes. *Curr. Opin. Cell Biol.* 8, 106–119. doi:10.1016/s0955-0674(96)80054-8

Longtine, M. S., Fares, H., and Pringle, J. R. (1998). Role of the Yeast Gin4p Protein Kinase in Septin Assembly and the Relationship Between Septin Assembly and Septin Function. *J. Cell Biol.* 143, 719–736. doi:10.1083/jcb.143.3.719

Longtine, M. S., Theesfeld, C. L., Mcmillan, J. N., Weaver, E., Pringle, J. R., and Lew, D. J. (2000). Septin-dependent Assembly of a Cell Cycle-Regulatory Module in *Saccharomyces cerevisiae*. *Mol. Cell Biol.* 20, 4049–4061. doi:10.1128/mcb.20.11.4049-4061.2000

Lord, M., Yang, M. C., Mischke, M., and Chant, J. (2000). Cell Cycle Programs of Gene Expression Control Morphogenetic Protein Localization. *J. Cell Biol.* 151, 1501–1512. doi:10.1083/jcb.151.7.1501

Luedeke, C., Frei, S. B., Sbalzarini, I., Schwarz, H., Spang, A., and Barral, Y. (2005). Septin-Dependent Compartmentalization of the Endoplasmic Reticulum During Yeast Polarized Growth. *J. Cell Biol.* 169, 897–908. doi:10.1083/jcb.200412143

Marquardt, J., Chen, X., and Bi, E. (2019). Architecture, Remodeling, and Functions of the Septin Cytoskeleton. *Cytoskeleton.* 76, 7–14. doi:10.1002/cm.21475

Marquardt, J., Yao, L.-L., Okada, H., Svitkina, T., and Bi, E. (2020). The LKB1-Like Kinase Elm1 Controls Septin Hourglass Assembly and Stability by Regulating Filament Pairing. *Curr. Biol.* 30, 2386–2394. doi:10.1016/j.cub.2020.04.035

Mccartney, R. R., Garnar-Wortzel, L., Chandrashekarappa, D. G., and Schmidt, M. C. (2016). Activation and Inhibition of Snf1 Kinase Activity by Phosphorylation within the Activation Loop. *Biochim. Biophys. Acta (Bba) - Proteins Proteomics.* 1864, 1518–1528. doi:10.1016/j.bbapap.2016.08.007

Mcmurray, M. A., and Thorner, J. (2009). Septins: Molecular Partitioning and the Generation of Cellular Asymmetry. *Cell Div.* 4, 18. doi:10.1186/1747-1028-4-18

Mcquilken, M., Jentzsch, M. S., Verma, A., Mehta, S. B., Oldenbourg, R., and Gladfelter, A. S. (2017). Analysis of Septin Reorganization at Cytokinesis Using Polarized Fluorescence Microscopy. *Front. Cell Dev. Biol.* 5, 42. doi:10.3389/fcell.2017.00042

Mendonça, D. C., Macedo, J. N., Guimarães, S. L., Barroso Da Silva, F. L., Cassago, A., Garratt, R. C., et al. (2019). A Revised Order of Subunits in Mammalian Septin Complexes. *Cytoskeleton.* 76, 457–466. doi:10.1002/cm.21569

Mino, A., Tanaka, K., Kamei, T., Umikawa, M., Fujiwara, T., and Takai, Y. (1998). Shs1p: A Novel Member of Septin That Interacts with Spa2p, Involved in Polarized Growth inSaccharomyces Cerevisiae. *Biochem. Biophysical Res. Commun.* 251, 732–736. doi:10.1006/bbrc.1998.9541

Mortensen, E. M., Mcdonald, H., Yates, J., 3rd, and Kellogg, D. R. (2002). Cell Cycle-Dependent Assembly of a Gin4-Septin Complex. *MBoC.* 13, 2091–2105. doi:10.1091/mbc.01-10-0500

Mostowy, S., and Cossart, P. (2012). Septins: the Fourth Component of the Cytoskeleton. *Nat. Rev. Mol. Cell. Biol.* 13, 183–194. doi:10.1038/nrm3284

Muñoz, S., Manjón, E., and Sánchez, Y. (2014). The Putative Exchange Factor Gef3p Interacts With Rho3p GTPase and the Septin Ring During Cytokinesis in Fission Yeast. *J. Biol. Chem.* 289, 21995–22007. doi:10.1074/jbc.m114.548792

Nakano, A., and Takashima, S. (2012). LKB 1 and AMP -Activated Protein Kinase: Regulators of Cell Polarity. *Genes Cells.* 17, 737–747. doi:10.1111/j.1365-2443.2012.01629.x

Oh, Y., and Bi, E. (2011). Septin Structure and Function in Yeast and beyond. *Trends Cell Biol.* 21, 141–148. doi:10.1016/j.tcb.2010.11.006

Okada, S., Leda, M., Hanna, J., Savage, N. S., Bi, E., and Goryachev, A. B. (2013). Daughter Cell Identity Emerges From the Interplay of Cdc42, Septins, and Exocytosis. *Developmental Cell.* 26, 148–161. doi:10.1016/j.devcel.2013.06.015

Ong, K., Wloka, C., Okada, S., Svitkina, T., and Bi, E. (2014). Architecture and Dynamic Remodelling of the Septin Cytoskeleton During the Cell Cycle. *Nat. Commun.* 5, 5698. doi:10.1038/ncomms6698

Ozsarac, N., Bhattacharyya, M., Dawes, I. W., and Clancy, M. J. (1995). The SPR3 Gene Encodes a Sporulation-Specific Homologue of the Yeast CDC3/10/11/12 Family of Bud Neck Microfilaments and Is Regulated by ABFI. *Gene.* 164, 157–162. doi:10.1016/0378-1119(95)00438-c

Pan, F., Malmberg, R. L., and Momany, M. (2007). Analysis of Septins Across Kingdoms Reveals Orthology and New Motifs. *BMC Evol. Biol.* 7, 103. doi:10.1186/1471-2148-7-103

Patasi, C., Godočíková, J., Michlíková, S., Nie, Y., Káčeriková, R., Kválová, K., et al. (2015). The Role of Bni5 in the Regulation of Septin Higher-Order Structure Formation. *Biol. Chem.* 396, 1325–1337. doi:10.1515/hsz-2015-0165

Perez, A. M., Finnigan, G. C., Roelants, F. M., and Thorner, J. (2016). Septin-Associated Protein Kinases in the Yeast *Saccharomyces cerevisiae*. *Front. Cell Dev. Biol.* 4, 119. doi:10.3389/fcell.2016.00119

Pringle, J. R., Bi, E., Harkins, H. A., Zahner, J. E., De Virgilio, C., Chant, J., et al. (1995). Establishment of Cell Polarity in Yeast. *Cold Spring Harbor Symposia Quantitative Biol.* 60, 729–744. doi:10.1101/sqb.1995.060.01.079

Renshaw, M. J., Liu, J., Lavoie, B. D., and Wilde, A. (2014). Anillin-Dependent Organization of Septin Filaments Promotes Intercellular Bridge Elongation and Chmp4B Targeting to the Abscission Site. *Open Biol.* 4, 130190. doi:10.1098/rsob.130190

Robertson, C., Church, S. W., Nagar, H. A., Price, J., Hall, P. A., and Russell, S. H. (2004). Properties ofSEPT9 Isoforms and the Requirement for GTP Binding. *J. Pathol.* 203, 519–527. doi:10.1002/path.1551

Rodal, A. A., Kozubowski, L., Goode, B. L., Drubin, D. G., and Hartwig, J. H. (2005). Actin and Septin Ultrastructures at the Budding Yeast Cell Cortex. *MBoC.* 16, 372–384. doi:10.1091/mbc.e04-08-0734

Roeseler, S., Sandrock, K., Bartsch, I., and Zieger, B. (2009). Septins, a Novel Group of GTP-Binding Proteins - Relevance in Hemostasis, Neuropathology and Oncogenesis. *Klin. Padiatr.* 221, 150–155. doi:10.1055/s-0029-1220706

Rothbauer, U., Zolghadr, K., Tillib, S., Nowak, D., Schermelleh, L., Gahl, A., et al. (2006). Targeting and Tracing Antigens in Live Cells With Fluorescent Nanobodies. *Nat. Methods.* 3, 887–889. doi:10.1038/nmeth953

Rubenstein, E. M., Mccartney, R. R., and Schmidt, M. C. (2006). Regulatory Domains of Snf1-Activating Kinases Determine Pathway Specificity. *Eukaryot. Cell.* 5, 620–627. doi:10.1128/ec.5.4.620-627.2006

Sanders, S. L., and Herskowitz, I. (1996). The BUD4 Protein of Yeast, Required for Axial Budding, Is Localized to the Mother/BUD Neck in a Cell Cycle-Dependent Manner. *J. Cell Biol.* 134, 413–427. doi:10.1083/jcb.134.2.413

Schneider, C., Grois, J., Renz, C., Gronemeyer, T., and Johnsson, N. (2013). Septin Rings Act as a Template for Myosin Higher-Order Structures and Inhibit Redundant Polarity Establishment. *J. Cell Sci.* 126, 3390–3400. doi:10.1242/jcs.125302

Sellin, M. E., Sandblad, L., Stenmark, S., and Gullberg, M. (2011). Deciphering the Rules Governing Assembly Order of Mammalian Septin Complexes. *MBoC.* 22, 3152–3164. doi:10.1091/mbc.e11-03-0253

Sellin, M. E., Stenmark, S., and Gullberg, M. (2012). Mammalian SEPT9 Isoforms Direct Microtubule-Dependent Arrangements of Septin Core Heteromers. *MBoC.* 23, 4242–4255. doi:10.1091/mbc.e12-06-0486

Shaw, R. J., Kosmatka, M., Bardeesy, N., Hurley, R. L., Witters, L. A., Depinho, R. A., et al. (2004). The Tumor Suppressor LKB1 Kinase Directly Activates AMP-Activated Kinase and Regulates Apoptosis in Response to Energy Stress. *Proc. Natl. Acad. Sci.* 101, 3329–3335. doi:10.1073/pnas.0308061100

Shcheprova, Z., Baldi, S., Frei, S. B., Gonnet, G., and Barral, Y. (2008). A Mechanism for Asymmetric Segregation of Age During Yeast Budding. *Nature.* 454, 728–734. doi:10.1038/nature07212

Shen, Y.-R., Wang, H.-Y., Kuo, Y.-C., Shih, S.-C., Hsu, C.-H., Chen, Y.-R., et al. (2017). SEPT12 Phosphorylation Results in Loss of the Septin Ring/Sperm Annulus, Defective Sperm Motility and Poor Male Fertility. *Plos Genet.* 13, e1006631. doi:10.1371/journal.pgen.1006631

Shulewitz, M. J., Inouye, C. J., and Thorner, J. (1999). Hsl7 Localizes to a Septin Ring and Serves as an Adapter in a Regulatory Pathway that Relieves Tyrosine Phosphorylation of Cdc28 Protein Kinase in *Saccharomyces cerevisiae*. *Mol. Cell. Biol.* 19, 7123–7137. doi:10.1128/mcb.19.10.7123

Sirajuddin, M., Farkasovsky, M., Hauer, F., Kühlmann, D., Macara, I. G., Weyand, M., et al. (2007). Structural Insight Into Filament Formation by Mammalian Septins. *Nature* 449, 311–315. doi:10.1038/nature06052

Soroor, F., Kim, M. S., Palander, O., Balachandran, Y., Collins, R. F., Benlekbir, S., et al. (2021). Revised Subunit Order of Mammalian Septin Complexes Explains Their *In Vitro* Polymerization Properties. *MBoC.* 32, 289–300. doi:10.1091/mbc.e20-06-0398

Szkotnicki, L., Crutchley, J. M., Zyla, T. R., Bardes, E. S. G., and Lew, D. J. (2008). The Checkpoint Kinase Hsl1p Is Activated by Elm1p-Dependent Phosphorylation. *MBoC.* 19, 4675–4686. doi:10.1091/mbc.e08-06-0663

Tada, T., Simonetta, A., Batterton, M., Kinoshita, M., Edbauer, D., and Sheng, M. (2007). Role of Septin Cytoskeleton in Spine Morphogenesis and Dendrite Development in Neurons. *Curr. Biol.* 17, 1752–1758. doi:10.1016/j.cub.2007.09.039

Tamborrini, D., Juanes, M. A., Ibanes, S., Rancati, G., and Piatti, S. (2018). Recruitment of the Mitotic Exit Network to Yeast Centrosomes Couples Septin Displacement to Actomyosin Constriction. *Nat. Commun.* 9, 4308. doi:10.1038/s41467-018-06767-0

Tasto, J. J., Morrell, J. L., and Gould, K. L. (2003). An Anillin Homologue, Mid2p, Acts During Fission Yeast Cytokinesis to Organize the Septin Ring and Promote Cell Separation. *J. Cell Biol.* 160, 1093–1103. doi:10.1083/jcb.200211126

Van Eunen, K., Bouwman, J., Daran-Lapujade, P., Postmus, J., Canelas, A. B., Mensonides, F. I. C., et al. (2010). Measuring Enzyme Activities Under Standardized In Vivo-Like Conditions for Systems Biology. *FEBS J.* 277, 749–760. doi:10.1111/j.1742-4658.2009.07524.x

Vrabioiu, A. M., and Mitchison, T. J. (2006). Structural Insights Into Yeast Septin Organization From Polarized Fluorescence Microscopy. *Nature.* 443, 466–469. doi:10.1038/nature05109

Wang, K., Wloka, C., and Bi, E. (2019). Non-Muscle Myosin-II Is Required for the Generation of a Constriction Site for Subsequent Abscission. *iScience.* 13, 69–81. doi:10.1016/j.isci.2019.02.010

Wang, N., Wang, M., Zhu, Y.-H., Grosel, T. W., Sun, D., Kudryashov, D. S., et al. (2015). The Rho-GEF Gef3 Interacts With the Septin Complex and Activates the GTPase Rho4 During Fission Yeast Cytokinesis. *MBoC.* 26, 238–255. doi:10.1091/mbc.e14-07-1196

Watts, J. L., Morton, D. G., Bestman, J., and Kemphues, K. J. (2000). The *C. elegans* Par-4 Gene Encodes a Putative Serine-Threonine Kinase Required for Establishing Embryonic Asymmetry. *Development.* 127, 1467–1475. doi:10.1242/dev.127.7.1467

Weems, A., and Mcmurray, M. (2017). The Step-wise Pathway of Septin Hetero-Octamer Assembly in Budding Yeast. *eLife.* 6, e23689. doi:10.7554/eLife.23689

Weirich, C. S., Erzberger, J. P., and Barral, Y. (2008). The Septin Family of GTPases: Architecture and Dynamics. *Nat. Rev. Mol. Cell Biol.* 9, 478–489. doi:10.1038/nrm2407

Westfall, P. J., and Momany, M. (2002). Aspergillus nidulansSeptin AspB Plays Pre- and Postmitotic Roles in Septum, Branch, and Conidiophore Development. *MBoC.* 13, 110–118. doi:10.1091/mbc.01-06-0312

Wloka, C., Nishihama, R., Onishi, M., Oh, Y., Hanna, J., Pringle, J. R., et al. (2011). Evidence that a Septin Diffusion Barrier Is Dispensable for Cytokinesis in Budding Yeast. *Biol. Chem.* 392, 813–829. doi:10.1515/bc.2011.083

Woods, A., Johnstone, S. R., Dickerson, K., Leiper, F. C., Fryer, L. G. D., Neumann, D., et al. (2003). LKB1 Is the Upstream Kinase in the AMP-Activated Protein Kinase cascade. *Curr. Biol.* 13, 2004–2008. doi:10.1016/j.cub.2003.10.031

Wu, H., Guo, J., Zhou, Y.-T., and Gao, X.-D. (2015). The Anillin-Related Region of Bud4 Is the Major Functional Determinant for Bud4's Function in Septin Organization During Bud Growth and Axial Bud Site Selection in Budding Yeast. *Eukaryot. Cell.* 14, 241–251. doi:10.1128/ec.00268-14

Xie, Y., Vessey, J. P., Konecna, A., Dahm, R., Macchi, P., and Kiebler, M. A. (2007). The GTP-Binding Protein Septin 7 Is Critical for Dendrite Branching and Dendritic-Spine Morphology. *Curr. Biol.* 17, 1746–1751. doi:10.1016/j.cub.2007.08.042

Yadav, S., Oses-Prieto, J. A., Peters, C. J., Zhou, J., Pleasure, S. J., Burlingame, A. L., et al. (2017). TAOK2 Kinase Mediates PSD95 Stability and Dendritic Spine Maturation Through Septin7 Phosphorylation. *Neuron.* 93, 379–393. doi:10.1016/j.neuron.2016.12.006

Conflict of Interest: The authors declare that the research was conducted in the absence of any commercial or financial relationships that could be construed as a potential conflict of interest.

Publisher's Note: All claims expressed in this article are solely those of the authors and do not necessarily represent those of their affiliated organizations, or those of the publisher, the editors and the reviewers. Any product that may be evaluated in this article, or claim that may be made by its manufacturer, is not guaranteed or endorsed by the publisher.

frontiers in Cell and Developmental Biology

REVIEW
published: 09 December 2021
doi: 10.3389/fcell.2021.801507

Septins in Stem Cells

*Tanja Schuster and Hartmut Geiger**

Institute of Molecular Medicine, Ulm University, Ulm, Germany

Septins were first described in yeast. Due to extensive research in non-yeast cells, Septins are now recognized across all species as important players in the regulation of the cytoskeleton, in the establishment of polarity, for migration, vesicular trafficking and scaffolding. Stem cells are primarily quiescent cells, and this actively maintained quiescent state is critical for proper stem cell function. Equally important though, stem cells undergo symmetric or asymmetric division, which is likely linked to the level of symmetry found in the mother stem cell. Due to the ability to organize barriers and be able to break symmetry in cells, Septins are thought to have a significant impact on organizing quiescence as well as the mode (symmetric vs asymmetric) of stem cell division to affect self-renewal versus differentiation. Mechanisms of regulating mammalian quiescence and symmetry breaking by Septins are though still somewhat elusive. Within this overview article, we summarize current knowledge on the role of Septins in stem cells ranging from yeast to mice especially with respect to quiescence and asymmetric division, with a special focus on hematopoietic stem cells.

Keywords: septin, Borg, Cdc42, HSC, aging, stem cells, polarity, yeast

OPEN ACCESS

Edited by:
Hitoshi Takizawa,
Kumamoto University, Japan

Reviewed by:
Ayako Nakamura-Ishizu,
Tokyo Women's Medical University, Japan
Dirk Loeffler,
St. Jude Children's Research Hospital, United States

***Correspondence:**
Hartmut Geiger
hartmut.geiger@uni-ulm.de

Specialty section:
This article was submitted to Signaling, a section of the journal Frontiers in Cell and Developmental Biology

Received: *25 October 2021*
Accepted: *24 November 2021*
Published: *09 December 2021*

Citation:
Schuster T and Geiger H (2021) Septins in Stem Cells. Front. Cell Dev. Biol. 9:801507. doi: 10.3389/fcell.2021.801507

SEPTINS: A HIGHER-ORDER STRUCTURE FOR COMPLEX FUNCTIONS OF CELLS

The first image of Septins was an electron microscopy image taken in 1976 (Byers and Goetsch, 1976), 6 years after the discovery of Septins in yeast by L. H. Hartwell (Hartwell et al., 1970). It shows the budding of Saccharomyces cerevisiae and examines the neck in cytokinesis which evolves during budding. On the inner side of the plasma membrane 10 nm filaments are highly ordered in a ring-like structure. Yeast has seven different Septins: Cdc11, Cdc12, Cdc3, Cdc10, Shs1, Spr3 and Spr28 (Pan et al., 2007). These Septins form palindromic hetero-octamers in the order: Cdc11/Shs1-Cdc12-Cdc3-Cdc10-Cdc10-Cdc3-Cdc12-Cdc11/Shs1 (Weems et al., 2017). Spr3 and Spr28 are sporulation-specific Septins and can replace Cdc12 and Shs1, respectively (McMurray and Thorner, 2008; Heasley and McMurray, 2015). According to amino acid sequence homology mammalian Septins are separated among themselves in groups (Kinoshita, 2003). 13 different Septins can be found in animals/humans that belong to four groups: Sept3 (consisting of Sept3, Sept9, Sept12), Sept6 (consisting of Sept6, Sept8, Sept10, Sept11, Sept14), Sept2 (consisting of Sept1, Sept2, Sept4, Sept5) and Sept7 (consisting of Sept7). It is evident that Sept7 is a special group as it only has one member. Septins can form hetero-oligomer filaments and the Kinoshita rule states that a Septin of a group can be exchanged by another Septin of the same group within these filaments which do have a canonical order with Sept7-Sept6-Sept2-Sept9, and can form hexamers (Sept2-Sept6-Sept7-Sept7-Sept6-Sept2) and octamers (Sept2-Sept6-Sept7-Sept9-Sept9-Sept7-Sept6-Sept2) (McMurray and Thorner, 2019; Mendonça et al., 2019; Soroor et al., 2021), but other orders of Septin groups were also reported (Sandrock et al., 2011). The hexamers and octamers can interact with each other and form higher-order structures by end-to-end joining or filament pairing by N-termini face (Jiao et al., 2020) or postulated antiparallel homodimeric coiled-coils (Leonardo et al., 2021) resulting in longer and

TABLE1 | Septins in HSCs.

Septin type	Phenotype in HSCs	Murine HSC modification
Sept1 Ni et al. (2019)	Sept1 phosphorylation elevated, impaired cytoskeletal remodeling, decreased cell rigidity, stem cell egress from niche, HSCs with enhanced mobility, decreased quiescence, increased apoptosis and defective reconstitution capacity	Ptpn21$^{-/-}$ HSCs
Sept6 Senger et al. (2017)	Increased engraftment of Sept6$^{-/-}$ HSCs upon transplantation, decreased contribution to T cells and increased contribution to B cells, no influence on cell cycle kinetics, cell cycle status, homing, stress tolerance	Sept6$^{-/-}$ HSCs
Sept7 Kandi et al. (2021)	Sept7 polarity is regulated by Cdc42 activity; regulation of Cdc42-Borg4-Sept7 interaction in HSCs by Cdc42 activity level	Control HSCs
	Sept7$^{-/-}$ and Borg4$^{-/-}$ HSCs present impaired function upon transplantation and show changed Cdc42 distribution	
	Sept7$^{-/-}$ HSCs: impaired proliferation, loss of HSC and progenitor potential upon cell division	Sept7$^{-/-}$ HSCs Borg4$^{-/-}$ HSCs

thicker nonpolar polypeptide filaments or rings (Caviston et al., 2003), gauzes (Garcia et al., 2011) and cages (Lobato-Márquez et al., 2021). High-order Septin structures are more stable than other dynamic cytoskeletal polymers (Hagiwara et al., 2011; Bridges et al., 2014) which makes Septins a good choice for acting both as barriers or scaffolds.

Interestingly though, Septins can be organized in multiple types of structures, implying a versatile but also likely a cell type-specific organization of Septins to serve a special purpose within a cell. Septins show spot-like and blob-like distributions within cells under certain conditions (isolated BD3 domain expression of Borg3 (Joberty et al., 2001)) and in certain cell types as well (Kandi et al., 2021) which are likely not linked to fibers. The ring structure of Septins is associated with cytokinesis in yeast, but Septin rings are also formed around internalized bacteria upon infection of mammalian cell lines with *Listeria* and *Shigella* bacteria (Mostowy et al., 2009) and intra-cytosolic *Shigella* are compartmentalized in Septin cage-like structures for autophagy as a host defense (Mostowy et al., 2010). There is a functional interdependence between Septin and Actin cytoskeleton resulting in O- and C-shaped rings as well as bundles of Septins (Schmidt and Nichols, 2004), and Septins can co-align with microtubules to form bundles (Targa et al., 2019). Arc-shaped (together with ring-like) co-localizing clusters of Sept7, Sept5 and Sept11 could be found in neurons at the base of dendritic spines with the function of building a diffusion barrier for membrane proteins (Xie et al., 2007; Ewers et al., 2014). While Septins are known for their ability to break symmetry within cells (Spiliotis and McMurray, 2020), little is known about the role of Septins in mammalian stem cells. They are though designated candidates for being involved in the organization of symmetry and polarity and thus function of stem cells.

The process of blood cell formation (which is termed hematopoiesis) depends on hematopoietic stem cells (HSCs). Roughly 75% of HSCs are in the quiescent G0 state, about 20% are in G1, <2% can be found in an active-cycling state (G2/S/M) (Cheshier et al., 1999; Wilson et al., 2008). Symmetry in quiescent, resting HSCs has been defined by the distribution of polarity proteins and nuclear markers within HSCs (Florian and Geiger, 2010; Grigoryan et al., 2018). In addition, the extent of this symmetry correlates with the age of the HSCs. With respect to the distribution of Septins within HSCs, recent published data show that both spots and blobs of certain Septins (Sept7, Sept6, Sept2) are found within HSCs (Senger et al., 2017; Kandi et al., 2021b, see **Table1**). The distinct roles of these specific structures (spots, blobs) remain elusive.

In young HSCs (from mice that are 4 months old) there is a polar distribution of the polarity proteins RhoGTPase Cell division control 42 protein (Cdc42), Histone 4 Lysine 16 acetylation (H4K16ac), Per2, Numb, Tubulin and also Sept7, with usually one big blob at one spot with perhaps several smaller spots, while in aged HSCs (from animals 18 months and older), this distribution is apolar: more smaller spots, and a much more dispersed distribution (**Figure 1B**). It is thought that the level of polarity is linked to the mode (symmetric/asymmetric) of stem cell division to balance self-renewal versus differentiation (Florian et al., 2018) and to regulate the homing capability to allow for successful immune system reconstitution after transplantation (Liang et al., 2005; Janzen et al., 2006; Florian and Geiger, 2010; Dykstra et al., 2011; Florian et al., 2012; Sun et al., 2014; Kandi et al., 2021).

Upon aging, the activity of the small RhoGTPase Cdc42, in itself also a polarity protein, is elevated in almost all tissue analyzed so far (Yang et al., 2007b; Florian et al., 2012). This elevated activity of Cdc42 causes a reduced frequency of polar HSCs among aged HSCs. Cdc42 can bind to the effector protein group binders of Rho GTPases (Borgs), which themselves were shown to interact with Septins (Joberty et al., 2001; Sheffield et al., 2003). However, it is neither completely understood how the organization and reorganization of HSCs occurs with respect to Cdc42 and Borgs, nor how the Septin network behaves and changes upon aging in HSCs.

DECIPHER SEPTIN CONTRIBUTION TO MAMMALIAN STEM CELLS AND AGING VIA YEAST

Yeast as Role Model for Stem Cells?

As there is more information on Septins in yeast, findings in yeast might inform on Septin biology also in mammalian HSCs. This will help in formulating open questions that need to be addressed in the future. Yeast possesses characteristic traits of stem cells: quiescence and asymmetric division (Werner-Washburne et al., 1993; Gray et al., 2004; Higuchi-Sanabria et al., 2014). In the past, yeast has already successfully been taken as a comparison model for metabolic changes in quiescence entry and exit (Dhawan and Laxman, 2015). Replicative life span and chronological life span

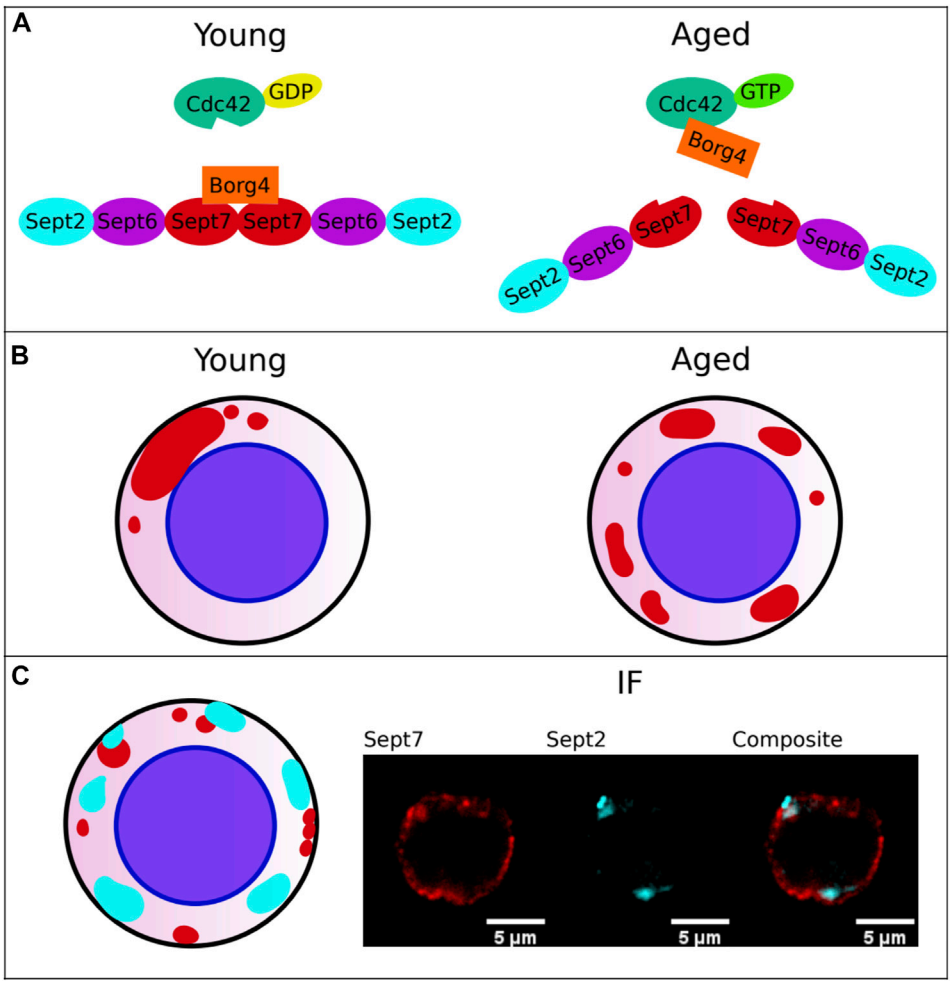

FIGURE 1 | Septin behavior in hematopoietic stem cells (HSCs). **(A)** Change in Cdc42-Borg4-Sept7 axis upon aging. Interaction of Borg4 with Sept7 is shifted upon aging according to elevated activity level of Cdc42 to interaction of Cdc42 with Borg4. **(B)** Change in protein distribution of Sept7 upon aging: Elevated Cdc42 activity leads to a more apolar distribution. **(C)** Interaction of Septins among themselves. Sept7 and Sept2 don't show same distribution. The Septin Network is more complex and demands further studies.

can be straightforward examined in yeast (Postnikoff and Harkness, 2014). Elevated activity of Cdc42 is linked to aging in HSCs and to replicative lifespan in yeast (Kang et al., 2021). Thus, yeast is both a good stem cell and aging model from which processes involved in impairing functions upon aging could be translated into HSCs. This could lead to clinical translations in improving transplantation success and immune system.

On the other hand, there are of course also distinct roles for Septins in yeast and HSCs. Septins for example are indispensable for yeast division (Hartwell et al., 1970), yet especially for the hematopoietic system it was shown that cytokinesis may occur without Septins, while Septins are indispensable for cytokinesis in fibroblasts (Menon et al., 2014). Novel anti-Septin cancer drugs for solid tumors might thus benefit from the fact that Septins are dispensable for hematopoietic cytokinesis while being critical for cancer cells (Menon and Gaestel, 2015). In summary, published data imply that while yeast can serve as a stem cell model and inform on roles of Septins in HSCs, Septins also show a cell type-specific behavior, which requires a careful approach when translating findings in yeast to HSCs.

Quiescence

Quiescence is a cell state in which cells exit the cell cycle and rest in a more robust, withstanding state (G0) till they respond to a signal and reenter the cell cycle. Features of quiescence spanning across species are: reduction of cell size, arrest of cell cycle, condensation of chromosomes, reduction of rRNA synthesis and reduction of protein translation, increase in autophagic activity and increase in stress resistance (Hendil, 1981; Kniss and Burry, 1988; Nagele et al., 1999; Kops et al., 2002; Yusuf and Fruman, 2003; Zhang et al., 2003; Gray et al., 2004; Dhawan and Laxman, 2015; Roche et al., 2017; Wang et al., 2017; Sun and Gresham, 2021).

Many types of extrinsic and intrinsic signals maintain HSCs in quiescence (Liu et al., 2009; Matsumoto et al., 2011; Yamazaki et al., 2011; Nakamura-Ishizu et al., 2014).

As HSC quiescence entry and exit is dependent on the conversion of the cytoskeleton, changes in the localization and structure of organelles will thus likely depend on the well-known properties of Septins like organizing, scaffolding and barricading. Currently, there is no direct data on the role of Septins upon HSCs leaving or entering the quiescent state. The role of Septins in quiescent yeast cells might thus help to inform on likely roles of Septins in quiescent mammalian HSCs.

Yeast enters the quiescent state upon nutrient deprivation or desiccation and several pathways like Target of rapamycin complex I (TORC1), Sucrose non-fermenting 1 (SNF1) protein kinase, Protein kinase A (PKA) and Pho80-Pho85 (Forget et al., 2002; Sopko et al., 2007; Xu et al., 2012) all contribute to this decision. Downregulation of TORCI, a downregulation of PKA, a downregulation of Pho80-Pho85 or an upregulation of SNF1 results in entering of the quiescent state in yeast. These signals are, at the end, all integrated and feed into the regulation of the activity of Cdc42. For mammalian cells similar pathways have been reported for being responsible for the regulation of quiescence in HSCs (Chen et al., 2008; Gan et al., 2010; Cheng et al., 2014), and it was shown that Cdc42 is important for quiescence in HSCs, as the Cdc42 knockout mouse model, which though does not represent physiological Cdc42 deviations upon aging, results in HSC cycling (Yang and Zheng, 2007a).

These findings lead to the following questions with respect to the role of Septins in quiescence: 1) How is Cdc42 linked to Septins? 2) How does Cdc42 affect Septins? and 3) Do interactions of Septins with other cytoskeletal proteins change upon quiescence?

1) A whole family of interaction partners linking Cdc42 to Septins was found in 1997: Gic1 and Gic2 bind specifically to Cdc42-guanosine triphosphate (Cdc42-GTP) (Brown et al., 1997) as well as to Septins (Sadian et al., 2013). It was shown that Gic1 behaves as a scaffolding protein for Septin filaments and Cdc42-GTP binding to Gic1 results in dissociation of Gic1 from Septin filaments. Cdc42-GDP can directly disassemble Septin filaments in yeast when Gic1 is missing. A functional mammalian equivalent was found in 1999 by Joberty et al.: Borgs (Binder of Rho GTPases) 1-5, also entitled as Cdc42 effector proteins 1-5, bind Cdc42 in a GTP-dependent manner (Joberty et al., 1999). HSCs do also express Borg proteins (Kandi et al., 2021). Among the above mentioned pathways linked to quiescence, also Iqg1 of the yeast TORC1 pathway was shown to be involved in Septin ring organization and regulation of Cdc42 activity (Iwase et al., 2007; Atkins et al., 2013). The mammalian homologue IQGAP1 binds the Exocyst-Septin complex via its N-terminus, probably via Sept2, and Cdc42-GTP via its C-terminus (Hedman et al., 2015; Wang et al., 2009) showing functional interdependence like regulation of secretion (Rittmeyer et al., 2008). Normal levels of Cdc42 activity (more GDP) regulate the assembly of Septin fibers via "free to bind Borgs", and Borgs lead to a stabilization and bundling of Septin filaments, which is consistent with the strong focal assembly (big blob) of Septins seen in young HSCs (**Figure 1B**). Such a view is further consistent with the recent finding from our laboratory that upon aging of HSCs, there is a switch in the Cdc42-Borg-Septin relationship: Elevated Cdc42 activity in aged correlated with co-localization of Cdc42 and Borg4, whereas in young HSCs (lower Cdc42 activity) Borg4 and Sept7 co-localized (Kandi et al., 2021) (**Figure 1A**). In conclusion, these data support that Cdc42 activity influences Septin behavior in both yeast and adult stem cells like HSCs and might also be critical for the role of Septins in quiescence.

2) Cdc42 activity changes upon quiescence as quiescence requires a downregulation of mTOR, of PKA, of Pho80-Pho85 and an upregulation of Snf1/AMPK, which altogether means more Septin-Exocyst complexes being bound to Iqg1 (mTOR, Snf1) (Xu et al., 2012), a dampened activity of Cdc42 (Pho80-Pho85) (Paglini et al., 2001; Sopko et al., 2007) with more membrane-bound Cdc42 (PKA) (Forget et al., 2002; Johnson et al., 2009). In summary, there is indeed a switch of Septin-Gic/Borg interactions regulated by Cdc42 activity in yeast and HSCs, which influences bundling and stabilization of Septin filaments. As it has not been tested though whether Cdc42-GDP indeed disturbs Septin filaments in HSCs like it does in yeast, it still remains a possibility that the Cdc42-Borg-Septin axis is somewhat distinct between yeast and HSCs with respect to quiescence.

3) While Septins also actively participate in forming the cytoskeleton (Kinoshita et al., 2002; Mavrakis et al., 2014; Kuzmić et al., 2021), they are not directly involved in the reorganization and restructuring of Actin and microtubules upon quiescence in yeast (Sagot et al., 2006; Laporte et al., 2013; Laporte et al., 2015). However, in HSCs a link of Septins to the cytoskeleton was shown by the finding that Ptpn21 localizing to Actin filaments is important for Sept1 dephosphorylation and Sept1 dephosphorylation level is crucial for HSC stiffness and retention in the bone marrow niche (Ni et al., 2019 and see **Table1**). Thus, in this case, investigations into the role of Septins in HSCs might inform on likely mechanisms of interactions of Septins with the cytoskeleton in yeast. Nonetheless, the involvement of Septins in reorganization of the other cytoskeleton components upon quiescence is still uncharted territory. An in depth understanding of the role Septins play in regulating quiescence will be important for basic stem cell biology, aging and cancer research.

Asymmetric Division

Asymmetric divisions first allow stem cells to provide a more differentiated cell that will contribute to tissue homeostasis while maintaining the pool of stem cells. Asymmetric division is also thought to be the key to produce one daughter cell which is free of already damaged products and one daughter cell which takes all these damaged products, and is regarded as kind of a rejuvenation strategy (Higuchi-Sanabria et al., 2014). Several organelles, proteins and mRNAs are asymmetrically inherited to daughters in yeast (McFaline-Figueroa et al., 2011; Shcheprova et al., 2008; Kennedy and McCormick, 2011; Henderson et al., 2014; Yang et al., 2015; Spokoini et al., 2012). The same holds true for mammalian stem cells (Inaba and Yamashita, 2012; Katajisto et al., 2015; Wang X. et al., 2009; Paridaen et al., 2013; Kuo et al., 2011; Rujano et al., 2006; Fuentealba et al., 2008; Loeffler et al., 2019; Hinge et al., 2020; Vannini et al., 2019; Loeffler at al., 2021). Proteins and organelles need to be distributed in a polar fashion

in cells during mitosis to allow for an asymmetric split-up. Our data show that polarity/symmetry in quiescent cells correlates with the type of division mode (symmetric/asymmetric) (Florian et al., 2018). Similar findings were made for mitochondria inheritance in HSCs (Hinge et al., 2020) and inheritance of lysosomes, autophagosomes, mitophagosomes, NUMB, Notch1 and CD63 which functionally predict the activation of daughter cells and thus their fates (Loeffler et al., 2019).

As Septins are master regulators of asymmetry and polarity (Spiliotis and McMurray, 2020), it is very likely that they play a role not only in the asymmetric division of budding yeast but as well also in HSC division and general asymmetric distribution of proteins within HSCs. We could recently demonstrate that Sept7 is indeed involved in regulating the distribution of polarity proteins in HSCs (Kandi et al., 2021, see **Table1**). Budding yeast achieves polarity and thus asymmetry during cell cytokinesis by three consecutive steps with enduring Septin support: 1) deciding upon a bud site and 2) passage of cellular components through a barrier and 3) active retainment of components within a compartmentalized space.

1) The first step is made by landmark proteins that then activate Rsr1 at a specific location. Rsr1-GTP recruits Cdc24, which functions as guanine-nucleotide-exchange factor (GEF) for Cdc42. Cdc42 is activated by Cdc24. Cdc42 further accumulates by positive feedback mechanisms that result in an area of high density of Cdc42-GTP. Septins then move to the high density Cdc42-GTP area. Right before budding Cdc24 interacts with the Septin Cdc11, which is essential for Septin recruitment and stability of the polarity patch (Park et al., 1997; Kang et al., 2001; Shimada et al., 2004; Chollet et al., 2020). Septins then form the characteristic ring-like filaments at the bud site (Okada et al., 2013). Cdc42 activity therefore plays a role in the polarization of the Septin ring. Whether there is a ring-like structure of Septins upon initiation of division of HSCs is currently not known.

2) The second step is regulated by the Septin ring which functions like a lateral diffusion barrier and compartmentalizes the bud. Septins can via this means function as a barrier for misfolded proteins of endoplasmic reticulum (ER) in the mother cell in a Septin-, Bud1-and sphingolipid-dependent manner (Chao et al., 2014; Clay et al., 2014). Similar mechanisms are proposed for the role of Septins in neurons, in which dendritic spines are restricted in the diffusion of ER proteins (Tada et al., 2007; Xie et al., 2007). It is thus likely that Septins can also play a similar role in HSCs, and also function in HSCs both as scaffold and as barrier in the process of asymmetric divisions.

3) The third step, active retainment, is fulfilled by anchor proteins that are transported to the bud and retain transported organelles and proteins in the bud or in the mother cell. While asymmetrically inherited mRNA is transported by Actin (Munchow et al., 1999; Takizawa et al., 2000), Septins act like a diffusion barrier by holding proteins that anchor organelles to the bud tip like Mmr1. (Fehrenbacher et al., 2004; McFaline-Figueroa et al., 2011; Swayne et al., 2011; Higuchi et al., 2013). Septins were also shown to interact with membrane components like phosphatidylinositol-4,5-bisphospate (PIP2). Septins are curvature-sensitive and capable of shaping the form of membranes (Gladfelter et al., 2005; Tanaka-Takiguchi et al., 2009; Bertin et al., 2010; Beber et al., 2019; Cannon et al., 2019). It is thus a possibility that Septins form lipid scaffolds for proteins, which themselves do not interact with Septins but are retained due to specific lipid or protein composition of the lipid scaffold. Research into the interaction of the lipidome with Septins will be necessary to obtain novel information on this likely novel role of Septins in the regulation of asymmetry, also presumably in HSCs.

While there has been ample progress in understanding the role of Septins for asymmetric division in yeast, so far, there have been no investigations published on the role of Septins and the Septin network in HSCs or even other stem cells for retaining or repulsing proteins and organelles upon division. Mammalian stem cell research has been focused on the role of individual Septins and their role for organelles. A disruption of mitochondrial fission in human mammary stem-like cells leads to symmetrical inheritance (Katajisto et al., 2015). A Drp1-mediated, distinct localization of old mitochondria is important for this asymmetric inheritance (Hinge et al., 2020). Sept2 is a known Drp1 interaction partner involved in mitochondria fission, implying indeed that Sept2 might be involved in an asymmetric inheritance of mitochondria upon division (Pagliuso et al., 2016). Centriole and cilium inheritance is asymmetric in radial glial progenitor cells (Wang X. et al., 2009; Paridaen et al., 2013). As Sept7 is a centrosomal protein and is involved in the process of mitotic spindle pole formation (Chen et al., 2021), it is possible that it also plays a role in asymmetric inheritance of centrioles and primary cilium in progenitor cells. A main unsolved question remains the nature of the role of the Septin network and thus filaments in HSCs and even in yeast. While the function of Septins has been frequently linked to their function within the filament network, recent data from our laboratory imply a non-filament linked, distinct polar/apolar distribution of Sept7, Sept2 and Sept6 in HSCs (Kandi et al., 2021b). For example, the distribution of Sept7 and Sept2 in HSCs is quite distinct (**Figure 1C**), which questions whether these Septins are indeed strongly interacting. Novel research on the role of Septins for the division of HSCs will thus need to focus on both the role of the Septin network as well as the role of individual Septins.

PERSPECTIVES

While Septins have been investigated since the early 1970s, even after now more than these 50 years of Septin research, the Septin field is still an emerging field with recent novel exciting developments like a revisited order of human Septins (instead of the previously postulated hexamer form "Sept7-Sept6-Sept2-Sept2-Sept6-Sept7" the novel hexamer form reads "Sept2-Sept6-Sept7-Sept7-Sept6-Sept2" and instead of the postulated octamer form "Sept9-Sept7-Sept6-Sept2-Sept2-Sept6-Sept7-Sept9" the novel octamer form reads "Sept2-Sept6-Sept7-Sept9-Sept9-Sept7-Sept6-Sept2"). (McMurray and Thorner, 2019; Mendonça et al., 2019; Soroor et al., 2021). So far, little is known about the role of Septins in maintenance of quiescence in yeast and stem cells, while the same holds true for the role of

Septins in asymmetric division and asymmetric protein distribution in stem cells. The role of Septins for an asymmetric division in yeast has been extensively studied, and in general, Septin biology in yeast might thus serve indeed as an initial blueprint for Septins in other types of stem cells like HSCs.

It is becoming more and more obvious though that Septins act also very cell type-specific, and have specific functions in distinct types of cells, especially among differentiated cells or cell lines. It will become therefore critical to investigate the role of Septins in a variety of cell types in order to understand their distinct behavior and to initiate transition of knowledge for example to drug development approaches to harvest differential sensitivities of cells to drugs targeting specific Septins (Menon and Gaestel, 2015). Another critical question that requires more attention is the organization state of Septins within cells, as both Septin filaments but also individual Septins outside of filaments are likely to have major biological function. Novel proteomics, lipidomics and immunofluorescence approaches that work on a few or even single cells will support the hunt for interaction partners of Septins and the organization of the Septin network in rare stem cells. It is likely that stem cells, due to their requirement of balancing quiescence and cycling and symmetric and asymmetric division might provide a fertile ground for elucidating these complex and context-dependent roles already within 1 cell type, as the underlying complexity that requires a versatile function of Septins might likely not be found in differentiated cells.

AUTHOR CONTRIBUTIONS

TS and HG wrote the manuscript.

FUNDING

TS is supported by the RTG 1789 CEMMA funded by the DFG.

ACKNOWLEDGMENTS

We thank the members of the Geiger lab for the input on the manuscript.

REFERENCES

Atkins, B. D., Yoshida, S., Saito, K., Wu, C.-F., Lew, D. J., and Pellman, D. (2013). Inhibition of Cdc42 during Mitotic Exit Is Required for Cytokinesis. *J. Cel Biol* 202, 231–240. doi:10.1083/jcb.201301090

Beber, A., Taveneau, C., Nania, M., Tsai, F.-C., Di Cicco, A., Bassereau, P., et al. (2019). Membrane Reshaping by Micrometric Curvature Sensitive Septin Filaments. *Nat. Commun.* 10, 420. doi:10.1038/s41467-019-08344-5

Bertin, A., McMurray, M. A., Thai, L., Garcia, G., Votin, V., Grob, P., et al. (2010). Phosphatidylinositol-4,5-bisphosphate Promotes Budding Yeast Septin Filament Assembly and Organization. *J. Mol. Biol.* 404, 711–731. doi:10.1016/j.jmb.2010.10.002

Bridges, A. A., Zhang, H., Mehta, S. B., Occhipinti, P., Tani, T., and Gladfelter, A. S. (2014). Septin Assemblies Form by Diffusion-Driven Annealing on Membranes. *Proc. Natl. Acad. Sci. USA* 111, 2146–2151. doi:10.1073/pnas.1314138111

Brown, J. L., Jaquenoud, M., Gulli, M.-P., Chant, J., and Peter, M. (1997). Novel Cdc42-Binding Proteins Gic1 and Gic2 Control Cell Polarity in Yeast. *Genes Dev.* 11, 2972–2982. doi:10.1101/gad.11.22.2972

Byers, B., and Goetsch, L. (1976). A Highly Ordered Ring of Membrane-Associated Filaments in Budding Yeast. *J. Cel. Biol.* 69, 717–721. doi:10.1083/jcb.69.3.717

Cannon, K. S., Woods, B. L., Crutchley, J. M., and Gladfelter, A. S. (2019). An Amphipathic helix Enables Septins to Sense Micrometer-Scale Membrane Curvature. *J. Cel Biol* 218, 1128–1137. doi:10.1083/jcb.201807211

Carolina Florian, M., and Geiger, H. (2010). Concise Review: Polarity in Stem Cells, Disease, and Aging. *Stem cells* 28, 1623–1629. doi:10.1002/stem.481

Caviston, J. P., Longtine, M., Pringle, J. R., and Bi, E. (2003). The Role of Cdc42p Gtpase-Activating Proteins in Assembly of the Septin Ring in Yeast. *MBoC* 14, 4051–4066. doi:10.1091/mbc.e03-04-0247

Chao, J. T., Wong, A. K. O., Tavassoli, S., Young, B. P., Chruscicki, A., Fang, N. N., et al. (2014). Polarization of the Endoplasmic Reticulum by Er-Septin Tethering. *Cell* 158, 620–632. doi:10.1016/j.cell.2014.06.033

Chen, C., Liu, Y., Liu, R., Ikenoue, T., Guan, K.-L., Liu, Y., et al. (2008). Tsc-mtor Maintains Quiescence and Function of Hematopoietic Stem Cells by Repressing Mitochondrial Biogenesis and Reactive Oxygen Species. *J. Exp. Med.* 205, 2397–2408. doi:10.1084/jem.20081297

Chen, T. Y., Lin, T. C., Kuo, P. L., Chen, Z. R., Cheng, H. l., Chao, Y. Y., et al. (2021). Septin 7 Is a Centrosomal Protein that Ensures S Phase Entry and Microtubule Nucleation by Maintaining the Abundance of P150 Glued. *J. Cel Physiol* 236, 2706–2724. doi:10.1002/jcp.30037

Cheng, C.-W., Adams, G. B., Perin, L., Wei, M., Zhou, X., Lam, B. S., et al. (2014). Prolonged Fasting Reduces Igf-1/pka to Promote Hematopoietic-Stem-Cell-Based Regeneration and Reverse Immunosuppression. *Cell stem cell* 14, 810–823. doi:10.1016/j.stem.2014.04.014

Cheshier, S. H., Morrison, S. J., Liao, X., and Weissman, I. L. (1999). *In Vivo* proliferation and Cell Cycle Kinetics of Long-Term Self-Renewing Hematopoietic Stem Cells. *Proc. Natl. Acad. Sci.* 96, 3120–3125. doi:10.1073/pnas.96.6.3120

Chollet, J., Dünkler, A., Bäuerle, A., Vivero-Pol, L., Mulaw, M. A., Gronemeyer, T., et al. (2020). Cdc24 Interacts with Septins to Create a Positive Feedback Loop during Bud Site Assembly in Yeast. *J. Cel Sci* 133, jcs240283. doi:10.1242/jcs.240283

Clay, L., Caudron, F., Denoth-Lippuner, A., Boettcher, B., Buvelot Frei, S., Snapp, E. L., et al. (2014). A Sphingolipid-dependent Diffusion Barrier Confines Er Stress to the Yeast Mother Cell. *Elife* 3, e01883. doi:10.7554/eLife.01883

Dhawan, J., and Laxman, S. (2015). Decoding the Stem Cell Quiescence Cycle - Lessons from Yeast for Regenerative Biology. *J. Cel. Sci.* 128, 4467–4474. doi:10.1242/jcs.177758

Dykstra, B., Olthof, S., Schreuder, J., Ritsema, M., and De Haan, G. (2011). Clonal Analysis Reveals Multiple Functional Defects of Aged Murine Hematopoietic Stem Cells. *J. Exp. Med.* 208, 2691–2703. doi:10.1084/jem.20111490

Ewers, H., Tada, T., Petersen, J. D., Racz, B., Sheng, M., and Choquet, D. (2014). A Septin-dependent Diffusion Barrier at Dendritic Spine Necks. *PloS one* 9, e113916. doi:10.1371/journal.pone.0113916

Fehrenbacher, K. L., Yang, H.-C., Gay, A. C., Huckaba, T. M., and Pon, L. A. (2004). Live Cell Imaging of Mitochondrial Movement along Actin Cables in Budding Yeast. *Curr. Biol.* 14, 1996–2004. doi:10.1016/j.cub.2004.11.004

Florian, M. C., Dörr, K., Niebel, A., Daria, D., Schrezenmeier, H., Rojewski, M., et al. (2012). Cdc42 Activity Regulates Hematopoietic Stem Cell Aging and Rejuvenation. *Cell stem cell* 10, 520–530. doi:10.1016/j.stem.2012.04.007

Florian, M. C., Klose, M., Sacma, M., Jablanovic, J., Knudson, L., Nattamai, K. J., et al. (2018). Aging Alters the Epigenetic Asymmetry of HSC Division. *Plos Biol.* 16 (9), e2003389. doi:10.1371/journal.pbio.2003389

Forget, M.-A., Desrosiers, R. R., Gingras, D., and Béliveau, R. (2002). Phosphorylation States of Cdc42 and Rhoa Regulate Their Interactions with Rho Gdp Dissociation Inhibitor and Their Extraction from Biological Membranes. *Biochem. J.* 361, 243–254. doi:10.1042/bj3610243

Fuentealba, L. C., Eivers, E., Geissert, D., Taelman, V., and De Robertis, E. M. (2008). Asymmetric Mitosis: Unequal Segregation of Proteins Destined for Degradation. *Proc. Natl. Acad. Sci.* 105, 7732–7737. doi:10.1073/pnas.0803027105

Gan, B., Hu, J., Jiang, S., Liu, Y., Sahin, E., Zhuang, L., et al. (2010). Lkb1 Regulates Quiescence and Metabolic Homeostasis of Haematopoietic Stem Cells. *Nature* 468, 701–704. doi:10.1038/nature09595

Garcia, G., Bertin, A., Li, Z., Song, Y., McMurray, M. A., Thorner, J., et al. (2011). Subunit-dependent Modulation of Septin Assembly: Budding Yeast Septin Shs1 Promotes Ring and Gauze Formation. *J. Cel Biol* 195, 993–1004. doi:10.1083/jcb.201107123

Gladfelter, A. S., Kozubowski, L., Zyla, T. R., and Lew, D. J. (2005). Interplay between Septin Organization, Cell Cycle and Cell Shape in Yeast. *J. Cel. Sci.* 118, 1617–1628. doi:10.1242/jcs.02286

Gray, J. V., Petsko, G. A., Johnston, G. C., Ringe, D., Singer, R. A., and Werner-Washburne, M. (2004). "sleeping beauty": Quiescence in saccharomyces Cerevisiae. *Microbiol. Mol. Biol. Rev.* 68, 187–206. doi:10.1128/mmbr.68.2.187-206.2004

Grigoryan, A., Guidi, N., Senger, K., Liehr, T., Soller, K., Marka, G., et al. (2018). LaminA/C Regulates Epigenetic and Chromatin Architecture Changes upon Aging of Hematopoietic Stem Cells. *Genome Biol.* 19, 189. doi:10.1186/s13059-018-1557-3

Hagiwara, A., Tanaka, Y., Hikawa, R., Morone, N., Kusumi, A., Kimura, H., et al. (2011). Submembranous Septins as Relatively Stable Components of Actin-Based Membrane Skeleton. *Cytoskeleton* 68, 512–525. doi:10.1002/cm.20528

Hartwell, L. H., Culotti, J., and Reid, B. (1970). Genetic Control of the Cell-Division Cycle in Yeast, I. Detection of Mutants. *Proc. Natl. Acad. Sci.* 66, 352–359. doi:10.1073/pnas.66.2.352

Heasley, L. R., and McMurray, M. A. (2016). Roles of Septins in Prospore Membrane Morphogenesis and Spore wall Assembly inSaccharomyces Cerevisiae. *MBoC* 27, 442–450. doi:10.1091/mbc.e15-10-0721

Hedman, A. C., Smith, J. M., and Sacks, D. B. (2015). The Biology of IQGAP Proteins: beyond the Cytoskeleton. *EMBO Rep.* 16, 427–446. doi:10.15252/embr.201439834

Henderson, K. A., Hughes, A. L., and Gottschling, D. E. (2014). Mother-daughter Asymmetry of Ph Underlies Aging and Rejuvenation in Yeast. *Elife* 3, e03504. doi:10.7554/eLife.03504

Hendil, K. B. (1981). Autophagy of Metabolically Inert Substances Injected into Fibroblasts in Culture. *Exp. Cel. Res.* 135, 157–166. doi:10.1016/0014-4827(81)90308-6

Higuchi, R., Vevea, J. D., Swayne, T. C., Chojnowski, R., Hill, V., Boldogh, I. R., et al. (2013). Actin Dynamics Affect Mitochondrial Quality Control and Aging in Budding Yeast. *Curr. Biol.* 23, 2417–2422. doi:10.1016/j.cub.2013.10.022

Higuchi-Sanabria, R., Pernice, W. M. A., Vevea, J. D., Alessi Wolken, D. M., Boldogh, I. R., and Pon, L. A. (2014). Role of Asymmetric Cell Division in Lifespan Control inSaccharomyces Cerevisiae. *FEMS Yeast Res.* 14, 1133–1146. doi:10.1111/1567-1364.12216

Hinge, A., He, J., Bartram, J., Javier, J., Xu, J., Fjellman, E., et al. (2020). Asymmetrically Segregated Mitochondria Provide Cellular Memory of Hematopoietic Stem Cell Replicative History and Drive HSC Attrition. *Cell Stem CellPMCID* 26 (3), 420PMC7212526–430. doi:10.1016/j.stem.2020.01.016

Inaba, M., and Yamashita, Y. M. (2012). Asymmetric Stem Cell Division: Precision for Robustness. *Cell stem cell* 11, 461–469. doi:10.1016/j.stem.2012.09.003

Iwase, M., Luo, J., Bi, E., and Toh-e, A. (2007). Shs1 Plays Separable Roles in Septin Organization and Cytokinesis in *Saccharomyces cerevisiae*. *Genetics* 177, 215–229. doi:10.1534/genetics.107.073007

Janzen, V., Forkert, R., Fleming, H. E., Saito, Y., Waring, M. T., Dombkowski, D. M., et al. (2006). Stem-cell Ageing Modified by the Cyclin-dependent Kinase Inhibitor p16INK4a. *Nature* 443, 421–426. doi:10.1038/nature05159

Jiao, F., Cannon, K. S., Lin, Y.-C., Gladfelter, A. S., and Scheuring, S. (2020). The Hierarchical Assembly of Septins Revealed by High-Speed Afm. *Nat. Commun.* 11, 5062. doi:10.1038/s41467-020-18778-x

Joberty, G., Perlungher, R. R., and Macara, I. G. (1999). The Borgs, a New Family of Cdc42 and Tc10 Gtpase-Interacting Proteins. *Mol. Cel Biol* 19, 6585–6597. doi:10.1128/mcb.19.10.6585

Joberty, G., Perlungher, R. R., Sheffield, P. J., Kinoshita, M., Noda, M., Haystead, T., et al. (2001). Borg Proteins Control Septin Organization and Are Negatively Regulated by Cdc42. *Nat. Cel Biol* 3, 861–866. doi:10.1038/ncb1001-861

Johnson, J. L., Erickson, J. W., and Cerione, R. A. (2009). New Insights into How the Rho Guanine Nucleotide Dissociation Inhibitor Regulates the Interaction of Cdc42 with Membranes. *J. Biol. Chem.* 284, 23860–23871. doi:10.1074/jbc.m109.031815

Kandi, R., Senger, K., Grigoryan, A., Soller, K., Sakk, V., Schuster, T., et al. (2021b). A Cdc42-Borg4-Septin 7 axis Regulates HSCs Polarity and Function. *bioRxiv*. doi:10.1101/2021.03.17.435817

Kandi, R., Senger, K., Grigoryan, A., Soller, K., Sakk, V., Schuster, T., et al. (2021). Cdc42-Borg4-Septin7 axis Regulates HSC Polarity and Function. *EMBO Rep.*, e52931. doi:10.15252/embr.202152931

Kang, P. J., Mullner, R., Li, H., Hansford, D., Shen, H.-W., and Park, H.-O. (2021). Upregulation of the Cdc42 GTPase Limits Replicative Lifespan in Budding Yeast. *bioRxiv*. doi:10.1101/2021.04.27.441634

Kang, P. J., Sanson, A., Lee, B., and Park, H.-O. (2001). A GDP/GTP Exchange Factor Involved in Linking a Spatial Landmark to Cell Polarity. *Science* 292, 1376–1378. doi:10.1126/science.1060360

Katajisto, P., Döhla, J., Chaffer, C. L., Pentinmikko, N., Marjanovic, N., Iqbal, S., et al. (2015). Asymmetric Apportioning of Aged Mitochondria between Daughter Cells Is Required for Stemness. *Science* 348, 340–343. doi:10.1126/science.1260384

Kennedy, B. K., and McCormick, M. A. (2011). Asymmetric Segregation: the Shape of Things to Come? *Curr. Biol.* 21, R149–R151. doi:10.1016/j.cub.2011.01.018

Kinoshita, M. (2003). Assembly of Mammalian Septins. *J. Biochem.* 134, 491–496. doi:10.1093/jb/mvg182

Kinoshita, M., Field, C. M., Coughlin, M. L., Straight, A. F., and Mitchison, T. J. (2002). Self- and Actin-Templated Assembly of Mammalian Septins. *Develop. Cel.* 3, 791–802. doi:10.1016/s1534-5807(02)00366-0

Kniss, D. A., and Burry, R. W. (1988). Serum and Fibroblast Growth Factor Stimulate Quiescent Astrocytes to Re-enter the Cell Cycle. *Brain Res.* 439, 281–288. doi:10.1016/0006-8993(88)91485-0

Kops, G. J. P. L., Dansen, T. B., Polderman, P. E., Saarloos, I., Wirtz, K. W. A., Coffer, P. J., et al. (2002). Forkhead Transcription Factor Foxo3a Protects Quiescent Cells from Oxidative Stress. *Nature* 419, 316–321. doi:10.1038/nature01036

Kuo, T.-C., Chen, C.-T., Baron, D., Onder, T. T., Loewer, S., Almeida, S., et al. (2011). Midbody Accumulation through Evasion of Autophagy Contributes to Cellular Reprogramming and Tumorigenicity. *Nat. Cel Biol* 13, 1214–1223. doi:10.1038/ncb2332

Kuzmić, M., Linares, G. C., Fialova´, J. L., Iv, F., Salau¨n, D., Llewellyn, A., et al. (2021). Septin Microtubule Association Requires a Map-like Motif Unique to Sept9 Isoform 1 Embedded into Septin Octamers. *BioRxiv*.

Laporte, D., Courtout, F., Pinson, B., Dompierre, J., Salin, B., Brocard, L., et al. (2015). A Stable Microtubule Array Drives Fission Yeast Polarity Reestablishment upon Quiescence Exit. *J. Cel Biol.* 210, 99–113. doi:10.1083/jcb.201502025

Laporte, D., Courtout, F., Salin, B., Ceschin, J., and Sagot, I. (2013). An Array of Nuclear Microtubules Reorganizes the Budding Yeast Nucleus during Quiescence. *J. Cel Biol.* 203, 585–594. doi:10.1083/jcb.201306075

Leonardo, D. A., Cavini, I. A., Sala, F. A., Mendonça, D. C., Rosa, H. V. D., Kumagai, P. S., et al. (2021). Orientational Ambiguity in Septin Coiled Coils and its Structural Basis. *J. Mol. Biol.* 433, 166889. doi:10.1016/j.jmb.2021.166889

Liang, Y., Van Zant, G., and Szilvassy, S. J. (2005). Effects of Aging on the Homing and Engraftment of Murine Hematopoietic Stem and Progenitor Cells. *Blood* 106, 1479–1487. doi:10.1182/blood-2004-11-4282

Liu, Y., Elf, S. E., Miyata, Y., Sashida, G., Liu, Y., Huang, G., et al. (2009). p53 Regulates Hematopoietic Stem Cell Quiescence. *Cell stem cell* 4, 37–48. doi:10.1016/j.stem.2008.11.006

Lobato-Márquez, D., Xu, J., Güler, G. Ö., Ojiakor, A., Pilhofer, M., and Mostowy, S. (2021). Mechanistic Insight into Bacterial Entrapment by Septin Cage Reconstitution. *Nat. Commun.* 12, 4511. doi:10.1038/s41467-021-24721-5

Loeffler, D., Schneiter, F., Wang, W., Wehling, A., Kull, T., Lengerke, C., et al. (2021). Asymmetric Organelle Inheritance Predicts Human Blood Stem Cell Fate. *Blood, blood*, 2020009778. doi:10.1182/blood.2020009778

Loeffler, D., Wehling, A., Schneiter, F., Zhang, Y., Müller-Bötticher, N., Hoppe, P. S., et al. (2019). Asymmetric Lysosome Inheritance Predicts Activation of Haematopoietic Stem Cells. *Nature* 573, 426–429. doi:10.1038/s41586-019-1531-6

Matsumoto, A., Takeishi, S., Kanie, T., Susaki, E., Onoyama, I., Tateishi, Y., et al. (2011). p57 Is Required for Quiescence and Maintenance of Adult Hematopoietic Stem Cells. *Cell stem cell* 9, 262–271. doi:10.1016/j.stem.2011.06.014

Mavrakis, M., Azou-Gros, Y., Tsai, F.-C., Alvarado, J., Bertin, A., Iv, F., et al. (2014). Septins Promote F-Actin Ring Formation by Crosslinking Actin Filaments into Curved Bundles. *Nat. Cel Biol* 16, 322–334. doi:10.1038/ncb2921

McFaline-Figueroa, J. R., Vevea, J., Swayne, T. C., Zhou, C., Liu, C., Leung, G., et al. (2011). Mitochondrial Quality Control during Inheritance Is Associated with Lifespan and Mother-Daughter Age Asymmetry in Budding Yeast. *Aging cell* 10, 885–895. doi:10.1111/j.1474-9726.2011.00731.x

McMurray, M. A., and Thorner, J. (2008). Septin Stability and Recycling during Dynamic Structural Transitions in Cell Division and Development. *Curr. Biol.* 18, 1203–1208. doi:10.1016/j.cub.2008.07.020

McMurray, M. A., and Thorner, J. (2019). Turning it inside Out: the Organization of Human Septin Heterooligomers. *Cytoskeleton* 76, 449–456. doi:10.1002/cm.21571

Mendonça, D. C., Macedo, J. N., Guimarães, S. L., Barroso da Silva, F. L., Cassago, A., Garratt, R. C., et al. (2019). A Revised Order of Subunits in Mammalian Septin Complexes. *Cytoskeleton (Hoboken)* 76, 457–466. doi:10.1002/cm.21569

Menon, M. B., and Gaestel, M. (2015). Sep(t)arate or Not - How Some Cells Take Septin-independent Routes through Cytokinesis. *J. Cel. Sci.* 128, 1877–1886. doi:10.1242/jcs.164830

Menon, M. B., Sawada, A., Chaturvedi, A., Mishra, P., Schuster-Gossler, K., Galla, M., et al. (2014). Genetic Deletion of Sept7 Reveals a Cell Type-specific Role of Septins in Microtubule Destabilization for the Completion of Cytokinesis. *Plos Genet.* 10, e1004558. doi:10.1371/journal.pgen.1004558

Mostowy, S., Bonazzi, M., Hamon, M. A., Tham, T. N., Mallet, A., Lelek, M., et al. (2010). Entrapment of Intracytosolic Bacteria by Septin Cage-like Structures. *Cell Host & Microbe* 8, 433–444. doi:10.1016/j.chom.2010.10.009

Mostowy, S., Nam Tham, T., Danckaert, A., Guadagnini, S., Boisson-Dupuis, S., Pizarro-Cerdá, J., et al. (2009). Septins Regulate Bacterial Entry into Host Cells. *PloS one* 4, e4196. doi:10.1371/journal.pone.0004196

Munchow, S., Sauter, C., and Jansen, R. P. (1999). Association of the Class V Myosin Myo4p with a Localised Messenger Rna in Budding Yeast Depends on She Proteins. *J. Cel. Sci.* 112, 1511–1518. doi:10.1242/jcs.112.10.1511

Nagele, R. G., Freeman, T., McMorrow, L., Thomson, Z., Kitson-Wind, K., and Lee, H. (1999). Chromosomes Exhibit Preferential Positioning in Nuclei of Quiescent Human Cells. *J. Cel. Sci.* 112, 525–535. doi:10.1242/jcs.112.4.525

Nakamura-Ishizu, A., Takubo, K., Fujioka, M., and Suda, T. (2014). Megakaryocytes Are Essential for Hsc Quiescence through the Production of Thrombopoietin. *Biochem. biophysical Res. Commun.* 454, 353–357. doi:10.1016/j.bbrc.2014.10.095

Ni, F., Yu, W.-M., Wang, X., Fay, M. E., Young, K. M., Qiu, Y., et al. (2019). Ptpn21 Controls Hematopoietic Stem Cell Homeostasis and Biomechanics. *Cell stem cell* 24, 608–620. doi:10.1016/j.stem.2019.02.009

Okada, S., Leda, M., Hanna, J., Savage, N. S., Bi, E., and Goryachev, A. B. (2013). Daughter Cell Identity Emerges from the Interplay of Cdc42, Septins, and Exocytosis. *Develop. Cel* 26, 148–161. doi:10.1016/j.devcel.2013.06.015

Paglini, G., Peris, L., Diez-Guerra, J., Quiroga, S., and Cáceres, A. (2001). The Cdk5-p35 Kinase Associates with the Golgi Apparatus and Regulates Membrane Traffic. *EMBO Rep.* 2, 1139–1144. doi:10.1093/embo-reports/kve250

Pagliuso, A., Tham, T. N., Stevens, J. K., Lagache, T., Persson, R., Salles, A., et al. (2016). A Role for Septin 2 in Drp1-mediated Mitochondrial Fission. *EMBO Rep.* 17, 858–873. doi:10.15252/embr.201541612

Pan, F., Malmberg, R. L., and Momany, M. (2007). Analysis of Septins across Kingdoms Reveals Orthology and New Motifs. *BMC Evol. Biol.* 7, 103. doi:10.1186/1471-2148-7-103

Paridaen, J. T. M. L., Wilsch-Bräuninger, M., and Huttner, W. B. (2013). Asymmetric Inheritance of Centrosome-Associated Primary Cilium Membrane Directs Ciliogenesis after Cell Division. *Cell* 155, 333–344. doi:10.1016/j.cell.2013.08.060

Park, H.-O., Bi, E., Pringle, J. R., and Herskowitz, I. (1997). Two Active States of the Ras-Related Bud1/Rsr1 Protein Bind to Different Effectors to Determine Yeast Cell Polarity. *Proc. Natl. Acad. Sci.* 94, 4463–4468. doi:10.1073/pnas.94.9.4463

Postnikoff, S. D. L., and Harkness, T. A. A. (2014). *Replicative and Chronological Life-Span Assays*. Springer, 223–227. doi:10.1007/978-1-4939-0799-1_17

Rittmeyer, E. N., Daniel, S., Hsu, S.-C., and Osman, M. A. (2008). A Dual Role for Iqgap1 in Regulating Exocytosis. *J. Cel. Sci.* 121, 391–403. doi:10.1242/jcs.016881

Roche, B., Arcangioli, B., and Martienssen, R. (2017). Transcriptional Reprogramming in Cellular Quiescence. *RNA Biol.* 14, 843–853. doi:10.1080/15476286.2017.1327510

Rujano, M. A., Bosveld, F., Salomons, F. A., Dijk, F., Van Waarde, M. A. W. H., Van Der Want, J. J. L., et al. (2006). Polarised Asymmetric Inheritance of Accumulated Protein Damage in Higher Eukaryotes. *Plos Biol.* 4, e417. doi:10.1371/journal.pbio.0040417

Sadian, Y., Gatsogiannis, C., Patasi, C., Hofnagel, O., Goody, R. S., Farkasovský, M., et al. (2013). The Role of Cdc42 and Gic1 in the Regulation of Septin Filament Formation and Dissociation. *Elife* 2, e01085. doi:10.7554/eLife.01085

Sagot, I., Pinson, B., Salin, B., and Daignan-Fornier, B. (2006). Actin Bodies in Yeast Quiescent Cells: an Immediately Available Actin reserve? *MBoC* 17, 4645–4655. doi:10.1091/mbc.e06-04-0282

Sandrock, K., Bartsch, I., Bläser, S., Busse, A., Busse, E., and Zieger, B. (2011). Characterization of Human Septin Interactions. *Characterization Hum. septin interactions* 392, 751–761. doi:10.1515/BC.2011.081

Schmidt, K., and Nichols, B. J. (2004). Functional Interdependence between Septin and Actin Cytoskeleton. *BMC Cel Biol* 5, 43–13. doi:10.1186/1471-2121-5-43

Senger, K., Marka, G., Soller, K., Sakk, V., Florian, M. C., and Geiger, H. (2017). Septin 6 Regulates Engraftment and Lymphoid Differentiation Potential of Murine Long-Term Hematopoietic Stem Cells. *Exp. Hematol.* 55, 45–55. doi:10.1016/j.exphem.2017.07.005

Shcheprova, Z., Baldi, S., Frei, S. B., Gonnet, G., and Barral, Y. (2008). A Mechanism for Asymmetric Segregation of Age during Yeast Budding. *Nature* 454, 728–734. doi:10.1038/nature07212

Sheffield, P. J., Oliver, C. J., Kremer, B. E., Sheng, S., Shao, Z., and Macara, I. G. (2003). Borg/septin Interactions and the Assembly of Mammalian Septin Heterodimers, Trimers, and Filaments. *J. Biol. Chem.* 278, 3483–3488. doi:10.1074/jbc.m209701200

Shimada, Y., Wiget, P., Gulli, M.-P., Bi, E., and Peter, M. (2004). The Nucleotide Exchange Factor Cdc24p May Be Regulated by Auto-Inhibition. *Embo J* 23, 1051–1062. doi:10.1038/sj.emboj.7600124.

Sopko, R., Huang, D., Smith, J. C., Figeys, D., and Andrews, B. J. (2007). Activation of the Cdc42p Gtpase by Cyclin-dependent Protein Kinases in Budding Yeast. *Embo J.* 26, 4487–4500. doi:10.1038/sj.emboj.7601847

Soroor, F., Kim, M. S., Palander, O., Balachandran, Y., Collins, R. F., Benlekbir, S., et al. (2021). Revised Subunit Order of Mammalian Septin Complexes Explains Their *In Vitro* Polymerization Properties. *MBoC* 32, 289–300. doi:10.1091/mbc.e20-06-0398

Spiliotis, E. T., and McMurray, M. A. (2020). Masters of Asymmetry - Lessons and Perspectives from 50 Years of Septins. *MBoC* 31, 2289–2297. doi:10.1091/mbc.e19-11-0648

Spokoini, R., Moldavski, O., Nahmias, Y., England, J. L., Schuldiner, M., and Kaganovich, D. (2012). Confinement to Organelle-Associated Inclusion Structures Mediates Asymmetric Inheritance of Aggregated Protein in Budding Yeast. *Cel Rep.* 2, 738–747. doi:10.1016/j.celrep.2012.08.024

Sun, D., Luo, M., Jeong, M., Rodriguez, B., Xia, Z., Hannah, R., et al. (2014). Epigenomic Profiling of Young and Aged Hscs Reveals Concerted Changes during Aging that Reinforce Self-Renewal. *Cell stem cell* 14, 673–688. doi:10.1016/j.stem.2014.03.002

Sun, S., and Gresham, D. (2021). Cellular Quiescence in Budding Yeast. *Yeast* 38, 12–29. doi:10.1002/yea.3545

Swayne, T. C., Zhou, C., Boldogh, I. R., Charalel, J. K., McFaline-Figueroa, J. R., Thoms, S., et al. (2011). Role for Cer and Mmr1p in anchorage of Mitochondria at Sites of Polarized Surface Growth in Budding Yeast. *Curr. Biol.* 21, 1994–1999. doi:10.1016/j.cub.2011.10.019

Tada, T., Simonetta, A., Batterton, M., Kinoshita, M., Edbauer, D., and Sheng, M. (2007). Role of Septin Cytoskeleton in Spine Morphogenesis and Dendrite Development in Neurons. *Curr. Biol.* 17, 1752–1758. doi:10.1016/j.cub.2007.09.039

Takizawa, P. A., DeRisi, J. L., Wilhelm, J. E., and Vale, R. D. (2000). Plasma Membrane Compartmentalization in Yeast by Messenger Rna Transport and a Septin Diffusion Barrier. *Science* 290, 341–344. doi:10.1126/science.290.5490.341

Tanaka-Takiguchi, Y., Kinoshita, M., and Takiguchi, K. (2009). Septin-mediated Uniform Bracing of Phospholipid Membranes. *Curr. Biol.* 19, 140–145. doi:10.1016/j.cub.2008.12.030

Targa, B., Klipfel, L., Cantaloube, I., Salameh, J., Benoit, B., Poüs, C., et al. (2019). Septin Filament Coalignment with Microtubules Depends on SEPT9_i1 and Tubulin Polyglutamylation, and Is an Early Feature of Acquired Cell Resistance to Paclitaxel. *Cell Death Dis* 10, 54–14. doi:10.1038/s41419-019-1318-6

Vannini, N., Campos, V., Girotra, M., Trachsel, V., Rojas-Sutterlin, S., Tratwal, J., et al. (2019). The NAD-Booster Nicotinamide Riboside Potently Stimulates Hematopoiesis through Increased Mitochondrial Clearance. *Cell Stem Cell* 24 (3), 405–418. doi:10.1016/j.stem.2019.02.012

Wang, J.-B., Sonn, R., Tekletsadik, Y. K., Samorodnitsky, D., and Osman, M. A. (2009). Iqgap1 Regulates Cell Proliferation through a Novel Cdc42-Mtor Pathway. *J. Cel. Sci.* 122, 2024–2033. doi:10.1242/jcs.044644

Wang, X., Fujimaki, K., Mitchell, G. C., Kwon, J. S., Della Croce, K., Langsdorf, C., et al. (2017). Exit from Quiescence Displays a Memory of Cell Growth and Division. *Nat. Commun.* 8, 321–411. doi:10.1038/s41467-017-00367-0

Wang, X., Tsai, J.-W., Imai, J. H., Lian, W.-N., Vallee, R. B., and Shi, S.-H. (2009b). Asymmetric Centrosome Inheritance Maintains Neural Progenitors in the Neocortex. *Nature* 461, 947–955. doi:10.1038/nature08435

Weems, A., McMurray, M., and Barral, Y. (2017). The Step-wise Pathway of Septin Hetero-Octamer Assembly in Budding Yeast. *eLife* 6, e23689. doi:10.7554/eLife.23689

Werner-Washburne, M., Braun, E., Johnston, G. C., and Singer, R. A. (1993). Stationary Phase in the Yeast saccharomyces Cerevisiae. *Microbiol. Rev.* 57, 383–401. doi:10.1128/mr.57.2.383-401.1993

Wilson, A., Laurenti, E., Oser, G., van der Wath, R. C., Blanco-Bose, W., Jaworski, M., et al. (2008). Hematopoietic Stem Cells Reversibly Switch from Dormancy to Self-Renewal during Homeostasis and Repair. *Cell* 135, 1118–1129. doi:10.1016/j.cell.2008.10.048

Xie, Y., Vessey, J. P., Konecna, A., Dahm, R., Macchi, P., and Kiebler, M. A. (2007). The Gtp-Binding Protein Septin 7 Is Critical for Dendrite Branching and Dendritic-Spine Morphology. *Curr. Biol.* 17, 1746–1751. doi:10.1016/j.cub.2007.08.042

Xu, J., Ji, J., and Yan, X.-H. (2012). Cross-talk between Ampk and Mtor in Regulating Energy Balance. *Crit. Rev. Food Sci. Nutr.* 52, 373–381. doi:10.1080/10408398.2010.500245

Yamazaki, S., Ema, H., Karlsson, G., Yamaguchi, T., Miyoshi, H., Shioda, S., et al. (2011). Nonmyelinating Schwann Cells Maintain Hematopoietic Stem Cell Hibernation in the Bone Marrow Niche. *Cell* 147 (5), 1146–1158. doi:10.1016/j.cell.2011.09.053

Yang, J., McCormick, M. A., Zheng, J., Xie, Z., Tsuchiya, M., Tsuchiyama, S., et al. (2015). Systematic Analysis of Asymmetric Partitioning of Yeast Proteome between Mother and Daughter Cells Reveals "Aging Factors" and Mechanism of Lifespan Asymmetry. *Proc. Natl. Acad. Sci. USA* 112, 11977–11982. doi:10.1073/pnas.1506054112

Yang, L., Wang, L., Geiger, H., Cancelas, J. A., Mo, J., and Zheng, Y. (2007b). Rho GTPase Cdc42 Coordinates Hematopoietic Stem Cell Quiescence and Niche Interaction in the Bone Marrow. *Proc. Natl. Acad. Sci.* 104, 5091–5096. doi:10.1073/pnas.0610819104

Yang, L., and Zheng, Y. (2007a). Cdc42: a Signal Coordinator in Hematopoietic Stem Cell Maintenance. *Cell cycle* 6, 1444–1449. doi:10.4161/cc.6.12.4371

Yusuf, I., and Fruman, D. A. (2003). Regulation of Quiescence in Lymphocytes. *Trends Immunology* 24, 380–386. doi:10.1016/s1471-4906(03)00141-8

Zhang, H., Pan, K.-H., and Cohen, S. N. (2003). Senescence-specific Gene Expression Fingerprints Reveal Cell-type-dependent Physical Clustering of Up-Regulated Chromosomal Loci. *Proc. Natl. Acad. Sci.* 100, 3251–3256. doi:10.1073/pnas.2627983100

Conflict of Interest: The authors declare that the research was conducted in the absence of any commercial or financial relationships that could be construed as a potential conflict of interest.

Publisher's Note: All claims expressed in this article are solely those of the authors and do not necessarily represent those of their affiliated organizations, or those of the publisher, the editors and the reviewers. Any product that may be evaluated in this article, or claim that may be made by its manufacturer, is not guaranteed or endorsed by the publisher.

frontiers in Cell and Developmental Biology

ORIGINAL RESEARCH
published: 21 December 2021
doi: 10.3389/fcell.2021.794807

Deficits Associated With Loss of STIM1 in Purkinje Neurons Including Motor Coordination Can Be Rescued by Loss of Septin 7

Sreeja Kumari Dhanya[1,2] *and Gaiti Hasan*[1]*

[1]National Centre for Biological Sciences, Tata Institute of Fundamental Research, Bangalore, India, [2]SASTRA University, Thanjavur, India

Septins are cytoskeletal proteins that can assemble to form heteromeric filamentous complexes and regulate a range of membrane-associated cellular functions. SEPT7, a member of the septin family, functions as a negative regulator of the plasma membrane–localized store-operated Ca^{2+} entry (SOCE) channel, Orai in *Drosophila* neurons, and in human neural progenitor cells. Knockdown of STIM, a Ca^{2+} sensor in the endoplasmic reticulum (ER) and an integral component of SOCE, leads to flight deficits in *Drosophila* that can be rescued by partial loss of SEPT7 in neurons. Here, we tested the effect of reducing and removing SEPT7 in mouse Purkinje neurons (PNs) with the loss of STIM1. Mice with the complete knockout of STIM1 in PNs exhibit several age-dependent changes. These include altered gene expression in PNs, which correlates with increased synapses between climbing fiber (CF) axons and Purkinje neuron (PN) dendrites and a reduced ability to learn a motor coordination task. Removal of either one or two copies of the *SEPT7* gene in *STIM1*^{KO} PNs restored the expression of a subset of genes, including several in the category of neuron projection development. Importantly, the rescue of gene expression in these animals is accompanied by normal CF-PN innervation and an improved ability to learn a motor coordination task in aging mice. Thus, the loss of SEPT7 in PNs further modulates cerebellar circuit function in *STIM1*^{KO} animals. Our findings are relevant in the context of identifying SEPT7 as a putative therapeutic target for various neurodegenerative diseases caused by reduced intracellular Ca^{2+} signaling.

Keywords: Ca2+ signaling, gene expression, climbing fibers, VGLUT2, SOCE, synaptic function, neurodegenerative disorders

OPEN ACCESS

Edited by:
Manoj B. Menon,
Indian Institute of Technology Delhi, India

Reviewed by:
Laura N. Borodinsky,
University of California, Davis, United States
Jeremy Smyth,
Uniformed Services University of the Health Sciences, United States

***Correspondence:**
Gaiti Hasan
gaiti@ncbs.res.in

Specialty section:
This article was submitted to Signaling, a section of the journal Frontiers in Cell and Developmental Biology

Received: *14 October 2021*
Accepted: *15 November 2021*
Published: *21 December 2021*

Citation:
Dhanya SK and Hasan G (2021) Deficits Associated With Loss of STIM1 in Purkinje Neurons Including Motor Coordination Can Be Rescued by Loss of Septin 7. Front. Cell Dev. Biol. 9:794807. doi: 10.3389/fcell.2021.794807

INTRODUCTION

Septins (SEPT) constitute a family of filament-forming GTPases that can assemble into hetero-oligomeric complexes in cells and regulate various cellular functions such as cytokinesis (Kinoshita et al., 1997; Gladfelter et al., 2001; Kinoshita and Noda, 2001), cell polarity determination and maintenance (Drees et al., 2001; Faty et al., 2002; Irazoqui and Lew, 2004), microtubule and actin dynamics (Kinoshita et al., 1997; Finger, 2002; Surka et al., 2002; Nagata et al., 2003), membrane associations, cell movement (Finger et al., 2003), vesicle trafficking (Hsu et al., 1998), and exocytosis (Beites et al., 1999). There are thirteen septin-encoding genes in mice and humans that can be classified into four different subgroups based primarily on sequence homology. The subgroups are

SEPT2 consisting of SEPT1, 2, 4, and 5; SEPT3 consisting of SEPT3, 9, and 12; SEPT6 consisting of SEPT6, 8, 10, 11, and 14; and SEPT7 which is encoded by a single gene (Kartmann & Roth, 2001; Macara et al., 2002; Kinoshita, 2003; Pan et al., 2014; Soroor et al., 2021). Functionally, septins from each subgroup occupy distinct positions in septin heteromers that can in turn assemble to form higher order septin filaments and structures (Sirajuddin et al., 2007; Mendonça et al., 2019; Soroor et al., 2021).

Regulation of cellular Ca^{2+} signaling by septins was first demonstrated in an siRNA screen in HeLa cells that identified mammalian septins of the SEPT2 class (SEPT2/4/5) as positive regulators of STIM/Orai-mediated store-operated Ca^{2+} entry (SOCE) (Sharma et al., 2013) and is further supported by recent studies (de Souza et al., 2021). Unlike the SEPT2 subclass, a mutant for the single SEPT7 gene in *Drosophila* was found to function as a negative regulator of SOCE. Heterozygotes of the *Drosophila SEPT7* mutant could rescue cellular and systemic phenotypes associated with neuronal knockdown of the SOCE molecules STIM/Orai in adult *Drosophila*. Subsequent genetic and cellular studies support the idea that SEPT7 function in human stem cell–derived neural precursors and differentiated neurons is similar to *Drosophila*. In both human neuronal cells and *Drosophila* neurons, SEPT7 orthologs prevent spontaneous Ca^{2+} entry through the SOCE channel, Orai (Deb et al., 2016; Deb et al., 2020).

Altered intracellular Ca^{2+} signaling has been associated with several neurodegenerative disorders in mouse models and in humans (Street et al., 1997; Bezprozvanny and Hayden, 2004; Van De Leemput et al., 2007; Klejman et al., 2009; Sun et al., 2014; Zhou et al., 2016; Klar et al., 2017; Ando et al., 2018; Czeredys, 2020). For example, mutations in a gene encoding the ER-Ca^{2+} release channel *IP_3R1* in humans are associated with spinocerebellar ataxias 15 and 29 (SCA 15 and 29), leading to cerebellar atrophy with the loss of Purkinje neurons and resulting in impaired coordination of movements (Hasan and Sharma, 2020). Loss of the gene encoding the ER-Ca^{2+} sensor STIM1 in mouse cerebellar Purkinje neurons affects their intrinsic excitability (Ryu et al., 2017), mGluR1-dependent synaptic transmission along with age-dependent changes that include a reduced ability to learn a motor coordination task (Hartmann et al., 2014), and changes in synaptic connectivity and gene expression (Dhanya and Hasan, 2021). Interestingly, in a mouse model of familial Alzheimer's disease, raising SOCE by overexpressing STIM2 rescued loss of mushroom spines in hippocampal neurons (Sun et al., 2014). These findings suggest that restoring intracellular Ca^{2+} homeostasis by modulating SOCE in the initial stages of neurodegenerative disease conditions could be a therapeutic strategy for the treatment of these neurodegenerative disorders. In this study, we investigated the cellular and behavioral effects of reducing SEPT7 and thus increasing spontaneous Ca^{2+} entry through SOCE channels, in mice with loss of STIM1 in Purkinje neurons.

MATERIALS AND METHODS

Animals

All experimental procedures were conducted in accordance with the Institutional Animal Ethics Committee which is approved by the Control and Supervision of Experiments on Animals (CPCSEA), New Delhi, India. All transgenic mice used for the experiments were bred and maintained in the NCBS Animal Facility, Bangalore, India. The conditional Cre-lox system (Nagy, 2000; Kim et al., 2018) was used to generate a double knockout compound mouse strain with deletion of *STIM1* and *SEPT7* together in Purkinje neurons. Mice were obtained where *loxP* sites flanked the EF hand of the *STIM1* gene encoded by exon 2 (*STIM1 flox*; Oh-hora et al., 2008) and the GTP-binding P-loop of the *SEPT7* gene encoded by exon 4 (*SEPT7 flox;* Menon et al., 2014). *Pcp2 Cre* mice [B6.129-Tg (Pcp2-cre) 2Mpin/J-The Jacksons Laboratory, RRID: IMSR_JAX: 004146 (Barski et al., 2000)] that express Cre under the control of the PCP2 promoter, thus allowing Cre-mediated recombination exclusively in the Purkinje neurons, were used for the experiment. Triple transgenic mice, $STIM1^{flox/flox}$; $SEPT7^{flox/flox}$; $PCP_2^{Cre/+}$ ($STIM1^{PKO}$; $SEPT7^{PKO}$), were generated by crossing the homozygous double transgenic $STIM1^{flox/flox}$; $SEPT7^{flox/flox}$ with $STIM1^{flox/+}$; $PCP2\text{-}Cre^{cre/+}$ mice. Mice heterozygous for the *SEPT7* floxed and homozygous for the *STIM1* floxed allele with *PCP2 (L7)-Cre* are referred to as $STIM1^{PKO}$; $SEPT7^{PHet}$ ($STIM1^{flox/flox}$; $SEPT7^{flox/+}$; $PCP2\text{-}Cre^{cre/+}$). Double transgenic mice, $STIM1^{flox/flox}$; $SEPT7^{flox/+}$ and $STIM1^{flox/flox}$; $SEPT7^{flox/flox}$, were used as controls for heterozygous and homozygous *SEPT7* knockout strains, respectively. The offspring obtained were further genotyped by PCR of genomic DNA extracted from tail clippings. Primer pairs used to detect the wild-type *STIM1* gene (348 bp) and the floxed *STIM1* gene (399 bp) are from Oh-hora et al. (2008) and are given in **Table 1**. Primers used to detect the presence or absence of Cre are listed in **Table 1**, and the presence of the *Cre* transgene was determined by observing a product length of 421 bp (Hartmann et al., 2014). The wild-type *SEPT7* gene and the floxed *SEPT7* gene were confirmed using the primer pairs shown in **Table 1**. The product length for the wild-type *SEPT7* gene is 151 bp, whereas the product length for the floxed *SEPT7* gene is 197 bp (Menon et al., 2014).

Microdissection and RNA Isolation

Sagittal cerebellar sections of about 250 µm thickness were obtained from mice aged 1 year using a vibratome (Leica, VT1200) and following isoflurane anesthesia and decapitation. The slices were sectioned in ice-cold cutting solution that contains the following reagents (in mM): 87 NaCl, 2.5 KCl, 0.5 $CaCl_2$, 7 $MgCl_2$, 1.25 NaH_2PO_4, 26 $NaHCO_3$, 75 sucrose, and 10 glucose, bubbled with 95% O_2 and 5% CO_2. Cerebellar slices were then microdissected into Purkinje neuronal and molecular layer (PNL + ML) that was separated from the granular neuronal layer (GNL) with white matter under an illuminated stereomicroscope (Ryu et al., 2017).

RNA was isolated from PNL with ML and GNL with white matter using TRIzol according to the manufacturer's protocol. Microdissected tissue was homogenized in 500 µl TRIzol (Invitrogen Cat# 15596026) using a micropestle homogenizer, and the samples were vortexed prior to proceeding with the RNA isolation protocol. Isolated RNA was analyzed by a NanoDrop spectrophotometer (Thermo Scientific) to check for its purity, followed by running it on a 1% Tris–EDTA agarose gel to check its integrity. For cDNA synthesis, approximately 500 ng of total

TABLE 1 | Primers used for genotyping transgenic mice and for quantitative real-time PCR.

Gene	Forward (5′>3′)	Reverse (5′>3′)
Stim1 (DNA)	CGATGGTCTCACGGTCTCTAGTTTC	GGCTCTGCTGACCTGGAACTATAGTG
Cre (DNA)	GCCGAAATTGCCAGGATCAG	AGCCACCAGCTTGCATGATC
SEPT7 (DNA)	CTTTGCACATATGACTAAGC	GGTATAGGGGACTTTGGGG
Pcp2	CCAGGCCAGAACCCAGAAAG	CCCAGGTCGTTTCTGCATTC
Stim1	ACAACTGGACTGTGGATGAGG	TGGTTACTGCTAGCCTTGGC
Gabra6	TGCTGGAAGGCTATGACAACC	GTCTGGCGGAAGAAAACATCC
Pvalb	ATGGGGACGGCAAGATTGG	GCGAGAAGGACTGAGATGGG
Calm1	CGTTCTTCCTTCCTTCGCTCG	TTCCTTGGTTGTGATGGTGCC
Dlg4	ACCAAGATGAAGACACGCCC	TTCCGTTCACATATCCTGGGG
Robo2	CTGCCATCTAGACCTGACTCC	ACGAGATCCTTGACCTTGCC
Map4	AGCCAGGTTGAAGGTATCCC	TGGCTGCTCTGATAATCCGG
Gigyf2	GGACCGCAGTGTTAAAAAGACC	TCTGCTGCCATTCTTCTCCG
Atp1a3	CTGCCGACATGATTCTGCTGG	AGGAAGGGTGTGATCTCAGGG
Itpr1	TGAAGGGGAACAGAACGAGC	AGGCCGATTCTTTGTTTCTGC
Orai3	CCTGTGGCCTGGTTTTTATC	GTGCCCGGTGTTAGAGAATG
Casq2	AGCCCAACGTCATCCCTAAC	AGTCGTCTTCTCCTGTAGTCC
S100b	GATGTCTTCCACCAGTACTCCG	AGCGTCTCCATCACTTTGTCC
Cacng5	CTTCCTGTGATGTGAGGGCG	CAAAAGTTGGAGTCGAGCGC
Kctd17	GGCTCCTCCTACAACTATGGG	GGAGGGAGAAAAGGTTAGCGG
Vamp1	CCCGTCTCGTTGCATTCTCC	GTCATGTTGGGAGGAGGACC
Syt11	CAAGAGGAACATTCAGAAGTGC	CCTGAGAGACCGGTGATATCC
Setd6	TGGTTTTGCTGAGCCCTATCC	CCCCTACCATCTCCTGTTTGC
Gapdh	CTTTGGCATTGTGGAAGGGC	TGCAGGGATGATGTTCTGGG

Sequences of primers used for standard PCR for genotyping transgenic mice and for quantitative real-time PCR for all sets of genes are listed in the table. Standard PCR is carried out on genomic DNA extracted from tail clippings of transgenic mice. The PCR product length of the wild-type STIM1 *gene and the floxed* STIM1 *gene are 348 bp and 399 bp, respectively (Oh-hora et al., 2008). The presence of Cre is identified by a PCR product length of 421 bp (Hartmann et al., 2014). The wild-type* SEPT7 *gene and the floxed* SEPT7 *gene were confirmed by PCR product lengths of 151 bp and 197 bp, respectively (Menon et al., 2014). All primers used for qPCR were designed using primer 3 (http://bioinfo.ut.ee/primer3-0.4.0/).* Pcp2, *Purkinje cell protein 2;* Stim1, *stromal interaction molecule 1;* Gabra6, *gamma-aminobutyric acid type A receptor subunit alpha 6).* Pvalb, *parvalbumin;* Calm1,*calmodulin 1;* Dlg4, *discs large homolog 4;* Robo2, *roundabout guidance receptor 2;* Map4, *microtubule-associated protein 4;* Gigyf2, *GRB10-interacting GYF protein 2;* Atp1a3, *Na+/K+-ATPase transporting subunit alpha 3;* Itpr1, *inositol 1,4,5-trisphosphate receptor 1,* Orai3—*Orai3;* Casq2, *calsequestrin 2,* S100b—*S100B;* Cacng5, *calcium voltage-gated channel auxiliary subunit gamma 5;* Kctd17, *potassium channel tetramerization domain containing 17;* Vamp1, *vesicle-associated membrane protein 1;* Syt11, *synaptotagmin 11;* Setd6, *SET domain containing 6;* Gapdh, *glyceraldehyde 3-phosphate dehydrogenase.*

RNA isolated was used per sample. DNase treatment was carried out with a reaction volume of 22.1 µl containing 500 ng of isolated RNA, 1 mM DTT, 0.5 U of DNase I (amplification grade), and 20 U of RNase inhibitor (RNase OUT) which was incubated at 37°C for 30 min, followed by heat inactivation at 70°C for 10 min. DNase-treated samples were further subjected to cDNA synthesis with 200 U of Moloney murine leukemia virus reverse transcriptase, 1 mM deoxyribonucleotide triphosphate, and 50 µM random hexamers in a final volume of 20 µl. The reaction mixture was then incubated at 25°C for 10 min, followed by treatment at 42°C for 60 min, and finally heat inactivation at 70°C for 10 min. All reagents used for this experiment were purchased from Invitrogen (Life Technologies).

Real-Time Quantitative PCRs

Real-time quantitative PCRs (qPCRs) were performed with the KAPA SYBR FAST qPCR kit (Sigma-Aldrich Cat# KK4601) in a total volume of 10 µl on an ABI 7500 Fast machine (Applied Biosystems) which is operated with ABI 7500 software version 2. Primer 3 (http://bioinfo.ut.ee/primer3-0.4.0/) was used to design primers. Sequences of primers for all set of genes are listed in **Table 1**. The fold change of gene expression levels in experimental conditions relative to control was normalized according to the $2^{-\Delta\Delta Ct}$ method, where ΔΔCt = [(Ct (target gene)—Ct (GAPDH)] Expt.—[(Ct (target gene)—Ct (GAPDH)] control. GAPDH was used as a housekeeping gene.

Immunohistochemistry

Mice were anesthetized and then transcardially perfused with 1X PBS, followed by perfusion with 4% PFA in 1X PBS. Brains were harvested following perfusion and postfixed with 4% PFA overnight, followed by cryoprotection in 30% sucrose in 1X PBS. The fixed cerebellum was then embedded in 5% low melting agar and sliced using a vibratome into 35-µm-thin sections. The cerebellar sections were washed in 1X PBS, blocked for 1 h at 4°C in 0.1% Triton X-100 and 5% normal goat serum, and stained with antibodies overnight at 4°C against guinea pig anti-VGLUT2 (1:1,000; Synaptic Systems Cat# 135 404, RRID: AB_887884). The sections were then washed in PBS-T (0.1% Triton X-100 in 1X PBS) thrice and incubated with secondary antibody goat anti-guinea pig which is coupled to Alexa Fluor 488 (Invitrogen Cat# A-11073, RRID: AB_2534117) for 1 h at room temperature. The slices were then washed in 1X PBS, mounted in Vectashield medium (Vector Labs, Cat#: H-1000), and imaged using an Olympus confocal microscope FV3000 with FV31S-SW 2.1 viewer software.

Confocal Imaging and Image Analysis

Confocal images were captured using a confocal laser microscope (Olympus FV3000 laser scanning confocal microscope) with a 40X objective (PlanApo, NA 1.0; Olympus oil-immersion). Confocal images were acquired at 1.0-µm-thickness intervals

with the frame size of 512 × 512 pixels. For estimation of VGLUT2 puncta along PC dendrites at proximal ends, Imaris software (Bitplane, v 9.1.2) was used (Kaneko et al., 2011). The Filament Tracer software (Auto Depth) of Imaris was used to trace each dendritic filament setting the largest diameter threshold at 3 µm and the smallest diameter at 1.86 µm. To quantify VGLUT2 puncta along Purkinje neuron dendrites, spot detection in Imaris software was used by setting the spot diameter threshold as 2 µm and the total distance close to the filament as 3 µm for proximal dendrites.

Rotarod Test

The rotarod assay was performed by first habituating mice to a rotarod (IITC, model# 775, Series 8 Software) by providing a short training session where they were subjected to a constant speed of 5 rpm for 400 s. The mice were then tested for four trials a day for 5 days consecutively. Each session began from 5 rpm and finally attained 45 rpm, with a ramp speed at 240 s (Hartmann et al., 2014). The velocity of rotation was thus increased, keeping a constant acceleration of 9 rpm/min. The time at which each mouse fell off the rotarod was recorded for each session, and the mean latency on the rod was then calculated for all four trials for each mouse across 5 days of sessions.

Statistical Analysis

Statistical analysis was performed using GraphPad Prism 7.0 or Origin 8.0 software. The statistical methods used in each experiment are mentioned in the figure legends. All bar graphs indicate means and standard error of means, and statistical significance was defined as $p < 0.05$ (*), highly significant for $p < 0.01$ (**) and $p < 0.001$ (***) as determined using paired Student's *t*-test or one-way analysis of variance (ANOVA). In case of the rotarod test, two-way ANOVA, followed by Tukey's multiple comparison test, was adopted for comparisons between groups.

RESULTS

Generation of *STIM1-SEPT7* Double Knockout Mice

To understand if negative regulation of store-operated Ca^{2+} entry (SOCE) by SEPT7 is conserved among murine models and to investigate if motor deficits observed in *STIM1* knockout ($STIM1^{PKO}$) mice (Hartmann et al., 2014; Dhanya and Hasan, 2020) could be rescued by altering SEPT7 levels, we generated Purkinje neuron (PN)–specific compound *STIM1-SEPT7* double knockout mice strains using the conditional Cre-lox system (**Figures 1A,B** and methods). Exon 4, which encodes the GTP-binding P-loop of *SEPT7*, and exon 2, which encodes the EF hand of *STIM1*, were deleted in the progeny that included a *PCP2 (L7)-Cre* transgene as judged by the size of DNA fragments from appropriate PCRs from genomic DNA (**Figure 1C** and methods). Mice homozygous for the *SEPT7* floxed and *STIM1* floxed allele along with *PCP2 (L7)-Cre* are referred to as $STIM1^{PKO}$; $SEPT7^{PKO}$ [$STIM1^{flox/flox}$; $SEPT7^{flox/flox}$; *PCP2* (*L7*)-$Cre^{cre/+}$, **Figures 1B,C**]. Mice heterozygous for the *SEPT7* floxed and homozygous for the *STIM1* floxed allele with *PCP2 (L7)-Cre* are referred to as $STIM1^{PKO}$; $SEPT7^{PHet}$ ($STIM1^{flox/flox}$; $SEPT7^{flox/+}$; *PCP2-*$Cre^{cre/+}$, **Figure 1C**). $STIM1^{flox/flox}$; $SEPT7^{flox/flox}$ and $STIM1^{flox/flox}$; $SEPT7^{flox/+}$ mouse strains in the absence of *PCP2* (*L7*)-$Cre^{cre/+}$ were used as controls for homozygous and heterozygous *SEPT7* knockout strains, respectively.

Characterization of *SEPT7* and *STIM1* Expression Levels in *STIM1-SEPT7* Double Knockout Mice

Purkinje neurons present in the molecular layer were separated from the granule cell layer by hand microdissection of isolated cerebella from 1-year-old *STIM1-SEPT7* double knockout mice (**Figure 2**, green bars) and control mice of the appropriate genotypes (**Figure 2**, blue and pink bars). Enrichment of PNs and their separation from the granule cell layer was estimated by measuring relative gene expression levels of a Purkinje neuronal marker, Purkinje cell protein-2 (PCP2), and a granule cell layer marker GABA(A) receptor α6 subunit (GABRA6) (Boyden et al., 2006). Microdissected Purkinje layer samples from control and *STIM1-SEPT7* double knockout cerebella showed approximately three- to four-fold enrichment of PCP2 compared to the granule cell layer (**Figure 2A**) and a 10- to 14-fold lower expression of the granule cell marker GABRA6 (**Figure 2B**), indicating the minimal presence of granule neurons in the microdissected PN samples. The extent of SEPT7 knockdown in heterozygous and homozygous *SEPT7* knockout mouse strains was examined next. A significant reduction in *SEPT7* mRNA levels was observed in Purkinje layers isolated from the $STIM1^{PKO}$; $SEPT7^{PHet}$ and $STIM1^{PKO}$; $SEPT7^{PKO}$ animals as compared to control mice (**Figure 2C**). The expression of *STIM1* was also tested and found to be significantly reduced as expected in the three genotypes with homozygous $STIM1^{PKO}$. Thus, both heterozygous and homozygous conditions of *SEPT7* knockout in *STIM1* knockout backgrounds led to a significant reduction in *SEPT7* mRNA expression in PNs.

Altered Expression of *SEPT7* in *STIM1* Knockout Mice Modulates Gene Expression in Purkinje Neurons

Age-dependent changes in gene expression have been reported recently in Purkinje neurons from $STIM1^{PKO}$ mice (Dhanya and Hasan, 2021). If reduced SEPT7 indeed raises Ca^{2+} entry in PNs, we hypothesized that gene expression changes that arise directly due to reduced SOCE should revert in PNs of $SEPT7^{PHet}$; $STIM1^{PKO}$ and $SEPT7^{PKO}$; $STIM1^{PKO}$ mice with age. This idea was tested by measuring the expression of a subset of genes, belonging to various gene ontology classes (**Table 2**), which are all significantly downregulated in PNs from 1-year-old $STIM1^{PKO}$ mice but not when tested in mice aged 4 months or less (Dhanya and Hasan, 2020). Expression levels of genes encoding the Ca^{2+}-binding proteins parvalbumin (*Pvalb*) and calmodulin 1 (*Calm1*) were restored in PNs of both $STIM1^{PKO}$; $SEPT7^{PHet}$ and $STIM1^{PKO}$; $SEPT7^{PKO}$ mice when tested at 1 year (**Figures**

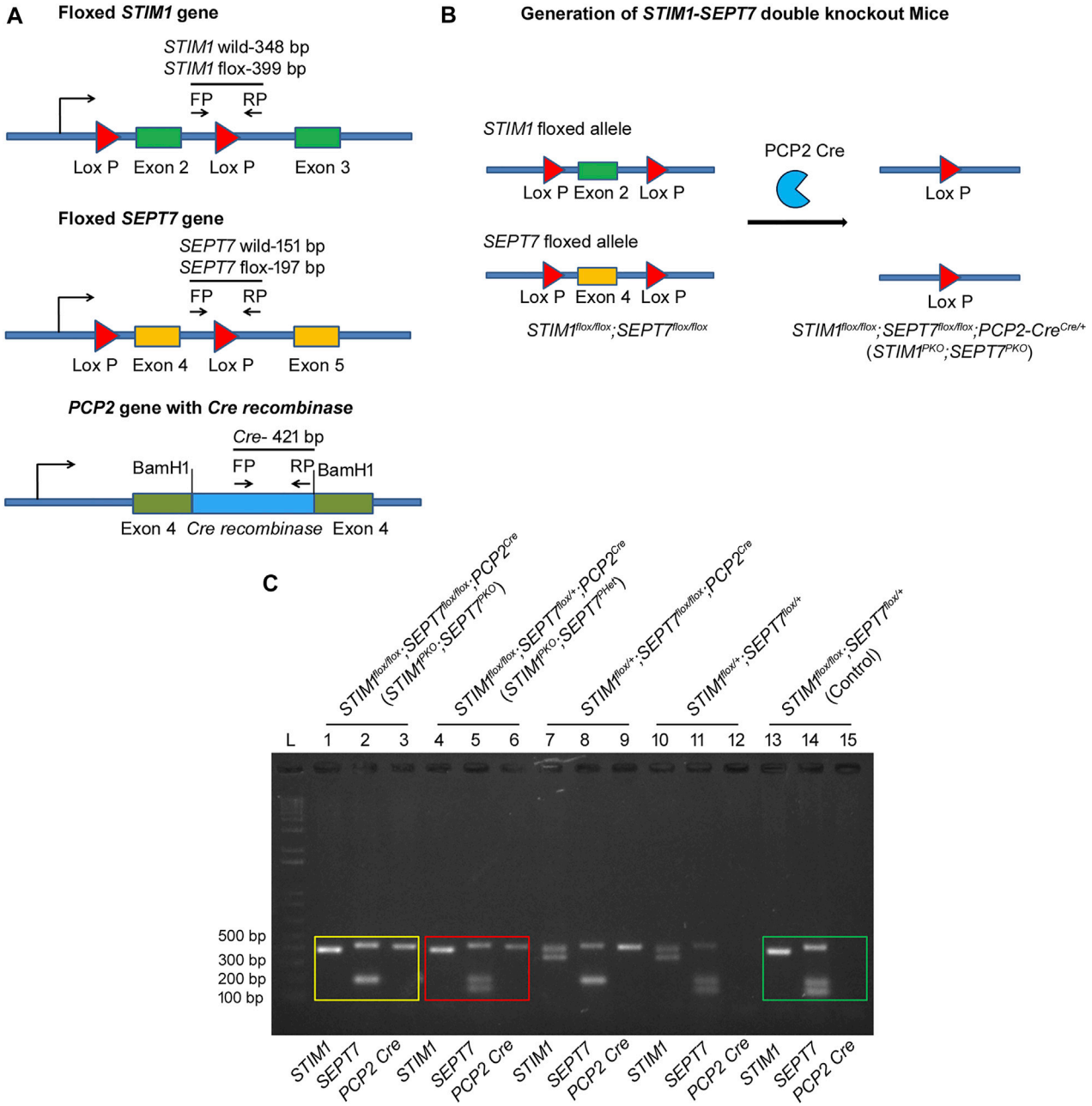

FIGURE 1 | Generation of *STIM1–SEPT7* double knockout mice. **(A) (Top)** Schematic diagram with exon 2 of *STIM1* gene flanked by *loxP* recombination sites (red triangles). Cre-mediated recombination will result in the deletion of exon 2. **(Middle)** Schematic diagram with exon 4 of *SEPT7* gene flanked by *loxP* recombination sites (red triangles). **(Bottom)** Schematic diagram showing insertion of Cre-recombinase cDNA into the exon 4 of *PCP2* gene. Primers used for genotyping are indicated by arrows (FP, forward primer and RP, reverse primer). **(B)** Triple transgenic mouse strain $STIM1^{flox/flox}$; $SEPT7^{flox/flox}$; $PCP_2{}^{Cre/+}$ ($STIM1^{PKO}$; $SEPT7^{PKO}$) was generated by cross-breeding homozygous double transgenic $STIM1^{flox/flox}$; $SEPT7^{flox/flox}$ mice with $STIM1^{flox/+}$; $PCP2\text{-}Cre^{cre/+}$ mice to generate STIM1 and SEPT7 double knockout mice. **(C)** Agarose gel showing the genotyping of *STIM1–SEPT7* double knockout mice. PCRs of genomic DNA from $STIM1^{flox/flox}$; $SEPT7^{flox/flox}$; $PCP_2{}^{Cre/+}$ ($STIM1^{PKO}$; $SEPT7^{PKO}$) mice are shown on Lanes 1–3. PCRs were performed separately for each gene, and PCR products were loaded separately in different lanes. A single band at 399 bp indicates homozygous *STIM1 flox* (Lane 1), a band at 197 bp indicates homozygous *SEPT7 flox* (Lane 2), and the 421-bp band is from the *PCP2-Cre* allele (Lane 3). PCRs with genomic DNA from $STIM1^{flox/flox}$; $SEPT7^{flox/+}$; $PCP_2{}^{Cre/+}$ ($STIM1^{PKO}$; $SEPT7^{PHet}$) mice are shown in Lanes 4–6. Lanes 13–15 indicate genotyping of control mice $STIM1^{flox/flox}$; $SEPT7^{flox/+}$. DNA band sizes are as described before. "L" denotes DNA ladder.

3A,B). Similarly, the expression of four genes, *Dlg4* (discs large homolog 4), *Robo2* (roundabout guidance receptor 2), *Map4* (microtubule-associated protein 4), and *Gigyf2* (GRB10 interacting GYF protein 2), was restored (**Figures 3A,B**). All four genes belong to the GO (gene ontology) category of neuron projection development (**Table 2**). In addition, reducing *SEPT7*

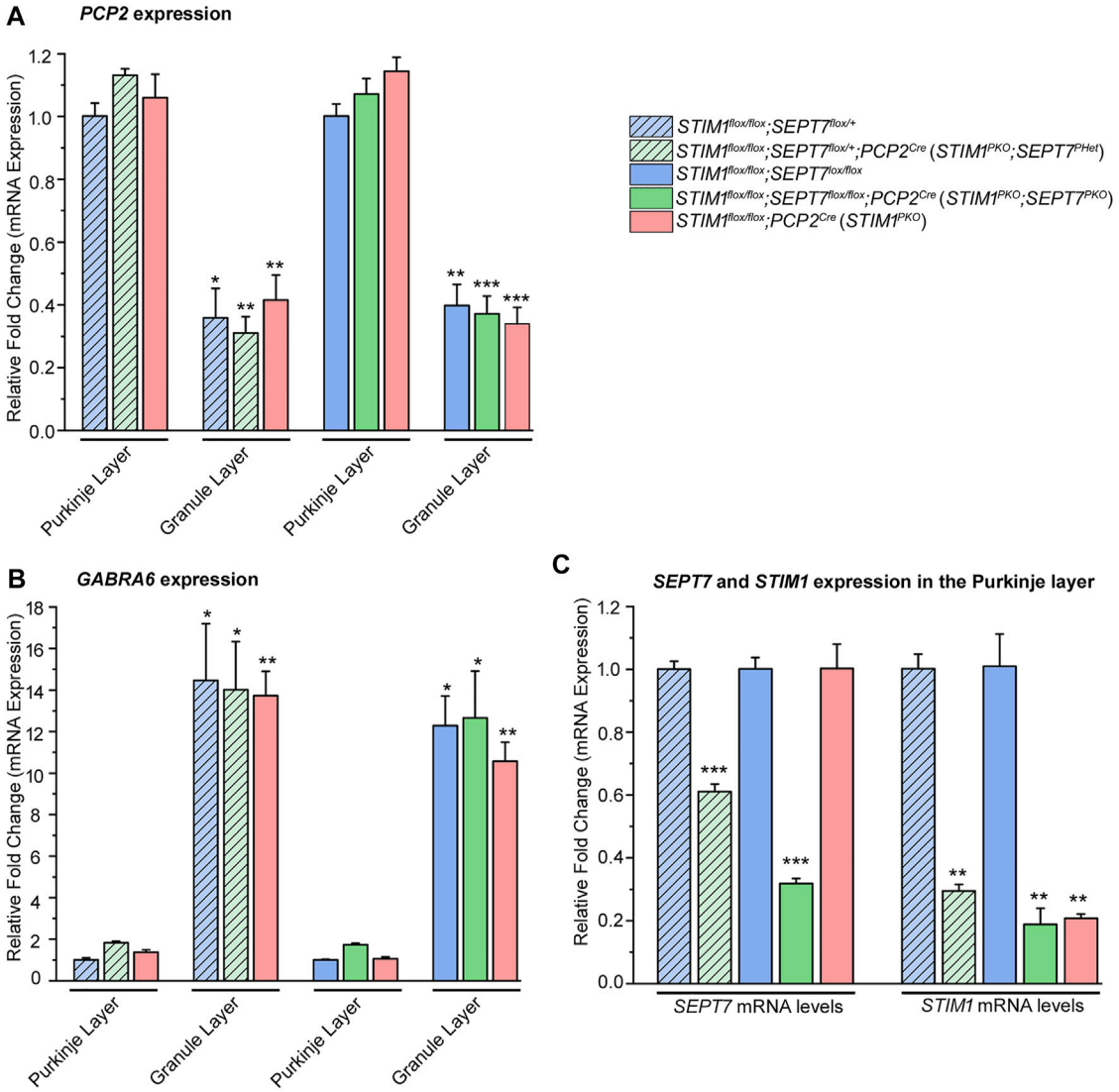

FIGURE 2 | Characterization of *SEPT7* and *STIM1* expression levels. **(A)** Bar graphs indicating relative expression of Purkinje neuron marker, *PCP2* (Purkinje cell protein 2) normalized to *GAPDH* (glyceraldehyde 3-phosphate dehydrogenase) in samples of the Purkinje neuronal layer (PNL) and the granule layer (GL). *PCP2* expression levels of GL are relative to PNL for each genotype, and statistical significance is indicated above the bar graph. **(B)** Bar graphs with relative expression of granule layer marker, *GABRA6* (gamma-aminobutyric acid type A receptor subunit alpha 6) normalized to *GAPDH* levels in samples of the Purkinje neuronal layer and the granule layer. *GABRA6* expression levels of GL are compared relative to those of PNL for each genotype, and statistical significance is indicated above the bar graph. **(C)** Bar graphs indicating fold changes in expression of *SEPT7* and *STIM1* normalized to *GAPDH* from microdissected Purkinje neuronal layer of each genotype. Fold changes are relative to that of its respective controls, and statistical significance is indicated above the bar graph. Data are presented as mean ± SEM, $^{*}p < 0.05$, $^{**}p < 0.01$, $^{***}p < 0.001$; one-way ANOVA with post hoc Tukey's test ($n = 3$ mice for all groups and $n = 4$ for $STIM1^{PKO}$; $SEPT7^{PHet}$, age—1-year-old mice).

in $STIM1^{PKO}$ PNs restored the expression of an ion channel gene *Atp1a3* encoding a Na^+/K^+-transporting ATPase subunit alpha 3 (**Figures 3A,B**). Thus, in 7 out of 16 genes tested (**Figure 3** and **Supplementary Figure S1**), expression was restored significantly to control or near-control levels. The expression of genes like *Orai3* (SOCE channel), *Cacng5* (voltage-gated Ca^{2+} channel), *Vamp1* (vesicle-associated membrane protein 1), and *Syt11* (synaptotagmin 11) went up marginally in PNs from $STIM1^{PKO}$; $SEPT7^{PKO}$ animals as compared to PNs from $STIM1^{PKO}$ mice (**Supplementary Figure S1A**). Although, due to technical limitations (Dhanya and Hasan 2021), we were unable to measure Ca^{2+} entry directly in PNs from *STIM1-SEPT7* double mutant conditions, these data support the idea that either reduction ($SEPT7^{PHet}$) or loss of SEPT7 ($SEPT7^{PKO}$) in PNs allows spontaneous extracellular Ca^{2+} entry, as observed previously in human stem cell–derived precursors and differentiated neurons (Deb et al., 2020). This putative mode of Ca^{2+} entry in PNs might partially compensate for loss of STIM1-mediated SOCE and concomitant gene expression changes.

TABLE 2 | Table with downregulated genes identified under enriched GO biological and cellular process.

GO Term	Pathway	LogP	Genes
GO:0010975	Regulation of neuron projection development	−4.69	*Dlg4*, *Robo2*, *Gigyf2*, *S100b*, *Map4*, *Itpr1*, *Kctd17*
GO:0098984	Neuron to neuron synapse	-4.60	*Dlg4*, *Itpr1*, *Map4*, *Cacng5*, *Syt11*, *Atp1a3*, *Vamp1*
GO:0006898	Receptor-mediated endocytosis	−4.19	*Atp5b*, *Dlg4*, *Cacng5*, *Syt11*
GO:0090316	Positive regulation of intracellular protein transport	−4.10	*Syt11*, *Vamp1*, *Itpr1*
GO:0032469	Endoplasmic reticulum calcium ion homeostasis	−3.02	*Itpr1*, *Orai3*, *Dlg4*, *Casq2*, *S100b*, *Atp1a3*, *Cacng5*, *Kctd17*
GO:0061024	Membrane organization	−2.48	*Dlg4*, *Vamp1*, *Cacng5*, *Syt11*
GO:0098793	Presynapse	−2.35	*Calm1*, *Dlg4*, *Itpr1*, *Syt11*, *Atp1a3*

GO classification of biological and cellular processes of selected genes downregulated upon STIM1 *knockout in PNs. Enriched categories with associated GO term, log* p *value, and lists of genes associated with each process and tested here are shown. Metascape was used for gene enrichment using parameters specific for* Mus musculus*, with a* p *value cutoff as 0.01 (data from Dhanya and Hasan, 2021).*

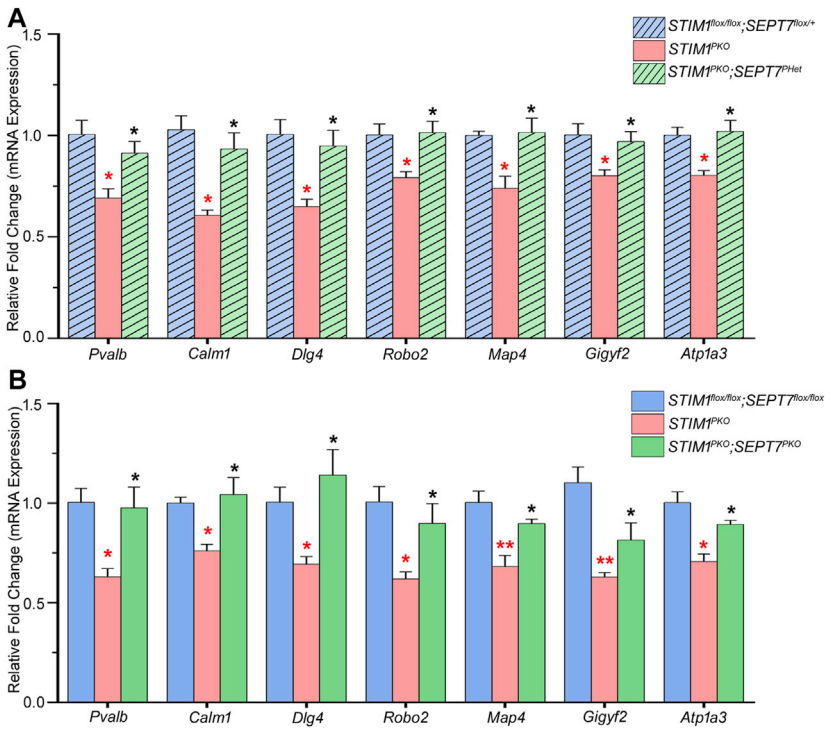

FIGURE 3 | Partial or complete deletion of *SEPT7* can reverse the expression of a subset of genes that are downregulated by *STIM1* knockout in Purkinje neurons. **(A)** Bar graph with relative fold changes in expression of the indicated genes in the indicated genotypes. Red asterisks above each bar represent statistically significant change between $STIM1^{PKO}$ (pink bars) and the control genotype $STIM1^{flox/flox}$; $SEPT7^{flox/+}$ (light blue bars). Black asterisks above each bar represent statistically significant change between $STIM1^{PKO}$ (pink bars) and the experimental genotype, $STIM1^{PKO}$; $SEPT7^{PHet}$ (light green bars). **(B)** Bar graph of relative gene expression changes in the indicated genotypes. Red asterisks over each bar represent statistically significant change between $STIM1^{PKO}$ (pink bars) and the control genotype $STIM1^{flox/flox}$; $SEPT7^{flox/flox}$ (blue bars). Black asterisks above each bar represent a statistically significant change between $STIM1^{PKO}$ (pink bars) and $STIM1^{PKO}$; $SEPT7^{PKO}$ (green bars). Fold changes were normalized to *GAPDH*. Data are presented as mean ± SEM, $^{*}p < 0.05$, $^{**}p < 0.01$; one-way ANOVA with post hoc Tukey's test. All measurements are taken by qRT-PCR of cDNA prepared from RNA isolated from microdissected Purkinje layers ($n = 3$ mice for all groups and $n = 4$ for $STIM1^{PKO}$; $SEPT7^{PHet}$, age—1 year). *Pvalb*—Parvalbumin, *Calm1*—Calmodulin 1, *Dlg4*—Discs large homolog 4, *Robo2*—Roundabout guidance receptor 2, *Map4*—Microtubule-associated protein 4, *Gigyf2*—GRB10 interacting GYF Protein 2, *Atp1a3*—Na+/K+-transporting ATPase subunit alpha 3.

Loss of SEPT7 Modulates Synaptic Connectivity Among Climbing Fiber Axons and Purkinje Neuron Dendrites in *STIM1* Knockout Purkinje Neurons

Next, we investigated if reducing or abolishing SEPT7 from $STIM1^{PKO}$ Purkinje neurons modulates synaptic connectivity between climbing fibers and Purkinje neurons. Climbing fibers (CFs) are axonal projections from inferior olive neurons. They innervate Purkinje neurons dendrites through glutamatergic synapses that express VGLUT2 (vesicular glutamate transporter type 2; Fremeau et al., 2001). Activity from CFs greatly influences individual Purkinje neurons and cerebellar output (Smeets and Verbeek, 2016). Excess CF-PN innervation

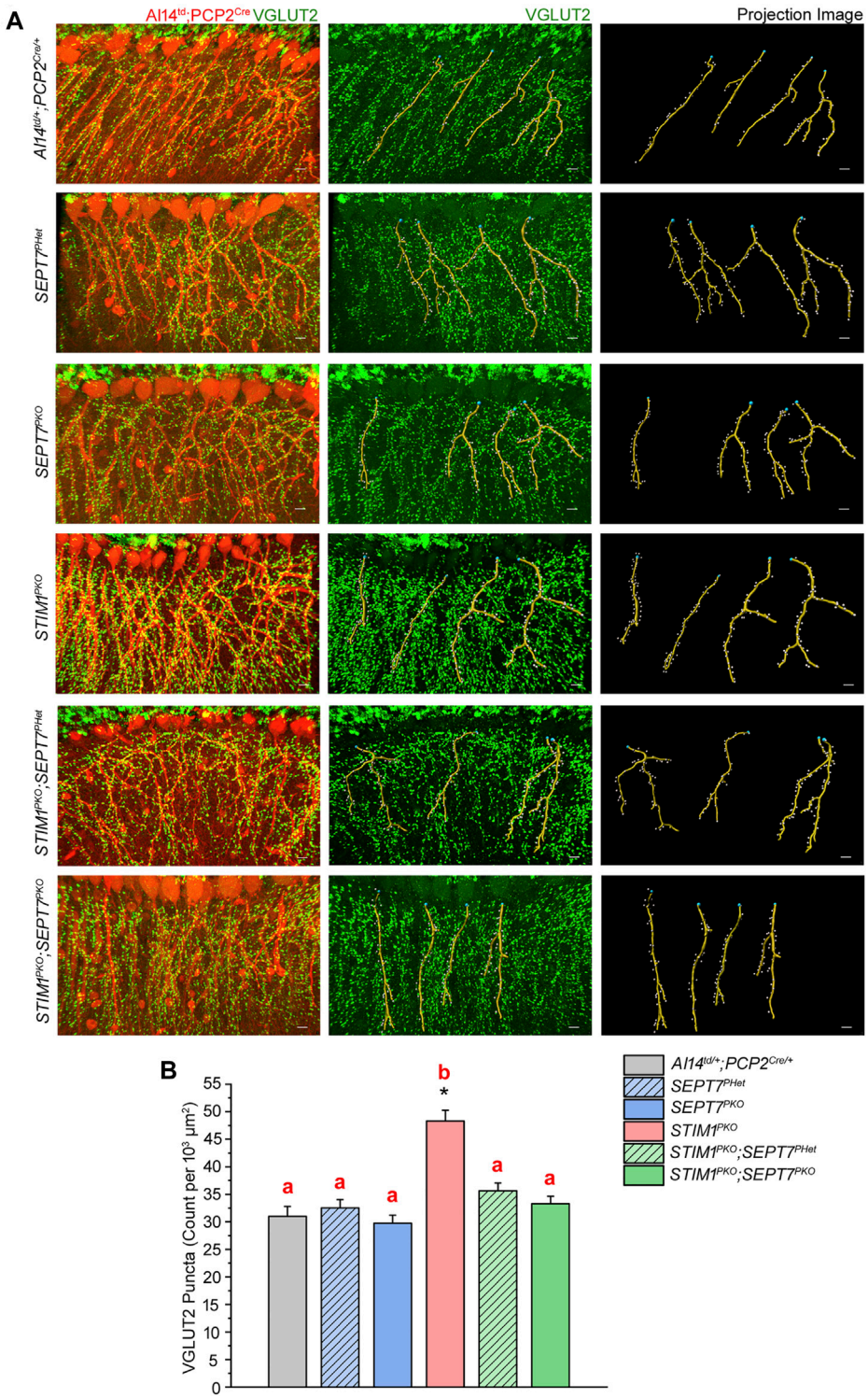

FIGURE 4 | Excess innervation between climbing fibers and Purkinje neuron dendrites in *STIM1* mice can be reversed by reduction and loss of *SEPT7*. **(A)** Immunohistochemical images and quantitative analysis of climbing fiber innervations on the proximal dendrites of Purkinje neurons in the indicated mice genotypes. **(Left panel)** PN soma and proximal dendrites with Td tomato expression (red). VGLUT2 puncta are visible as green dots along the dendrites; **(middle panel)** VGLUT2 puncta (green) with projection images of dendritic filaments (yellow) obtained computationally using Imaris software and **(right panel)** projection images from Imaris analysis with dendritic filaments marked in yellow and VGLUT2 puncta as white dots. Scale bars are 10 µm. **(B)** Bar graph depicting the density of VGLUT2 puncta (count per 10^3 µm^2) presents at the proximal dendritic regions of PNs of the indicated mice genotypes. Quantification of VGLUT2 puncta density was from three mice of each genotype, all aged 1 year, and 27 or more PNs from each genotype. Data are presented as mean ± SEM; one-way ANOVA with post hoc Tukey's test; *$p < 0.00001$. Same alphabets above the bar graphs represent statistically indistinguishable groups, and a different alphabet represents a statistically different group with the minimal significance of $p < 0.05$.

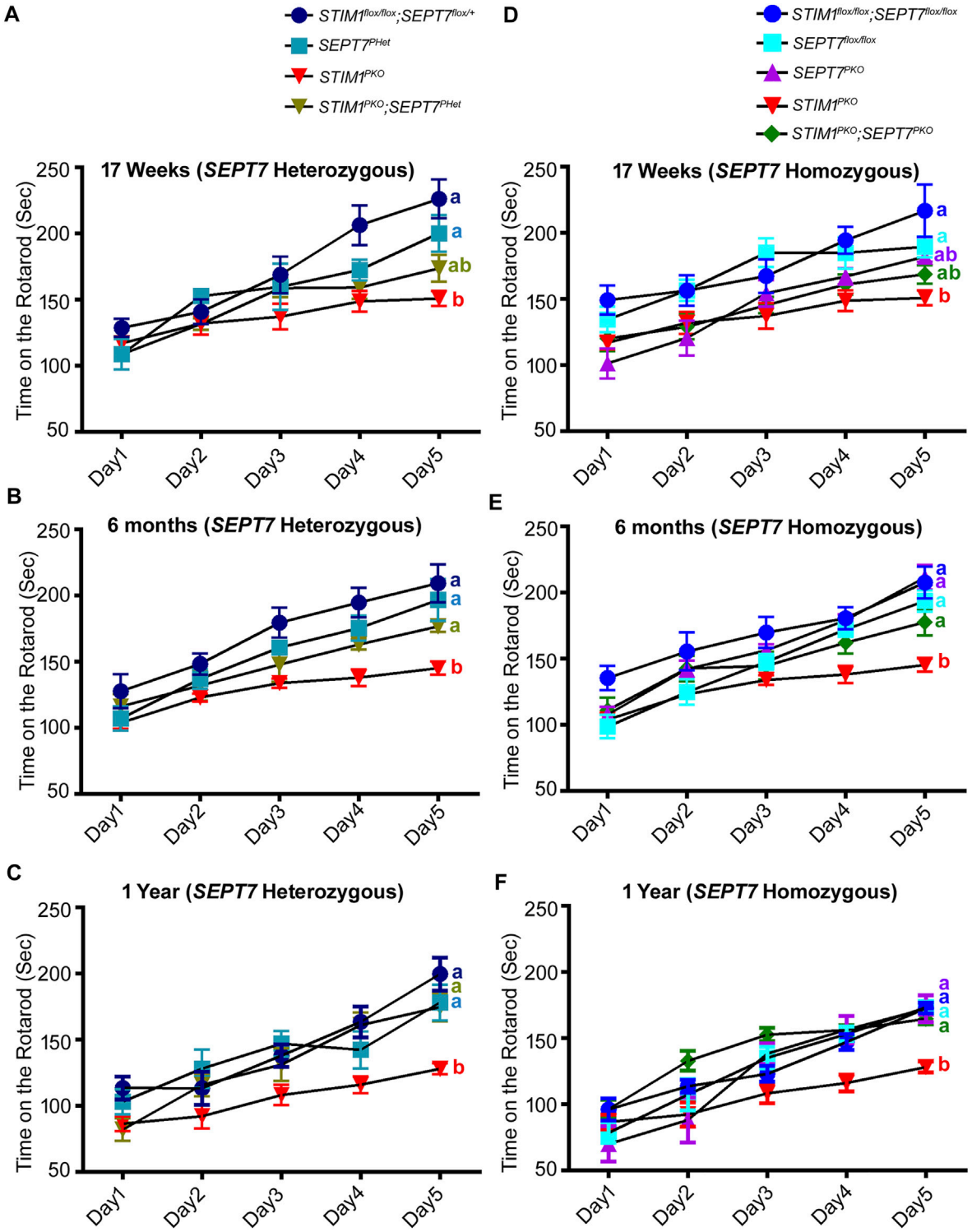

FIGURE 5 | Reduction and loss of SEPT7 rescue loss of motor learning and coordination arising from loss of STIM1 in Purkinje neurons mean latency times on the rotarod are shown for the indicated genotypes at **(A, D)** 17 weeks, **(B, E)** 6 months, and **(C, F)** 1 year of age. The number of mice tested for each genotypes is *STIM1*$^{flox/flox}$; *SEPT7*$^{flox/+}$ (n = 6), *SEPT7*^{PHet} (n = 4), *STIM1*^{PKO} (n = 7), *STIM1*^{PKO}; *SEPT7*^{PHet} (n = 5), *STIM1*$^{flox/flox}$; *SEPT7*$^{flox/flox}$ (n = 6), *SEPT7*$^{flox/flox}$ (n = 8), *SEPT7*^{PKO} (n = 6), *STIM1*^{PKO} (n = 7), *STIM1*^{PKO}; *SEPT7*^{PKO} (n = 8). Same alphabets at the end of line plots represent statistically indistinguishable groups, the color of the alphabets denotes the respective line plots, and different alphabets represent $p < 0.05$. Two-way ANOVA, a post hoc test, followed by Tukey's multiple comparisons test were used.

has been seen in a number of genetic mouse models with impaired Ca^{2+} signaling and reduced motor coordination (Alba et al., 1994; Chen et al., 1995; Kano et al., 1995; Kashiwabuchi et al., 1995; Kano et al., 1997; Hashimoto et al., 2001). Moreover, *STIM1*^{PKO} mice at 1 year exhibit increased CF-PN synapse numbers that correlate with reduced motor coordination (Dhanya and Hasan, 2020). To evaluate the density and distribution of CF-PN synapses, we quantified VGLUT2 (vesicular glutamate transporter type 2) puncta along the proximal dendrites of PNs (**Figure 4**). As described previously, a significant increase in VGLUT2 puncta is observed along the proximal dendrites of *STIM1*^{PKO} PNs as compared with the control genotype of *AI14*^{td}; *PCP2*^{Cre} (**Figures 4A,B**; Dhanya and Hasan, 2021). Importantly, the density of VGLUT2 puncta along the PN dendrites of both *STIM1*^{PKO}; *SEPT7*^{PHet} and *STIM1*^{PKO}; *SEPT7*^{PKO} mice was comparable to that of the control mice. There was no change in the density of VGLUT2 puncta on PN dendrites of either *SEPT7*^{PHet} or *SEPT7*^{PKO} mice (**Figures 4A,B**). Restoration of CF-PN innervation upon reducing SEPT7 in STIM1 knockout Purkinje neurons suggests that Ca^{2+} homeostasis impacts synaptic plasticity and together the two could alter cerebellar circuit function.

Reduced SEPT7 Levels Improve Motor Performance in *STIM1* Knockout Mice

A well-established readout of PN and cerebellar function is the ability to learn a motor coordination task such as time spent on a rotarod with increasing rotational speed (Koopmans et al., 2007; Shiotsuki et al., 2010; Stroobants et al., 2013). Loss of STIM1 in PNs reduces the ability to perform this motor learning task (Hartmann et al., 2014). Further impairment is seen with age both in controls and in *STIM1*^{PKO} animals (Dhanya and Hasan, 2021). Restored expression of a subset of genes and rescue of CF-PN connectivity motivated us to compare the motor learning deficits of *STIM1*^{PKO} mice with *STIM1*^{PKO}; *SEPT7*^{PHet} and *STIM1*^{PKO}; *SEPT7*^{PKO} mice, along with their appropriate genetic controls in the rotarod assay across various ages. Initially, we tested motor learning in mice with either partial or complete loss of SEPT7 in Purkinje neurons (**Figure 5**). Motor learning deficits were not observed in *SEPT7*^{PHet} and *SEPT*^{PKO} mice at 17 weeks, 6 months, or 1 year of age (**Figures 5A–F**), suggesting the limited function of SEPT7 in adult PNs. Next, we tested motor learning in the double mutant combinations of *STIM1*^{PKO}; *SEPT7*^{PHet} and *STIM1*^{PKO}; *SEPT7*^{PKO} mice. *STIM1*$^{flox/flox}$, *SEPT7*$^{flox/+}$, and *SEPT7*^{PHet} were the controls for *STIM1*^{PKO}; *SEPT7*^{PHet} mice, whereas *STIM1*$^{flox/flox}$, *SEPT7*$^{flox/flox}$, and *SEPT7*^{PKO} were controls for *STIM1*^{PKO}; *SEPT7*^{PKO} mice. The same batch of mice was tested at 17 weeks, 6 months, and 1 year of age. At all ages, tested motor learning in *STIM1*$^{flox/flox}$, *SEPT7*$^{flox/+}$, and *SEPT7*^{PHet} mice is significantly better than in *STIM1*^{PKO} mice (**Figure 5A**). For example, at 17 weeks, *STIM1*$^{flox/flox}$; *SEPT7*$^{flox/+}$ control mice improved their latency on the rotarod from 128.8 ± 6.9 s on the 1st day to 226.3 ± 14.7 s on the 5th day (**Figure 5A**), whereas *STIM1*^{PKO} mice showed similar performance as that of control mice on day 1 (mean latency of 117.1 ± 5.1 s) but did not improve to the same extent

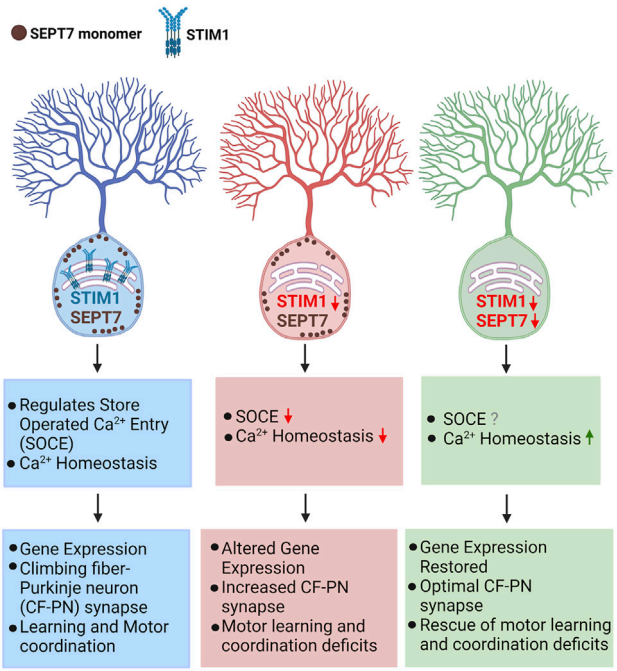

FIGURE 6 | Cellular and behavioral effects of reducing SEPT7 in mice with loss of STIM1 in Purkinje neurons loss of STIM1 in Purkinje neurons attenuate Ca^{2+} entry and affect ER-Ca^{2+} refilling which in turn suppresses mGluR1-stimulated Ca^{2+} signals and Purkinje neuron excitability (Hartmann et al., 2014; Ryu et al., 2017; Dhanya and Hasan, 2021). These changes affect gene expression and optimal synaptic connectivity of cerebellar Purkinje neurons with age (Dhanya and Hasan, 2021). Reducing or abolishing *SEPT7* in *STIM1*^{KO} PNs restored gene expression which is accompanied by normal CF-PN innervation and an improved ability to learn a motor coordination task in aging mice. [Model created using Biorender (BioRender.com).]

(150.9 ± 5.6 s, **Figures 5A,B**) as the controls over 5 days of training. Performance of *STIM1*^{PKO}; *SEPT7*^{PHet} mice at 17 weeks is not statistically indistinguishable from either controls or *STIM1*^{PKO} animals (**Figure 5A**). However, the age performance of *STIM1*^{PKO}; *SEPT7*^{PHet} mice improves on the rotarod as evident at 6 months (**Figure 5B**; **Supplementary Figure S2**) and 1 year (**Figure 5C**). A similar age-dependent improvement in motor coordination learning is evident in *STIM1*^{PKO}; *SEPT7*^{PKO} homozygotes from 17 weeks to 1 year (**Figures 5D–F**; **Supplementary Figure S2**, **Supplementary Video S1**). However, as compared to *STIM1*^{PKO}; *SEPT7*^{PHet} mice (**Figure 5C**), the *STIM1*^{PKO}; *SEPT7*^{PKO} mice (**Figure 5F**) exhibit an overall reduction in motor learning with age, which is also evident for the control genotypes and is possibly due to the sustained loss of SEPT7 from PNs. Thus, deleting either single or both copies of *SEPT7* in PNs of *STIM1*^{PKO} mice partially rescues their motor learning deficits.

DISCUSSION

In this study, we show that partial or complete deletion of SEPT7 from adult murine Purkinje neurons reverses multiple

phenotypes associated with PN-specific loss of the ER-Ca^{2+} sensor and SOCE protein STIM1. The phenotypes reverted include changes in gene expression in part, expression of VGLUT2 puncta that serve as a marker for altered neuronal connectivity between climbing fiber axons and PN dendrites, and the ability to learn a motor coordination task in aging mice. From a previous study, we know that loss of motor coordination is seen as early as 17 weeks of age in $STIM1^{PKO}$ mice, whereas changes in CF-PN synapse numbers and changes in gene expression become evident in mice aged 1 year (Dhanya and Hasan, 2021). $STIM1^{PKO}$–$SEPT^{PHet/PKO}$ mice also exhibit early motor learning deficits. Importantly, the progression of these deficits undergoes reversal with age (**Figure 5**, **Supplementary Figure S2**, **Supplementary Video S1**). Taken together, these findings support the idea that reduction/loss of SEPT7 in adult PNs reverts key age-dependent changes in neuronal Ca^{2+} homeostasis that occurs from loss of STIM1. Consequently, there is reversion of other age-dependent cellular (VGLUT2 puncta) and molecular (gene expression) deficits, and this reversion correlates with better learning of motor coordination with age in $STIM1^{PKO}$–$SEPT7^{PHet/PKO}$ mice (**Figure 6**). The reversion of motor coordination deficits observed in mice is in agreement with previous findings in *Drosophila* where partial genetic depletion of SEPT7 could rescue flight deficits due to STIM knockdown (Deb et al., 2016). Early changes (17 weeks) in mGluR1-dependent Ca^{2+} transients, of which STIM1 is an integral component, are very likely not restored by loss/reduction of SEPT7. The status of mGluR1-initiated Ca^{2+} signals in PNs from $STIM1^{PKO}$–$SEPT7^{PHet/PKO}$ mice needs further investigation.

SEPT7 May Function as a Monomer for Regulating Ca^{2+} Entry at the Plasma Membrane

Most cellular functions of septins are associated with their ability to form filaments and higher order cytoskeletal structures (Marquardt et al., 2019). Recent findings demonstrate that filament formation requires linear hexamers/octamers consisting of SEPT7 at the core, followed by other SEPT subunits in a specific order (Mendonça et al., 2019; Soroor et al., 2021). Differential regulation of SOCE by SEPT2/4 (positive regulators; Sharma et al., 2013; de Souza et al., 2021) and SEPT7 (negative regulator; Deb et al., 2016; Deb et al., 2020) is difficult to reconcile with SEPT7 as the core subunit of a minimally functional septin multimer. Unicellular organisms such as *Chlamydomonas reinhardtii* encode a single gene for septin (Pinto et al., 2017), raising the possibility that monomeric septin function may precede septin filament formation. For the negative regulation of SOCE channels, we propose that SEPT7 very likely functions as a monomer (**Figure 6**). At this stage, however, there is no direct evidence demonstrating the presence of SEPT7 monomers near the ER-PM junctions where SOCE is known to occur.

The mechanism by which SEPT7 regulates Ca^{2+} entry remains poorly understood. In human stem cell–derived neurons, spontaneous Ca^{2+} entry by loss of SEPT7 requires the polybasic N-terminal region known to interact with membrane-localized phospholipids such as PIP2 and PIP3 (Zhang et al., 1999; Deb et al., 2020). We predict that the interaction of SEPT7 monomers with membrane phospholipid(s) prevents the opening of a STIM1-regulated Ca^{2+} entry channel in PNs. Concomitant loss of SEPT7 with STIM1 possibly allows a low level of spontaneous Ca^{2+} entry through such channels and thus restores PN Ca^{2+} homeostasis and associated long-term deficits.

Among the deficits tested here, we did not find any significant change in $SEPT7^{PKO}$ animals, suggesting that in mature PNs, septin filaments have either no role or a very minor role. Possible effects of SEPT7 on dendritic branching were not investigated though a role for SEPT7 in regulating spine morphogenesis and dendrite development during neuronal maturation has been demonstrated in hippocampal neurons (Tada et al., 2007). SEPT7 monomers are possibly one among several regulators of STIM1-mediated Ca^{2+} entry, and presumably, their loss can be compensated by other regulators of Ca^{2+} signaling in PNs.

Gene Expression Changes in Purkinje Neurons With Loss of STIM1, and Restored by SEPT7, Are Associated With Neurodegeneration

Purkinje neurons express a range of Ca^{2+}-binding proteins, Ca^{2+} channels, Ca^{2+}-dependent kinases, and phosphatases that not only tune PN excitability but also help maintain cellular Ca^{2+} homeostasis, regulate different Ca^{2+}-dependent processes, and modulate multiple inputs received by PNs (Prestori et al., 2020). Changes in gene expression by loss of STIM1 suggest that the maintenance of Ca^{2+} homeostasis by STIM1 is required for appropriate age-dependent expression of multiple genes. Restored expression of genes encoding the Ca^{2+}-binding proteins parvalbumin (*Pvalb*) and calmodulin 1 (*Calm1*) (**Figure 3**) is of interest because parvalbumin is expressed abundantly in PNs (Caillard et al., 2000; Schwaller et al., 2002) and significant reduction in parvalbumin expression is reported from PNs of SCA1 (spinocerebellar ataxia 1) patients (Vig et al., 1996) and transgenic mice carrying the human SCA1-causing gene (Vig et al., 1998). Calmodulin 1, which is an EF hand containing Ca^{2+}-binding protein, is known to regulate the activity of several Ca^{2+}-regulated enzymes such as αCaMKII and βCaMKII that are required for cerebellar long-term depression (LTD) and motor learning (Hansel et al., 2006; Van Woerden et al., 2009). Reduced calmodulin levels are reported in the cerebellar vermis of the spontaneously ataxic mouse, *Pogo* (Lee et al., 2011).

The expression of certain genes classified under the GO category of neuron projection development is also restored in $STIM1^{PKO}$–$SEPT^{PHet/PKO}$ mice (**Figure 3**). Dlg4 is a major scaffolding protein in the excitatory postsynaptic density that regulates synaptic strength (Kim et al., 2004; Funke et al., 2005; Cheng et al., 2006), and previous work has reported impaired motor coordination in *Dlg4* knockout mice (Feyder et al., 2010). Robo2 is a transmembrane receptor for the secreted molecule slit homolog 2 protein (Slit2) and plays an important role in axon guidance and cell migration (Ma and Tessier-Lavigne, 2007; Giovannone et al., 2012). It is highly expressed by PNs during dendritic arbor development, and PN-specific *Robo2*-deficient

mice exhibit gait alterations (Gibson et al., 2014). Gigyf2 interacts with an adapter protein Grb10, which binds to activated IGF-I and insulin receptors (Giovannone et al., 2003; Holt and Siddle, 2005). Mice heterozygous for *Gigyf2* exhibit motor dysfunction (Giovannone et al., 2009). Loss of SEPT7 however does not restore the expression of every gene downregulated in $STIM^{PKO}$ PNs. This is possibly because reduced expression of some downregulated genes may be many steps downstream of Ca^{2+} entry, and slow restoration of PN Ca^{2+} homeostasis in either $SEPT7^{PHet}$; $STIM1^{PKO}$ or $SEPT7^{PKO}$;$STIM1^{PKO}$ animals may be insufficient to revert such changes. Moreover, SEPT7 may not restore precise Ca^{2+} dynamics related to STIM1 signaling that may be necessary for the expression of certain genes.

Climbing Fiber–Purkinje Neuron Synaptic Connectivity and Motor Behavior

Climbing fibers provide one of the major excitatory inputs to Purkinje neurons (Lin et al., 2014). Climbing fiber–Purkinje neuron (CF-PN) synaptic wiring influences processing and integration of information at the PN dendrites essential for proper control of cerebellar motor learning and coordination (Ichikawa et al., 2016). The distribution of CF-PN synapses on Purkinje dendrites is regulated and required for the proper physiological function of Purkinje neurons (Watanabe, 2008). Abnormal CF-PN innervation has been reported in various genetic mouse models with impaired Ca^{2+} signaling and motor coordination deficits (Alba et al., 1994; Chen et al., 1995; Kano et al., 1995; Kashiwabuchi et al., 1995; Kano et al., 1997; Hashimoto et al., 2001). Defective CF–PN connections have also been observed in the initial stages of Purkinje neuron degeneration in various forms of spinocerebellar ataxias and in conditions of abnormal activity in climbing fibres (Cheng et al., 2013; Koeppen et al., 2013; Helmich et al., 2013). Restoration of CF–PN innervation in $STIM1^{PKO}$–$SEPT7^{PHet/PKO}$ mice (**Figure 4**) is thus an important observation and very likely causative in the restoration of motor learning with age.

In conclusion, our data demonstrate that partial or complete loss of SEPT7 in *STIM1* knockout Purkinje neurons could restore age-dependent gene expression changes observed in $STIM1^{PKO}$ PNs. This is accompanied by normal climbing fiber–Purkinje neuron synaptic connectivity and an improved ability to learn and perform motor coordination task in aging mice. These findings suggest that loss of SEPT7 in Purkinje neurons allows spontaneous extracellular Ca^{2+} entry, as reported previously in *Drosophila* neurons (Deb et al., 2016) and in human neural progenitor cells (Deb et al., 2020), and this mode of Ca^{2+} entry could partially compensate for loss of STIM1-mediated SOCE in $STIM1^{PKO}$ PNs. This negative regulation of SOCE by SEPT7 in PNs could further modulate synaptic wiring and cerebellar circuit function in $STIM1^{PKO}$ mice. Our findings are relevant in the context of deciphering the therapeutic potential of SEPT7 inhibitors for neurodegenerative conditions where Ca^{2+} dyshomeostasis is observed over time.

DATA AVAILABILITY STATEMENT

The original contributions presented in the study are included in the article/**Supplementary Material**, and further inquiries can be directed to the corresponding author.

ETHICS STATEMENT

The animal study was reviewed and approved by the Institutional Animal Ethics Committee which is approved by the Control and Supervision of Experiments on Animals (CPCSEA), New Delhi, India.

AUTHOR CONTRIBUTIONS

SD contributed to conceptualization, developed methodology, performed and analyzed the experiments, assisted with data curation, and wrote the original manuscript. GH contributed to conceptualization, supervision, funding acquisition, and writing and editing of the manuscript.

FUNDING

This work was funded by Department of Biotechnology, Ministry of Science and Technology, Government of India (BT/PR6371/COE/34/19/2013) and core funds from National Centre for Biological Sciences (NCBS), Tata Institute for Fundamental Research, Bangalore, India. SD was supported by a fellowship from the Indian Council of Medical Research (ICMR). Government of India (ICMR-JRF-2015/LS/133/92183).

ACKNOWLEDGMENTS

We are thankful to the National Centre for Biological Sciences (NCBS), Tata Institute for Fundamental Research, and the Department of Biotechnology, government of India, for funding the project. We thank Prof. Anjana Rao from La Jolla Institute for Allergy and Immunology, La Jolla, California, for providing us with $Stim1^{flox/flox}$ mice. We are grateful to Prof. Matthias Gaestel, Institute of Biochemistry, Hannover Medical School, Hanover, Germany, for sending the $SEPT7^{flox/flox}$ mice. We are very thankful to the Animal Facility at the NCBS for maintaining the experimental mice. We thank the NCBS Central Imaging and Flow Facility for the use of confocal microscopes.

SUPPLEMENTARY MATERIAL

The Supplementary Material for this article can be found online at: https://www.frontiersin.org/articles/10.3389/fcell.2021.794807/full#supplementary-material

Supplementary Figure S1 | Analysis of gene expression in *SEPT7–STIM1* knockout Purkinje neurons (related to **Figure 3**) **(A)** Bar graph showing relative fold changes in expression levels of the indicated genes of various control genotypes of $STIM1^{PKO}$; $SEPT7^{PHet}$. Red asterisks above each bar represent statistically significant groups compared between $STIM1^{PKO}$ (pink bars) and $STIM1^{flox/flox}$; $SEPT^{flox/+}$(light blue bars). **(B)** Bar graph showing relative gene expression changes of the indicated genes of various control genotypes of $STIM1^{PKO}$; $SEPT7^{PKO}$. Red asterisks over each bar represent statistically significant groups compared between $STIM1^{PKO}$(pink bars) and $STIM1^{flox/flox}$; $SEPT^{flox/flox}$(blue bars). Fold changes were normalized to *GAPDH*. Data are presented as mean ± SEM, $^{*}p < 0.05$, $^{**}p < 0.01$; One-way ANOVA with post hoc Tukey's test. All measurements are taken by qRT-PCR of cDNA prepared from RNA isolated from microdissected Purkinje layers ($n = 3$ mice for all groups and $n = 4$ for $STIM1^{PKO}$; $SEPT7^{PHet}$, age: 1-year-old mice). *Itpr1*, inositol 1,4,5-trisphosphate receptor 1, *Orai3*—Orai3; *Casq2*, calsequestrin 2, *S100b*—S100b; *Cacng5*, calcium voltage-gated channel auxiliary subunit gamma 5; *Kctd17*, pPotassium channel tetramerization domain containing 17; *Vamp1*, vesicle-associated membrane protein 1; *Syt11*, synaptotagmin 11, *Setd6*, SET domaincontaining 6, *Gapdh*, glyceraldehyde 3-phosphate dehydrogenase.

Supplementary Figure S2 | Experimental setup of rotarod assay with mice of various genotypes of *SEPT7–STIM1* mutant strain (Related to **Figure 5**) Snapshots of mice of indicated genotypes on an accelerated rotarod at 0, 45, and 102 s. Lane 1–$STIM1^{flox/flox}$; $SEPT7^{flox/flox}$ (wild), Lane 2–$STIM1^{PKO}$, Lane 3–$STIM1^{PKO}$, Lane 4–$STIM1^{PKO}$; $SEPT7^{PHet}$, Lane 5–$STIM1^{PKO}$; $SEPT7^{PKO}$. All animals were aged 6 months. Mice that have fallen from the accelerating rod are indicated by red arrows.

Supplementary Video S1 | Rotarod assay of *SEPT7–STIM1* mutant mice strain (related to **Figure 5**). Video of the rotarod assay with mice of indicated genotypes. Lane 1: $STIM1^{flox/flox}$; $SEPT7^{flox/flox}$ (wild), Lane 2: $STIM1^{PKO}$, Lane 3: $STIM1^{PKO}$, Lane 4: $STIM1^{PKO}$; $SEPT7^{PHet}$, Lane 5: $STIM1^{PKO}$; $SEPT7^{PKO}$. All mice were 6 months old in this video.

REFERENCES

Alba, A., Kano, M., Chen, C., Stanton, M. E., Fox, G. D., Herrup, K., et al. (1994). Deficient Cerebellar Long-Term Depression and Impaired Motor Learning in mGluR1 Mutant Mice. *Cell* 79 (2), 377–388. doi:10.1016/0092-8674(94)90205-4

Ando, H., Hirose, M., and Mikoshiba, K. (2018). Aberrant IP3 Receptor Activities Revealed by Comprehensive Analysis of Pathological Mutations Causing Spinocerebellar Ataxia 29. *Proc. Natl. Acad. Sci. USA* 115 (48), 12259–12264. doi:10.1073/pnas.1811129115

Barski, J. J., Dethleffsen, K., and Meyer, M. (2000). Cre Recombinase Expression in Cerebellar Purkinje Cells. *Genesis* 28 (34), 93–98. doi:10.1002/1526-968x(200011/12)28:3/4<93:aid-gene10>3.0.co;2-w

Beites, C. L., Xie, H., Bowser, R., and Trimble, W. S. (1999). The Septin CDCrel-1 Binds Syntaxin and Inhibits Exocytosis. *Nat. Neurosci.* 2 (5), 434–439. doi:10.1038/8100

Bezprozvanny, I., and Hayden, M. R. (2004). Deranged Neuronal Calcium Signaling and Huntington Disease. *Biochem. Biophysical Res. Commun.* 322, 1310–1317. doi:10.1016/j.bbrc.2004.08.035

Boyden, E. S., Katoh, A., Pyle, J. L., Chatila, T. A., Tsien, R. W., and Raymond, J. L. (2006). Selective Engagement of Plasticity Mechanisms for Motor Memory Storage. *Neuron* 51 (6), 823–834. doi:10.1016/j.neuron.2006.08.026

Caillard, O., Moreno, H., Schwaller, B., Llano, I., Celio, M. R., and Marty, A. (2000). Role of the Calcium-Binding Protein Parvalbumin in Short-Term Synaptic Plasticity. *Proc. Natl. Acad. Sci.* 97 (24), 13372–13377. doi:10.1073/pnas.230362997

Chen, C., Kano, M., Abeliovich, A., Chen, L., Bao, S., Kim, J. J., et al. (1995). Impaired Motor Coordination Correlates with Persistent Multiple Climbing Fiber Innervation in PKC*γ* Mutant Mice. *Cell* 83 (7), 1233–1242. doi:10.1016/0092-8674(95)90148-5

Cheng, D., Hoogenraad, C. C., Rush, J., Ramm, E., Schlager, M. A., Duong, D. M., et al. (2006). Relative and Absolute Quantification of Postsynaptic Density Proteome Isolated from Rat Forebrain and Cerebellum. *Mol. Cell Proteomics* 5 (6), 1158–1170. doi:10.1074/mcp.D500009-MCP200

Cheng, M. M., Tang, G., and Kuo, S.-H. (2013). Harmaline-Induced Tremor in Mice: Videotape Documentation and Open Questions about the Model. *Tremor and Other Hyperkinetic Movements* 3 (0), 03. doi:10.5334/tohm.139

Czeredys, M. (2020). Dysregulation of Neuronal Calcium Signaling via Store-Operated Channels in Huntington's Disease. *Front. Cel Dev. Biol.* 8. doi:10.3389/fcell.2020.611735

de Souza, L. B., Ong, H. L., Liu, X., and Ambudkar, I. S. (2021). PIP2 and Septin Control STIM1/Orai1 Assembly by Regulating Cytoskeletal Remodeling via a CDC42-Wasp/wave-Arp2/3 Protein Complex. *Cell Calcium* 99, 102475. doi:10.1016/j.ceca.2021.102475

Deb, B. K., Chakraborty, P., Gopurappilly, R., and Hasan, G. (2020). SEPT7 Regulates Ca2+ Entry through Orai Channels in Human Neural Progenitor Cells and Neurons. *Cell Calcium* 90, 102252. doi:10.1016/j.ceca.2020.102252

Deb, B. K., Pathak, T., and Hasan, G. (2016). Store-independent Modulation of Ca2+ Entry through Orai by Septin 7. *Nat. Commun.* 7, 11751. doi:10.1038/ncomms11751

Dhanya, S. K., and Hasan, G. (2021). Purkinje Neurons with Loss of STIM1 Exhibit Age-dependent Changes in Gene Expression and Synaptic Components. *J. Neurosci.* 41 (17), 3777–3798. doi:10.1523/jneurosci.2401-20.2021

Drees, B. L., Sundin, B., Brazeau, E., Caviston, J. P., Chen, G.-C., Guo, W., et al. (2001). A Protein Interaction Map for Cell Polarity Development. *J. Cel Biol.* 154 (3), 549–576. doi:10.1083/jcb.200104057

Faty, M., Fink, M., and Barral, Y. (2002). Septins: A Ring to Part Mother and Daughter. *Curr. Genet.* 41, 123–131. doi:10.1007/s00294-002-0304-0

Feyder, M., Karlsson, R.-M., Mathur, P., Lyman, M., Bock, R., Momenan, R., et al. (2010). Association of MouseDlg4(PSD-95) Gene Deletion and HumanDLG4Gene Variation with Phenotypes Relevant to Autism Spectrum Disorders and Williams' Syndrome. *Ajp* 167 (12), 1508–1517. doi:10.1176/appi.ajp.2010.10040484

Finger, F. P., Kopish, K. R., and White, J. G. (2003). A Role for Septins in Cellular and Axonal Migration in *C. elegans*. *Developmental Biol.* 261 (1), 220–234. doi:10.1016/S0012-1606(03)00296-3

Finger, F. P. (2002). One Ring to Bind Them. *Developmental Cel* 3, 761–763. doi:10.1016/S1534-5807(02)00371-4

Fremeau, R. T., Troyer, M. D., Pahner, I., Nygaard, G. O., Tran, C. H., Reimer, R. J., et al. (2001). The Expression of Vesicular Glutamate Transporters Defines Two Classes of Excitatory Synapse. *Neuron* 31 (2), 247–260. doi:10.1016/S0896-6273(01)00344-0

Funke, L., Dakoji, S., and Bredt, D. S. (2005). Membrane-associated Guanylate Kinases Regulate Adhesion and Plasticity at Cell Junctions. *Annu. Rev. Biochem.* 74, 219–245. doi:10.1146/annurev.biochem.74.082803.133339

Gibson, D. A., Tymanskyj, S., Yuan, R. C., Leung, H. C., Lefebvre, J. L., Sanes, J. R., et al. (2014). Dendrite Self-Avoidance Requires Cell-Autonomous Slit/robo Signaling in Cerebellar Purkinje Cells. *Neuron* 81 (5), 1040–1056. doi:10.1016/j.neuron.2014.01.009

Giovannone, B., Lee, E., Laviola, L., Giorgino, F., Cleveland, K. A., and Smith, R. J. (2003). Two Novel Proteins that Are Linked to Insulin-like Growth Factor (IGF-I) Receptors by the Grb10 Adapter and Modulate IGF-I Signaling. *J. Biol. Chem.* 278 (34), 31564–31573. doi:10.1074/jbc.M211572200

Giovannone, B., Tsiaras, W. G., De la Monte, S., Klysik, J., Lautier, C., Karashchuk, G., et al. (2009). GIGYF2 Gene Disruption in Mice Results in Neurodegeneration and Altered Insulin-like Growth Factor Signaling. *Hum. Mol. Genet.* 18 (23), 4629–4639. doi:10.1093/hmg/ddp430

Giovannone, D., Reyes, M., Reyes, R., Correa, L., Martinez, D., Ra, H., et al. (2012). Slits Affect the Timely Migration of Neural Crest Cells via Robo Receptor. *Dev. Dyn.* 241 (8), 1274–1288. doi:10.1002/dvdy.23817

Gladfelter, A., Pringle, J. R., and Lew, D. J. (2001). The Septin Cortex at the Yeast Motherâ€"bud Neck. *Curr. Opin. Microbiol.* 4, 681–689. doi:10.1016/S1369-5274(01)00269-7

Hansel, C., de Jeu, M., Belmeguenai, A., Houtman, S. H., Buitendijk, G. H. S., Andreev, D., et al. (2006). αCaMKII Is Essential for Cerebellar LTD and Motor Learning. *Neuron* 51 (6), 835–843. doi:10.1016/j.neuron.2006.08.013

Hartmann, J., Karl, R. M., Alexander, R. P. D., Adelsberger, H., Brill, M. S., Rühlmann, C., et al. (2014). STIM1 Controls Neuronal Ca2+ Signaling, mGluR1-dependent Synaptic Transmission, and Cerebellar Motor Behavior. *Neuron* 82 (3), 635–644. doi:10.1016/j.neuron.2014.03.027

Hasan, G., and Sharma, A. (2020). Regulation of Neuronal Physiology by Ca2+ Release through the IP3R. *Curr. Opin. Physiol.* 17, 1–8. doi:10.1016/j.cophys.2020.06.001

Hashimoto, K., Ichikawa, R., Takechi, H., Inoue, Y., Aiba, A., Sakimura, K., et al. (2001). Roles of Glutamate Receptor δ2 Subunit (GluRδ2) and Metabotropic Glutamate Receptor Subtype 1 (mGluR1) in Climbing Fiber Synapse Elimination during Postnatal Cerebellar Development. *J. Neurosci.* 21 (24), 9701–9712. doi:10.1523/jneurosci.21-24-09701.2001

Helmich, R. C., Toni, I., Deuschl, G., and Bloem, B. R. (2013). The Pathophysiology of Essential Tremor and Parkinson's Tremor. *Curr. Neurol. Neurosci. Rep.* 13 (9), 1–10. doi:10.1007/s11910-013-0378-8

Holt, L. J., and Siddle, K. (2005). Grb10 and Grb14: Enigmatic Regulators of Insulin Action - and More? *Biochem. J.* 388 (2), 393–406. doi:10.1042/BJ20050216

Hsu, S.-C., Hazuka, C. D., Roth, R., Foletti, D. L., Heuser, J., and Scheller, R. H. (1998). Subunit Composition, Protein Interactions, and Structures of the Mammalian Brain Sec6/8 Complex and Septin Filaments. *Neuron* 20 (6), 1111–1122. doi:10.1016/S0896-6273(00)80493-6

Ichikawa, R., Hashimoto, K., Miyazaki, T., Uchigashima, M., Yamasaki, M., Aiba, A., et al. (2016). Territories of Heterologous Inputs onto Purkinje Cell Dendrites Are Segregated by Mglur1-dependent Parallel Fiber Synapse Elimination. *Proc. Natl. Acad. Sci. USA* 113 (8), 2282–2287. doi:10.1073/pnas.1511513113

Irazoqui, J. E., and Lew, D. J. (2004). Polarity Establishment in Yeast. *J. Cel Sci.* 117, 2169–2171. doi:10.1242/jcs.00953

Kaneko, M., Yamaguchi, K., Eiraku, M., Sato, M., Takata, N., Kiyohara, Y., et al. (2011). Remodeling of Monoplanar Purkinje Cell Dendrites during Cerebellar Circuit Formation. *PLoS One* 6 (5), e20108. doi:10.1371/journal.pone.0020108

Kano, M., Hashimoto, K., Chen, C., Abeliovich, A., Aiba, A., Kurihara, H., et al. (1995). Impaired Synapse Elimination during Cerebellar Development in PKCγ Mutant Mice. *Cell* 83 (7), 1223–1231. doi:10.1016/0092-8674(95)90147-7

Kano, M., Hashimoto, K., Kurihara, H., Watanabe, M., Inoue, Y., Aiba, A., et al. (1997). Persistent Multiple Climbing Fiber Innervationof Cerebellar Purkinje Cellsin Mice Lacking mGluR1. *Neuron* 18 (1), 71–79. doi:10.1016/S0896-6273(01)80047-7

Kartmann, B., and Roth, D. (2001). Novel Roles for Mammalian Septins: From Vesicle Trafficking to Oncogenesis. *J. Cel Sci.* 114 (5), 839–844. doi:10.1242/jcs.114.5.839

Kashiwabuchi, N., Ikeda, K., Araki, K., Hirano, T., Shibuki, K., Takayama, C., et al. (1995). Impairment of Motor Coordination, Purkinje Cell Synapse Formation, and Cerebellar Long-Term Depression in GluRδ2 Mutant Mice. *Cell* 81 (2), 245–252. doi:10.1016/0092-8674(95)90334-8

Kim, E., and Sheng, M. (2004). PDZ Domain Proteins of Synapses. *Nat. Rev. Neurosci.* 5, 771–781. doi:10.1038/nrn1517

Kim, H., Kim, M., Im, S.-K., and Fang, S. (2018). Mouse Cre-LoxP System: General Principles to Determine Tissue-specific Roles of Target Genes. *Lab. Anim. Res.* 34 (4), 147. doi:10.5625/lar.2018.34.4.147

Kinoshita, M. (2003). Assembly of Mammalian Septins. *J. Biochem.* 134 (4), 491–496. doi:10.1093/jb/mvg182

Kinoshita, M., Kumar, S., Mizoguchi, A., Ide, C., Kinoshita, A., Haraguchi, T., et al. (1997). Nedd5, a Mammalian Septin, Is a Novel Cytoskeletal Component Interacting with Actin-Based Structures. *Genes Dev.* 11 (12), 1535–1547. doi:10.1101/gad.11.12.1535

Kinoshita, M., and Noda, M. (2001). Advances in Cytokinesis Research. Roles of Septins in the Mammalian Cytokinesis Machinery. *Cell Struct. Funct.* 26, 667–670. doi:10.1247/csf.26.667

Klar, J., Ali, Z., Farooq, M., Khan, K., Wikström, J., Iqbal, M., et al. (2017). A Missense Variant in ITPR1 Provides Evidence for Autosomal Recessive SCA29 with Asymptomatic Cerebellar Hypoplasia in Carriers. *Eur. J. Hum. Genet.* 25, 848–853. doi:10.1038/ejhg.2017.54

Klejman, M. E., Gruszczynska-Biegala, J., Skibinska-Kijek, A., Wisniewska, M. B., Misztal, K., Blazejczyk, M., et al. (2009). Expression of STIM1 in Brain and Puncta-like Co-localization of STIM1 and ORAI1 upon Depletion of Ca2+ Store in Neurons. *Neurochem. Int.* 54 (1), 49–55. doi:10.1016/j.neuint.2008.10.005

Koeppen, A. H., Ramirez, R. L., Bjork, S. T., Bauer, P., and Feustel, P. J. (2013). The Reciprocal Cerebellar Circuitry in Human Hereditary Ataxia. *Cerebellum* 12 (4), 493–503. doi:10.1007/s12311-013-0456-0

Koopmans, G. C., Deumens, R., Brook, G., Gerver, J., Honig, W. M. M., Hamers, F. P. T., et al. (2007). Strain and Locomotor Speed Affect Over-ground Locomotion in Intact Rats. *Physiol. Behav.* 92 (5), 993–1001. doi:10.1016/j.physbeh.2007.07.018

Lee, K. Y., Kim, J. S., Kim, S. H., Park, H. S., Jeong, Y.-G., Lee, N.-S., et al. (2011). Altered Purkinje Cell Responses and Calmodulin Expression in the Spontaneously Ataxic Mouse, Pogo. *Eur. J. Neurosci.* 33 (November 2009), 1493–1503. doi:10.1111/j.1460-9568.2011.07641.x

Lin, C.-Y., Louis, E. D., Faust, P. L., Koeppen, A. H., Vonsattel, J.-P. G., and Kuo, S.-H. (2014). Abnormal Climbing Fibre-Purkinje Cell Synaptic Connections in the Essential Tremor Cerebellum. *Brain* 137 (12), 3149–3159. doi:10.1093/brain/awu281

Ma, L., and Tessier-Lavigne, M. (2007). Dual branch-promoting and branch-repelling Actions of Slit/Robo Signaling on Peripheral and central Branches of Developing Sensory Axons. *J. Neurosci.* 27 (25), 6843–6851. doi:10.1523/JNEUROSCI.1479-07.2007

Macara, I. G., Baldarelli, R., Field, C. M., Glotzer, M., Hayashi, Y., Hsu, S.-C., et al. (2002). Mammalian Septins Nomenclature. *MBoC* 13, 4111–4113. doi:10.1091/mbc.E02-07-0438

Marquardt, J., Chen, X., and Bi, E. (2019). Architecture, Remodeling, and Functions of the Septin Cytoskeleton. *Cytoskeleton* 76, 7–14. doi:10.1002/cm.21475

Mendonça, D. C., Macedo, J. N., Guimarães, S. L., Barroso da Silva, F. L., Cassago, A., Garratt, R. C., et al. (2019). A Revised Order of Subunits in Mammalian Septin Complexes. *Cytoskeleton* 76 (9–10), 457–466. doi:10.1002/cm.21569

Menon, M. B., Sawada, A., Chaturvedi, A., Mishra, P., Schuster-gossler, K., Galla, M., et al. (2014). Genetic Deletion of SEPT7 Reveals a Cell Type-specific Role of Septins in Microtubule Destabilization for the Completion of Cytokinesis. *Plos Genet.* 10 (8), e1004558. doi:10.1371/journal.pgen.1004558

Nagata, K.-i., Kawajiri, A., Matsui, S., Takagishi, M., Shiromizu, T., Saitoh, N., et al. (2003). Filament Formation of MSF-A, a Mammalian Septin, in Human Mammary Epithelial Cells Depends on Interactions with Microtubules. *J. Biol. Chem.* 278 (20), 18538–18543. doi:10.1074/jbc.M205246200

Nagy, A. (2000). Cre Recombinase: The Universal Reagent for Genome Tailoring. *Genesis* 26, 99–109. doi:10.1002/(sici)1526-968x(200002)26:2<99:aid-gene1>3.0.co;2-b

Oh-hora, M., Yamashita, M., Hogan, P. G., Sharma, S., Lamperti, E., Chung, W., et al. (2008). Dual Functions for the Endoplasmic Reticulum Calcium Sensors STIM1 and STIM2 in T Cell Activation and Tolerance. *Nat. Immunol.* 9 (4), 432–443. doi:10.1038/ni1574

Pan, Z., Brotto, M., and Ma, J. (2014). Store-operated Ca2+entry in Muscle Physiology and Diseases. *BMB Rep.* 47 (2), 69–79. doi:10.5483/BMBRep.2014.47.2.015

Pinto, A. P. A., Pereira, H. M., Zeraik, A. E., Ciol, H., Ferreira, F. M., Brandão-Neto, J., et al. (2017). Filaments and Fingers: Novel Structural Aspects of the Single Septin from Chlamydomonas Reinhardtii. *J. Biol. Chem.* 292 (26), 10899–10911. doi:10.1074/jbc.M116.762229

Prestori, F., Moccia, F., and D'Angelo, E. (2020). Disrupted Calcium Signaling in Animal Models of Human Spinocerebellar Ataxia (SCA). *Ijms* 21 (1), 216–228. doi:10.3390/ijms21010216

Ryu, C., Jang, D. C., Jung, D., Kim, Y. G., Shim, H. G., Ryu, H.-H., et al. (2017). STIM1 Regulates Somatic Ca2+ Signals and Intrinsic Firing Properties of Cerebellar Purkinje Neurons. *J. Neurosci.* 37 (37), 8876–8894. doi:10.1523/JNEUROSCI.3973-16.2017

Schwaller, B., Meyer, M., and Schiffmann, S. (2002). 'New' Functions for 'old' Proteins: The Role of the Calcium-Binding Proteins Calbindin D-28k, Calretinin and Parvalbumin, in Cerebellar Physiology. Studies with Knockout Mice. *The Cerebellum* 1 (4), 241–258. doi:10.1080/147342202320883551

Sharma, S., Quintana, A., Findlay, G. M., Mettlen, M., Baust, B., Jain, M., et al. (2013). An siRNA Screen for NFAT Activation Identifies Septins as Coordinators of Store-Operated Ca2+ Entry. *Nature* 499 (7457), 238–242. doi:10.1038/nature12229

Shiotsuki, H., Yoshimi, K., Shimo, Y., Funayama, M., Takamatsu, Y., Ikeda, K., et al. (2010). A Rotarod Test for Evaluation of Motor Skill Learning. *J. Neurosci. Methods* 189 (2), 180–185. doi:10.1016/j.jneumeth.2010.03.026

Sirajuddin, M., Farkasovsky, M., Hauer, F., Kühlmann, D., Macara, I. G., Weyand, M., et al. (2007). Structural Insight into Filament Formation by Mammalian Septins. *Nature* 449 (7160), 311–315. doi:10.1038/nature06052

Smeets, C. J. L. M., and Verbeek, D. S. (2016). Climbing Fibers in Spinocerebellar Ataxia: A Mechanism for the Loss of Motor Control. *Neurobiol. Dis.* 88, 96–106. doi:10.1016/j.nbd.2016.01.009

Soroor, F., Kim, M. S., Palander, O., Balachandran, Y., Collins, R. F., Benlekbir, S., et al. (2021). Revised Subunit Order of Mammalian Septin Complexes Explains Their *In Vitro* Polymerization Properties. *MBoC* 32 (3), 289–300. doi:10.1091/MBC.E20-06-0398

Street, V. A., Bosma, M. M., Demas, V. P., Regan, M. R., Lin, D. D., Robinson, L. C., et al. (1997). The Type 1 Inositol 1,4,5-Trisphosphate Receptor Gene Is Altered in theopisthotonosMouse. *J. Neurosci.* 17 (2), 635–645. doi:10.1523/jneurosci.17-02-00635.1997

Stroobants, S., Gantois, I., Pooters, T., and D'Hooge, R. (2013). Increased Gait Variability in Mice with Small Cerebellar Cortex Lesions and normal Rotarod Performance. *Behav. Brain Res.* 241 (1), 32–37. doi:10.1016/j.bbr.2012.11.034

Sun, S., Zhang, H., Liu, J., Popugaeva, E., Xu, N.-J., Feske, S., et al. (2014). Reduced Synaptic STIM2 Expression and Impaired Store-Operated Calcium Entry Cause Destabilization of Mature Spines in Mutant Presenilin Mice. *Neuron* 82 (1), 79–93. doi:10.1016/j.neuron.2014.02.019

Surka, M. C., Tsang, C. W., and Trimble, W. S. (2002). The Mammalian Septin MSF Localizes with Microtubules and Is Required for Completion of Cytokinesis. *MBoC* 13 (10), 3532–3545. doi:10.1091/mbc.E02-01-0042

Tada, T., Simonetta, A., Batterton, M., Kinoshita, M., Edbauer, D., and Sheng, M. (2007). Role of Septin Cytoskeleton in Spine Morphogenesis and Dendrite Development in Neurons. *Curr. Biol.* 17, 1752–1758. doi:10.1016/j.cub.2007.09.039

Van De Leemput, J., Chandran, J., Knight, M. A., Holtzclaw, L. A., Scholz, S., Cookson, M. R., et al. (2007). Deletion at ITPR1 Underlies Ataxia in Mice and Spinocerebellar Ataxia 15 in Humans. *Plos Genet.* 3 (6), e108. doi:10.1371/journal.pgen.0030108

Van Woerden, G. M., Hoebeek, F. E., Gao, Z., Nagaraja, R. Y., Hoogenraad, C. C., Kushner, S. A., et al. (2009). βCaMKII Controls the Direction of Plasticity at Parallel Fiber-Purkinje Cell Synapses. *Nat. Neurosci.* 12 (7), 823–825. doi:10.1038/nn.2329

Vig, P. J. S., Fratkin, J. D., Desaiah, D., Currier, R. D., and Subramony, S. H. (1996). Decreased Parvalbumin Immunoreactivity in Surviving Purkinje Cells of Patients with Spinocerebellar Ataxia-1. *Neurology* 47 (1), 249–253. doi:10.1212/WNL.47.1.249

Vig, P. J. S., Subramony, S. H., Burright, E. N., Fratkin, J. D., McDaniel, D. O., Desaiah, D., et al. (1998). Reduced Immunoreactivity to Calcium-Binding Proteins in Purkinje Cells Precedes Onset of Ataxia in Spinocerebellar Ataxia-1 Transgenic Mice. *Neurology* 50 (1), 106–113. doi:10.1212/WNL.50.1.106

Watanabe, M. (2008). Molecular Mechanisms Governing Competitive Synaptic Wiring in Cerebellar Purkinje Cells. *Tohoku J. Exp. Med.* 214, 175–190. doi:10.1620/tjem.214.175

Zhang, J., Kong, C., Xie, H., McPherson, P. S., Grinstein, S., and Trimble, W. S. (1999). Phosphatidylinositol Polyphosphate Binding to the Mammalian Septin H5 Is Modulated by GTP. *Curr. Biol.* 9 (24), 1458–1467. doi:10.1016/S0960-9822(00)80115-3

Zhou, Q., Yen, A., Rymarczyk, G., Asai, H., Trengrove, C., Aziz, N., et al. (2016). Impairment of PARK14-dependent Ca2+ Signalling Is a Novel Determinant of Parkinson's Disease. *Nat. Commun.* 7. doi:10.1038/ncomms10332

Conflict of Interest: The authors declare that the research was conducted in the absence of any commercial or financial relationships that could be construed as a potential conflict of interest.

Publisher's Note: All claims expressed in this article are solely those of the authors and do not necessarily represent those of their affiliated organizations, or those of the publisher, the editors, and the reviewers. Any product that may be evaluated in this article, or claim that may be made by its manufacturer, is not guaranteed or endorsed by the publisher.

frontiers in Cell and Developmental Biology

BRIEF RESEARCH REPORT
published: 06 January 2022
doi: 10.3389/fcell.2021.795798

Lyz2-Cre-Mediated Genetic Deletion of *Septin7* Reveals a Role of Septins in Macrophage Cytokinesis and *Kras*-Driven Tumorigenesis

Manoj B. Menon[1,2], Tatiana Yakovleva[1], Natalia Ronkina[1], Abdulhadi Suwandi[1], Ivan Odak[3], Sonam Dhamija[1,4], Inga Sandrock[3], Florian Hansmann[5,6], Wolfgang Baumgärtner[5], Reinhold Förster[3], Alexey Kotlyarov[1†] and Matthias Gaestel[1†]*

[1]Institute of Cell Biochemistry, Hannover Medical School, Hannover, Germany, [2]Kusuma School of Biological Sciences, Indian Institute of Technology Delhi, New Delhi, India, [3]Institute of Immunology, Hannover Medical School, Hannover, Germany, [4]Institute of Genomics and Integrative Biology (CSIR-IGIB), New Delhi, India, [5]Institute of Pathology, Stiftung Tierärztliche Hochschule, Hannover, Germany, [6]Institute of Veterinary Pathology, Veterinary Faculty of Leipzig University, Leipzig, Germany

OPEN ACCESS

Edited by:
Ana Cuenda, Spanish National Research Council (CSIC), Spain

Reviewed by:
Simon Arthur, University of Dundee, United Kingdom
Francisco Iñesta-Vaquera, University of Dundee, United Kingdom

***Correspondence:**
Matthias Gaestel
gaestel.matthias@mh-hannover.de

[†]These authors share senior authorship

Specialty section:
This article was submitted to Signaling, a section of the journal Frontiers in Cell and Developmental Biology

Received: *15 October 2021*
Accepted: *16 December 2021*
Published: *06 January 2022*

Citation:
Menon MB, Yakovleva T, Ronkina N, Suwandi A, Odak I, Dhamija S, Sandrock I, Hansmann F, Baumgärtner W, Förster R, Kotlyarov A and Gaestel M (2022) Lyz2-Cre-Mediated Genetic Deletion of Septin7 Reveals a Role of Septins in Macrophage Cytokinesis and Kras-Driven Tumorigenesis. Front. Cell Dev. Biol. 9:795798. doi: 10.3389/fcell.2021.795798

By crossing *septin7*-floxed mice with *Lyz2*-Cre mice carrying the Cre recombinase inserted in the Lysozyme-M (*Lyz2*) gene locus we aimed the specific deletion of septin7 in myeloid cells, such as monocytes, macrophages and granulocytes. *Septin7*$^{flox/flox}$:*Lyz2*-Cre mice show no alterations in the myeloid compartment. *Septin7*-deleted macrophages (BMDMs) were isolated and analyzed. The lack of Septin7 expression was confirmed and a constitutive double-nucleation was detected in Septin7-deficient BMDMs indicating a defect in macrophage cytokinesis. However, phagocytic function of macrophages as judged by uptake of labelled *E. coli* particles and LPS-stimulated macrophage activation as judged by induction of TNF mRNA expression and TNF secretion were not compromised. In addition to myeloid cells, Lyz2-Cre is also active in type II pneumocytes (AT2 cells). We monitored lung adenocarcinoma formation in these mice by crossing them with the conditional knock-in *Kras*-LSL-G12D allele. Interestingly, we found that control mice without septin7 depletion die after 3–5 weeks, while the Septin7-deficient animals survived 11 weeks or even longer. Control mice sacrificed in the age of 4 weeks display a bronchiolo-alveolar hyperplasia with multiple adenomas, whereas the Septin7-deficient animals of the same age are normal or show only a weak multifocal brochiolo-alveolar hyperplasia. Our findings indicate an essential role of Septin7 in macrophage cytokinesis but not in macrophage function. Furthermore, septin7 seems absolutely essential for oncogenic *Kras*-driven lung tumorigenesis making it a potential target for anti-tumor interventions.

Keywords: septins, septin7, Lyz2-Cre, phagocytosis, myeloid cells, tumor model, Kras-G12D

INTRODUCTION

Septins, a conserved family of filament forming GTPases, build heteropolymeric higher-order structures and participate in diverse cellular processes, and are being widely accepted as the fourth component of eukaryotic cytoskeleton (Mostowy and Cossart, 2012). Originally discovered as genes required for cytokinesis in budding yeast, septins associate with mitotic

spindle, contractile ring and midbody and participate in cytokinesis of metazoan cells, (Hartwell et al., 1970; Fededa and Gerlich, 2012; Green et al., 2012; Karasmanis et al., 2019; Chen et al., 2021). Non-canonical septin functions in mammalian cells range from neuronal morphogenesis to control of bacterial and viral infections (Bridges and Gladfelter, 2015; Van Ngo and Mostowy, 2019; Robertin and Mostowy, 2020).

Mammalian cells express 13 septin gene products with partially redundant functions. Depletion of one of the major subunits, such as the pivotal subunit Septin7 affects multiple steps in mitosis and cytokinesis (Kinoshita et al., 1997; Estey et al., 2010; Sellin et al., 2011; Karasmanis et al., 2019; Chen et al., 2021). Deletion of *Septin7* gene is associated with the co-depletion of the core septin subunits making it a pan-septin depletion model (Menon et al., 2014). *Septin7*$^{-/-}$ fibroblasts display cytokinetic failure and undergo obligate multinucleation (Menon et al., 2014). While *Septin7*$^{-/-}$ embryos fail to gastrulate, *Septin7*-deletion in lymphoid cells does not have an impact on T and B-lymphocyte development. However, *Septin7*-deleted CD8^{+} T cells display cytokinetic failure upon cytokine stimulation in the absence of antigen-presenting cells (Menon et al., 2014; Mujal et al., 2016). Furthermore, siRNA mediated Septin7 depletion in T-lymphocytes *in vitro* had no impact on lymphocyte proliferation, despite clear motility defects (Tooley et al., 2009). Septin7-deficient myeloid progenitors are capable of colony formation *in vitro* (Menon et al., 2014) and siRNA-mediated Septin7 depletion in myeloid K562 cell line had no impact on cell proliferation (Sellin et al., 2011). Septins assemble at the base of phagosomes in myeloid cells and siRNA mediated depletion of septin 2 and 11 in macrophages has been shown to suppress FcγR-mediated phagocytosis (Huang et al., 2008). Septins participate in the cell entry and pathogenicity of intracellular bacteria such as *Listeria* and *Shigella* (Mostowy et al., 2010; Van Ngo and Mostowy, 2019). While most of the studies investigating the role of septins in bacterial pathogenesis have been performed in non-phagocytic cells, an infection model in zebrafish has shown a role for macrophages and neutrophil septins in limiting *Shigella* infection (Mostowy et al., 2013). In the present study, we crossed the *Septin7*^{flox} mice with the myeloid-specific *Lyz2*-Cre line (Clausen et al., 1999) to generate a tissue-specific *Septin7*-knockout (KO) mice and to investigate the role of septins in myeloid cells.

Adenocarcinoma, the major form of lung cancer, is associated with activating mutations in the oncogenic small GTPase KRAS (Cancer Genome Atlas Research Network, 2014). Most tumor cells located in lung periphery express surfactant protein C, indicating that they originate from alveolar type 2 (AT2) cells or from their progenitors (Desai et al., 2014). Since the *Lyz2* locus is active not only in myeloid lineage but also in AT2 cells (Desai et al., 2014), the Cre-Lyz2 knock-in strain could be used to analyze the effect of gene deletion in AT2 cells. Interestingly, AT2 proliferation is selectively induced by Cre-regulated oncogenic Kras-G12D *in vivo* (Jackson et al., 2001), efficiently generating multifocal, clonal adenomas in the lungs with replacement of almost the entire alveolar region and death of the animals within a month after birth (Desai et al., 2014). The generation and initial analyses of the *Septin7* whole-animal and hematopoietic-specific knockout models had revealed a cell-type specific role for septins in mammalian cytokinesis (Menon et al., 2014). These findings support a hypothesis that differential targeting of cytokinesis could form the basis for specific anti-proliferative therapies to target solid tumors, without impairing hematopoiesis that is less dependent on septins (Menon and Gaestel, 2015). Here, we present genetic evidence that septins are indispensable for Kras-induced lung tumorigenesis and thus septin targeting may be a feasible strategy of therapeutic intervention.

MATERIALS AND METHODS

Generation of *Lyz2*-Cre Driven *Septin7* Conditional KO Mice

All mice experiments were conducted according to German and international guidelines and were in accordance with the ethical oversight by the local government for the administrative region of Lower Saxony (permit 17/2593), Germany. *Septin7*$^{flox/flox}$ mice (*Sept7*^{tm1Mgl}) targeting the exon 4 of Septin7 gene was reported previously (Menon et al., 2014). For the generation of myeloid specific knockout animals, *Septin7* homozygous floxed mice (back-crossed for six generations with C57Bl/6J) were crossed with *B6- Lyz2*$^{tm1(cre)Ifo}$ deletor line (Clausen et al., 1999). For the generation of the Ras-induced tumor model the *Sept7*$^{flox/flox}$*:Lyz2-Cre* strain was crossed with *B6.129S4-Kras*^{tm4Tyj} animals (Jackson et al., 2001). In animal experiments, age and sex matched, Cre-expressing *Septin7* wt/flox (heterozygous control, n = 18) and flox/flox (homozygous floxed, n = 17) mice were compared. Mice were monitored daily for survival.

DNA Isolation and Genotyping

Tail biopsies and BM samples were overnight digested at 53°C in lysis buffer [50 mM Tris-Cl (pH 8.0), 100 mM EDTA, 100 mM NaCl and 1% SDS] containing proteinase-K (0.5 mg/ml) (Roche). Proteins were salted out with extra NaCl. DNA was precipitated with isopropanol, washed with 70% ethanol and dissolved in water. Genotyping PCRs were performed with Top Taq DNA polymerase (Qiagen) with extra Mg^{2+} under standard conditions with annealing temperature at 53°C. The primers used for *Septin7* and *Cre* genotyping were described previously (Menon et al., 2014). Lyz2-Cre locus was genotyped using primers described in the Jackson laboratory Genotyping protocol (#28518) for the strain using standard PCR conditions. For genotyping *Kras*, the following primers were used: Kras-y117: 5'-CTAGCCACCATG GCTTGAGT-3'; Kras-y118: 5'-ATGTCTTTCCCCAGCACA GT-3'; Kras-y116: TCCGAATTCAGTGACTACAGATG-3'. For *Kras* wildtype, y117/y118 primer pairs generated a PCR product of 450-bp. For *Kras LSL* allele y117/y116 primer pairs generated a PCR product of 327-bp (Thakkar et al., 2018) PCR reactions were separated on 2% agarose gels and images acquired using INTAS Gel documentation system.

BMDM Generation and Treatments

To obtain bone marrow-derived macrophages (BMDMs), femurs of 6–8 weeks-old mice were flushed and plated on one 10 cm plate

with 100 ng/ml M-CSF (Wyeth/Pfizer) in DMEM supplemented with 10% FCS, antibiotics and 1× non-essential amino-acids. The next day, non-adherent floaters were transferred to a new 10 cm plate and new medium containing M-CSF was added to the first plate. Medium was renewed on both plates every 3–4 days. Cells were scraped and seeded for experiments between 10 and 14 days after initial plating. For experimental treatments, cells were seeded in the same growth medium without MCSF. For stimulation, BMDMs were treated with LPS (Sigma, *E. coli* O127:B8, 1 μg/ml) for indicated time-periods before cells and/or supernatants were used for further analyses.

For monitoring phagocytosis, the cells were treated with BODIPY™ FL conjugated *E. coli* (K-12 strain) Bioparticles (Molecular Probes, Cat#E2864) for 75 min. Immediately after the incubation, cells were cooled on ice, were 3× washed with ice-cold PBS and were fixed and stained with Septin7 antibodies and DAPI as described below. For semi-quantitative measurement of phagocytosis BMDMs were treated with Fluorescein-labeled *Escherichia coli* K-12 Bioparticles (Vybrant™ Phagocytosis Assay Kit, Molecular Probes, Cat#V-6694) for 75 min. After incubation, cells were immediately cooled on ice and trypan blue was added and incubated for 1 min to extinguish fluorescence of non-internalized bacteria. The cells were washed 3× with ice-cold PBS, fixed with 4% PFA and stained with DAPI as described below. The images were acquired on Cytation 1 (BioTek) at 40× magnification in eight fields of view (FOV) per samples using BioTek Gen5™ Software. Quantification of mean fluorescence intensity (MFI) was determined using Cellular Analysis tools from BioTek Gen5™ Software. DAPI staining was defined as primary mask to identify the cells. Furthermore, the secondary mask was defined from GFP channel by expanding the primary mask to 20 μm that cover the perinuclear region. Green MFI in that area were measured. The results are defined as the mean of green fluorescence intensity per cells per FOV. For monitoring the efficiency of Septin7 depletion, control cells were fixed and stained for Septin7 (Alexa fluor-555 channel) and images were acquired and processed as above. DAPI staining was defined as primary mask to identify the cells and the standard RFP channel was used to detect Septin7. RFP mean fluorescence intensity (MFI) were measured and a minimum threshold RFP signal in the Septin7 positive cells were defined. The number of cells with red fluorescence intensity higher than the threshold were counted, and then the percentage of positive cells to total cells (DAPI positive cells) were calculated. The results are the mean of % RFP positive cells per FOV.

Antibodies and Reagents

Primary antibodies used were: Septin7 (#JP18991, IBL International), EF2 (sc-13004-R, Santa Cruz Biotech) and Phospho-p38 MAPK (#9211, Cell Signaling Technology). Anti-rabbit Alexa fluor-555 (#A31572), anti-rabbit Alexa fluor-488 (cat# A21206) and anti-mouse Alexa fluor-546 -dye labeled secondary antibodies, tetramethyl rhodamine-conjugated WGA (#W849) and Alexa fluor-647-conjugated phalloidin (#A22287) were from Invitrogen. DAPI for DNA staining was from Carl Roth (#6335.1). HRP-labeled anti-rabbit (#111035-003) secondary antibodies for immunoblots were from Dianova.

Western Immunoblotting

Cells were lysed directly in SDS gel loading dye and western blotting was performed as previously described using gradient SDS-PAGE gels (Menon et al., 2010).

Immunofluorescence Staining

BMDMs were grown on glass coverslips and fixed with 4% paraformaldehyde (PFA) in PBS. Fixation was performed for 2–5 min at room temperature (RT) followed by 20 min at 4°C and were permeabilized with 0.25% Triton X-100–PBS for 30 min at RT. Blocking was done using 4% bovine serum albumin (BSA) for 1 h at 4°C. Primary antibodies were used at a 1:50 to 1:200 dilution in 1% BSA–PBS for 1–2 h. Secondary antibodies or Alexa Fluor 647-conjugated phalloidin/tetramethy rhodamine conjugated WGA was used at a 1:500 dilution in 1% BSA–PBS. Slides were mounted with ROTI® Mount (Carl-Roth) after staining with DAPI. Imaging was performed using a Leica TCS SP2 confocal microscope with standard settings. For phagocytosis assays, images were acquired using a standard fluorescence microscope or the Cytation 1 imaging multimode reader (Biotek).

Flow Cytometry Analysis

For immunophenotyping analysis of bone marrow, cells were isolated, RBC lysed (Pharmlyse, BD Biosciences) and analyzed for surface staining with Gr1-PE (clone-RB6-8CS), Sca1-PE (D7), ckit-APC (2B8; BD Biosciences), CD11b-APC (M1/70; eBiosciences), CD11b-PE (M1/70.15; Immunotools)and F4/80-PE (BM8; eBiosciences) as described previously (Mingay et al., 2018). In short, Propidium-Iodide-negative cells were gated and probed for c-Kit-APC/Sca1-PE double positive, CD11b-APC/F4/80-PE double positive (monocytes) and CD11b-APC/Gr1-PE double positive (granulocytes) cells as shown in the representative gating scheme (**Supplementary Figure S1**). BMDMs were scraped out, pelleted and resuspended in PBS-2mM EDTA before staining. Samples were analyzed using a FACSCalibur Flow-cytometer (BD Biosciences).

For Septin7 staining, nucleated BM cells were fixed with 3× by volume PFA (4%) at RT for 30 min. Washed and resuspended in PBS and absolute methanol was added to 90% concentration final with constant mixing. The methanol permeabilization was continued for 30 min on ice. After 2× PBS wash cells were resuspended in 4% BSA-PBS and blocked at 4°C for 30 min. Cells were stained with primary Septin7 antibodies (1:100 in 1% BSA-PBS) at RT for 30 min. After 1× PBS wash, samples were resuspended in Alexa fluor-488-labelled secondary antibody dilution (1:500 diluted in 1% BSA-PBS) and incubated for additional 30 min before PBS wash and analysis in Accuri- C6 flow cytometer.

Gene Expression Analyses by Real-Time qPCR and ELISA

RNA was isolated using the NucleoSpin RNA extraction kit (Macherey and Nagel) according to the manufacturer's instructions. cDNA was synthesized with the first strand cDNA synthesis kit (Fermentas/Thermo) using random hexamer primers. qRT-PCRs were run on a Rotor-Gene-Q

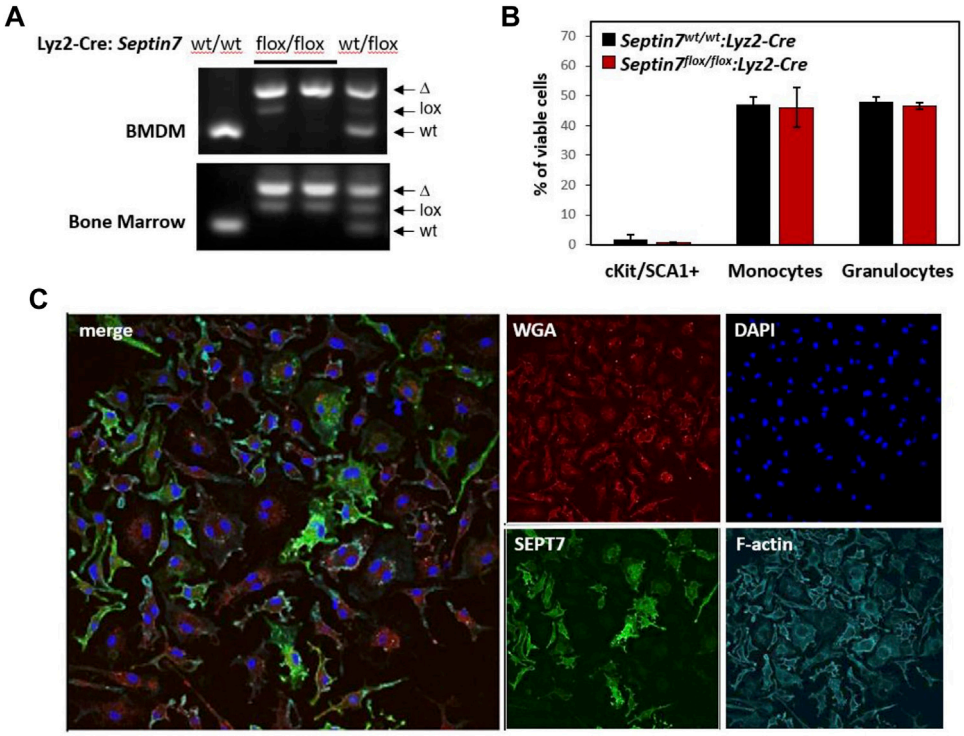

FIGURE 1 | Effect of myeloid Septin7-deletion in myelopoiesis and BMDM proliferation. **(A)** Septin7-genotye analyses of bone marrow (BM) cells and BM-derived macrophages (BMDM) from the myeloid specific Septin7-KO mice show efficient deletion of the floxed allele. **(B)** Cell surface marker analysis of BM cells from *Septin7*$^{flox/flox}$*:Lyz2-Cre* and *Septin7*$^{wt/wt}$*:Lyz2-Cre* reveal no significant differences (n = 3 mice each, p value > 0.3) in stem/progenitors (cKit$^+$ and Sca1$^+$), monocytes (CD11b$^+$ and F4/80$^+$) and granulocyte (Gr1$^+$ and CD11b$^+$) populations. **(C)** Immunofluorescence analysis showing obligatory binucleation of *Septin7*-KO BMDMs. DAPI is used for nuclear staining, WGA and Phalloidin (staining F-actin) are shown as counter stains. Septin7-negative cells display more than one nucleus, whereas Septin7-positive cells (stained green) display only one.

(Qiagen) device using 2× SYBR-Green SensiFast mixes (no ROX, Bioline) and the gene expression for *Tnfα* and *Nfkbiα* were normalized to *Gapdh* and presented. Primers used are *Tnfα*-fwd- 5'-TGCCTATGTCTCAGCCTCTTC-3', *Tnfα* -rev- 5'- GA GGCCATTTGGGAACTTCT -3', *Gapdh*-fwd- 5'- CATGGCCTT CCGTGTTCCTA- 3', *Gapdh*-rev-"CCTGCTTCACCACCTTCT TGAT", *Nfkbiα* -fwd-5'- GACGCAGACCTGCACACCCC- 3' and *Nfkbiα*-rev-5'-TGGAGGGCTGTCCGGCCATT-3'. BMDM supernatants were collected and quantification of murine TNFα by ELISA was performed as described previously using commercial kits (Tiedje et al., 2012).

Histopathology

Lungs were harvested and inflation fixed with 10% neutral buffered formalin. Lungs were trimmed at different levels and embedded in paraffin wax. For histological examinations 2–3 µm thick sections were prepared and stained with hematoxylin and eosin.

Statistical Analyses

Students 2-tailed t-tests was used to check the statistical significance of differences between Septin7-wt and KO myeloid cells (in **Figure 1B**, **Figures 2C,D**, p-values non-significant > 0.3). For the animal experiments, p-values were derived by the Kaplan-Meier log-rank (Mantel-Cox) test using GraphPad Prism 8 software. The survival curves are significantly different with a χ^2 = 36.29 resulting in a p value < 0.0001.

RESULTS

Deletion of *Septin7* Does Not Alter the Myeloid Compartment, But Leads to Cytokinesis Failure in Macrophages *In Vitro*

By *in vitro* deletion of *Septin7* in hematopoietic cells, we had previously shown that *Septin7*-deficient myeloid progenitors can form colonies in a semi-solid medium (Menon et al., 2014). To further investigate the *in vivo* consequences of *Septin7* deletion in myeloid cells, we crossed the *Septin7*-floxed mice with the *Lyz2*-Cre deleter line (Clausen et al., 1999) to generate a myeloid-specific *Septin7*-KO. *Septin7*$^{flox/flox}$*:Lyz2-Cre* animals developed normally without any perceived abnormalities. Efficient Cre-mediated recombination was detectable in the bone marrow (BM) of the heterozygous and homozygous floxed mice in the presence of *Lyz2*-Cre as indicated by the genotyping data (**Figure 1A**). Residual amounts of the floxed allele were detected, as expected from the presence of additional non-

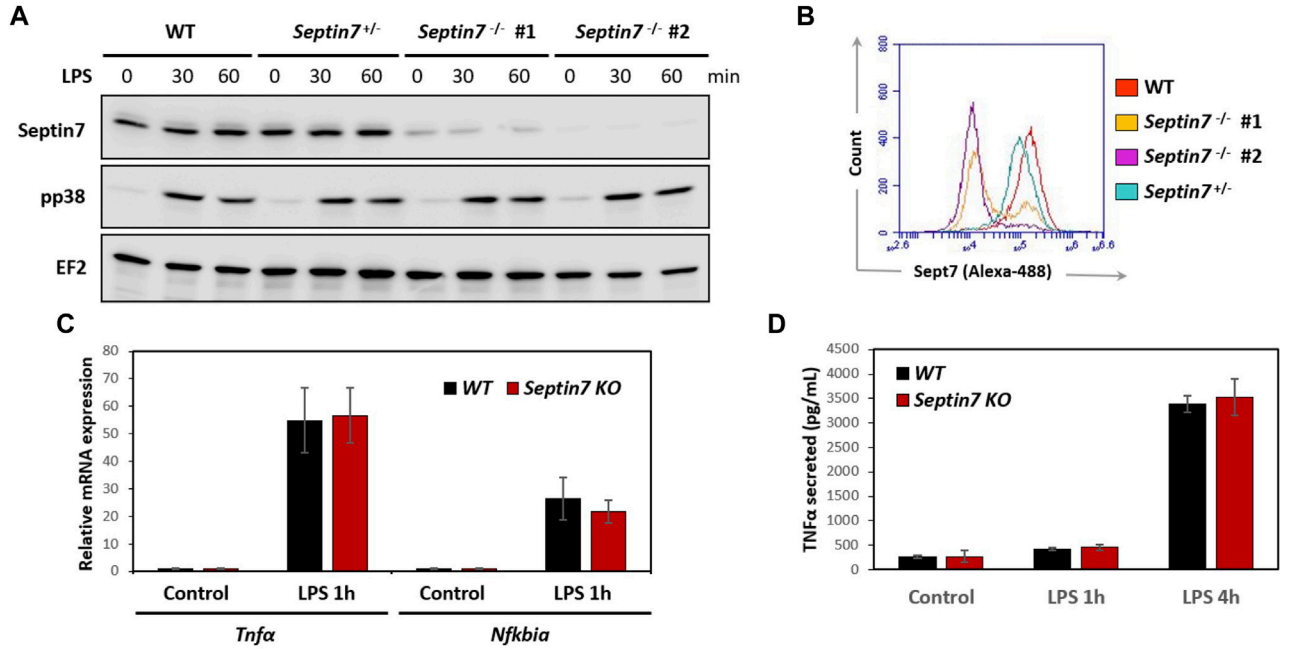

FIGURE 2 | Septin7 KO BMDMs respond normally to LPS stimulation. **(A,B)** Immunoblot analyses of LPS-stimulated BMDM lysates **(A)** and Flow-cytometry **(B)** show efficient depletion of Septin7 in two homozygous *Septin7*-KO cells. However, p38 activation is indistinguishable between the KO and control cells **(A)**. EF2 is shown as loading control. **(C)** LPS-induced expression of *Tnfα* and *Nfkbiα* are not significantly affected upon *Septin7*-deletion in BMDMs (n = 4 independent treated culture wells, p-values > 0.3 for 1 h LPS-stimulated samples). **(D)** LPS-induced secretion of Tnfα quantified by ELISA reveal no significant difference between *Septin7*-KO and *Septin7*-Wt (WT) BMDMs (n = 4 independent treated culture wells, p-values > 0.3 for 1 and 4 h LPS-treated).

myeloid cells in the BM. Flow-cytometric analysis for the myeloid lineage cells revealed no significant difference between the wild-type and *Septin7*-KO mice BM, indicating septin-independent development of myeloid lineage cells (**Figure 1B**).

In regard to the cell-type specificity of septin-dependent cytokinesis, a recent hypothesis is the requirement of septins specifically for the proliferation of adherent cell-types (Sellin et al., 2011). To verify this hypothesis, we generated adherent BM-derived macrophages (BMDMs) from the *Septin7*-KO mice. As indicated by the genotyping data, the BMDMs displayed almost complete deletion of the *Septin7*-floxed allele (**Figure 1A**). However, microscopic analyses of Septin7 expression revealed significant heterogeneity in the cells even after 10 days of BMDM differentiation showing a mosaic of Septin7-depleted and Septin7 positive cells (**Figure 1C**). Interestingly, cells without Septin7 expression were almost exclusively double-nucleated, establishing a role for septins in BMDM cytokinesis.

Septin7-Deleted Macrophages are Functional, Despite Defective Cytokinesis

Considering the cytokinetic defect observed in Septin7-deficient macrophages, we further investigated whether they are impaired in their functionality. Expression of myeloid markers including CD11b and F4/80 was comparable between control and Septin7$^{-/-}$ BMDMs indicating normal differentiation *in vitro* (**Supplementary Figure S2**). Immunoblotting revealed strong depletion of Septin7 protein levels in the *Septin7$^{flox/flox}$:Lyz2-Cre* BMDMs, which was consistent with the flow-cytometric analysis (**Figures 2A,B**). To understand the effects of Septin depletion of macrophage functions, we monitored the lipopolysaccharide (LPS) induced activation of BMDMs by analyzing downstream p38 MAPK phosphorylation. As expected, strong p38 activation was observed upon LPS-stimulation, but there were no differences between Septin7-depleted and wild-type cells (**Figure 2A**). Real-time qPCR analyses for the expression of mRNA of *Tnfα* (TNFα) and *Nfκbia* (IκBα), two downstream targets of LPS, also showed no significant changes upon *Septin7* deletion (**Figure 2C**). Moreover, the LPS-induced secretion of TNFα was also normal in Septin7-deficient BMDMs (**Figure 2D**). Since the alterations in septin cytoskeleton may have consequences in vesicular transport and processes involving the cell cortex, we also performed macrophage phagocytosis assays using labelled *E. coli* particles. Since Lyz2-Cre mediated deletion of Septin7 usually results in a mixed population of *Septin7*-positive and negative cells in the early stages, we used this model to monitor the role of septins in phagocytosis. As indicated by the images, the BMDMs efficiently phagocytosed the bacterial particles independent of Septin expression and multinucleation (**Figure 3A**). Semi-quantitative analysis using immunofluorescence microcopy showed no differences in phagocytosed bacterial particles between WT and Septin 7 KO BMDMs (**Figure 3B**). A control analysis of untreated cells revealed that majority of BMDMs from Septin7 KO were indeed depleted of Septin7 protein (**Figure 3C**).

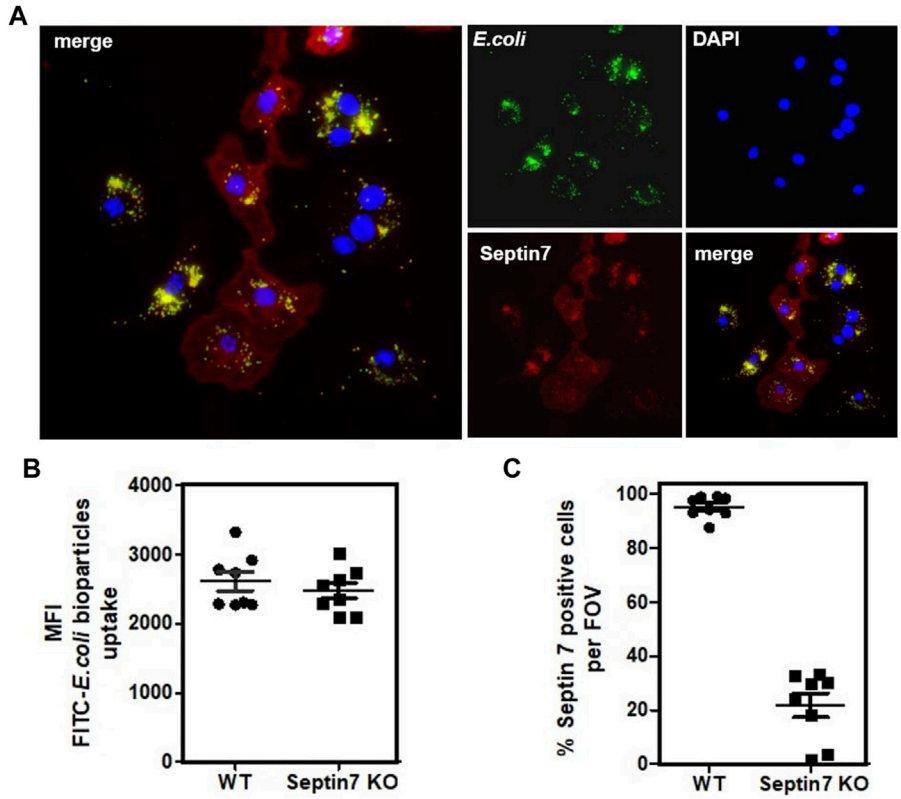

FIGURE 3 | Septin7 KO BMDMs phagocytose bacterial particles. **(A)** BMDMs generated from *Septin7*$^{flox/flox}$*:Lyz2-Cre* mice BM were subjected to phagocytosis assay with fluorescent labeled *E. coli* particles (Green) and were fixed and stained with Septin7 antibodies (Red) and DAPI (blue). Both Septin7-positive mono-nucleated cells and Septin7-deficient predominantly multinucleated BMDMs efficiently phagocytose the bacterial particles as indicated by their intracellular accumulation. **(B)** Semi-quantitative analysis of phagocytosed bacterial particles of WT and Septin 7 KO BMDMs—mean of green fluorescence intensity (MFI) of phagocytosed green-fluorescent particles is shown per cells per field of view. **(C)** Percentage of Septin7-positive cells quantified as detailed in methods section and shown as percentage per field of view (FOV).

In summary, while Septin7-depleted macrophages displayed cytokinetic failure leading to bi-nucleated and multinucleated cells, they were normal for the functions tested. It is interesting to note that fully differentiated and activated macrophage populations usually harbor significant amount of multinucleated cells (Pereira et al., 2018).

Septin7 in Tumor Cell Proliferation *In Vivo*

Lysozyme M (*Lyz2*)-Cre is often used as the deleter line of choice for gene deletion in myeloid lineages including monocytes, macrophages and granulocytes. However, the *Lyz2* locus is active not only in myeloid lineages but also in the lung alveolar type-2 (AT2) cells. Hence, the *Cre*-Lyz2 knock-in strain could nicely be used to analyze the effect of gene deletion in AT2 cells. AT2 cells, among other things are involved in the secretion of surfactants that prevents alveolar collapse. Analysis of the *Septin7*$^{flox/flox}$*:Lyz2-Cre* mice revealed no defects in lung development (data not shown). To analyze the role of Septin7 in tumor development, we decided to establish a Septin7-dependent *in vivo* mouse model of lung adenocarcinoma formation, the major form of lung cancer associated with activating mutations in the *Kras* oncogene. We used Cre-Lyz2-mediated recombination to activate the conditional knock-in *Kras-LSL-G12D* allele (Jackson et al., 2001) in AT2 cells (Desai et al., 2014). In this model, AT2 proliferation is selectively induced by knock-in of oncogenic *Kras-G12D in vivo*, efficiently generating multifocal, clonal adenomas with replacement of almost the entire alveolar region and death of the animals within 1 month after birth. We genetically combined the knock-in of oncogenic *Kras* with the deletion of *Septin7* in AT2 cells *in vivo* by crossing mice to introduce the *Sept7*^{flox}-allele in addition to *Kras-LSL-G12D* and *Lyz2-Cre* alleles (**Figure 4A**). We then compared adenocarcinoma formation between *Kras-LSL-G12D:Lyz2-Cre:Sept7*$^{flox/flox}$ and *Kras*-LSL-G12D:Lyz2-Cre:*Sept7*$^{flox/wt}$. All animals analyzed were heterozygous for the *Kras-LSL-G12D* allele and littermates were used to avoid other variables. We detected a significant difference in survival time between the homozygous *Septin7*-KO and the control *Septin7*$^{+/-}$ mice. While control mice die between 3–5 weeks, the Septin7-deficient animals survived 11 weeks or even longer (**Figure 4B**). In parallel, lungs from both groups of animals were investigated using histopathology. The occurrence of bronchiolo-alveolar hyperplasia as well as adenomas was assessed semi-

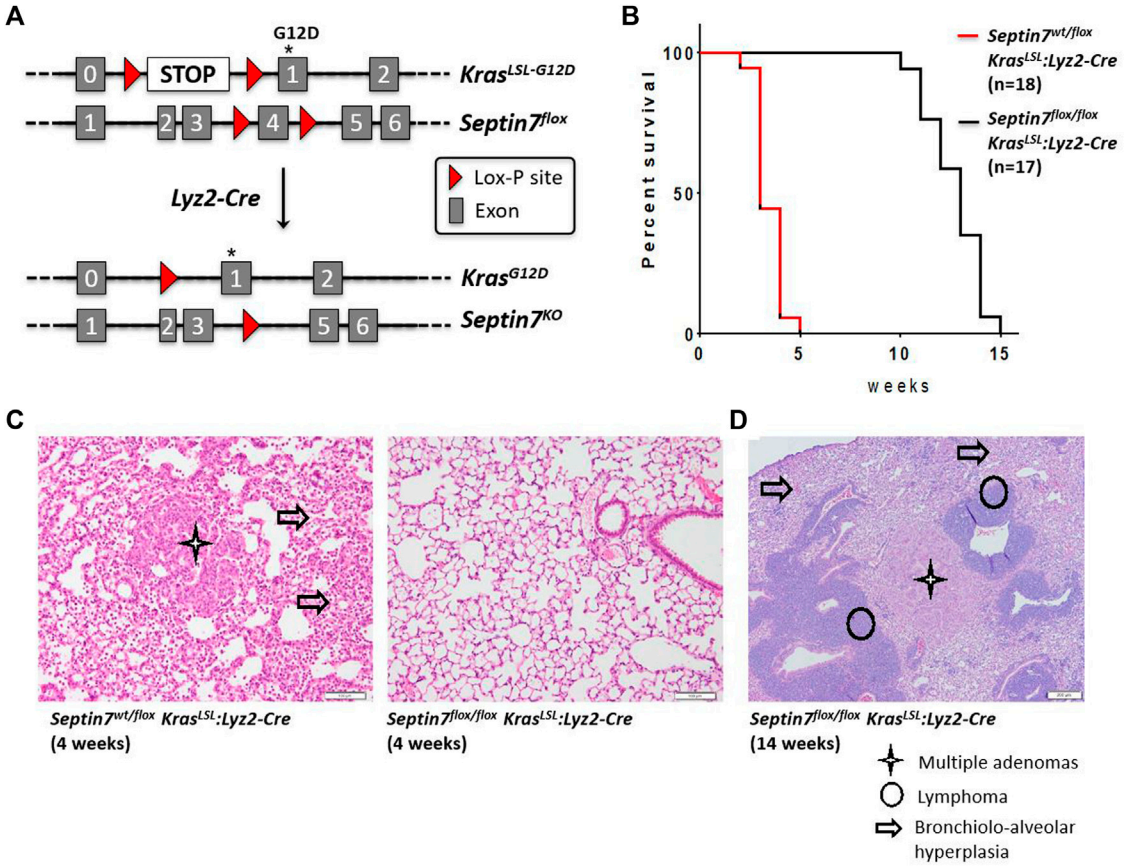

FIGURE 4 | Septin7 is essential for Ras-induced lung tumor formation and lethality *in vivo*. **(A)** The gene targeting strategy employed for the generation of a Kras-G12D-induced lung tumor model to monitor the effects of Septin7-deficiency using the Lyz2-Cre deleter line. **(B)** Kaplan-Meier survival plots showing the essential role of Septin7 in lung cancer induced lethality in the Kras-induced tumor model. The survival curves are significantly different with a $\chi^2 = 36.29$ resulting in a p-value < 0.0001. **(C)** Representative images of hematoxylin and eosin (H and E) stained lung sections from the mice of indicated genotype at 4 weeks after birth. Cancer associated tissue alterations visible are indicated (scale bar = 100 μm). **(D)** Lungs from Septin7-KO mice show late-onset adenomas and lymphomas as revealed in the standard histology H and E staining. Arrow = bronchiolo-alveolar hyperplasia, star = multiple adenomas and circle = T cells lymphoma (scale bar = 200 μm).

quantitatively by light microscopy. Analyses of control mice sacrificed at the age of 4 weeks displayed a bronchiolo-alveolar hyperplasia with multiple adenomas, whereas lungs of Septin7-deficient animals of the same age were unremarkable or showed only a weaker multifocal brochiolo-alveolar hyperplasia (**Figures 4C,D** and **Supplementary Figure S4**). This indicates an essential role of Septin7 in oncogenic Kras-induced lung tumorigenesis.

DISCUSSION

Our findings from the myeloid-specific *Septin7*-KO model indicate an essential role of *Septin7* in macrophage cytokinesis but not in macrophage functions. Furthermore, septin7 seems to be essential for Kras-driven tumor development in the lung making it a potential target for anti-tumor interventions. Even though it was a known fact that septins are required for the proliferation of several tumor-derived epithelial cell lines and Septin7-deficient fibroblasts undergo obligate multinucleation *in vitro*, this is the first report establishing a clear role for septins in tumorigenesis *in vivo*.

The *Lyz2-Cre*-mediated *Septin7* deletion was very efficient in the BM, but did not lead to perceivable defects in the development of monocytes and granulocytes (**Figures 1A,B**). However, *in vitro* differentiated BMDMs displayed clear double nucleation upon Septin7-depletion. Interestingly, this supports the hypothesis that adherent hematopoietic lineages and not the suspension cells require septins for completion of cytokinesis. It should be noted that the complete depletion of Septin7 in majority of the BMDMs was only achieved upon prolonged differentiation of BM cells with MCSF. While 1 week of MCSF treatment is used in standard BMDM generation protocols, much longer periods were required to achieve Septin7 deletion in majority of the population (**Supplementary Figure S5**). Despite the defects in cytokinesis, the *Septin7*-KO macrophages were not compromised in their functions including activation, gene expression, cytokine secretion and phagocytosis. Previous studies using knockdown approaches targeting Septins 2 and 11 in macrophage cell lines have shown a role for septins in phagosome assembly (Huang

et al., 2008). Moreover, they observed a septin collar-like structure at the base of phagosomes during FcγR-mediated phagocytosis in macrophages and neutrophils. This discrepancy with our observations could be due to the differences in the experimental settings as the previous study specifically focused on FcγR-mediated phagocytosis of IgG-coated latex beads and we followed phagocytosis of bacteria by primary macrophages. A role for septins in bacterial and yeast infection or invasion has been established predominantly in non-phagocytic epithelial cells and the *Septin7*$^{flox/flox}$*:Lyz2-Cre* mouse model will be an invaluable tool in further studies investigating the role of septins in infection biology using septin-depleted macrophages and neutrophils.

The protection of the Septin7-depleted mice from rapid-onset lung tumors and resultant lethality was clearly evident. However, *Septin7*-KO mice also eventually succumbed to the oncogene-induced lethality. We could detect adenomas similar to that of the 4 weeks-old control mice in *Septin7*$^{flox/flox}$ animals sacrificed at the age of 14 weeks. These "late" (slow growing) adenomas could result from cells adapted to *Septin7* ablation or could also arise from a minor cell population with Cre-driven recombined *Kras* but without Cre-driven *Septin7* deletion. Interestingly, adenomas in the lungs of *Septin7*$^{flox/flox}$ animals were accompanied with morphological distinct tumor foci (myeloma or lymphoma), which were not detected in the control animals. A possible explanation is that the growth of adenoma was inhibited in the absence of Septin7 and other cell types with activated *Kras* form tumors with a slower kinetics. It is to be noted that *Lyz2-Cre* expression is not restricted to myeloid cells and AT2 cells (Ye et al., 2003). Another possibility is that the appearance of this novel (non-adenoma) tumor cells is caused by *Kras* activation combined with genetic instability caused by the loss of Septin7. Interestingly, a recent multi-omics study correlated low SEPTIN7 expression levels and an intronic single-nucleotide polymorphism in the *SEPTIN7* gene with higher survival rates for long-term former smoking lung cancer patients (Shen et al., 2021). While the presence of Septin7 seems indispensable for oncogenic Ras-induced lung-adenocarcinoma formation, further investigations in the *Septin7* conditional knockout model is necessary to completely understand the role of septins in tumorigenesis.

DATA AVAILABILITY STATEMENT

The raw data supporting the conclusions of this article will be made available by the authors, without undue reservation.

ETHICS STATEMENT

The animal study was reviewed and approved by Animal handling was performed according to strict governmental and international guidelines and ethical oversight by the local government for the administrative region of Lower Saxony (permit 17/2593), Germany, at Niedersächsisches Landesamt für Verbraucherschutz und Lebensmittelsicherheit.

AUTHOR CONTRIBUTIONS

Conceived and designed the experiments: MM, AK, and MG. Performed the experiments: MM, TY, NR, AS, FH, IO, IS, and SD. Analyzed the data: MM, AK, NR, SD, AS, FH, WB, IO, IS, and RF. Writing of the manuscript: MM, AK, and MG. Provided conceptual insight: AK and MG. All read and approved the submitted version of the manuscript.

ACKNOWLEDGMENTS

We thank Anuhar Chaturvedi for help with the flow cytometry analyses. MM thanks the Science and Engineering Research Board (DST-SERB) for financial support (#SRG/2020/001396). SD thanks Department of Biotechnology, India for Ramalingaswami Re-entry Fellowship. We thank Dr. Michael Saborowski (MHH) and Dr. Kai Wollert (MHH) for sharing the *Ras-LSL-G12D* and Lyz2-Cre mice line, respectively.

SUPPLEMENTARY MATERIAL

The Supplementary Material for this article can be found online at: https://www.frontiersin.org/articles/10.3389/fcell.2021.795798/full#supplementary-material

Supplementary Figure S1 | The gating scheme used for immunophenotyping of the bone-marrow. The simple gating scheme involving forward, and side-scatter based gating, followed by dead-cell exclusion by selecting propidium-iodide negative cells is shown with a representative example bone-marrow staining with the indicated antibody cocktails.

Supplementary Figure S2 | Septin7-KO BMDMs have normal surface marker expression. Septin7-KO and wild-type BMDMs were surface stained for CD11b or F4/80 and were analysed by BD Accuri-C6 flow-cytometer.

Supplementary Figure S3 | Isotype controls show specific staining of Septin7 in BMDMs. Additional controls for the flow-cytometry data presented in **Figure 2B**. An indirect flow-cytometry protocol is used with anti-Septin7 antibodies and anti-Rabbit Alexa Fluor-488 labelled secondary antibodies are 13 combined to detect septin. Here, staining with the secondary antibody alone is included which shows immunofluorescence intensities similar to that seen in the Septin7-KO cells.

Supplementary Figure S4 | Higher magnification images showing the abnormalities observed in old Septin7 KO mice upon Ras-induced tumorigenesis. Representative higher magnification images (scale bar = 100 μm) of H&E stained sections from Septin7-KO mice (14 weeks old, shown in **Figure 4D**).

Supplementary Figure S5 | Effect of longer BMDM culture on Septin7 depletion in floxed cells. BM cells from WT and Septin7-floxed mice were treated with MCSF for the indicated time-periods to generate BMDMs. The adherent cells were fixed and stained for Septin7, alpha-tubulin and nuclei (DAPI). The data clearly indicate significantly higher number of Septin7-depleted cells in 2 weeks differentiated compared to 1 week differentiated KO cells.

REFERENCES

Bridges, A. A., and Gladfelter, A. S. (2015). Septin Form and Function at the Cell Cortex. *J. Biol. Chem.* 290, 17173–17180. doi:10.1074/jbc.r114.634444

Cancer Genome Atlas Research Network (2014). Comprehensive Molecular Profiling of Lung Adenocarcinoma. *Nature* 511, 543–550. doi:10.1038/nature13385

Chen, T. Y., Lin, T. C., Kuo, P. L., Chen, Z. R., Cheng, H. l., Chao, Y. Y., et al. (2021). Septin 7 Is a Centrosomal Protein that Ensures S Phase Entry and Microtubule Nucleation by Maintaining the Abundance of P150 Glued. *J. Cel Physiol* 236, 2706–2724. doi:10.1002/jcp.30037

Clausen, B. E., Burkhardt, C., Reith, W., Renkawitz, R., and Förster, I. (1999). Conditional Gene Targeting in Macrophages and Granulocytes Using LysMcre Mice. *Transgenic Res.* 8, 265–277. doi:10.1023/a:1008942828960

Desai, T. J., Brownfield, D. G., and Krasnow, M. A. (2014). Alveolar Progenitor and Stem Cells in Lung Development, Renewal and Cancer. *Nature* 507, 190–194. doi:10.1038/nature12930

Estey, M. P., Di Ciano-Oliveira, C., Froese, C. D., Bejide, M. T., and Trimble, W. S. (2010). Distinct Roles of Septins in Cytokinesis: SEPT9 Mediates Midbody Abscission. *J. Cel Biol* 191, 741–749. doi:10.1083/jcb.201006031

Fededa, J. P., and Gerlich, D. W. (2012). Molecular Control of Animal Cell Cytokinesis. *Nat. Cel Biol* 14, 440–447. doi:10.1038/ncb2482

Green, R. A., Paluch, E., and Oegema, K. (2012). Cytokinesis in Animal Cells. *Annu. Rev. Cel Dev. Biol.* 28, 29–58. doi:10.1146/annurev-cellbio-101011-155718

Hartwell, L. H., Culotti, J., and Reid, B. (1970). Genetic Control of the Cell-Division Cycle in Yeast, I. Detection of Mutants. *Proc. Natl. Acad. Sci.* 66, 352–359. doi:10.1073/pnas.66.2.352

Huang, Y.-W., Yan, M., Collins, R. F., Diciccio, J. E., Grinstein, S., and Trimble, W. S. (2008). Mammalian Septins Are Required for Phagosome Formation. *MBoC* 19, 1717–1726. doi:10.1091/mbc.e07-07-0641

Jackson, E. L., Willis, N., Mercer, K., Bronson, R. T., Crowley, D., Montoya, R., et al. (2001). Analysis of Lung Tumor Initiation and Progression Using Conditional Expression of Oncogenic K-Ras. *Genes Dev.* 15, 3243–3248. doi:10.1101/gad.943001

Karasmanis, E. P., Hwang, D., Nakos, K., Bowen, J. R., Angelis, D., and Spiliotis, E. T. (2019). A Septin Double Ring Controls the Spatiotemporal Organization of the ESCRT Machinery in Cytokinetic Abscission. *Curr. Biol.* 29, 2174–2182. e2177. doi:10.1016/j.cub.2019.05.050

Kinoshita, M., Kumar, S., Mizoguchi, A., Ide, C., Kinoshita, A., Haraguchi, T., et al. (1997). Nedd5, a Mammalian Septin, Is a Novel Cytoskeletal Component Interacting with Actin-Based Structures. *Genes Dev.* 11, 1535–1547. doi:10.1101/gad.11.12.1535

Menon, M. B., and Gaestel, M. (2015). Sep(t)arate or Not - How Some Cells Take Septin-independent Routes through Cytokinesis. *J. Cel Sci* 128, 1877–1886. doi:10.1242/jcs.164830

Menon, M. B., Sawada, A., Chaturvedi, A., Mishra, P., Schuster-Gossler, K., Galla, M., et al. (2014). Genetic Deletion of SEPT7 Reveals a Cell Type-specific Role of Septins in Microtubule Destabilization for the Completion of Cytokinesis. *Plos Genet.* 10, e1004558. doi:10.1371/journal.pgen.1004558

Menon, M. B., Schwermann, J., Singh, A. K., Franz-Wachtel, M., Pabst, O., Seidler, U., et al. (2010). p38 MAP Kinase and MAPKAP Kinases MK2/3 Cooperatively Phosphorylate Epithelial Keratins*. *J. Biol. Chem.* 285, 33242–33251. doi:10.1074/jbc.m110.132357

Mingay, M., Chaturvedi, A., Bilenky, M., Cao, Q., Jackson, L., Hui, T., et al. (2018). Vitamin C-Induced Epigenomic Remodelling in IDH1 Mutant Acute Myeloid Leukaemia. *Leukemia* 32, 11–20. doi:10.1038/leu.2017.171

Mostowy, S., Bonazzi, M., Hamon, M. A., Tham, T. N., Mallet, A., Lelek, M., et al. (2010). Entrapment of Intracytosolic Bacteria by Septin Cage-like Structures. *Cell Host & Microbe* 8, 433–444. doi:10.1016/j.chom.2010.10.009

Mostowy, S., Boucontet, L., Mazon Moya, M. J., Sirianni, A., Boudinot, P., Hollinshead, M., et al. (2013). The Zebrafish as a New Model for the *In Vivo* Study of Shigella Flexneri Interaction with Phagocytes and Bacterial Autophagy. *Plos Pathog.* 9, e1003588. doi:10.1371/journal.ppat.1003588

Mostowy, S., and Cossart, P. (2012). Septins: the Fourth Component of the Cytoskeleton. *Nat. Rev. Mol. Cel Biol* 13, 183–194. doi:10.1038/nrm3284

Mujal, A. M., Gilden, J. K., Gérard, A., Kinoshita, M., and Krummel, M. F. (2016). A Septin Requirement Differentiates Autonomous and Contact-Facilitated T Cell Proliferation. *Nat. Immunol.* 17, 315–322. doi:10.1038/ni.3330

Pereira, M., Petretto, E., Gordon, S., Bassett, J. H. D., Williams, G. R., and Behmoaras, J. (2018). Common Signalling Pathways in Macrophage and Osteoclast Multinucleation. *J. Cel Sci* 131, jcs216267. doi:10.1242/jcs.216267

Robertin, S., and Mostowy, S. (2020). The History of Septin Biology and Bacterial Infection. *Cell Microbiol* 22, e13173. doi:10.1111/cmi.13173

Sellin, M. E., Sandblad, L., Stenmark, S., and Gullberg, M. (2011). Deciphering the Rules Governing Assembly Order of Mammalian Septin Complexes. *MBoC* 22, 3152–3164. doi:10.1091/mbc.e11-03-0253

Shen, S., Wei, Y., Li, Y., Duan, W., Dong, X., Lin, L., et al. (2021). A Multi-Omics Study Links TNS3 and SEPT7 to Long-Term Former Smoking NSCLC Survival. *Npj Precis. Onc.* 5, 39. doi:10.1038/s41698-021-00182-3

Thakkar, A., Desai, P., Chenreddy, S., Modi, J., Thio, A., Khamas, W., et al. (2018). Novel Nano-Drug Combination Therapeutic Regimen Demonstrates Significant Efficacy in the Transgenic Mouse Model of Pancreatic Ductal Adenocarcinoma. *Am. J. Cancer Res.* 8, 2005–2019.

Tiedje, C., Ronkina, N., Tehrani, M., Dhamija, S., Laass, K., Holtmann, H., et al. (2012). The p38/MK2-Driven Exchange between Tristetraprolin and HuR Regulates AU-Rich Element-dependent Translation. *Plos Genet.* 8, e1002977. doi:10.1371/journal.pgen.1002977

Tooley, A. J., Gilden, J., Jacobelli, J., Beemiller, P., Trimble, W. S., Kinoshita, M., et al. (2009). Amoeboid T Lymphocytes Require the Septin Cytoskeleton for Cortical Integrity and Persistent Motility. *Nat. Cel Biol* 11, 17–26. doi:10.1038/ncb1808

Van Ngo, H., and Mostowy, S. (2019). Role of Septins in Microbial Infection. *J. Cel Sci* 132, jcs226266. doi:10.1242/jcs.226266

Ye, M., Iwasaki, H., Laiosa, C. V., Stadtfeld, M., Xie, H., Heck, S., et al. (2003). Hematopoietic Stem Cells Expressing the Myeloid Lysozyme Gene Retain Long-Term, Multilineage Repopulation Potential. *Immunity* 19, 689–699. doi:10.1016/s1074-7613(03)00299-1

Conflict of Interest: The authors declare that the research was conducted in the absence of any commercial or financial relationships that could be construed as a potential conflict of interest.

frontiers in Cell and Developmental Biology

REVIEW
published: 17 January 2022
doi: 10.3389/fcell.2021.824850

Septins From Protists to People

*Brent Shuman and Michelle Momany**

Fungal Biology Group and Plant Biology Department, University of Georgia, Athens, GA, United States

Septin GTPases form nonpolar heteropolymers that play important roles in cytokinesis and other cellular processes. The ability to form heteropolymers appears to be critical to many septin functions and to have been a major driver of the high conservation of many septin domains. Septins fall into five orthologous groups. Members of Groups 1–4 interact with each other to form heterooligomers and are known as the "core septins." Representative core septins are present in all fungi and animals so far examined and show positional orthology with monomer location in the heteropolymer conserved within groups. In contrast, members of Group 5 are not part of canonical heteropolymers and appear to interact only transiently, if at all, with core septins. Group 5 septins have a spotty distribution, having been identified in specific fungi, ciliates, chlorophyte algae, and brown algae. In this review we compare the septins from nine well-studied model organisms that span the tree of life (*Homo sapiens*, *Drosophila melanogaster*, *Schistosoma mansoni*, *Caenorhabditis elegans*, *Saccharomyces cerevisiae*, *Aspergillus nidulans*, *Magnaporthe oryzae*, *Tetrahymena thermophila*, and *Chlamydomonas reinhardtii*). We focus on classification, evolutionary relationships, conserved motifs, interfaces between monomers, and positional orthology within heteropolymers. Understanding the relationships of septins across kingdoms can give new insight into their functions.

Keywords: interface, evolution, heteropolymer, septin, domains

OPEN ACCESS

Edited by:
Matthias Gaestel,
Hannover Medical School, Germany

Reviewed by:
Richard Garratt,
University of São Paulo, Brazil
Michael McMurray,
University of Colorado Anschutz Medical Campus, United States

****Correspondence:***
Michelle Momany
mmomany@uga.edu

Specialty section:
This article was submitted to Signaling, a section of the journal Frontiers in Cell and Developmental Biology

Received: *29 November 2021*
Accepted: *16 December 2021*
Published: *17 January 2022*

Citation:
Shuman B and Momany M (2022) Septins From Protists to People. Front. Cell Dev. Biol. 9:824850. doi: 10.3389/fcell.2021.824850

INTRODUCTION

Septin GTPases form nonpolar heteropolymers and are a component of the cytoskeleton (Mostowy and Cossart 2012). The first septins were identified in *Saccharomyces cerevisiae* in the classic cell division cycle (*cdc*) mutant screen. The four prototypical septin mutants, *cdc3*, *cdc10*, *cdc11*, and *cdc12*, made elongated buds and did not complete cytokinesis at restrictive temperature (Hartwell et al., 1970; Hartwell et al., 1973). In the 50 years since their discovery, septins have been identified in organisms across kingdoms and much work has been done to understand septin evolution, structure, assembly, and function (Angelis and Spiliotis 2016; Momany and Talbot 2017; Spiliotis and McMurray 2020; Spiliotis and Nakos 2021; Woods and Gladfelter 2021). The purpose of this review is to allow researchers to understand the relationships of septins across kingdoms so that they can use insights from other systems to inform their own work. We will do this by comparing septins from nine model systems (**Figure 1**), focusing on classifications based on evolutionary relationships and conserved motifs, including interfaces. We chose these nine organisms because they span the tree of life and are well-studied, but we urge researchers to remember that there is great diversity in septin structure and function and we are covering only a small, though hopefully representative, slice. Much of the knowledge presented in this review builds on many structural and functional studies conducted in many labs over many years. We apologize to our colleagues whose work might be missed.

Momany Group[1]	Kinoshita Group[2]	Hs[3]	Dm	Sm	Ce	Sc	An	Mo	Tt	Cr
1a	SEPT3	SEPT3 SEPT9 SEPT12				Cdc10	AspD	Sep4		
1b	SEPT6	SEPT6 SEPT8 SEPT10 SEPT11 SEPT14	Sep2 Sep5	SEPT10	UNC61					
2a						Cdc3	AspB	Sep3		
2b	SEPT2	SEPT1 SEPT2 SEPT4 SEPT5	Sep1 Sep4	SEPT5						
	SEPT7	SEPT7	Pnut	SEPT7.1 SEPT7.2	UNC59					
3						Cdc11 Shs1 Spr28	AspA	Sep5		
4						Cdc12 Spr3	AspC	Sep6		
5							AspE	Sep7	Sep2 Sep3	Sep1

FIGURE 1 | Groupings of septins across Kingdoms. Septin designations for representative model organisms across kingdoms are shown. Protein sequences were retrieved from UniProt, WormBase, NCBI, or FungiDB.[1]All 161 then-available septin sequences were classified into 5 groups by the Momany lab (Pan et al., 2007).[2]All 12 then-available human septins were classified into 4 homologous groups, members of which were proposed to substitute for each other in a polymer ("Kinoshita rule") by the Kinoshita lab (Kinoshita 2003b).[3]Hs, *Homo sapiens*; SEPT1(*Q8WYJ6*), SEPT2(*Q15019*), SEPT3(*Q9UH03*), SEPT4(*Q6ZU15*), SEPT5(*Q99719*), SEPT6(*Q14141*), SEPT7(*Q16181*), SEPT8(*Q92599*), SEPT9(*Q9UHD8*), SEPT10(*Q9P0V9*), SEPT11(*Q9NVA2*), SEPT12(*Q8IYM1*), SEPT14(*Q6ZU15*); Dm, *Drosophila melanogaster*; Sep1(*P42207*), Sep2(*P54359*), Sep4(*Q0KHR7*), Sep5(*Q7KLG8*), Pnut(*P40797*); Sm, *Schistosoma mansoni*; SEPT5(*KC916723*), SEPT7.1(*KC916724*), SEPT7.2(*KC916725*), SEPT10(*KC916726*); Ce, *Caenorhabditis elegans*; UNC-59 (*CE20165*), UNC-61(*CE47829*); Sc, *Saccharomyces cerevisiae*; Cdc3(*YLR314C*), Cdc10(*YCR002C*), Cdc11(*YJR076C*), Cdc12(*YHR107C*), Shs1(*YDL225W*), Spr3(*YGR059W*), Spr28(*YDR218C*); An, *Aspergillus nidulans*: AspA(*AN4667*), AspB(*AN6688*), AspC(*AN8182*), AspD(*AN1394*), AspE(*AN10595*); Mo, *Magnaporthe oryzae*; Sep3(*MGG_01521*), Sep4(*MGG_06726*), Sep5(*MGG_03087*), Sep6(*MGG_07466*), Sep7(*MGG_02626*); Tt, *Tetrahymena thermophila;* Sep2(*I7M2Q5*), Sep3(*Q240L4*); Cr, *Chlamydomonas reinhardtii*; Sep1(*EDP03113*).

CLASSIFICATION AND EVOLUTION

The first attempt to classify the fungal septins was in 2001 when the Momany lab analyzed 27 septins from eight fungi (Momany et al., 2001). They concluded that most fungal septins could be grouped with one of the four *S. cerevisiae* prototypical, or core, septins, and referred to each class based on the *S. cerevisiae* septin member (Cdc3, Cdc10, Cdc11, or Cdc12). They also noted a few fungal septins did not appear to group with others and suggested these might be part of a fifth class.

The first attempt to classify the mammalian septins was in 2003 when Makoto Kinoshita placed the 12 human septins known at the time into four groups based on sequence similarity (Kinoshita 2003a). He also proposed that group members were interchangeable within heteropolymers, an idea that is often now called the "Kinoshita rule." This rule was very important in shaping septin research because while it was clear that septin monomers interacted with each other to form nonpolar heterohexamers and heterooctamers, the principles that governed their assembly were not yet known. These four Kinoshita septin groups were named after their best-studied members: SEPT2 (group also contains SEPT1, SEPT4, and SEPT5), SEPT3 (also contains SEPT9 and SEPT12), SEPT6 (also contains SEPT8, SEPT10, and SEPT11), and SEPT7 (the only group with a single representative) (**Figure 1**). In 2003 Kinoshita widened his scope with a phylogenetic analysis of 33 septins from two yeasts and three animals (Kinoshita 2003b). He concluded that septins fell into 2-4 groups within these species. He also concluded that there were no orthologs between animal and fungal septins and suggested that this meant lessons learned from septins in one kingdom might not be informative for those in the

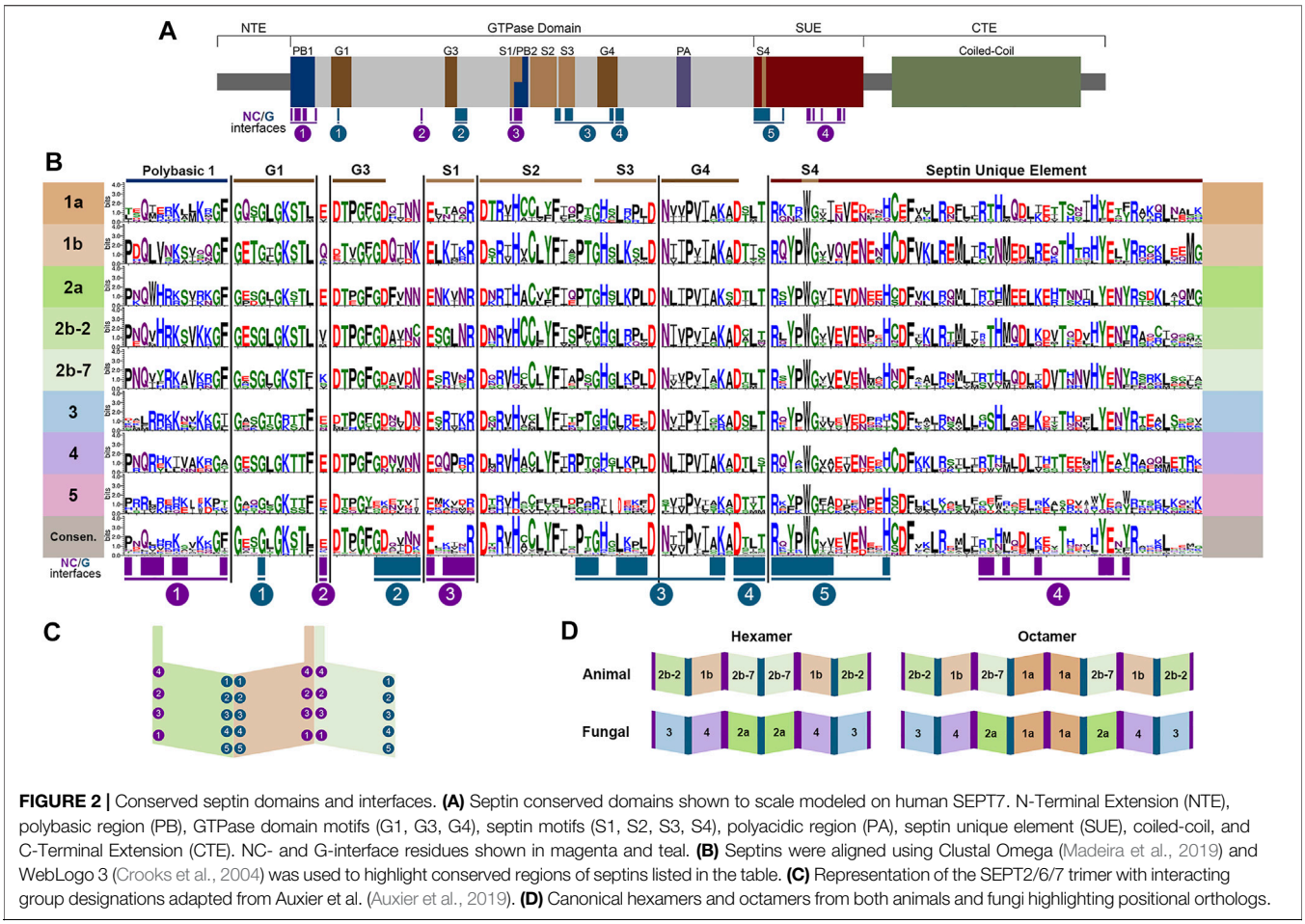

FIGURE 2 | Conserved septin domains and interfaces. **(A)** Septin conserved domains shown to scale modeled on human SEPT7. N-Terminal Extension (NTE), polybasic region (PB), GTPase domain motifs (G1, G3, G4), septin motifs (S1, S2, S3, S4), polyacidic region (PA), septin unique element (SUE), coiled-coil, and C-Terminal Extension (CTE). NC- and G-interface residues shown in magenta and teal. **(B)** Septins were aligned using Clustal Omega (Madeira et al., 2019) and WebLogo 3 (Crooks et al., 2004) was used to highlight conserved regions of septins listed in the table. **(C)** Representation of the SEPT2/6/7 trimer with interacting group designations adapted from Auxier et al. (Auxier et al., 2019). **(D)** Canonical hexamers and octamers from both animals and fungi highlighting positional orthologs.

other kingdom. Contrary to this view and as described below, later analysis of a wider range of genome sequences showed that there was orthology between animal and fungal septins and that some lessons learned could be applied across kingdoms. As more genome sequences became available, other researchers analyzed more septins and found that the Kinoshita classification system worked well for other animals in addition to humans. In work largely focused on mammalian septins, Martinez and Ware (Martinez et al., 2004) renamed the Kinoshita groups "Group I-IV" based on sequence similarity, though that designation doesn't seem to have been used much since. Later the Yu lab analyzed 78 septins from nine metazoan species, found they all fell into the four Kinoshita groups, and continued to use the Kinoshita Group names to describe them (Cao et al., 2007).

In 2007 the Momany lab performed an extensive phylogenetic analysis including all 161 septin sequences that were publicly available at the time (Pan et al., 2007). They found septins in animals, fungi, and microsporidia (which were later reclassified as fungi), but none in plants or protists. These septins were placed into five classes and were named Groups 1–5 (**Figure 1**). Animal septins were found only in Momany Groups 1 and 2, but those groups contained subgroups that were generally consistent with the Kinoshita classification (Momany Group 1a = Kinoshita Group SEPT3, 1b = SEPT6, 2b = SEPT2 and SEPT7). The Momany classification Group 2b contained both Kinoshita Group SEPT2 and Kinoshita Group SEPT7 septins.

In the Momany classification, fungal septins were found in all five groups, with Groups 3–5 being unique to fungi (**Figure 1**). The Group 5 septins were the most different from those in other groups and were only found in filamentous fungi leading the authors to speculate that Group 5 septins either diverged very recently in filamentous fungi or very early with subsequent loss in most species. Interestingly later work showed that the Group 5 septins don't participate in the heteropolymer like the prototypical core septins (Hernandez-Rodriguez et al., 2014).

As more high-quality genomes became publicly available, septin sequences were identified in organisms outside of animals and fungi including protists, ciliates, chlorophyte algae and brown algae (Merchant et al., 2007; Wloga et al., 2008; Nishihama et al., 2011). In 2011 the Pringle lab proposed that Group 5 septins were ancestral to animals and fungi based on their identification in Alveolata, Heterokonta, and Planta and additional phylogenetic research in fungal septins supports that proposition (Nishihama et al., 2011; Auxier et al., 2019). It is currently unclear if Group 5 septins are a single group or if they might contain multiple groups, a sort of "none of the above" category relative to the core septins in Groups 1–4. An analysis of septins including those from green algae, brown algae, ciliates, and diatoms published in 2013 by the Kawano lab (Yamazaki et al., 2013) suggests that Group 5 fungal septins are a distinct subgroup, separate from septins in green algae and ciliates.

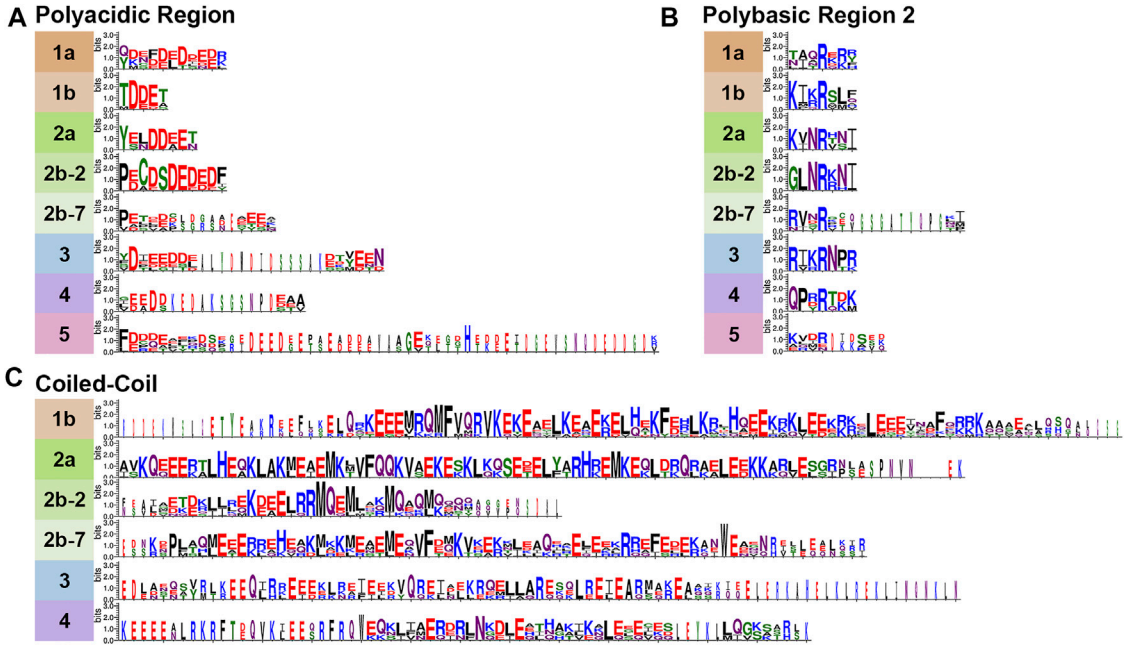

FIGURE 3 | Variable Septin domains. Septins were aligned using Clustal Omega (Madeira et al., 2019) and WebLogo 3 (Crooks et al., 2004) was used to view variable septin domains. **(A)** The polyacidic, **(B)** polybasic 2, and **(C)** coiled-coil regions vary between groups in size and residues.

HETEROPOLYMERS

With the publication of the first septin crystal structure, it became clear that core septin monomers form heteropolymers by interacting with each other via two distinct interface regions, called the G-interface and the NC-interface (**Figures 2C,D**) (Sirajuddin et al., 2007). Several highly conserved regions first noted in Pan et al. (Pan et al., 2007) were later shown to participate in monomer contacts across interfaces that defined four interacting groups at the NC-interface and five at the G-interface (Auxier et al., 2019; Castro et al., 2020) (**Figure 2**).

It should be noted that there are far more protein structures available for human septins than for others. Structures of septins from other species would certainly help to clarify many of the outstanding questions in the field. Still, based on known structures and other biochemical and genetic analyses it is clear that canonical octamer and hexamer heteropolymers are assembled following the same general plan; that is to say evolutionarily-related septins occupy the same positions within heteropolymers and bind using the same interfaces (McMurray and Thorner 2019; Mendonca et al., 2019; Soroor et al., 2021). This allows for the comparison of septins across evolutionary groups because they occupy equivalent positions within heteropolymers acting as "positional orthologs," though it should be noted that positional orthology does not necessarily mean that all activities are equivalent. Since SEPT2 and SEPT7 are within the same subgroup in the Momany classification, but are at different positions within polymers, we show them here as Groups 2b-2 (SEPT2) and 2b-7 (SEPT7). Octamer heteropolymers are formed with a central Group 1a septin dimer, flanked by Group 2 septins (2b-7 in animals or 2a in fungi), flanked by a Group 1b septin in animals or Group 4 septin in fungi, flanked by Group 2b-2 in animals or three in fungi (**Figure 2D**). The canonical hexamers are identical, except they lack the central Group 1a septin dimer.

Interestingly, *Caenorhaabditis elegans* has only two septins, UNC61 and UNC59. In all classifications, UNC61 was placed with the SEPT6/Group 1b septins. The placement of UNC59 has been less consistent. In the Momany lab analysis UNC59 was in a small Group 2b subclade with two septins from *Caenorhabditis briggsae*. This clade was an outlier, though it was closer to the subclade containing human SEPT2 than to that containing human SEPT7 (Pan et al., 2007). In the Kinoshita and Yu analyses (Kinoshita 2003a; Cao et al., 2007) UNC59 was again something of an outlier but fell into the same clade as human SEPT7.

In other model organisms examined here the Group 2b-7 septin is positioned in the interior of the heterohexamer or heterooctamer (**Figure 2D**). In contrast, UNC-59 appears to be the exposed subunit of the heterotetramer (John et al., 2007). Despite its lack of positional orthology, we show UNC59 as a member of Group 2b-7 in **Figures 1–4** because UNC59 was first identified by its homology to the *Drosophila melanogaster* SEPT7 ortholog PNUT (Nguyen et al., 2000). It will be very interesting to see which features of this unusual septin allow it to function as a heterotetramer rather than the more common heterohexamer or heterooctamer.

MOTIFS

Not surprisingly based on their evolutionary origin from a common ancestor, septins across species share several well-conserved motifs (**Figures 2–4**) including those shown in **Figure 2A**: the polybasic regions (PB1 and PB2), GTPase motifs (G1, G3, G4), septin conserved motifs (S1, S2, S3, S4), polyacidic region (PA), and the septin unique element (SUE) (Zhang et al., 1999; Leipe et al., 2002; Versele et al.,

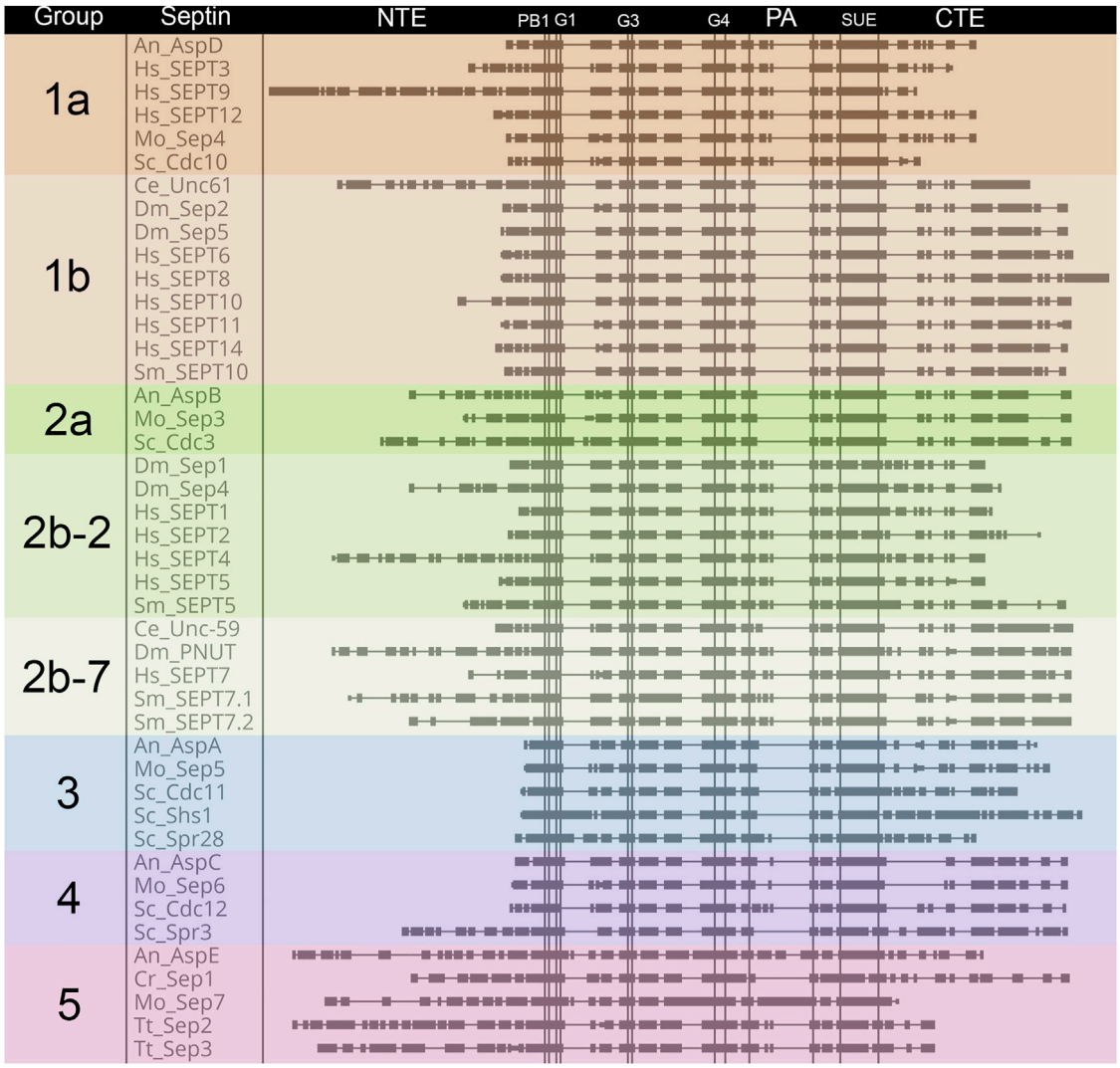

FIGURE 4 | Comparison of septin domain conservation. Large scale view of septins highlighting areas with variable sequence lengths. Septin proteins were aligned using Clustal Omega (Madeira et al., 2019), and placed in alphabetical order within groups. Domains are as shown for **Figure 2** and are indicated above the alignment. Vertical lines denote boundaries of domains. Rectangles indicate blocks of conservation. Thin horizontal lines indicate gaps introduced by Clustal to facilitate alignment.

2004; Pan et al., 2007; Valadares et al., 2017; Omrane et al., 2019). Comparing the nine representative model organisms highlights interesting features of the conserved motifs across the five septin groups (**Figures 1–4**):

N-Terminal Extension

The length of the NTE varies widely (**Figure 4**). Interestingly the extended NTE of SEPT9 has been shown to interact with the acidic tails of microtubules and crosslink F-actin, bridging three mammalian cytoskeletal elements (Bai et al., 2013; Smith et al., 2015). This does not appear to be a feature common to other Group 1a septins (even within humans), and may have evolved independently. Among the nine model organisms we examine here, fungal-specific Groups 3 and 4 have very short NTEs with the exception of the *S. cerevisiae* meiotic septin Spr3. Representative Group 5 septins also have longer NTEs than most, but their function is currently unknown.

Polybasic Regions (PB1 and PB2)

The PBs have been shown to bind phosphoinositides in fungi and humans (Zhang et al., 1999; Casamayor and Snyder 2003; Omrane et al., 2019). PB1 of these model organisms vary in the number of basic residues (between 1 and 7) and their relative positions within the conserved region (**Figure 2B**). However, none of these septins completely lack basic residues within this N-terminal region. Though less common, acidic residues are present in PB1 of some septins. It has been shown that adding an acidic residue can reduce the ability of PB1 to bind phosphatidylinositides (Casamayor and Snyder 2003).

First identified in 2019 in human septins, PB2 has also been shown to bind phosphoinositides, and in SEPT9 both polybasic regions are thought to increase the selectivity of the septin to particular membrane curvatures (Omrane et al., 2019). PB2 overlaps with the previously identified highly conserved Sep1 (S1) by four residues where it takes part in an NC-interface interacting group

(**Figure 2**). Among the model organisms we analyzed, the presence of a PB2 region is highly conserved across groups; however, except for the highly conserved central arginine residue, the sequence of PB2 is conserved within groups, not across them (**Figure 3B**).

GTPase Motifs (G1, G3, G4)

Septins contain three of the five motifs that define P-loop GTPases (Leipe et al., 2002). The G1, G3, and G4 motifs interact with the GTP nucleotide and/or its cofactor. As expected, based on this critical function, the GTPase domains are highly conserved across septins. The Group 5 septins show the most variation in GTPase domains, though the conservation is still high.

Sep Motifs (S1-S4)

The Sep motifs were identified based on high levels of conservation across multiple species (Pan et al., 2007). Though their function was not clear at the time, it was later found that Sep1, Sep3, and Sep4 were likely involved in contacts between septin monomers within heteropolymers (Auxier et al., 2019). Once more the most variation is seen within Group 5 Sep motifs consistent with data suggesting they do not interact with other septins in the canonical manner (Hernandez-Rodriguez et al., 2014).

Polyacidic Region

First identified by the Araujo and Garratt labs in 2017 (Valadares et al., 2017), the polyacidic region is thought to interact with PB1 or PB2 at the center of the octamer depending on the conformation of the NC-interface (Castro et al., 2020). As shown for our nine model organisms the septin PA is highly variable in length and acidity across groups, but is conserved within groups (**Figures 3A**, **4**).

Septin Unique Element

The SUE is a large (53 amino acids) region first identified based on conservation in many septins (Versele et al., 2004). It was later shown to contain contact regions for both NC- and G-interfaces (Auxier et al., 2019). No other functions have been described for this motif.

C-Terminal Extension

The CTE of septins varies more than the central regions of the protein (**Figure 4**). One of the CTE features that has drawn notice is the presence or absence of a coiled-coiled. Coiled-coils are important for septin higher-order structure formation, and recent crystal structures of the coiled-coils reveal they interact both within and across polymers (Bertin et al., 2010; Leonardo et al., 2021). Septins from Groups 1a and five do not have predicted coiled-coils (Pan et al., 2007) (**Figure 3C**). The truncated CTE and lack of a coiled-coil is especially interesting for Group1a septins since they form the central dimer of the heterooctamer (**Figure 2D**). This central dimer is formed via the NC-interface which in all other heteropolymeric septins is the interface from which the coiled-coils emerge (**Figure 2C**).

Another feature of note is the presence of an amphipathic helix in many septin CTEs. The distinct hydrophobic and hydrophilic faces of amphipathic helices are thought to allow septins to sense membrane curvature. So far amphipathic helices have been identified in septins from groups 1b, 2b-2, 2b-7, 3, and 4 (Cannon et al., 2019; Woods et al., 2021).

CONCLUSION

Septins have duplicated and diversified from their common evolutionary ancestor to perform an amazing array of important functions across species from protists to people. The ability to form heteropolymers appears to be critical to many of those functions and to have been a major driver of the high conservation of many critical domains. Because of this, comparisons can be made between animal and fungal septins that are positional orthologs, though more structural studies on septins from other species are certainly needed to complement the studies on human septins.

The significance of the divergence in polymer composition is still unknown. Perhaps the most striking example of this divergence is in the Group 5 septins which are present in some fungi and protists, absent in animals, and which appear to interact with core septins only transiently. More studies on Group 5 septins from fungi and their non-opisthokont relatives may prove critical to understanding the origins of septins and their ability to interact with each other, with other proteins, and with the membrane. Studying positional orthologs across kingdoms should reveal the history of how septins have been added or removed from polymers and possible conserved functions of septins with shared evolutionary history.

AUTHOR CONTRIBUTIONS

BS and MM contributed to the conception and design of the study. BS performed analyses. BS wrote the first draft. BS and MM wrote sections of the manuscript and contributed to editing and revision.

FUNDING

This work has been supported by funding to MM from the Franklin College of Arts and Sciences Dean's Office. The funder has had no role in design or interpretation of the work.

ACKNOWLEDGMENTS

We thank Amy Shaub Maddox and Jenna A Perry (UNC Chapel Hill) for sharing useful insight on the *C. elegans* septins.

REFERENCES

Angelis, D., and Spiliotis, E. T. (2016). Septin Mutations in Human Cancers. *Front. Cel Dev. Biol.* 4, 122. doi:10.3389/fcell.2016.00122

Auxier, B., Dee, J., Berbee, M. L., and Momany, M. (2019). Diversity of Opisthokont Septin Proteins Reveals Structural Constraints and Conserved Motifs. *BMC Evol. Biol.* 19 (1), 4. doi:10.1186/s12862-018-1297-8

Bai, X., Bowen, J. R., Knox, T. K., Zhou, K., Pendziwiat, M., Kuhlenbäumer, G., et al. (2013). Novel Septin 9 Repeat Motifs Altered in Neuralgic Amyotrophy Bind and Bundle Microtubules. *J. Cel Biol* 203 (6), 895–905. doi:10.1083/jcb.201308068

Bertin, A., McMurray, M. A., Thai, L., Garcia, G., 3rd, Votin, V., Grob, P., et al. (2010). Phosphatidylinositol-4,5-bisphosphate Promotes Budding Yeast Septin

Filament Assembly and Organization. *J. Mol. Biol.* 404 (4), 711–731. doi:10.1016/j.jmb.2010.10.002

Cannon, K. S., Woods, B. L., Crutchley, J. M., and Gladfelter, A. S. (2019). An Amphipathic helix Enables Septins to Sense Micrometer-Scale Membrane Curvature. *J. Cel Biol* 218 (4), 1128–1137. doi:10.1083/jcb.201807211

Cao, L., Ding, X., Yu, W., Yang, X., Shen, S., and Yu, L. (2007). Phylogenetic and Evolutionary Analysis of the Septin Protein Family in Metazoan. *FEBS Lett.* 581 (28), 5526–5532. doi:10.1016/j.febslet.2007.10.032

Casamayor, A., and Snyder, M. (2003). Molecular Dissection of a Yeast Septin: Distinct Domains Are Required for Septin Interaction, Localization, and Function. *Mol. Cel Biol* 23 (8), 2762–2777. doi:10.1128/mcb.23.8.2762-2777.2003

Castro, D. K. S. D. V., da Silva, S. M. O., Pereira, H. D., Macedo, J. N. A., Leonardo, D. A., Valadares, N. F., et al. (2020). A Complete Compendium of crystal Structures for the Human SEPT3 Subgroup Reveals Functional Plasticity at a Specific Septin Interface. *IUCrJ* 7 (Pt 3), 462–479. doi:10.1107/S2052252520002973

Crooks, G. E., Hon, G., Chandonia, J.-M., and Brenner, S. E. (2004). WebLogo: A Sequence Logo Generator: Figure 1. *Genome Res.* 14 (6), 1188–1190. doi:10.1101/gr.849004

Hartwell, L. H., Culotti, J., and Reid, B. (1970). Genetic Control of the Cell-Division Cycle in Yeast, I. Detection of Mutants. *Proc. Natl. Acad. Sci.* 66 (2), 352–359. doi:10.1073/pnas.66.2.352

Hartwell, L. H., Mortimer, R. K., Culotti, J., and Culotti, M. (1973). Genetic Control of the Cell Division Cycle in Yeast: V. Genetic Analysis of Cdc Mutants. *Genetics* 74 (2), 267–286. V. Genetic Analysis of cdc Mutants. doi:10.1093/genetics/74.2.267

Hernández-Rodríguez, Y., Masuo, S., Johnson, D., Orlando, R., Smith, A., Couto-Rodriguez, M., et al. (2014). Distinct Septin Heteropolymers Co-exist during Multicellular Development in the Filamentous Fungus Aspergillus nidulans. *PLoS One* 9 (3), e92819. doi:10.1371/journal.pone.0092819

John, C. M., Hite, R. K., Weirich, C. S., Fitzgerald, D. J., Jawhari, H., Faty, M., et al. (2007). The *Caenorhabditis elegans* Septin Complex Is Nonpolar. *EMBO J.* 26 (14), 3296–3307. doi:10.1038/sj.emboj.7601775

Kinoshita, M. (2003a). Assembly of Mammalian Septins. *J. Biochem.* 134 (4), 491–496. doi:10.1093/jb/mvg182

Kinoshita, M. (2003b). The Septins. *Genome Biol.* 4 (11), 236. doi:10.1186/gb-2003-4-11-236

Leipe, D. D., Wolf, Y. I., Koonin, E. V., and Aravind, L. (2002). Classification and Evolution of P-Loop GTPases and Related ATPases. *J. Mol. Biol.* 317 (1), 41–72. doi:10.1006/jmbi.2001.5378

Leonardo, D. A., Cavini, I. A., Sala, F. A., Mendonça, D. C., Rosa, H. V. D., Kumagai, P. S., et al. (2021). Orientational Ambiguity in Septin Coiled Coils and its Structural Basis. *J. Mol. Biol.* 433 (9), 166889. doi:10.1016/j.jmb.2021.166889

Madeira, F., Park, Y. M., Lee, J., Buso, N., Gur, T., Madhusoodanan, N., et al. (2019). The EMBL-EBI Search and Sequence Analysis Tools APIs in 2019. *Nucleic Acids Res.* 47 (W1), W636–W641. doi:10.1093/nar/gkz268

Martínez, C., Sanjuan, M. A., Dent, J. A., Karlsson, L., and Ware, J. (2004). Human Septin-Septin Interactions as a Prerequisite for Targeting Septin Complexes in the Cytosol. *Biochem. J.* 382 (Pt 3), 783–791. doi:10.1042/BJ20040372

McMurray, M. A., and Thorner, J. (2019). Turning it inside Out: The Organization of Human Septin Heterooligomers. *Cytoskeleton (Hoboken)* 76 (9-10), 449–456. doi:10.1002/cm.21571

Mendonça, D. C., Macedo, J. N., Guimarães, S. L., Barroso da Silva, F. L., Cassago, A., Garratt, R. C., et al. (2019). A Revised Order of Subunits in Mammalian Septin Complexes. *Cytoskeleton (Hoboken)* 76 (9-10), 457–466. doi:10.1002/cm.21569

Merchant, S. S., Prochnik, S. E., Vallon, O., Harris, E. H., Karpowicz, S. J., Witman, G. B., et al. (2007). The Chlamydomonas Genome Reveals the Evolution of Key Animal and Plant Functions. *Science* 318 (5848), 245–250. doi:10.1126/science.1143609

Momany, M., and Talbot, N. J. (2017). Septins Focus Cellular Growth for Host Infection by Pathogenic Fungi. *Front. Cel Dev. Biol.* 5, 33. doi:10.3389/fcell.2017.00033

Momany, M., Zhao, J., Lindsey, R., and Westfall, P. J. (2001). Characterization of the Aspergillus nidulans Septin (Asp) Gene Family. *Genetics* 157 (3), 969–977. doi:10.1093/genetics/157.3.969

Mostowy, S., and Cossart, P. (2012). Septins: the Fourth Component of the Cytoskeleton. *Nat. Rev. Mol. Cel Biol* 13 (3), 183–194. doi:10.1038/nrm3284

Nguyen, T. Q., Sawa, H., Okano, H., and White, J. G. (2000). The *C. elegans* Septin Genes, Unc-59 and Unc-61, Are Required for normal Postembryonic Cytokineses and Morphogenesis but Have No Essential Function in Embryogenesis. *J. Cel Sci* 113, 3825–3837. doi:10.1242/jcs.113.21.3825

Nishihama, R., Onishi, M., and Pringle, J. R. (2011). New Insights into the Phylogenetic Distribution and Evolutionary Origins of the Septins. *Biol. Chem.* 392 (8-9), 681–687. doi:10.1515/BC.2011.086

Omrane, M., Camara, A. S., Taveneau, C., Benzoubir, N., Tubiana, T., Yu, J., et al. (2019). Septin 9 Has Two Polybasic Domains Critical to Septin Filament Assembly and Golgi Integrity. *iScience* 13, 138–153. doi:10.1016/j.isci.2019.02.015

Pan, F., Malmberg, R. L., and Momany, M. (2007). Analysis of Septins across Kingdoms Reveals Orthology and New Motifs. *BMC Evol. Biol.* 7, 103. doi:10.1186/1471-2148-7-103

Sirajuddin, M., Farkasovsky, M., Hauer, F., Kühlmann, D., Macara, I. G., Weyand, M., et al. (2007). Structural Insight into Filament Formation by Mammalian Septins. *Nature* 449 (7160), 311–315. doi:10.1038/nature06052

Smith, C., Dolat, L., Angelis, D., Forgacs, E., Spiliotis, E. T., and Galkin, V. E. (2015). Septin 9 Exhibits Polymorphic Binding to F-Actin and Inhibits Myosin and Cofilin Activity. *J. Mol. Biol.* 427 (20), 3273–3284. doi:10.1016/j.jmb.2015.07.026

Soroor, F., Kim, M. S., Palander, O., Balachandran, Y., Collins, R. F., Benlekbir, S., et al. (2021). Revised Subunit Order of Mammalian Septin Complexes Explains Their *In Vitro* Polymerization Properties. *MBoC* 32 (3), 289–300. doi:10.1091/mbc.e20-06-0398

Spiliotis, E. T., and McMurray, M. A. (2020). Masters of Asymmetry - Lessons and Perspectives from 50 Years of Septins. *MBoC* 31 (21), 2289–2297. doi:10.1091/mbc.e19-11-0648

Spiliotis, E. T., and Nakos, K. (2021). Cellular Functions of Actin- and Microtubule-Associated Septins. *Curr. Biol.* 31 (10), R651–R666. doi:10.1016/j.cub.2021.03.064

Valadares, N. F., d' Muniz Pereira, H., Ulian Araujo, A. P., and Garratt, R. C. (2017). Septin Structure and Filament Assembly. *Biophys. Rev.* 9 (5), 481–500. doi:10.1007/s12551-017-0320-4

Versele, M., Gullbrand, B., Shulewitz, M. J., Cid, V. J., Bahmanyar, S., Chen, R. E., et al. (2004). Protein-Protein Interactions Governing Septin Heteropentamer Assembly and Septin Filament Organization in *Saccharomyces Cerevisiae*. *MBoC* 15 (10), 4568–4583. doi:10.1091/mbc.e04-04-0330

Wloga, D., Strzyzewska-Jówko, I., Gaertig, J., and Jerka-Dziadosz, M. (2008). Septins Stabilize Mitochondria in Tetrahymena Thermophila. *Eukaryot. Cel* 7 (8), 1373–1386. doi:10.1128/EC.00085-08

Woods, B. L., Cannon, K. S., Vogt, E. J. D., Crutchley, J. M., and Gladfelter, A. S. (2021). Interplay of Septin Amphipathic Helices in Sensing Membrane-Curvature and Filament Bundling. *MBoC* 32 (20), br5. doi:10.1091/mbc.e20-05-0303

Woods, B. L., and Gladfelter, A. S. (2021). The State of the Septin Cytoskeleton from Assembly to Function. *Curr. Opin. Cel Biol.* 68, 105–112. doi:10.1016/j.ceb.2020.10.007

Yamazaki, T., Owari, S., Ota, S., Sumiya, N., Yamamoto, M., Watanabe, K., et al. (2013). Localization and Evolution of Septins in Algae. *Plant J.* 74 (4), 605–614. doi:10.1111/tpj.12147

Zhang, J., Kong, C., Xie, H., McPherson, P. S., Grinstein, S., and Trimble, W. S. (1999). Phosphatidylinositol Polyphosphate Binding to the Mammalian Septin H5 Is Modulated by GTP. *Curr. Biol.* 9 (24), 1458–1467. doi:10.1016/s0960-9822(00)80115-3

Conflict of Interest: The authors declare that the research was conducted in the absence of any commercial or financial relationships that could be construed as a potential conflict of interest.

Publisher's Note: All claims expressed in this article are solely those of the authors and do not necessarily represent those of their affiliated organizations, or those of the publisher, the editors and the reviewers. Any product that may be evaluated in this article, or claim that may be made by its manufacturer, is not guaranteed or endorsed by the publisher.

frontiers in Cell and Developmental Biology

BRIEF RESEARCH REPORT
published: 03 March 2022
doi: 10.3389/fcell.2022.771388

Biochemical Characterization of a Human Septin Octamer

Martin Fischer[1], *Dominik Frank*[1], *Reinhild Rösler*[2], *Nils Johnsson*[1] *and Thomas Gronemeyer*[1]*

[1]Institute of Molecular Genetics and Cell Biology, Ulm University, Ulm, Germany, [2]Core Unit Mass Spectrometry and Proteomics, Ulm University, Ulm, Germany

Septins are part of the cytoskeleton and polymerize into non-polar filaments of heteromeric hexamers or octamers. They belong to the class of P-loop GTPases but the roles of GTP binding and hydrolysis on filament formation and dynamics are not well understood. The basic human septin building block is the septin rod, a hetero-octamer composed of SEPT2, SEPT6, SEPT7, and SEPT9 with a stoichiometry of 2:2:2:2 (2-6-7-9-9-7-6-2). Septin rods polymerize by end-to-end and lateral joining into linear filaments and higher ordered structures such as rings, sheets, and gauzes. We purified a recombinant human septin octamer from *E. coli* for *in vitro* experimentation that is able to polymerize into filaments. We could show that the C-terminal region of the central SEPT9 subunit contributes to filament formation and that the human septin rod decreases the rate of *in vitro* actin polymerization. We provide further first kinetic data on the nucleotide uptake- and exchange properties of human hexameric and octameric septin rods. We could show that nucleotide uptake prior to hydrolysis is a dynamic process and that a bound nucleotide is exchangeable. However, the hydrolyzed γ-phosphate is not released from the native protein complex. We consequently propose that GTP hydrolysis in human septins does not follow the typical mechanism known from other small GTPases.

Keywords: septins, septin octamer, GTPases, nucleotide uptake, actin polymerization

OPEN ACCESS

Edited by:
Manoj B. Menon,
Indian Institute of Technology Delhi, India

Reviewed by:
Aurélie Bertin,
UMR168 Unite physico-chimie Curie (PCC), France
Michael McMurray,
University of Colorado Denver, United States

***Correspondence:**
Thomas Gronemeyer
thomas.gronemeyer@uni-ulm.de

Specialty section:
This article was submitted to Signaling, a section of the journal Frontiers in Cell and Developmental Biology

Received: *06 September 2021*
Accepted: *14 February 2022*
Published: *03 March 2022*

Citation:
Fischer M, Frank D, Rösler R, Johnsson N and Gronemeyer T (2022) Biochemical Characterization of a Human Septin Octamer. Front. Cell Dev. Biol. 10:771388. doi: 10.3389/fcell.2022.771388

1 INTRODUCTION

Septins were discovered in yeast in 1971 (Hartwell 1971) and are part of the cytoskeleton (Mostowy and Cossart 2012). They form non-polar filaments that unlike actin filaments and microtubules do not serve as railroad tracks for motor proteins. Being rather neglected for several years after their discovery, research on the septins gained a growing attention over the past few years (Menon and Gaestel, 2017). Initially labeled as passive scaffold proteins, septins were later discovered to actively participate in many dynamic intracellular processes. Septins regulate the organization of the cytoskeleton, vesicle transport and fusion, chromosome alignment and segregation, and cytokinesis (Surka et al., 2002; Estey et al., 2010; Bowen et al., 2011; Füchtbauer et al., 2011; Tokhtaeva et al., 2015).

The septin subunit SEPT9 was reported to bundle actin and microtubules (Bai et al., 2013; Dolat et al., 2014; Mavrakis et al., 2014; Smith et al., 2015).

The mammalian genome encodes thirteen different septins (SEPT1-SEPT12, SEPT14) (Russell and Hall, 2011), of which SEPT2, SEPT7 and SEPT9 are nearly ubiquitously expressed, while SEPT1, SEPT3, SEPT12, and SEPT14 appear tissue-specific. All septin subunits can be sorted into four subgroups based on sequence homology, namely the SEPT2, SEPT3, SEPT6 and SEPT7 subgroup (Kinoshita 2003; Pan et al., 2007).

The basic septin building block in mammalian cells is a hetero-octamer composed of the SEPT2, SEPT6, SEPT7, and SEPT9 at a stoichiometry of 2:2:2:2 (2-6-7-9-9-7-6-2) (Soroor et al., 2021). This building block is capable of polymerizing by end-to-end and lateral joining into higher ordered structures such as rings, filaments, and gauzes. Assembly into these higher ordered structures is achieved by alternating interactions between the G domains (G interface) or between the N- and C-termini (NC interface), respectively (Bertin et al., 2008).

All septins share a central GTP binding domain (short G domain) that is flanked by variable C- and N-terminal extensions (Sirajuddin et al., 2007) and contains a septin unique element including a β-meander and two further helices. The G domain is conserved among different species and is supposed to be loaded either with GTP or GDP. The available crystal structures of human and yeast septins (Sirajuddin et al., 2007; Sirajuddin et al., 2009; Zent et al., 2011; Brausemann et al., 2016; Valadares et al., 2017; Castro et al., 2020; Rosa et al., 2020) confirm that the G domain contains all structural features of small GTPases like the P-loop and the distinct Switch1 and Switch2 loops including the invariant DXXG motif. GTP binding and hydrolysis was confirmed for human septins. Standard assays aiming at detecting GTP hydrolysis in small GTPases employ usually loading of the GTPase with a GTP labeled at its γ-phosphate and subsequent detection of the released γ-phosphate (Frech et al., 1990) or detection of GTP decrease and GDP increase upon hydrolysis by HPLC (Tucker et al., 1986). However, detection of GTPase hydrolysis products in human septin subunits was so far only achieved after denaturation of the protein (Sirajuddin et al., 2009; Castro et al., 2020). GTP uptake and hydrolysis of entire rods composed of human septins was not yet examined. However, these experiments were conducted for entire rods from yeast, leading to partly contradictory results (Vrabioiu et al., 2004; Farkasovsky et al., 2005; Baur et al., 2018).

Only one of the available septin crystal structures, the human SEPT2/6/7 complex (Sirajuddin et al., 2007), shows a trimeric complex composed of more than two different subunits in the asymmetric unit. A recently presented hexameric structure of the same complex was built based on cryo-EM data (Mendonça et al., 2021). All other human septin structures contain various compositions of maximal two different subunits. Octameric rods for *in vitro* experimentation were only presented recently (DeRose et al., 2020; Iv et al., 2021) and now in this work. We present here a first biochemical characterization of the nucleotide binding- and hydrolysis properties of purified human octameric septin rods and measure the influence of septin complexes on actin filament assembly in real time.

2 MATERIALS AND METHODS

2.1 Molecular Cloning, Protein Purification- and Analysis

The ORFs of the isoforms i1 of SEPT2 and SEPT9 (or SEPT91-568) as well as SEPT7 and SEPT6 were cloned into two compatible bicistronic plasmids. SEPT6 was constructed with a N-terminal 6His-tag for IMAC purification while the other subunits were untagged.

Protein expression of hexameric and octameric rods was performed in the *E. coli* strain BL21DE3 in SB medium at 18°C. Protein purification from the crude extract was performed by immobilized metal affinity chromatography (IMAC) and subsequent size exclusion chromatography (SEC).

Integrity of the purified complex was determined by density gradient centrifugation and MS analysis. Western blot analysis was performed using an anti-SEPT9 antibody (mouse, clone 2C6, Sigma Aldrich). Detailed protocols on the cloning-expression and purification procedures as well as on the analytical assays can be found in the supporting methods.

2.2 Filament Formation Assays

Septin filament formation was performed as described elsewhere for yeast septins (Renz et al., 2013). Briefly, septin preparations were adjusted to 2 μM and cleared from aggregates by centrifugation. Filament formation was induced by dialysis into 50 mM Tris pH 8.0, followed by incubation at 4°C overnight and subsequent centrifugation at 100.000 xg. The pellet was resuspended in 50 mM Tris pH 8.0 and either subjected to SDS-PAGE or to negative staining for electron microscopy. Therefore, the protein solution was spotted onto a carbon coated TEM grid and negative stained with uranyl acetate using standard procedures. EM imaging was performed on a JEM 1400 TEM instrument (Jeol) at 120 kV acceleration voltage. The camera resolution was 2000 x 2000 px.

2.3 Nucleotide Uptake- and Hydrolysis Assays

The nucleotide content of the rod preparations was determined by analytical anion exchange chromatography. Briefly, purified protein from the SEC was dialyzed into buffer without salt and subsequently heat denatured to release bound nucleotide. The denatured protein was pelleted and the supernatant was loaded onto a MonoQ HR 5/5 column (Amersham Pharmacia Biotech). The nucleotides were eluted by a linear salt gradient and detected at 254 nm. GTP and GDP were used to determine the elution profiles of the pure compounds.

Uptake of [γ^{32}P]-GTP to hexameric and octameric rods and isolated SEPT9 was performed as described elsewhere for yeast septins (Baur et al., 2018). Briefly, septin preparations were incubated with [γ^{32}P]-GTP in exchange buffer containing 5 mM EDTA. For hydrolysis, the exchange reaction was transferred into hydrolysis buffer containing $MgCl_2$. Radioactivity retained in the native septin proteins during uptake or during hydrolysis was detected with a filter binding assay.

Further details of the procedure and the subsequent data processing are outlined in the supporting methods.

2.4 Actin Polymerization Assays

Pyrene-labeled G-actin (shortly pyrene actin) was prepared from rabbit muscle acetone powder as described elsewhere (Cooper et al., 1983) with some modifications outlined in the supporting

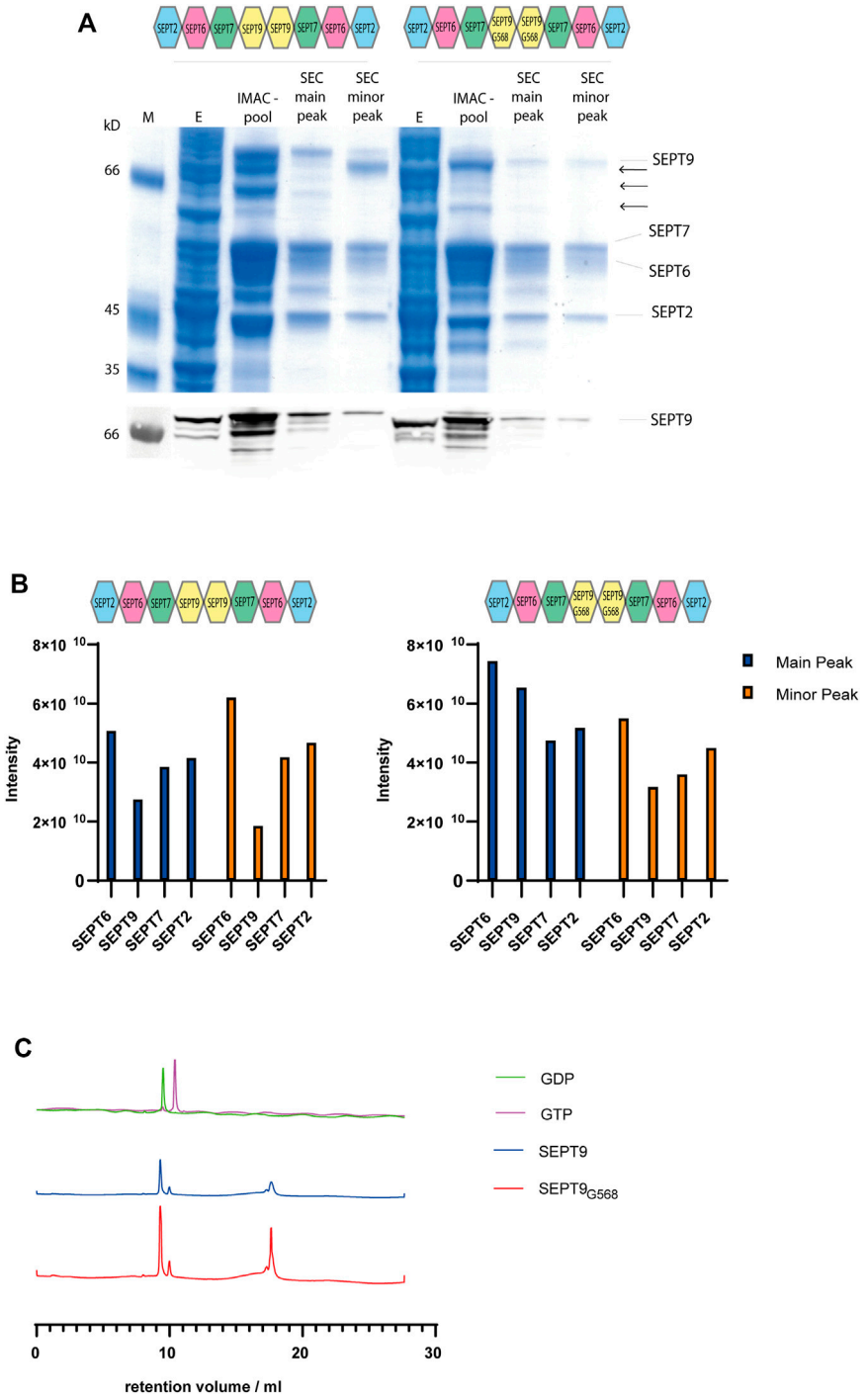

FIGURE 1 | Purification of octameric septin rods. **(A)** SDS-PAGE (Coomassie staining) of a representative purification of septin octamers containing $SEPT9_{FL}$ and $SEPT9_{G568}$. Fractions from IMAC and SEC including the major and minor peak are indicated. SEPT9 degradation products are marked with arrows. The anti-SEPT9 Western blot shows the SEPT9 degradation products. **(B)** Representative MS analysis of the purified septin complexes. Both the main product peak and the minor peak from SEC were analyzed. Peptide abundancies of the $SEPT_{FL}$ (left panel) and $SEPT9_{G568}$ (right panel) octamer are plotted; the indicated intensity score reflects the accumulated intensities of all peptides detected for the respective subunit. **(C)** Nucleotide content of octameric rods containing $SEPT9_{FL}$ or $SEPT9_{G568}$ detected by analytical anion exchange chromatography (representative runs out of at least three per rod species performed) after heat denaturation of the protein. Calibration runs with GTP and GDP are shown in the upper row.

methods. Pyrene actin fluorescence increases upon actin polymerization and can be recorded in actin polymerization buffer at an excitation of 365 nm and emission of 407 nm. Details on the pyrene actin preparation, the assay protocol and data processing are outlined in the supporting methods.

The unprocessed raw data are shown in **Supplementary Figure S4**.

3 RESULTS

3.1 Construction and Purification of Human Hexameric- and Octameric Septin Rods

We expressed the subunits of the human octameric and hexameric septin rods in *E.coli* from two compatible bicistronic plasmids. SEPT6 and SEPT7 were expressed from one plasmid and SEPT2 (and SEPT9 for octameric rods) from the second plasmid as in a previous study (Sheffield et al., 2003). Only SEPT6 carried a hexa-histidine tag for purification by immobilized metal affinity chromatography (IMAC). The enriched fractions were subsequently subjected to size exclusion chromatography (SEC). Complexes eluted in a shoulder in the second half of the main peak (the first half representing the void peak of the column) and in a minor peak directly adjacent to the main peak (**Supplementary Figure S1A**).

SDS-PAGE and Western blot analysis with an anti-SEPT9 antibody documented the presence of shorter fragments of SEPT9 (**Figure 1A**). SEPT9 has two flexible regions, a long extension at the N-terminus and a shorter one at the C-terminus. We suspected one or both of these extensions to cause the shorter fragments. The long SEPT9 isoforms used by Iv et al. (2021) in their rod preparations contained both the N-terminus or larger parts thereof, but their SEPT9i3 terminates at residue Glycine 568. This residue represents the terminal residue of the α6 helix of the G domain. We decided to test first if a version of SEPT9 truncated at Glycine 568 ($SEPT9_{G568}$) still produces degradation products in our purification pipeline. Octameric rods expressing $SEPT9_{G568}$ showed less degradation products than the native octamer and the purified complex could be readily separated from other subcomplexes and contaminants by the preparative SEC (**Figure 1A**). The IMAC enriched septin preparation was analyzed on a glycerol gradient centrifugation to confirm the integrity of the complex. Septin subunits, SEPT9 degradation products and contaminants migrated in the fractions corresponding to a lower molecular weight whereas the stoichiometric combination of all four subunits migrated just before the 670 kD marker protein became abundant, indicative of an octameric septin complex (**Supplementary Figure S1B**).

We analyzed the fractions from the major and minor peak from the SEC of $SEPT9_{FL}$ and $SEPT9_{G568}$ complexes by mass spectrometry (MS). All four subunits are present in nearly stoichiometric abundance (**Figure 1B**). We conclude that our septin preparation in the main peak is indeed an octameric complex containing all four subunits. We performed the MS analyses with several purified complexes. The peptide intensity scores of the individual subunits varied slightly between the preparations, but we observed in all MS runs that SEPT9 was less abundant in the complex of the minor SEC peak. As this subcomplex poorly formed filaments (see below), all subsequent experiments were conducted with a septin preparation from the main peak.

We subsequently determined the nucleotide content of our rod preparations. Bound nucleotide was released from the protein by heat denaturation and afterwards analyzed by analytical anion exchange chromatography (**Figure 1C**). We determined the peak integrals and calculated the ratio of GDP to GTP. Both $SEPT9_{FL}$ and $SEPT9_{G568}$ complexes contained between 3.5 and 5 times more GDP than GTP (varying between several purifications performed). Overall, we could not detect any difference in SEPT9 and $SEPT9_{G568}$ containing octamers regarding the nucleotide content after purification.

Hexameric SEPT2/6/7 complexes were purified using the same purification pipeline and yielded a highly purified after SEC (**Supplementary Figure 1C**).

3.2 Filament Forming Properties

We asked next whether septin filament formation is altered by the absence of the SEPT9 C-terminal extension. Septin preparations were cleared from aggregates by centrifugation, dialyzed into low salt buffer and subjected subsequently to ultracentrifugation. Surprisingly, we could detect filaments already at 300 mM NaCl for $SEPT9_{FL}$ octamers (**Supplementary Figure S2A**) whereas filaments of $SEPT9_{G568}$ containing octamers and hexamers required 50 mM NaCl to form (**Supplementary Figures S2B, C**). Filament formation was almost abolished at 100 mM NaCl. Negative stain EM of $SEPT9_{FL}$ octamers revealed the presence of long filament bundles consisting of parallel aligned septin filaments, consistent with the findings of Iv et al. (2021) (**Figure 2A**). $SEPT9_{G568}$ containing filaments formed also bundles, but the filaments forming the bundle appeared rather curved and less parallel aligned (**Figure 2B**). Complexes isolated from the minor peaks of the SEC only poorly formed filaments (data not shown) which we were not able to visualize by EM.

3.3 Effects of Human Septin Rods on the Polymerization Properties of Actin

The septin subunit SEPT9 was reported to bundle actin and microtubules (Bai et al., 2013; Dolat et al., 2014; Mavrakis et al., 2014; Smith et al., 2015).

To investigate the influence of septin rods on the formation of the actin cytoskeleton *in vitro*, we performed actin polymerization assays with 2 μM pyrene labeled G-actin and recorded the increase of fluorescence over time. G actin without additives or with purified GST (serving as control to exclude unwanted side effects by crowding) displayed a typical sigmoidal polymerization curve (**Supplementary Figure S3A**) (Cooper et al., 1983) which can be described mathematically by a growth curve including lag phase, exponential growth and plateau phase. From this curve, parameters such as the rate constant, the lag time or the doubling time can be calculated. All parameters calculated from the polymerization curves are summarized in

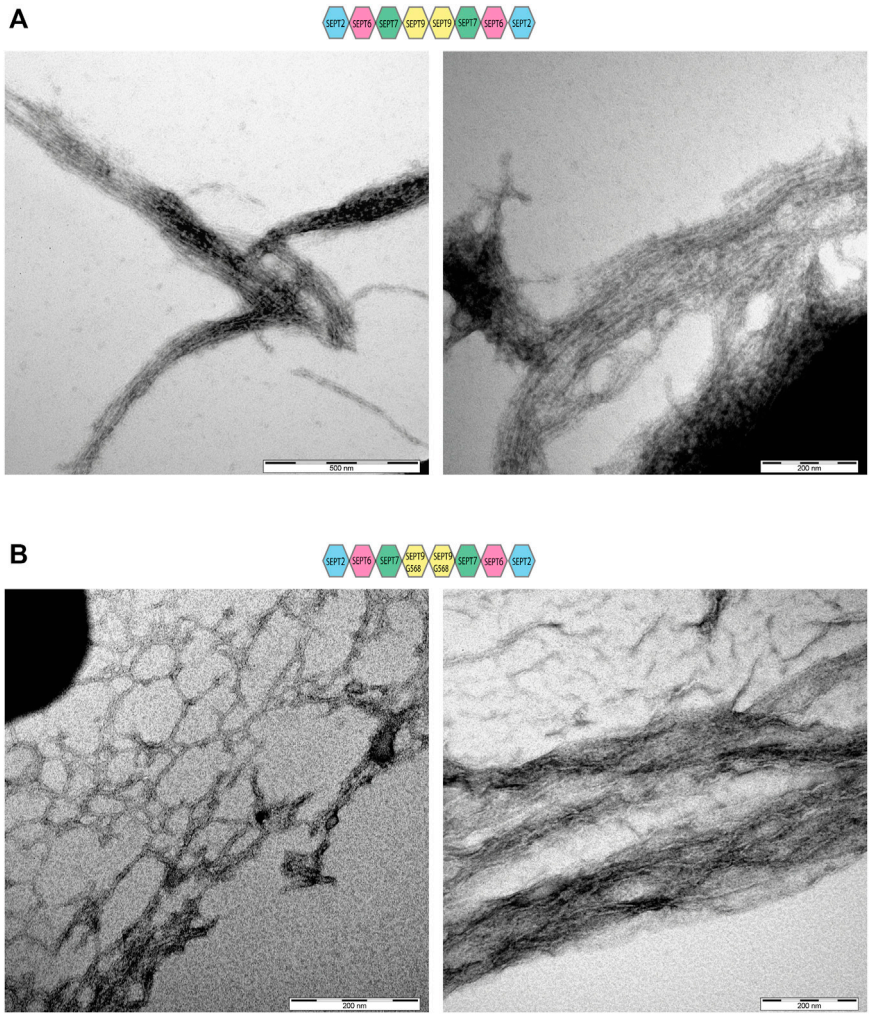

FIGURE 2 | Electron microscopy of $SEPT9_{FL}$ and $SEPT9_{G568}$ containing septin rods. Negative stains of septin filaments obtained by dialysis in low salt buffer showing bundles and network-like structures. **(A)** Electron microscopy of septin filaments containing $SEPT9_{FL}$. **(B)** Electron microscopy of septin filaments containing $SEPT9_{G568}$.

Supplementary Table S1. Actin polymerization did not occur in G-buffer without salts (**Supplementary Figure S3B**). The presence of hexameric septins increased the lag time in a concentration dependent manner, leading to a shift of the inflection point relative to the inflection point of the actin curve (**Figure 3A**). For octamers, the shift was more pronounced at lower concentration but did not change significantly at higher septin concentrations (**Figure 3B**). More important, the actin monomer turnover in the elongation phase (represented by τ, the inverse value of the rate constant) was slightly decreased about 1.4 fold for hexameric rods and 0.5 μM octamer relative to actin alone and more pronounced decreased by 2.1 fold for 1 μM octamer. Increased τ values are reflected by a shallower slope of the curve.

A spin down assay with septin octamers previously dialyzed in G buffer showed that septin filaments did not measurably bind G-actin (**Supplementary Figure 3C**).

3.4 Nucleotide Uptake and Hydrolysis Properties of the Human Septins

We have previously measured the uptake of [γ^{32}P] labelled GTP in the presence of EDTA by the hexameric- and octameric septin rods from yeast (Baur et al., 2018). All following experiments were conducted with $SEPT9_{G568}$ containing octamers. [γ^{32}P]-GTP uptake followed an exponential one phase association kinetics from which the rate constant and the reaction half time $t_{1/2}$ can be calculated. The reaction half time $t_{1/2}$ was 10 min for hexameric rods and 16 min for octameric rods, respectively (**Figure 4A**). All $t_{1/2}$ values of this and the subsequently performed experiments are summarized in **Figure 4C** and the full evaluation of all performed measurements are shown in the supporting information (**Supplementary Tables S2–S4**).

Unlike for yeast septin rods, adding $MgCl_2$ to the exchange reaction after 20 min did not change the overall shape of the

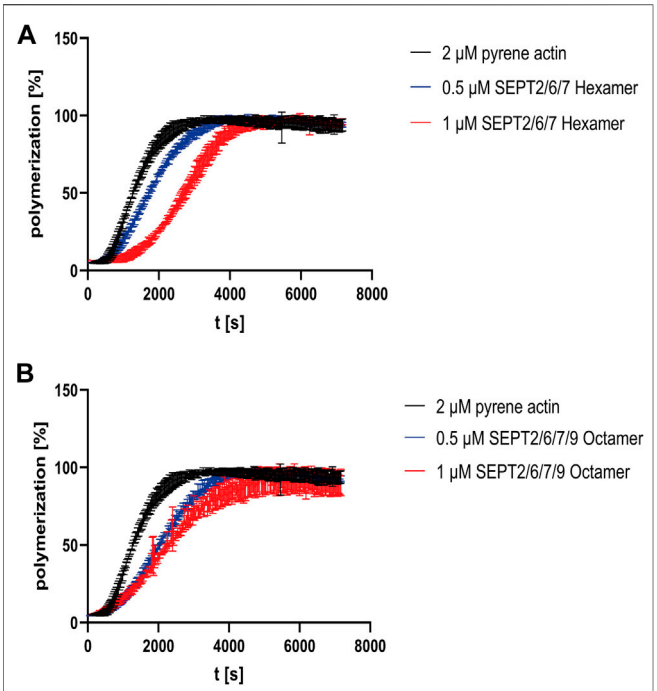

FIGURE 3 | Influence of human septin rods on actin polymerization. **(A)** Actin polymerization assay using pyrene actin with and without septin hexamers. **(B)** Actin polymerization assay using pyrene actin with and without $SEPT9_{G568}$ containing octamers. The assays shown were performed in triplicate and in quintuplicate for actin. The same averaged actin curve was used for evaluation of the assay. The unprocessed raw data are shown in **Supplementary Figure S4**.

uptake kinetics but prolonged $t_{1/2}$ slightly (and barely significantly) to 14.5 min for hexamers and 21 min for octamers (**Supplementary Figure S5A** and **Figure 4C**).

To evaluate whether the bound nucleotide remains in the septin rod or exchanges with free GTP, we pre-loaded septin preparations with non-radioactive GDP or GTP and removed excess nucleotide by micro-dialysis. Subsequent nucleotide exchange against [γ^{32}P]-GTP showed a shift in reaction half times to 42 min for both GDP and GTP loaded hexameric rods and to 33 min for GDP loaded octameric rods and 38 min for GTP loaded octameric rods, respectively (**Supplementary Figures S5B, C** and **Figure 4C**).

We also subjected the octameric rods to exchange of previously bound [γ^{32}P]-GTP against non-radioactive nucleotide. After loading, excess nucleotide was removed via a desalting column and the uptake of non-radioactive GTP was monitored via the decrease of protein-bound radioactivity. The calculated reaction half time of 46.5 min was slightly (and not significantly) slower than the $t_{1/2}$ for the inverse exchange reaction (GTP against [γ^{32}P]-GTP) (**Figure 4B**).

We conclude that human septin octamers exchange bound nucleotides quite readily.

Previous studies showed that isolated septin subunits may have other GTPase properties than septin rods (Sheffield et al., 2003). We tested the isolated $SEPT9_{FL}$ subunit and the SEPT9 G-domain ($SEPT9_{Q295\text{-}E567}$) for nucleotide uptake and found that both did not accept [γ^{32}P]-GTP (**Figure 4D**).

To find out whether human septins follow the same GTP hydrolysis mechanism like other small GTPases, we measured the released or protein-bound radioactivity by [γ^{32}P]-GTP preloaded septins under conditions used for other small GTPases (i.e. magnesium and an excess of non-radioactive GTP to avoid unwanted re-association of [γ^{32}P]-GTP molecules) (Tucker et al., 1986; Schweins et al., 1995). In contrast to common small GTPases of the Ras family, neither hexameric nor octameric rods showed a release of hydrolyzed [γ^{32}P] under these conditions in the applied time frame, regardless of the applied reaction temperature (25°C or 37°C, respectively) (**Figure 4E** and **Supplementary Figure S6**).

4 DISCUSSION

4.1 The C-Terminus of SEPT9 Contributes to Filament Formation

Human hexameric septin rods are available for *in vitro* experimentation and even crystallization for several years (Sheffield et al., 2003; Sirajuddin et al., 2007). However, purified octameric rods containing SEPT9 were only very recently obtained (Iv et al., 2021). We introduce here an additional two step purification protocol for human octameric rods harboring a hexa-histidine tag at only one of its subunits. Gycerol density gradient centrifugation of the complex after the first purification step separated contaminants and septin containing subcomplexes from the octamer, which migrated at the expected density in the gradient. After preparative SEC, we obtained the purified octamer including all four subunits in nearly stoichiometric abundance as judged by MS analysis.

The central subunit SEPT9 is prone to C-terminal degradation during expression and purification of the rod. Removal of the terminal 18 amino acids stabilized the protein and led to less degradation products. To our surprise we found that the $SEPT9_{FL}$ containing rods formed filaments already at 300 mM NaCl whereas filament formation by hexamers and $SEPT9_{G568}$ containing octamers was abolished already at 100 mM NaCl. The first study of filament formation of SEPT2/6/7 hexamers raised the expectation of another—at that time largely unknown - septin subunit (SEPT9) with a stabilizing effect on the filaments (Sheffield et al., 2003). Based on our herein presented experimental data we propose that the stabilizing effect of the SEPT9 subunit on filament formation is mediated by the α6 helix and its C-terminal extension. The α6 helix of the SEPT9 G domain is an essential component of the central SEPT9-SEPT9 NC interface, contributing to an interaction network with the α2 helix of the neighboring subunit (Castro et al., 2020). The C-terminal extensions would point out from the interface, maybe interacting with each other they further stabile the interface. We and others (Iv et al., 2021) postulate that the assembly of higher ordered septin structures is driven *in vitro* by the N- and C-terminal extensions.

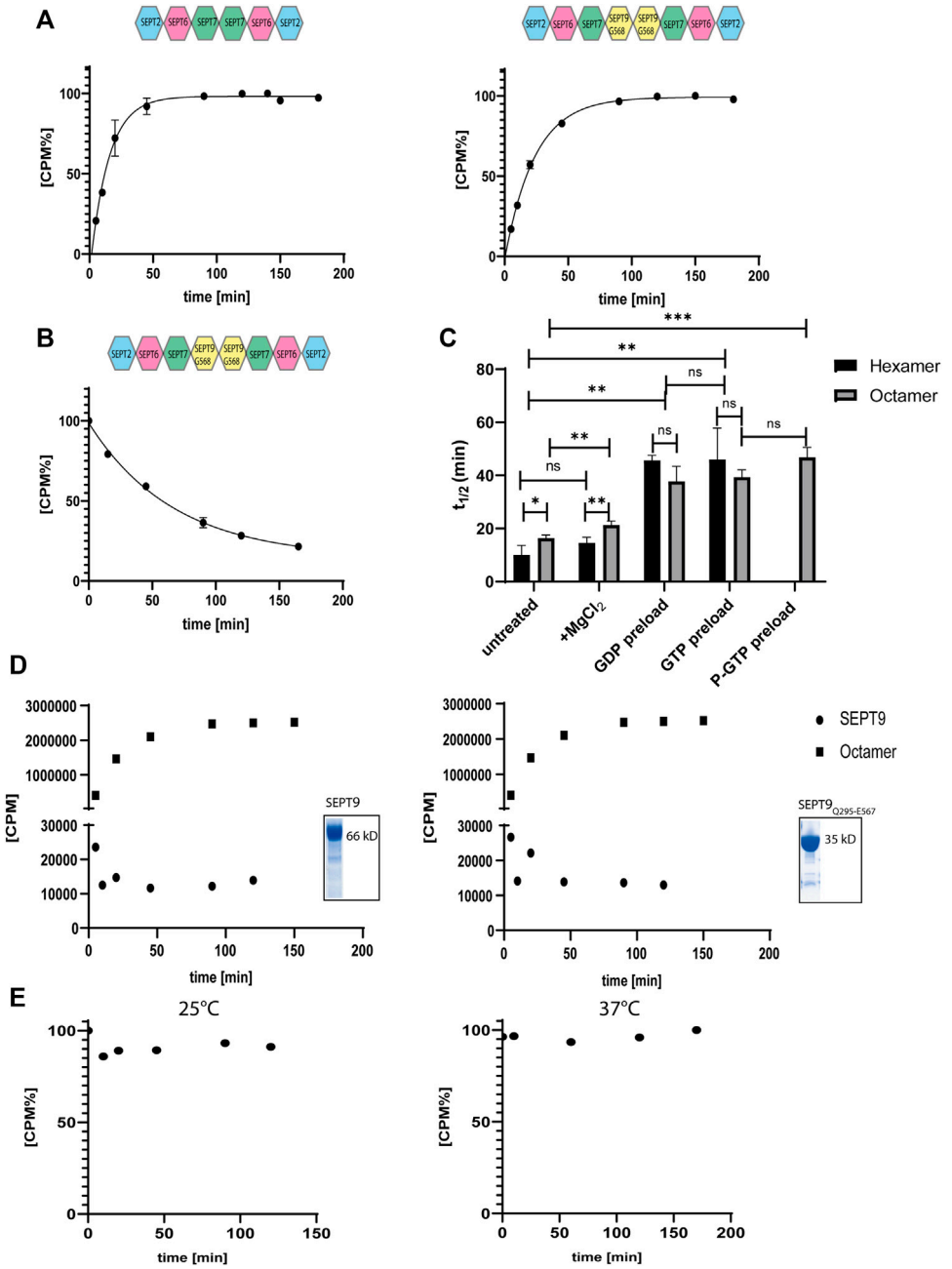

FIGURE 4 | Nucleotide uptake- and hydrolysis properties of hexameric and SEPT9$_{G568}$ octameric septin rods. **(A)** Nucleotide exchange reaction of hexameric (left panel) and octameric septins (right panel). Purified complexes were incubated with [γ^{32}P]-GTP and uptake was monitored at the indicated timepoints by a filter assay. [CPM%] values (normalized radioactive counts) are plotted vs. the reaction time. The connecting line represents the fitting curve of the exponential association. **(B)** Nucleotide exchange reaction of octameric septins preloaded with [γ^{32}P]-GTP. The preloaded complex was incubated with GTP and decrease of [γ^{32}P]-GTP was monitored at the indicated timepoints by a filter assay as in A. The connecting line represents the fitting curve of the exponential dissociation. **(C)** Compilation of the $t_{1/2}$ values of all performed nucleotide exchange assays. The parameters of the statistical evaluation are provided in **Supplementary Tables S2, S3**. Error bars represent the standard deviation. All assays [including those depicted in detail in (A,B)] were performed at least in triplicate. **(D)** Representative [γ^{32}P]-GTP uptake assay for isolated SEPT9$_{FL}$ (left panel) and SEPT9$_{Q295\text{-}E567}$ (right panel) subunits. The assay was performed as in (A). The raw, unprocessed CPM counts are plotted vs. the reaction time. For comparison, a representative nucleotide uptake reaction for a septin octamer is also plotted. The inlets show the Coomassie stained SDS-PAGE of both purifications. **(E)** Representative GTP hydrolysis assay for octameric septins. After preloading with [γ^{32}P]-GTP, the complex was subjected to hydrolysis conditions applicable for small GTPases. The reaction was performed at 25°C (left panel) and 37°C (right panel). Samples were taken at the indicated time points and the [γ^{32}P]-GTP content was detected by a filter assay. [CPM%] values (normalized radioactive counts) are plotted vs. the reaction time. GTP hydroloysis of hexameric rods is shown in **Supplementary Figure S4**.

4.2 Human Septin Complexes Reduce the Rate of Actin Polymerization *in vitro*

Several studies have already demonstrated the capability of SEPT9, septin hexamers and octamers to bind and bundle filamentous actin (Mavrakis et al., 2014; Smith et al., 2015; Iv et al., 2021). All these studies monitored the effects of septins on filamentous actin. Actin bundling was detected subsequently by electron- or fluorescence microscopy. The pyrene actin assay introduced in this study looks at actin polymerization in real time, however, it measures the net polymer weight and does not provide information on the longitudinal distribution of the filaments (Cooper et al., 1983). It was recently shown by *in vitro* microscopy that recombinant septin rods cross-link actin filaments into straight and curved bundles (Iv et al., 2021). Our assay revealed that the presence of septin rods decreases the rate of actin polymerization. As we could not detect any interaction between septin rods and G-actin we propose that the septins exert their influence on polymerization through interaction with the forming actin filament and subsequently bundle filaments by lateral joining. Why this effect is more pronounced for octamers requires further investigation. Maybe the interaction of the octamer with the actin filament is favored over hexamer binding.

Whether SEPT9 is a bundling factor on its own is currently under debate (Mavrakis et al., 2014; Smith et al., 2015; Iv et al., 2021). As the influence on actin monomer turnover is more pronounced for octamers, we support a the idea of a direct contribution of SEPT9 on actin polymerization.

4.3 Nucleotide Uptake- and Hydrolysis by Human Septin Complexes

Septins were first labeled as GTP binding proteins in Drosophila (Field et al., 1996) and afterwards nucleotide binding was confirmed also for human and yeast septin complexes (Sheffield et al., 2003; Vrabioiu et al., 2004) and subsequently evaluated in further studies (Farkasovsky et al., 2005; Baur et al., 2018). However, the functional role of nucleotide binding- and hydrolysis of the septins in cellular processes and in septin (proto-)filament assembly is still under debate and not well understood.

The availability of yeast and human septin octamers enabled us to measure nucleotide association kinetics in these protein complexes and to compare the properties of both species. GTP-loading in human septin rods remains on a constant level after reaching a plateau whereas in the yeast septin rods the radioactive signal decreases about 50% after reaching a maximum (Baur et al., 2018). This indicates the release of the γ-phosphate or the entire nucleotide in at least some subunits of the protofilaments. Mg^{2+} suppresses this release but shows no significant effect on the GTP association rate in the yeast septin rods. In contrast, Mg^{2+} slightly slows down the GTP binding in human septin rods. In the absence of Mg^{2+}, hexameric and octameric rods from both species are able to exchange previously bound GTP and GDP. The exchange rates for GDP and GTP of the human septin rods do not differ significantly. In contrast, the *S. cerevisiae* septin rods exhibit a much faster GDP-GTP than GTP-GTP exchange. These discrepancies indicate that, although displaying a high structural similarity, the septins from different species follow each an individual biochemistry. Even within one species the different subunits exhibit different properties. Comparing the GTP and GDP loaded structures of SEPT2 (PDB IDs 3FTQ and 2QNR, respectively) reveals a conformational change in the Switch1 region with the invariant Thr78 and Mg^{2+} being in close contact with the γ-phosphate exclusively in the GTP conformation. In the GDP conformation Switch1 is either unstructured or oriented away from the nucleotide (**Supplementary Figure S7A**). This conformational change cannot be seen in the structures of SEPT9 (PDB IDs 5CYP and 5CYO) where the corresponding Thr64 in Switch1 is associated with Mg^{2+} towards the nucleotide in both nucleotide states (**Supplementary Figure S7B**). This inflexibility of Switch1 might explain the inability of the isolated SEPT9 to accept [γ^{32}P]-GTP and why we do not detect significant differences in nucleotide uptake between hexamers and octamers. However, it should be kept in mind that the mentioned structures do not contain a native G interface and thus they can provide only indications explaining our experimental findings.

GTP hydrolysis is routinely detected in small GTPases of the Ras family. Experimentally, the small GTPase is loaded with GTP in the presence of EDTA and then subjected to a Mg^{2+} containing buffer without EDTA. The Mg^{2+} ion is an indispensable component for the GTPase reaction. The γ-phosphate is coordinated by invariant threonine and glycine residues in the Switch1 and Switch2 regions. The conformational change following the GTPase reaction was termed "loaded-spring mechanism" which allows the release of the γ-phosphate after hydrolysis and the relaxation of the switch regions into the GDP conformation (Vetter and Wittinghofer 2001). We were not able to detect the release of [γ^{32}P]-GTP or hydrolyzed [γ^{32}P] from any rod species examined. This indicates that bound nucleotides and presumable hydrolysis products remain in the binding pocket and are not released into the surrounding medium, at least not in the timeframe of the experiment (120–180 min) and at least not under the conditions applied. This is more in line with our findings for yeast septins (Baur et al., 2018) rather than with the properties of small GTPases of the Ras family.

GTPase hydrolysis products were detected in yeast and mammalian septin preparations after denaturation of the protein (Sheffield et al., 2003; Versele and Thorner 2004; Sirajuddin et al., 2009; Castro et al., 2020). In contrast, our assay was conducted under native conditions. Consequently, hydrolysis occurs either at very slow pace, undetectable within the chosen timeframe, or the hydrolysis products remain in the active site after the reaction took place. This raises the question which role nucleotides and their hydrolysis play. This question was addressed in yeast septins and it was proposed that nucleotide hydrolysis plays a role during formation of the rod (Weems and McMurray 2017). This would indeed imply that one GTP hydrolysis event is enough and that cycling between the GDP and GTP bound state would not be necessary. However, more studies both *in vivo* and *in vitro* are necessary to convincingly address this issue for human septins.

Taken together, we propose that GTP binding and hydrolysis in septins follow a different mechanism than in other small GTPases and that septin rods from budding yeast differ mechanistically in their guanine nucleotide interactions from their human counterparts. More structural information from yeast septins is needed to understand these differences.

DATA AVAILABILITY STATEMENT

The original contributions presented in the study are included in the article/**Supplementary Material**, further inquiries can be directed to the corresponding author.

AUTHOR CONTRIBUTIONS

MF and DF performed the experiments and prepared the figures. RR performed the MS analysis. NJ analyzed the data and improved the manuscript. TG performed experiments, analyzed the data, conceived the study and wrote the manuscript.

ACKNOWLEDGMENTS

The authors thank Matthias Hecht (Inst. f. Molecular Genetics, Ulm) for providing the SEPT9 G domain expression construct and 1306 fibroblast cDNA and Elias Spiliotis (Drexel University, PA, United States) for the kind gift of a GFP-SEPT9i1 expression plasmid. Paul Walther (Central EM Facility, Uni Ulm) is acknowledged for performing the negative stains. The authors thank Sebastian Iben and Tamara Pham (Uniklinik Ulm) for providing access and support to the gradient mixing device and Thomas Monecke (Inst. of Pharmaceutical Biotechnology, Ulm University) for providing access and support to the multiwell plate reader. Benjamin Grupp (Inst. f. Molecular Genetics, Ulm) is acknowledged for critically reading the manuscript and for technical assistance with the IEX nucleotide assay.

SUPPLEMENTARY MATERIAL

The Supplementary Material for this article can be found online at: https://www.frontiersin.org/articles/10.3389/fcell.2022.771388/full#supplementary-material

REFERENCES

Bai, X., Bowen, J. R., Knox, T. K., Zhou, K., Pendziwiat, M., Kuhlenbäumer, G., et al. (2013). Novel Septin 9 Repeat Motifs Altered in Neuralgic Amyotrophy Bind and Bundle Microtubules. *J. Cel Biol.* 203 (6), 895–905. doi:10.1083/jcb.201308068

Baur, J. D., Rösler, R., Wiese, S., Johnsson, N., and Gronemeyer, T. (2018). Dissecting the Nucleotide Binding Properties of the Septins from S. Cerevisiae.. *Cytoskeleton* 76 (1), 45–54. doi:10.1002/cm.21484

Bertin, A., McMurray, M. A., Grob, P., Park, S.-S., Garcia, G., 3rd, Patanwala, I., et al. (2008). Saccharomyces Cerevisiae Septins: Supramolecular Organization of Heterooligomers and the Mechanism of Filament Assembly. *Proc. Natl. Acad. Sci.* 105 (24), 8274–8279. doi:10.1073/pnas.0803330105

Bowen, J. R., Hwang, D., Bai, X., Roy, D., and Spiliotis, E. T. (2011). Septin GTPases Spatially Guide Microtubule Organization and Plus End Dynamics in Polarizing Epithelia. *J. Cel Biol.* 194 (2), 187–197. doi:10.1083/jcb.201102076

Brausemann, A., Gerhardt, S., Schott, A.-K., Einsle, O., Große-Berkenbusch, A., Johnsson, N., et al. (2016). Crystal Structure of Cdc11, a Septin Subunit from Saccharomyces cerevisiae. *J. Struct. Biol.* 193, 157–161. doi:10.1016/j.jsb.2016.01.004

Castro, D. K. S. d. V., da Silva, S. M. d. O., Pereira, H. D. M., Macedo, J. N. A., Leonardo, D. A., Valadares, N. F., et al. (2020). A Complete Compendium of Crystal Structures for the Human SEPT3 Subgroup Reveals Functional Plasticity at a Specific Septin Interface. *Int. Union Crystallogr. J.* 7 (3), 462–479. doi:10.1107/S2052252520002973

Cooper, J. A., Walker, S. B., and Pollard, T. D. (1983). Pyrene Actin: Documentation of the Validity of a Sensitive Assay for Actin Polymerization. *J. Muscle Res. Cel Motil* 4 (2), 253–262. doi:10.1007/BF00712034

DeRose, B. T., Kelley, R. S., Ravi, R., Kokona, B., Beld, J., Spiliotis, E. T., et al. (2020). Production and Analysis of a Mammalian Septin Hetero-Octamer Complex. *Cytoskeleton* 77 (11), 485–499. doi:10.1002/cm.21643

Dolat, L., Hunyara, J. L., Bowen, J. R., Karasmanis, E. P., Elgawly, M., Galkin, V. E., et al. (2014). Septins Promote Stress Fiber-Mediated Maturation of Focal Adhesions and Renal Epithelial Motility. *J. Cel Biol.* 207 (2), 225–235. doi:10.1083/jcb.201405050

Estey, M. P., Di Ciano-Oliveira, C., Froese, C. D., Bejide, M. T., and Trimble, W. S. (2010). Distinct Roles of Septins in Cytokinesis: SEPT9 Mediates Midbody Abscission. *J. Cel Biol.* 191 (4), 741–749. doi:10.1083/jcb.201006031

Farkasovsky, M., Herter, P., Voss, B., and Wittinghofer, A. (2005). Nucleotide Binding and Filament Assembly of Recombinant Yeast Septin Complexes. *Biol. Chem.* 386, 643–656. doi:10.1515/BC.2005.075

Field, C. M., Al-Awar, O., Rosenblatt, J., Wong, M. L., Alberts, B., and Mitchison, T. J. (1996). A Purified Drosophila Septin Complex Forms Filaments and Exhibits GTPase Activity. *J. Cel Biol.* 133 (3), 605–616. doi:10.1083/jcb.133.3.605

Frech, M., John, J., Pizon, V., Chardin, P., Tavitian, A., Clark, R., et al. (1990). Inhibition of GTPase Activating Protein Stimulation of Ras-P21 GTPase by the K Rev -1 Gene Product. *Science* 249, 169–171. doi:10.1126/science.2164710

Füchtbauer, A., Lassen, L. B., Jensen, A. B., Howard, J., Quiroga, A. d. S., Warming, S., et al. (2011). Septin9 Is Involved in Septin Filament Formation and Cellular Stability. *Biol. Chem.* 392 (8-9), 769–777. doi:10.1515/BC.2011.088

Hartwell, L. (1971). Genetic Control of the Cell Division Cycle in Yeast. IV. Genes Controlling Bud Emergence and Cytokinesis. *Exp. Cel Res.* 69 (2), 265–276. doi:10.1016/0014-4827(71)90223-0

Iv, F., Martins, C. S., Castro-Linares, G., Taveneau, C., Barbier, P., Verdier-Pinard, P., et al. (2021). Insights into Animal Septins Using Recombinant Human Septin Octamers with Distinct SEPT9 Isoforms. *J. Cel Sci.* 134 (15), jcs258484. doi:10.1242/jcs.258484

Kinoshita, M. (2003). Assembly of Mammalian Septins. *J. Biochem.* 134 (4), 491–496. doi:10.1093/jb/mvg182

Mavrakis, M., Azou-Gros, Y., Tsai, F.-C., Alvarado, J., Bertin, A., Iv, F., et al. (2014). Septins Promote F-Actin Ring Formation by Crosslinking Actin Filaments into Curved Bundles. *Nat. Cel Biol* 16 (4), 322–334. doi:10.1038/ncb2921

M. B. Menon and M. Gaestel (Editors) (2017). *Emerging Functions of Septins* (Lausanne: Frontiers Media). doi:10.3389/978-2-88945-287-3

Mendonça, D. C., Guimarães, S. L., Pereira, H. D. M., Pinto, A. A., de Farias, M. A., de Godoy, A. S., et al. (2021). An Atomic Model for the Human Septin Hexamer by Cryo-EM. *J. Mol. Biol.* 433 (15), 167096. doi:10.1016/j.jmb.2021.167096

Mostowy, S., and Cossart, P. (2012). Septins: the Fourth Component of the Cytoskeleton. *Nat. Rev. Mol. Cel Biol* 13 (3), 183–194. doi:10.1038/nrm3284

Pan, F., Malmberg, R. L., and Momany, M. (2007). Analysis of Septins across Kingdoms Reveals Orthology and New Motifs. *BMC Evol. Biol.* 7, 103. doi:10.1186/1471-2148-7-103

Renz, C., Johnsson, N., and Gronemeyer, T. (2013). An Efficient Protocol for the Purification and Labeling of Entire Yeast Septin Rods from E.Coli for Quantitative in Vitroexperimentation. *BMC Biotechnol.* 13, 60. doi:10.1186/1472-6750-13-60

Rosa, H. V. D., Leonardo, D. A., Brognara, G., Brandão-Neto, J., D'Muniz Pereira, H., Araújo, A. P. U., et al. (2020). Molecular Recognition at Septin Interfaces:

The Switches Hold the Key. *J. Mol. Biol.* 432 (21), 5784–5801. doi:10.1016/j.jmb.2020.09.001

Russell, S. E., and Hall, P. A. (2011). Septin Genomics: a Road Less Travelled. *Biol. Chem.* 392 (8-9), 763–767. doi:10.1515/BC.2011.079

Schweins, T., Geyer, M., Scheffzek, K., Warshel, A., Kalbitzer, H. R., and Wittinghofer, A. (1995). Substrate-assisted Catalysis as a Mechanism for GTP Hydrolysis of P21ras and Other GTP-Binding Proteins. *Nat. Struct. Mol. Biol.* 2 (1), 36–44. doi:10.1038/nsb0195-36

Sheffield, P. J., Oliver, C. J., Kremer, B. E., Sheng, S., Shao, Z., and Macara, I. G. (2003). Borg/Septin Interactions and the Assembly of Mammalian Septin Heterodimers, Trimers, and Filaments. *J. Biol. Chem.* 278 (5), 3483–3488. doi:10.1074/jbc.M209701200

Sirajuddin, M., Farkasovsky, M., Hauer, F., Kühlmann, D., Macara, I. G., Weyand, M., et al. (2007). Structural Insight into Filament Formation by Mammalian Septins. *Nature* 449 (7160), 311–315. doi:10.1038/nature06052

Sirajuddin, M., Farkasovsky, M., Zent, E., and Wittinghofer, A. (2009). GTP-induced Conformational Changes in Septins and Implications for Function. *Proc. Natl. Acad. Sci.* 106 (39), 16592–16597. doi:10.1073/pnas.0902858106

Smith, C., Dolat, L., Angelis, D., Forgacs, E., Spiliotis, E. T., and Galkin, V. E. (2015). Septin 9 Exhibits Polymorphic Binding to F-Actin and Inhibits Myosin and Cofilin Activity. *J. Mol. Biol.* 427 (20), 3273–3284. doi:10.1016/j.jmb.2015.07.026

Soroor, F., Kim, M. S., Palander, O., Balachandran, Y., Collins, R. F., Benlekbir, S., et al. (2021). Revised Subunit Order of Mammalian Septin Complexes Explains Their *In Vitro* Polymerization Properties. *Mol. Biol. Cel* 32 (3), 289–300. doi:10.1091/mbc.E20-06-0398

Surka, M. C., Tsang, C. W., and Trimble, W. S. (2002). The Mammalian Septin MSF Localizes with Microtubules and Is Required for Completion of Cytokinesis. *Mol. Biol. Cel* 13 (10), 3532–3545. doi:10.1091/mbc.E02-01-0042

Tokhtaeva, E., Capri, J., Marcus, E. A., Whitelegge, J. P., Khuzakhmetova, V., Bukharaeva, E., et al. (2015). Septin Dynamics Are Essential for Exocytosis. *J. Biol. Chem.* 290 (9), 5280–5297. doi:10.1074/jbc.M114.616201

Tucker, J., Sczakiel, G., Feuerstein, J., John, J., Goody, R. S., and Wittinghofer, A. (1986). Expression of P21 Proteins in Escherichia coli and Stereochemistry of the Nucleotide-Binding Site. *EMBO J.* 5 (6), 1351–1358. doi:10.1002/j.1460-2075.1986.tb04366.x

Valadares, N. F., d' Muniz Pereira, H., Ulian Araujo, A. P., and Garratt, R. C. (2017). Septin Structure and Filament Assembly. *Biophys. Rev.* 9, 481–500. doi:10.1007/s12551-017-0320-4

Versele, M., and Thorner, J. (2004). Septin Collar Formation in Budding Yeast Requires GTP Binding and Direct Phosphorylation by the PAK, Cla4, Cla4. *J. Cel Biol.* 164 (5), 701–715. doi:10.1083/jcb.200312070

Vetter, I. R., and Wittinghofer, A. (2001). The Guanine Nucleotide-Binding Switch in Three Dimensions. *Science* 294, 1299–1304. doi:10.1126/science.1062023

Vrabioiu, A. M., Gerber, S. A., Gygi, S. P., Field, C. M., and Mitchison, T. J. (2004). The Majority of the Saccharomyces cerevisiae Septin Complexes Do Not Exchange Guanine Nucleotides. *J. Biol. Chem.* 279 (4), 3111–3118. doi:10.1074/jbc.M310941200

Weems, A., and McMurray, M. (2017). The Step-wise Pathway of Septin Hetero-Octamer Assembly in Budding Yeast. *ELife* 6, e23689. doi:10.7554/eLife.23689

Zent, E., Vetter, I., and Wittinghofer, A. (2011). Structural and Biochemical Properties of Sept7, a Unique Septin Required for Filament Formation. *Biol. Chem.* 392, 791–797. doi:10.1515/BC.2011.082

Conflict of Interest: The authors declare that the research was conducted in the absence of any commercial or financial relationships that could be construed as a potential conflict of interest.

Publisher's Note: All claims expressed in this article are solely those of the authors and do not necessarily represent those of their affiliated organizations, or those of the publisher, the editors and the reviewers. Any product that may be evaluated in this article, or claim that may be made by its manufacturer, is not guaranteed or endorsed by the publisher.

frontiers | Frontiers in Cell and Developmental Biology

ORIGINAL RESEARCH
published: 04 May 2022
doi: 10.3389/fcell.2022.836746

Proteomic Identification of Phosphorylation-Dependent Septin 7 Interactors that Drive Dendritic Spine Formation

Sujin Byeon[1†], Bailey Werner[2†], Reilly Falter[2], Kristian Davidsen[3], Calvin Snyder[2], Shao-En Ong[2] and Smita Yadav[2]*

[1]Graduate Program in Neuroscience, University of Washington, Seattle, WA, United States, [2]Department of Pharmacology, University of Washington, Seattle, WA, United States, [3]Human Biology Division, Fred Hutchinson Cancer Research Center, Seattle, WA, United States

OPEN ACCESS

Edited by:
Matthias Gaestel,
Hannover Medical School, Germany

Reviewed by:
William Trimble,
University of Toronto, Canada
Gaiti Hasan,
National Centre for Biological Sciences, India

***Correspondence:**
Smita Yadav
smitay@uw.edu

[†]These authors have contributed equally to this work and share first authorship

Specialty section:
This article was submitted to Signaling, a section of the journal Frontiers in Cell and Developmental Biology

Received: 15 December 2021
Accepted: 30 March 2022
Published: 04 May 2022

Citation:
Byeon S, Werner B, Falter R, Davidsen K, Snyder C, Ong S-E and Yadav S (2022) Proteomic Identification of Phosphorylation-Dependent Septin 7 Interactors that Drive Dendritic Spine Formation. Front. Cell Dev. Biol. 10:836746. doi: 10.3389/fcell.2022.836746

Septins are a family of cytoskeletal proteins that regulate several important aspects of neuronal development. Septin 7 (Sept7) is enriched at the base of dendritic spines in excitatory neurons and mediates both spine formation and spine and synapse maturation. Phosphorylation at a conserved C-terminal tail residue of Sept7 mediates its translocation into the dendritic spine head to allow spine and synapse maturation. The mechanistic basis for postsynaptic stability and compartmentalization conferred by phosphorylated Sept7, however, is unclear. We report herein the proteomic identification of Sept7 phosphorylation-dependent neuronal interactors. Using Sept7 C-terminal phosphopeptide pulldown and biochemical assays, we show that the 14-3-3 family of proteins specifically interacts with Sept7 when phosphorylated at the T426 residue. Biochemically, we validate the interaction between Sept7 and 14-3-3 isoform gamma and show that 14-3-3 gamma is also enriched in the mature dendritic spine head. Furthermore, we demonstrate that interaction of phosphorylated Sept7 with 14-3-3 protects it from dephosphorylation, as expression of a 14-3-3 antagonist significantly decreases phosphorylated Sept7 in neurons. This study identifies 14-3-3 proteins as an important physiological regulator of Sept7 function in neuronal development.

Keywords: dendritic spines, septin, 14-3-3, phosphoregulation, proteomics

INTRODUCTION

Septins are evolutionarily conserved cytoskeletal proteins important for diverse cellular processes including cell division, regulation of actin and microtubule dynamics, localization of scaffolding proteins, and membrane trafficking (Mostowy and Cossart, 2012). Septins structurally contain a GTP-binding domain and a variable N- and C-terminal domain, which oligomerize with each other to form symmetric filaments and higher order structures such as rings (Sirajuddin et al., 2007; Mendonça et al., 2021). In humans, there are 13 septin genes within four homology groups: *SEPT2* (*SEPT1, SEPT2, SEPT4,* and *SEPT5*), *SEPT3* (*SEPT3, SEPT9,* and *SEPT12*), *SEPT6* (*SEPT6, SEPT8, SEPT10, SEPT11*, and *SEPT14*), and *SEPT7* (*SEPT7*) (Kinoshita, 2003a). Within these septin oligomers, septins from the same group are interchangeable, suggesting potential redundancy in

their function. Notably, forming its own group, Septin7 (Sept7) is a unique and non-redundant core component of the septin complexes (Kinoshita, 2003b).

Several members of the septin family were found to be enriched in postsynaptic density (PSD) fractions in the mouse brain, by a mass spectrometry analysis, with Sept7 suggested to be the most abundant (Walikonis et al., 2000). Sept7 is expressed throughout all stages of neuronal differentiation and localizes at axonal and dendritic branching points as well as at the base of dendritic protrusions (Tada et al., 2007; Xie et al., 2007). Depletion of Sept7 leads to decreased branching of axon and dendrites both *in vitro* and *in vivo* (Tada et al., 2007; Xie et al., 2007; Hu et al., 2012; Ageta-Ishihara et al., 2013). Moreover, an increase in the number of immature dendritic filopodia was observed when Sept7 was knocked down (Tada et al., 2007). Sept7 localizes at the base of dendritic spines to create an important diffusion barrier for membrane protein entry into the dendritic spine head (Ewers et al., 2014). Furthermore, Sept7 was found to be a phosphorylation target of thousand-and-one amino acid kinase 2 (TAOK2), a serine/threonine kinase encoded by the autism risk gene *TAOK2* (de Anda et al., 2012; Yadav et al., 2017; Richter et al., 2018; Nourbakhsh et al., 2021). Phosphorylation of Sept7 by *TAOK2* at an evolutionarily conserved C-terminal tail residue T426 was shown to be essential for spine maturation. While in its unphosphorylated state Sept7 localizes to the base of dendritic spines and filopodia, when phosphorylated at T426, Sept7 relocates to the dendritic spine head (Yadav et al., 2017). Although mechanisms through which phosphorylation induces Sept7 translocation are unclear, it was found that preventing this phosphorylation leads to increased dendritic filopodia as well as mislocalization of synaptic scaffold proteins to the dendritic shaft instead of the spine. This eventually led to formation of mislocalized synapses on the dendritic shafts (Yadav et al., 2017). How phosphorylation at the conserved T426 residue on the C-terminal tail of Sept7 regulates its function is unknown. The C-terminal tail extends perpendicularly out to the axis of the oligomeric septin filament (Sirajuddin et al., 2007). This is thought to facilitate protein–protein interactions in addition to lateral associations between septin filaments (Marques et al., 2012; Finnigan et al., 2015; Finnigan et al., 2016).

Herein, we show that phosphorylation of Sept7 C-terminal tail at the T426 residue can be mediated by several members of the TAO kinase family, including TAOK1 and two distinct isoforms of TAOK2 kinase. Furthermore, Sept7 phosphorylation at T426 was found to increase during development in rat embryonic hippocampal neurons. Sept7 phosphorylation was found to be important for spine maturation, as expression of phosphomimetic Sept7 T426D in early stages of neuronal development (DIV9) leads to precocious maturation of dendritic spines. Using live confocal imaging, we show that phosphorylated Sept7 is stably associated with the dendritic spine head over time in contrast with the wild-type and phosphomutant Sept7. To identify potential mechanisms through which phosphorylated Sept7 contributes to dendritic spine maturation, we performed an unbiased proteomic screening to identify phosphorylation-dependent binding partners of Sept7. Among the identified candidate interactors were several isoforms of 14-3-3 proteins and actin-binding proteins. Since 14-3-3 proteins bind and modulate functions of phosphorylated proteins, we tested whether phosphorylated Sept7 associates with 14-3-3 proteins. Using biochemical assays, we demonstrate that phosphorylated Sept7 interacts with the 14-3-3 gamma (14-3-3γ) isoform. Furthermore, we found that 14-3-3γ is enriched in dendritic spines compared to other 14-3-3 isoforms. Finally, we found that disrupting 14-3-3 and Sept7 interaction perturbs the level of phosphorylated Sept7 and maturation of dendritic spines in neurons, revealing an important role of this interaction in regulating neuronal development.

MATERIALS AND METHODS

Antibodies and Plasmids

Antibodies used for these experiments include: anti-HA-tag (Mouse, ProteinTech, Thermo Fisher Scientific, 50–173–6,449), phospho-TAOK2 (S181) (Rabbit, R&D Systems, PPS037), GFP (Mouse, Roche, 11,814,460,001), GST (Mouse, Invitrogen, MA4-004), 14-3-3 pan isoform (Rabbit, CST, #8312), and 14-3-3 gamma (Mouse, Sigma, MA1-16587). Rabbit phospho-Septin7 (pT426) antibody was generated, as described previously (Yadav et al., 2017). Human TAOK2α was PCR amplified from pCMV-Sp6-TAOK2 plasmid (Ultanir et al., 2014) and cloned into sfGFP-C1 vector (Addgene #54579) using restriction sites HindIII and MfeI. Human TAOK2β cDNA was obtained from Transomics (#BC152413) and cloned into the sfGFP-C1 vector using the same restriction sites. Similarly, TAOK1 cDNA from Transomics (#BC144067) was inserted into the sfGFP-C1 vector using restriction enzymes. Addgene plasmids used for these experiments include: HA-14-3-3 zeta (#116888) and pcDNA3-HA-14-3-3 gamma (#13274). EYFP-Difopein and EYFP-Control were gifts from Dr. Yi Zhou (Florida State University).

Immunoprecipitation Kinase Assays

HEK293T cells were grown in Dulbecco's modified Eagle medium (DMEM) containing 10% fetal bovine serum (FBS) and 1% penicillin–streptomycin (Thermo Fisher Scientific). Expression constructs sfGFP-tagged TAOK1, TAOK2α, and TAOK2β (3 μg) were transfected with JetOptimus, following the manufacturer's instructions. After 24 h post-transfection, cells were collected and incubated in HKT lysis buffer (25 mM HEPES pH 7.2, 150mM KCl, 1% Triton X-100, 2 mM DTT, and 1X protease inhibitor (Roche, cOmplete™ EDTA free)) for 30 min on ice prior to homogenization with a 25-gauge syringe needle. Pierce™ Protein G Agarose beads (Thermo Fisher Scientific) were washed with HKT buffer thrice. The supernatant was collected from cell lysates through centrifugation at 800g for 5 min, precleared with Protein G Agarose beads for 30 min, and immunoprecipitated with the GFP antibody overnight at 4°C. Beads were washed with HKT buffer twice, incubated with high salt HKT buffer (25 mM HEPES pH 7.2, 1M NaCl, 1% Triton X-100, 2 mM DTT, and 1X protease inhibitor (Roche, cOmplete™ EDTA free)) for 10 min, and washed with HK buffer (25 mM HEPES, 150mM KCl, 2 mM

DTT, and 1X protease inhibitor (Roche, cOmplete™ EDTA free)) twice and then with kinase buffer (20 mM Tris HCl pH 7.5, 10 mM MgCl2, 1 mM DTT, 1X protease inhibitor (Roche, cOmplete™ EDTA free)) twice at 4°C. Kinase assay was performed by incubating the beads with the kinase buffer, 1 mM ATP, and 10X phosphatase inhibitor (Thermo Fisher Scientific, Halt) at 30°C for 45 min at 920 rpm. To assay for phosphorylation of Septin7 by TAO kinases, purified GST-tagged Sept7 C-terminal tail (321–438 amino acids) was also added to the reaction. Samples were prepared by adding NuPAGE™ LDS sample buffer (Thermo Fisher Scientific) containing 125 mM DTT, heating for 10 min at 95°C, and centrifuging at 5,000g for 5 min. Samples were run on NuPAGE™ 4–12% bis-tris polyacrylamide gels (Thermo Fisher Scientific) with NuPAGE™ MOPS running buffer (Thermo Fisher Scientific) at 165 V for 20 min and then at 175 V for 50 min. Gels were transferred to Immobilon-P membrane at 100 V for 1 h. The blots were blocked with 5% BSA blocking buffer and probed with phospho-TAO2 (S181) and phospho-Sept7 (T426) antibodies at 1:500 dilution overnight at 4°C followed by 3 h incubation with HRP-conjugated secondary antibody at 1:5,000 dilution at room temperature. The kinase activity was quantified by normalizing phospho-TAOK2 signal intensity to that of the GFP signal and phospho-Sept7 signal intensity to that of the GST signal.

Protein Purification

Septin 7 C-terminal tail (321–438 amino acids) was cloned into pGEX4T1 vector using restriction sites BamHI and XhoI and transformed into the BL21 *E. coli* bacterial strain to bacterially express GST-tagged Sept7C-WT (Yadav et al., 2017). A 25 ml starter culture grown from a single colony overnight was used to inoculate 1 L culture, which was allowed to grow at 37°C until OD600 reached 0.6. Protein expression was induced by adding IPTG at the final concentration of 0.3 mM and growing the culture for additional 5 h at 30°C. Cells were harvested by centrifugation at 4500 g for 15 min at 4°C, washed with ice-cold PBS, and then resuspended in lysis buffer (50 mM Tris pH 8.0, 5 mM EDTA, 150 mM NaCl, 10% glycerol, 5 mM DTT, 1X protease inhibitor (Roche, cOmplete™ EDTA free), and 2 mM PMSF). To further lyse the cells, they were incubated with 4 mg of lysozyme on ice for 30 min followed by addition of 0.5% Triton X-100 and sonication. The supernatant was collected after a 30-min spin at 25,000 g and incubated with prewashed GST beads (Thermo Fisher Scientific) for 2 h. Beads were washed with wash buffer (PBS + 1 mM DTT +0.1% Tween 20) and then with wash buffer without detergent. Bound protein were eluted and collected in fractions by glutathione elution buffer at pH 8.0 (50 mM Tris pH 8.0, 250 mM KCl, 1 mM DTT, and 25 mM glutathione).

Co-Immunoprecipitation

Co-immunoprecipitation assays were performed in HEK293T cells grown in DMEM media (Thermo Fisher Scientific, Gibco) with 10% fetal bovine serum (Axenia) and 1% penicillin–streptomycin (Invitrogen). Cells were grown to confluence in a flat-bottom plate with 35-mm deep wells at 5% CO_2 and 37°C and transfected with 2.0 μg of HA-14-3-3 gamma, HA-14-3-3 zeta, or 1.5 μg of both gamma and zeta using JetOptimus, following the manufacturer's instructions. Cells were co-transfected with 1.0 μg of GFP-tagged Sept7-WT. Approximately 36 h post-transfection, cells were treated with 0.1 μM okadaic acid for 10 min and lysed with 1 ml HKT buffer (25 mM HEPES pH7.2, 100 mM KCl, 1% Triton X-100, 1 mM DTT, 1 mM EDTA, phosphatase inhibitor (Thermo Fisher Scientific, Halt), and protease inhibitor (Roche, cOmplete™ EDTA free)) per 2-well construct. Lysate was incubated on ice for 20 min prior to homogenization with a 25-gauge syringe needle. Homogenate was pelleted via centrifugation at 6,000 g and 4°C for 5 min. Pierce™ Protein G Agarose (Thermo Fisher Scientific) beads and EZview™ Red Anti-HA Affinity Gel (Millipore-Sigma) beads were washed twice for 5 min at 4°C and re-suspended in 150 μL HKT per sample tube. Pellet supernatant was pre-cleared with 20 μL Pierce™ Protein G Agarose (Thermo Fisher Scientific) beads, and pre-cleared supernatant was collected for input samples. Remaining volume of pre-cleared supernatant was immunoprecipitated with 20 μL EZview™ Red Anti-HA Affinity Gel (Millipore-Sigma) beads. Beads were washed three times with HKT and twice with HK buffer (25 mM HEPES pH 7.2, 100mM KCl, 1 mM DTT, and 1 mM EDTA). Both immunoprecipitation and input samples were prepared with 4X LDS sample buffer (Thermo Fisher Scientific) and 125 mM DTT followed by heat treatment at 95°C for 10 min. Samples were centrifuged at 14,000g for 5 min at 4°C and electrophoresed on NuPAGE™ 4–12% bis-tris polyacrylamide gels (Thermo Fisher Scientific) with NuPAGE™ MOPS running buffer (Thermo Fisher Scientific) for 40 min at 160 V.

Neuronal lysates were prepared at DIV18 with HKT buffer (25 mM HEPES pH7.2, 100 mM KCl, 1% Triton X-100, 1 mM DTT, 1 mM EDTA, and protease inhibitor (Roche, cOmplete). Lysates were precleared with agarose beads and then incubated with 14-3-3 gamma (mouse) or 14-3-3 pan (Rabbit)–bound sepharose beads overnight. Beads were washed thrice with HKT buffer and twice with buffer without detergent. In experiments where phosphospecific interaction was probed, Protein G beads with immunoprecipitated 14-3-3γ were incubated overnight with neuronal lysates that were prepared in 500 μL of lysis buffer (50 mM HEPES, 100 mM NaCl, 2 mM DTT, 1% TritonX100, and 1 mM $MnCl_2$) and pretreated with or without 10 μL of lambda protein phosphatase (NEB, Cat#P0753) at 30°C for an hour. Beads were then washed thrice with lysis buffer and twice with buffer without detergent before running on SDS-PAGE gels.

Western Blot

For Western blot analysis, gels were transferred to Immobilon-P PVDF membrane (Millipore-Sigma) with transfer buffer (25 mM Tris, 192 mM glycine, and 20% (v/v) Methanol) for 60 min at 100 V. Blots were cut below the 50 kDa mark to produce one half-membrane consisting of high molecular weights to detect phosphorylated Septin 7 and one half-membrane consisting of low molecular weights to detect 14-3-3 isoforms (endogenous or HA-tagged). Blots were blocked in 5% milk (5% milk powder (Carnation), 50 mM Tris-Cl, 150 mM NaCl, and 0.1% Tween™ 20 (Thermo Fisher Scientific)) or 2% BSA (2% bovine serum albumin (VWR), 50 mM Tris-Cl, 150 mM NaCl, and 0.1% Tween™ 20 (Thermo Fisher Scientific)) blocking buffer for

1 hour at room temperature and incubated in primary antibody overnight at 4°C. Primary rabbit antibody to detect phosphorylated Septin 7 (T426) was diluted to 1:250 and applied to high molecular weight half-membrane, and primary mouse antibody to detect HA-tag or endogenous 14-3-3 was diluted to 1:1,000 and applied to low molecular weight half-membrane. Blots were washed with blocking buffer at room temperature before secondary antibody incubation. Blots were incubated in HRP-conjugated secondary antibody at 1: 1,000 dilution for 3 hours at room temperature. Blots were washed successively with blocking buffer, TBST (50 mM Tris-Cl, 150 mM NaCl, and 0.1% Tween™ 20 (Thermo Fisher Scientific)), and TBS (50 mM and 150 mM NaCl). Western blot images were visualized with Pierce™ ECL Western Blotting Substrate (Thermo Fisher Scientific) and captured with the ChemiDoc Imager (Bio-Rad).

Peptide Pulldown and Mass Spectrometry

Synthetic peptide corresponding to Sept7 C-terminal tail residues 416–438 were commercially synthesized with an N-terminal cysteine residue and T426 in either phosphorylated or unphosphorylated forms (Elim Biopharmaceuticals). Peptides were coupled to SulfoLink beads (Invitrogen), according to manufacturer's protocol. In brief, 0.5 mg of peptide was dissolved in 1 ml of coupling buffer (50 mM Tris and 5 mM EDTA, pH8.5) and then TCEP was added to a final concentration of 25 mM. Beads (50 ul for each peptide) were washed four times in the coupling buffer, quenched with L-cysteine-HCl and then incubated with 100 ul of 0.5 mg/ml P15 mouse brain lysate. Beads were washed four times with lysis buffer, containing 20 mM Tris pH 7.5, 100 mM NaCl, 10 mM MgCl2, 0.5 mM DTT, 1% Triton X-100, 0.1% deoxycholic acid, and protease inhibitors (Roche), and thrice with lysis buffer without detergent. Proteins bound to beads were then denatured by adding 3x bead volumes of 8M urea/ 10 mM Tris pH 8.0 to resuspend beads. TCEP was added to a final concentration of 1 mM and incubated at room temperature for 30 min with thermomixer/slow vortex. Chloroacetamide (CAM) was added to final concentration of 3 mM and incubated at room temperature for 10 min with thermomixer/slow vortex. TCEP was added to quench excess CAM after alkylation is complete. The pH was then adjusted to 8. For protein digestion, LysC (Mass Spec Grade) at 1:100 enzyme:substrate ratio was added and incubated at 37°C for 2 h on a thermomixer with gentle agitation. Then 3x reaction volumes of TEAB was added to dilute urea to less than or equal to 2M urea. Then pH was adjusted to 8.0. Trypsin (MS grade, Promega) was added at 1:100 enzyme:substrate ratio and incubated at 37°C for 12–16 h with gentle agitation. Digestion was stopped by adding TFA to a final concentration of 1%. Peptide samples were desalted on C18 StageTips. Peptide samples were separated on an Thermo Dionex UltiMate 3000 RSLCnano System (Thermo Fisher Scientific) using 20-cm long fused silica capillary columns (100 µm ID, laser pulled in-house with Sutter P-2000, Novato CA) packed with 3 µm 120 Å reversed phase C18 beads (Dr. Maisch, Ammerbuch, DE). Liquid chromatography (LC) solvent A was 0.1% (v/v) aq. Acetic acid and LC solvent B was 20% of 0.1% (v/v) acetic acid and 80% acetonitrile. The LC gradient was 100-min long with 5–35% B at 300 nL/min. MS data was collected using an Orbitrap Elite mass spectrometer (Thermo Fisher Scientific).

Mass Spectrometry Data Analyses

Data-dependent analysis was applied using top15 selection with CID fragmentation. Data raw files were analyzed by MaxQuant/ Andromeda (Cox et al., 2011) version 1.6.2.8 using protein, peptide, and site FDRs of 0.01, a score minimum of 40 for modified peptides and 0 for unmodified peptides, and a delta score minimum of 17 for modified peptides and 0 for unmodified peptides. MS/MS spectra were searched against the UniProt mouse database (updated July 2016). MaxQuant search parameters are as follows: variable modifications included Oxidation (M) and Phospho (S/T/Y). Carbamidomethyl (C) was a fixed modification. Maximum missed cleavages were 2, enzyme was trypsin/P, and maximum charge was 7. The initial search tolerance for FTMS scans was 20 ppm and 0.5 Da for ITMS MS/MS scans. Label-free quantification (LFQ) of MS intensities from five process replicates/condition was processed with Perseus. Protein groups were filtered to remove proteins 'only identified by site' as well as reverse and potential contaminants. MS intensities were log2 transformed, and missing values were imputed by randomly selecting from a distribution downshifted by 1.8 and a width of 0.3. Significance was calculated by a two-sample Student's t-test.

MS raw data (ID MSV000088699) is publicly available at repository UCSD Massive database and can be accessed freely at https://massive.ucsd.edu.

Immunofluorescence

Rat embryonic hippocampal neurons were grown on coverslips coated with 0.1M borate buffer (50 mM boric acid and 12.5 mM sodium tetraborate in water, pH 8.5), 60 ug/mL poly-D-Lysine (Sigma), and 2.5 ug/mL laminin (Sigma) in 12-well plates. For immunofluorescence, neurons were fixed with warm 4% paraformaldehyde + 4% sucrose in PBS, followed by 60-min incubation in blocking buffer (0.2% Triton X-100, 10% normal goat serum (Jackson Labs), and 0.2M glycine pH 7.2) at room temperature. Primary antibody was incubated overnight at 4°C followed by secondary antibody for 3 hours at room temperature. Coverslips were mounted on slides using Fluoromount-G.

Neuronal Culture

Hippocampi were obtained from E17–E18 Sprague Dawley rat embryos (Envigo), trypsin dissociated, and plated at a density of 150,000 cells per 18 mm coverslip (Fisher Scientific) and 50,000–500,000 cells per 35 mm glass bottom dish (MatTek). Dishes were coated as previously described. Neurons were seeded in plating media (10% fetal bovine serum heat inactivated, 20% dextrose, 1x Glutamax (Invitrogen), 1x penicillin/streptomycin (Thermo Fisher Scientific), Eagle's MEM with Earle's BBS (Lonza)) for 4 hours. Media was changed to maintenance media (B27 (Invitrogen), 1x penicillin/streptomycin, 1x Glutamax, and neurobasal media (Invitrogen)). Half of the media was replaced with new maintenance media every 3–4 days. Transfection of mammalian expression constructs in neurons was performed using Lipofectamine 2000, following the manufacturer's instructions. Neurons were either fixed for 48 h after transfection using 4% PFA+ 4% sucrose, or imaged live 48 h after transfection.

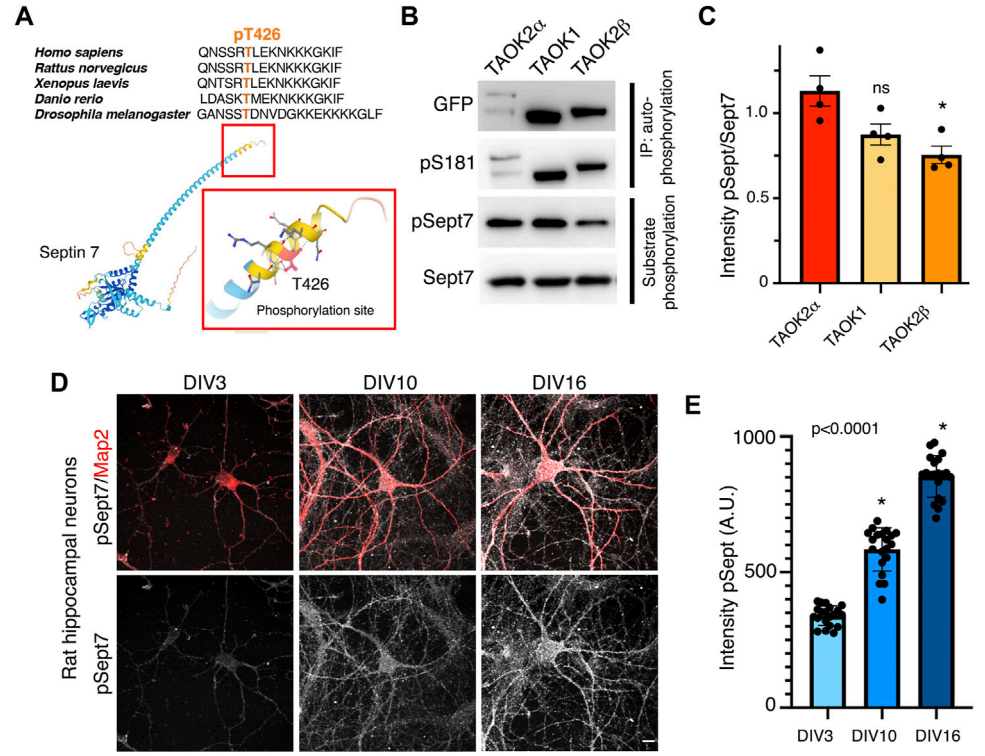

FIGURE 1 | TAO kinases phosphorylate the C-terminal tail of Sept7 during neuronal development. **(A)** Top: multiple sequence alignment of the C-terminal tail of Sept7 demonstrating its evolutionarily conserved sequence including the phosphorylation site. The phosphorylated residue T426 is shown in orange. Bottom: AlphaFold2.0 predicted protein structure of Sept7. Magnified inset depicts the T426 phosphorylation site (red) in the C terminal tail of Sept7. **(B)** Western blot shows kinase activity of sfGFP-TAOK2α, sfGFP-TAOK1, or sfGFP-TAOK2β expressed in HEK293T cells, immunoprecipitated with GFP antibody, and incubated with purified GST-Sept7 C-terminal tail (321–438 amino acids) for an *in vitro* kinase reaction. Substrate phosphorylation was determined by probing for phosphorylated Sept7 using the pT426 antibody. Total Sept7 was detected by antibody against GST tag. TAO kinase autophosphorylation was determined by probing for phosphorylated S181 residue. **(C)** Quantification of protein band intensity of Western blot in **(B)**. Bar graph displays the ratio of phosphorylated Sept7 band intensity to GST band intensity for each TAO kinase construct in which no significant difference was observed between TAOK2α and TAOK1 kinases. Error bars represent standard error of mean from $n = 4$ experiments. **(D)** Rat hippocampal neurons at DIV3, 10, and 16 were fixed and immunostained for endogenous phosphorylated Sept7 T426 and dendritic protein Map2. Scale bar represents 10 μm. **(E)** Mean fluorescence intensity of phosphorylated Sept7 T426 at distinct stages of neuronal development DIV3, 10, and 16 are plotted. Error bars represent standard error of mean for $n = 20$ neurons from three different experiments. Dunnett's multiple comparison shows significant changes in pSept7 levels between each stage.

Microscopy and Image Analyses

All live and fixed cell imaging was performed using a Nikon Ti2 Eclipse-CSU-X1 confocal spinning disk microscope equipped with four laser lines 405, 488, 561, and 670 nm and a sCMOS Andor camera for imaging. The microscope was caged within the OkoLab environmental control setup enabling temperature and CO_2 control during live imaging. Imaging was performed using Nikon 1.49 ×100 Apo, ×60, or ×40 oil objectives. All image analyses were done using the open access Fiji software.

Statistics

All statistics except for the mass spectrometry data were performed in GraphPad software Prism 9.0. Two group comparisons were made using unpaired *t*-test, unless otherwise stated. Statistically, p-value less than 0.05 was considered significant. All experiments were done in triplicate, unless stated otherwise, and experimental sample size and p-values are indicated with the corresponding figures.

RESULTS

Conserved C-Terminal Tail in Septin 7 is Phosphorylated by TAO Kinases During Neuronal Development

Sept7 was identified through an unbiased chemical and genetic screening as a phosphorylation target of TAOK2 (Yadav et al., 2017). The site of phosphorylation residue T426 lies in the extended C-terminal coiled coil tail of Sept7. This threonine residue which harbors the consensus site for TAO kinases p[S/T]-X-X[R/H/K] is evolutionarily highly conserved (**Figure 1A**). Members of thousand-and-one amino acid kinase (TAOK) family contain a highly conserved N-terminal kinase domain, while their C-terminal domains considerably vary (**Supplementary Figure S1A**). TAO kinases, TAOK1 and spliced isoforms of TAOK2, α and β, are highly expressed in the brain (de Anda et al., 2012 and Allen Brain Atlas), and both TAOK1 and TAOK2 have been associated

with neurodevelopmental disorders (Richter et al., 2018; Dulovic-Mahlow et al., 2019; van Woerden et al., 2021). TAOK2, both α and β, as well as TAOK1 have been shown to be important for several aspects of neuronal development including dendritic spine formation (Yasuda et al., 2007; Ultanir et al., 2014; Yadav et al., 2017; van Woerden et al., 2021). Recently, we discovered that TAOK2α is an endoplasmic reticulum–associated kinase with a transmembrane C-terminal region (Nourbakhsh et al., 2021). Given the structural conservation among the kinase domain of TAO kinases and their high expression in the brain (Hu et al., 2021), we tested whether closely related kinase TAOK1 and the alternatively spliced isoforms of TAOK2, TAOK2α, and TAOK2β could also phosphorylate Sept7 at T426. GFP-tagged TAOK1, TAOK2α, and TAOK2β were expressed independently in HEK293T cells, immuno-precipitated using GFP antibody and then incubated with purified GST-Septin7 protein (**Supplementary Figure S1B**) in an *in vitro* kinase reaction. Using a phosphospecific antibody (pT426) against the Sept7 T426 residue, we found that TAOK1, TAOK2α, and TAOK2β could each phosphorylate purified GST-Sept7 (**Figures 1B,C**). All of the immunoprecipitated TAO kinases were active as they could autophosphorylate themselves on the conserved residue S181 (TAOK1-2) in the kinase domain. Level of Sept7 phosphorylation by TAOK2α was significantly higher than that by TAOK2β, while phosphorylation by TAOK1 was not statistically different from TAOK2α. Furthermore, by immunostaining cultured hippocampal neurons at different stages of development, we found that phosphorylated Sept7 (T426) levels increased in neurons as it matured from DIV3 and DIV10 to DIV16 (**Figures 1D,E**). This is consistent with the increase in TAOK1, TAOK2α, and β expression in the mouse cortex from embryonic stages to the perinatal stage which then persists throughout adulthood (de Anda et al., 2012 and Allen Brain Atlas). These data suggest that the conserved family of TAO kinases show redundancy in Septin7 phosphorylation, where depending on the cellular context potentially multiple kinases of the TAO family can phosphorylate Sept7 C-terminal tail.

Altered Dynamics of Phosphorylated Septin 7

We had previously reported that phosphorylated Sept7 is enriched in the dendritic spine head and is important for dendritic spine formation and stability of PSD95 (Yadav et al., 2017). Expression of Sept7 phosphomutant T426A leads to failure of dendritic spine maturation, resulting in exuberant dendritic filopodia and shaft synapses (Yadav et al., 2017). To test the role of Sept7 phosphorylation during neuronal maturation, we expressed wild-type (WT), phosphomimetic (T426D), and phosphomutant (T426A) Sept7 in DIV9 neurons and imaged them at DIV11, a developmental stage where filopodial protrusions have not yet developed into mature mushroom dendritic spines. We found that expression of GFP-tagged phosphomimetic Sept7 (T426D) as opposed to WT Sept7 led to early maturation of dendritic spines in hippocampal neurons (**Figure 2A**). In contrast, expression of phosphomutant Sept7 T426A as expected resulted in extensive filopodial protrusions (**Figure 2A**). We found that even at this early stage of development at DIV11, there was accumulation of GFP-Sept7 in dendritic spines in neurons expressing phosphomimetic Sept7 T426D. We performed confocal live imaging of neurons expressing either the wild-type (WT), phosphomimetic (T426D), or phosphomutant (T426A) GFP-tagged Sept7. Live imaging of dendritic protrusions at DIV11 revealed that wild-type GFP-Sept7 exhibited dynamic changes in its accumulation within the filopodial protrusions within 10 s time period. In contrast, phosphomimetic Sept7 (T426D) remained stably localized within the dendritic spine head, while the phosphomutant Sept7 (T426A) predominantly was localized at the base of the dendritic spine (**Figure 2B**, montage over 10 s). Quantification of Sept7 intensity in dendritic protrusions in DIV11 neurons revealed a significant increase in Sept7 T426D expressing neurons compared to WT, while there was a dramatic decrease in intensity of Sept7 T426A compared to WT (n = 50 protrusions, 12 neurons from three experiments, and one way ANOVA). Based on these data showing distinct localization and dynamics of Sept7 in its phosphorylated and unphosphorylated states at residue T426, we hypothesized that there must be unique interaction partners of phosphorylated Sept7 that modulate its discrete properties.

Proteomic Identification of Septin 7 Phosphorylation-Dependent Binding Partners

We set out to identify proteins that specifically interact with Sept7 following phosphorylation at residue T426 in its C-terminal tail. This was achieved using an unbiased proteomic strategy to pull down proteins from P15 mouse brain lysate with a synthetic peptide corresponding to Sept7 C-terminal tail residues 416–438 (**Figure 3A**). This peptide of 22 amino acids was unique to Sept7, as BLAST analyses did not identify any other protein harboring this sequence. Next, the phosphorylated (pSept7) and non-phosphorylated (Sept7) peptides were coupled to beads. Agarose beads activated with iodoacetamide were used for covalent immobilization of peptides corresponding to pSept7 and Sept7 peptides. Peptide coupled beads were then incubated with mouse brain lysate. Proteins that were bound to peptide beads were enzymatically digested and then subjected to mass spectrometry-based identification. Label free quantification was used to measure the relative abundance of proteins bound to Sept7 and pT426-Sept7 (**Figure 3A**). In our analyses of five replicates of peptide pulldowns, we found 33 proteins (**Table 1**) that were significantly associated with phosphorylated Septin 7 peptide over unphosphorylated peptide (**Figure 3B**). These proteins were analyzed by STRING11.2 and the most significant biological process was identified as regulation of cytoskeletal organization including actin-binding proteins as well as the phosphoprotein regulating proteins of the 14-3-3 family (**Figures 3C,D**). The 14-3-3 protein family is a group of highly conserved acidic proteins highly expressed in the mammalian brain (Boston et al., 1982; Ferl et al., 2002). In humans, there are seven known isoforms of 14-3-3: β, γ, ε, η, δ, τ, and ζ (Gardino et al., 2006). 14-3-3 proteins are ubiquitous regulatory proteins that form both homo- and heterodimers, and their dimerization provides binding sites for association with one or two phosphorylated 'client' proteins (Gardino et al., 2006; Uhart and Bustos, 2013). Among the candidate pSept7-binding partners identified by our mass spectrometry experiment (**Figure 3C**), we were specifically interested in 14-3-3 proteins as 1) binding of 14-3-3 proteins is largely determined by phosphorylation of the client, with the isoforms typically binding phosphorylated

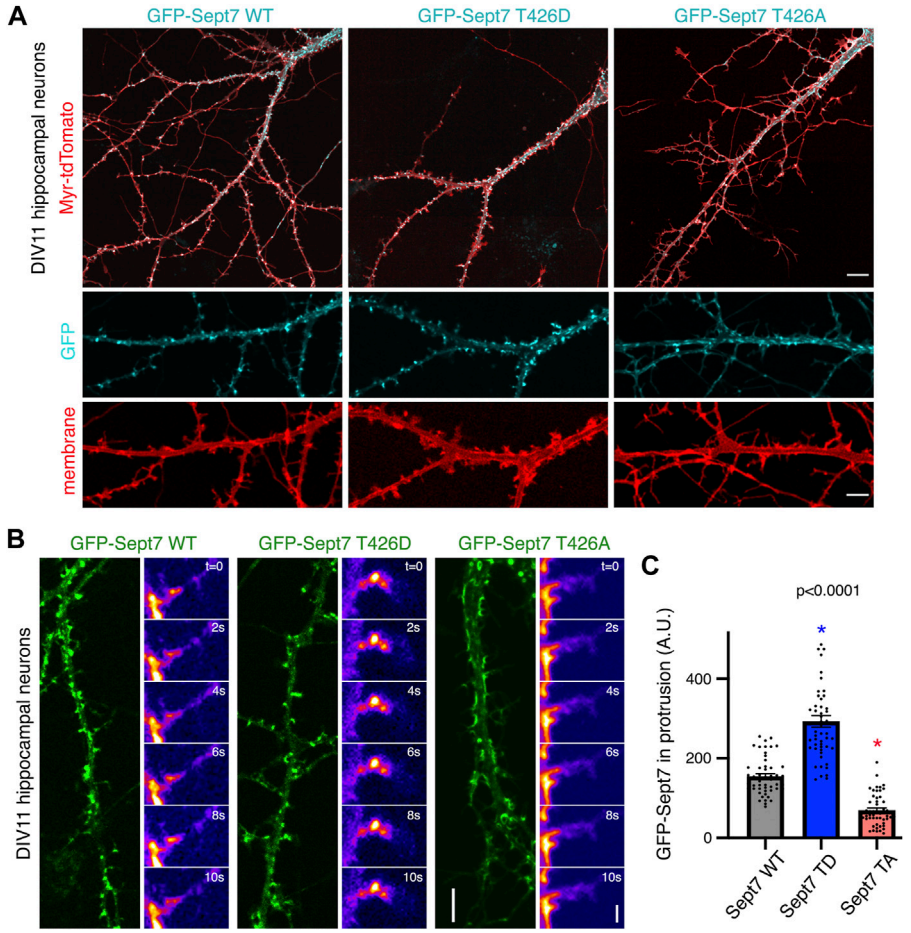

FIGURE 2 | Phosphorylation of Sept7 alters its localization and dynamics. **(A)** Hippocampal neurons were transfected with GFP-tagged Sept7-WT, phosphomimetic Sept7-T426D, or phosphomutant Sept7-T426A along with membrane marker myristoylated-tdTomato at DIV9 and then fixed at DIV11. Phosphomimetic GFP-Sept7 (T426D) expression leads to early maturation of dendritic spines compared to Sept7-WT, while phosphomutant Sept7-T426A expressing neurons exhibited only filopodial protrusions. **(B)** Montage of time lapse images showing DIV11 hippocampal neurons transfected at DIV9 with GFP-tagged wild-type Sept7-WT, phosphomimetic Sept7-T426D, or phosphomutant Sept7-T426A. Phosphomimetic Sept7-T426D is stably localized within the dendritic spine head, phosphomutant Sept7-T426A localizes to the base of the dendritic spine, whereas the wild-type Sept7-WT shows dynamic changes in its localization within protrusions. Scale bar represents 5 μm (green) and 1 μm (montage), respectively. **(C)** Quantification of GFP intensity in protrusions of DIV11 neurons transfected with GFP-tagged wild-type Sept7-WT, phosphomimetic Sept7-T426D, and phosphomutant Sept7-T426A. Values represent mean intensity, error bars represent SEM and $n = 50$ protrusions from 10 neurons in each condition. Dunnett's multiple comparison test, $p < 0.0001$.

serine/threonine motifs (Aitken, 1996; Fu et al., 2000); 2) 14-3-3 are expressed in the brain and important for synapse development; and 3) binding of phosphoproteins to 14-3-3 can serve diverse purposes, including preventing protein–protein interactions, scaffolding, inducing conformational changes, protecting phosphorylation sites, and promoting or preventing ubiquitination.

14-3-3 Proteins Associate with Septin 7

We next validated whether 14-3-3 proteins were *bona fide* interacting proteins of Sept7 using co-immunoprecipitation assays. Using an antibody that recognizes all isoforms of 14-3-3 (pan 14-3-3 polyclonal), we immunoprecipitated 14-3-3 proteins from neuronal lysate obtained from DIV18 cultured embryonic rat hippocampal neurons and then probed for phosphorylated Sept7 using the pT426 Sept7 antibody. We found that indeed pSept7 coimmunoprecipitated with 14-3-3 proteins from neuronal lysates (**Figure 4A**, $n = 3$ experiments). Since 14-3-3 zeta (ζ) and gamma (γ) were the isoforms most enriched in our proteomic data (**Figure 3D**), and are also highly expressed in the brain (Berg et al., 2003), we next tested if there was an interaction of these isoforms with phosphorylated Sept7. We co-expressed HEK293T cells with GFP-Sept7 along with either HA-tagged 14-3-3 zeta, 14-3-3 γ, or both isoforms together. Using the HA antibody, we pulled down the 14-3-3 isoforms and then probed for phosphorylated Sept7 using the pT426 antibody. We found that pSept7 co-immunoprecipitated strongly with 14-3-3 γ and 14-3-3(ζ + γ) but not 14-3-3ζ (**Figure 4B**, $n = 4$ experiments). Furthermore, using a gamma isoform specific antibody, we found that endogenous 14-3-3γ from neuronal lysates co-immunoprecipitated pSept7 (**Figure 4C**, $n = 3$). Next, we tested whether the interaction between Sept7 and

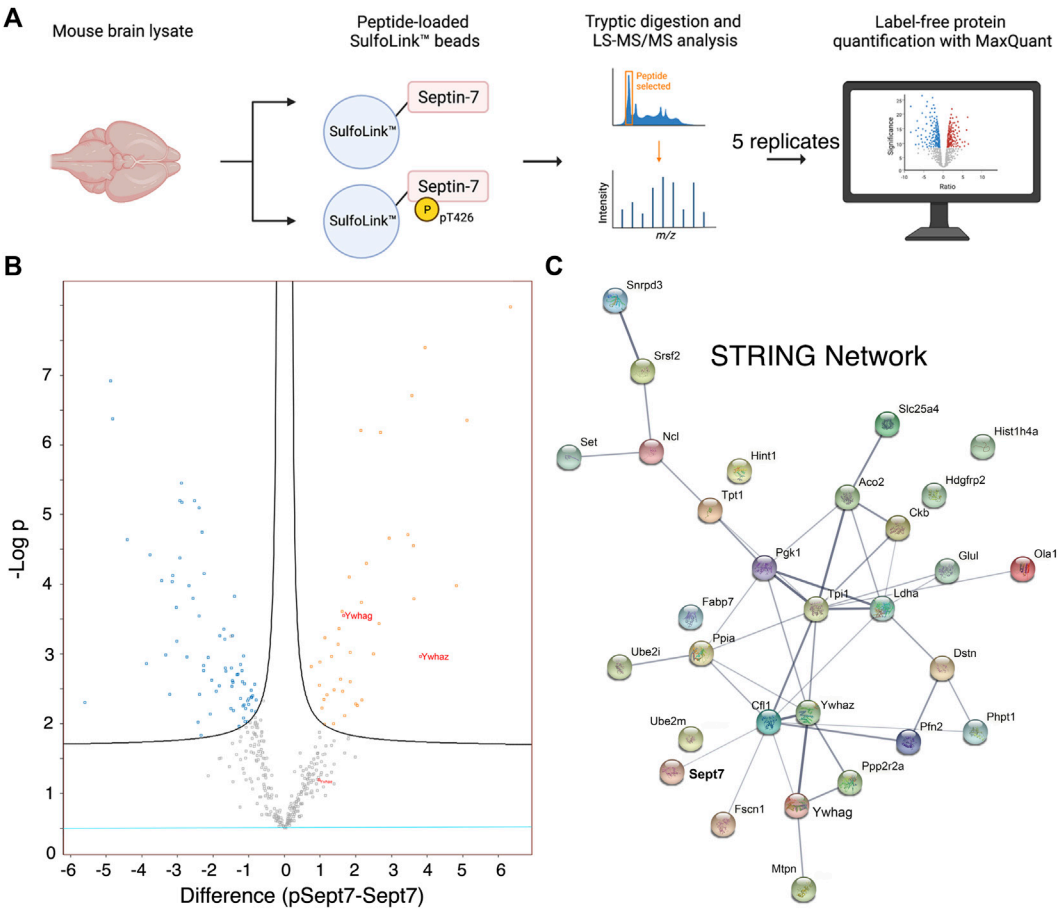

D

Gene	Protein	Function
Ywhag	14-3-3 gamma	Binds phosphoS/T proteins to modulates their activity
Ywhaz	14-3-3 zeta	Binds phosphoS/T proteins to modulates their activity
Cfl1	Cofilin-1	Binds to F-actin and depolymerizes actin
Fscn1	Fascin	Regulates organization of actin filament bundles
Mtpn	Myotrophin	Inhibits F-actin-capping protein complex
Pfn2	Profilin-2	Binds to actin and affects polymerization of actin
Dstn	Destrin	Actin-depolymerizing protein

FIGURE 3 | Proteomic identification of Septin 7 phosphorylation-dependent binding partners. **(A)** Workflow shows the proteomic strategy for identifying Sept7 phosphorylation-dependent binding partners. **(B)** Volcano plot displays the difference in association of proteins with phosphorylated (pT246) Sept7 versus unphosphorylated Sept7 based on five replicate pulldowns. 14-3-3 protein isoforms are labeled in red. **(C)** The protein–protein association network of candidate pSept7 interaction partners. The STRING network of identified proteins that significantly associate with phosphorylated Sept7 tail (pT426) versus non-phosphorylated Sept7 tail. Network nodes represent interacting proteins, and network edges indicate both functional and physical protein associations. Strength of the association is denoted by the thickness of the edges. **(D)** 14-3-3 family of proteins as well as several actin binding and depolymerizing proteins were found to significantly associate with Sept7 when phosphorylated at T426.

14-3-3γ was dependent on phosphorylation. Neuronal lysates at DIV18 were either treated with lambda protein phosphatase or buffer and then incubated with immunoprecipitated 14-3-3γ. When immunoprecipitates were then probed for the presence of total Sept7, we found that while in untreated condition Sept7 bound 14-3-3γ, this interaction was not detected when lysate was treated with protein phosphatase (**Figure 4D**, $n = 3$). These data suggest that the interaction between Sept7 and 14-3-3γ is phosphorylation dependent. Next, to determine the effect of expression of different 14-3-3 isoforms on dendritic spine maturation, we co-expressed HA-tagged 14-3-3γ and 14-3-3ζ along with membrane marker myr-tdTomato in cultured DIV12 hippocampal neurons. Neurons were fixed at DIV14 and stained with anti-HA antibody to visualize the localization of overexpressed 14-3-3 proteins (**Figure 4E**). In neurons overexpressing HA-14-3-3γ, about 52% of protrusions were spiny mushroom mature spines, while 42% of protrusions were spiny in neurons expressing HA-14-3-3ζ (**Figure 4F**). Interestingly, HA-14-3-3γ was enriched in dendritic spines with a spine/dendrite ratio of 1.2,

TABLE 1 | List of proteins identified by Mass Spectrometry that associate with Septin 7 when phosphorylated at residue T426.

Protein name	Gene	Function
14-3-3 protein gamma	Ywhag	Binds phospho S/T proteins and modulates their of activity
14-3-3 protein zeta/delta	Ywhaz	Binds phospho S/T proteins and modulates their of activity
Myotrophin	Mtpn	Regulates growth of actin filaments. Inhibits the activity of the F-actin-capping protein complex
Destrin	Dstn	Actin-depolymerizing protein. Severs actin filaments (F-actin) and binds to actin monomers (G-actin)
Fascin	Fscnl	Organization of actin filament bundles and the formation of microspikes and stress fibers
Profilin-2	Pfn2	Binds to actin and affects the structure of the cytoskeleton
Cofilin-1	Cfll	Binds to F-actin and exhibits F-actin depolymerizing activity
Glutamine synthetase	Glul	Catalyzes the production ofglutamine and 4-am inobutanoate (gamma-aminobutyric acid, GABA)
Histidine triad nucleotide-binding protein 1	Hintl	Hydrolyzes purine nucleotide phosphoramidates
Triosephosphate isomerase	Tpil	Triosephosphate isomerase 1
Eukaryotic translation initiationfactor 5A-1; 5A-2	Eif5a; Eif5a2	mRNA-binding protein involved in translation elongation
Fatty acid-binding protein, brain	Fabp7	Belongs to the calycin superfamily
Translationally-controlled tumor protein	Tptl	Involved in calcium binding and microtubule stabilization
Heterogenous nuclear ribonucleo protein A3	Gm6793; Gm9242; Hnrnpa3	Plays a role in cytoplasmic trafficking of RNA
SUMO-conjugating enzyme UBC9	Ube2i	Necessary for sumoylation
Protein SET	Set	Multitasking protein, involved in apoptosis, transcription, and histone chaperoning
Guanine nucleotide-binding protein G(I)/G(S)/G(T) subunit beta-1; beta-2; beta-4	Gnb1; Gnb2; Gnb4	Guanine nucleotide-bind ing proteins act as a modulator in various transmembrane signaling events
NEDD8-conjugating enzyme Ubc12	Ube2m	Ubiquitin conjugating enzyme
Ubiquitin-conjugating enzyme E2 D2; Ubiquitin-conjugating enzyme E2 D3; D2B	Ube2d2; Ube2d3; Ube2d2b	Ubiquitin conjugating enzyme
Serine/threonine-protein phosphatase 2A 55 kDa regulatory subunit B alpha isoform	Ppp2r2a	Protein Phosphatase
Serine/arginine-rich splicing factor 2	Srsf2	Necessary for thesplicing of pre-mRNA
ADP/ATP translocase 1	Slc25a4	Involved in mitochondrial ADP/ATP transport
Peptidyl-prolyl cis-trans isomerase A; Peptidyl-prolyl cis-trans isomerase A	Ppia	PPlases accelerate the folding of proteins
14 kDa phosphohistidine phosphatase	Phptl	Exhibits phosphohistidine phosphatase activity
Hepatoma-derived growth factor-related protein 2	Hdgfrp2	Associates with chromatin
Histone H4	Histlh4a	Core component of nucleosome
Obg-like ATPase 1	Olal	Obg-like ATPase 1; Hydrolyzes ATP, and can also hydrolyze GTP with lower efficiency
Small nuclear ribonucleoprotein Sm D3	Snrpd3	plays an important role in the splicing of cellular pre-mRNAs
L-lactate dehydrogenase A chain	Ldha	Lactatedehydrogenase A
Phosphoglycerate kinase 1	Pgkl	Catalyzes one ofthe two ATP producing reactions in theglycolytic pathway
Aconitate hydratase, mitochondrial	Aco2	Catalyzes the isomerization of citrateto isocitrate *via* cis-aconitate
Creatine kinase B-type	Ckb	Reversibly catalyzes thetransfer of phosphate between ATP and various phosphogens
Nucleolin	Ncl	Induces chromatin decondensation by binding to histone H1

whereas HA-14-3-3ζ primarily localized to the dendritic shaft and was not enriched in the spine head (**Figure 4G**). In summary, we found that Sept7 interacts with 14-3-3γ in a phosphorylation-dependent manner. Furthermore, overexpression of 14-3-3γ but not the zeta isoform leads to its enrichment in the dendritic spine head and enhances spine maturation.

Sept7 Association With 14-3-3 Protects its Phosphorylation at T426

To test the functional consequence of 14-3-3 association with phosphorylated Sept7, we utilized a genetically expressed inhibitor of 14-3-3, EYFP-Difopein (dimeric 14-3-3 peptide inhibitor). This construct EYFP-Difopein is based on R18, a Raf-1–derived phosphopeptide, which is a high-affinity peptide antagonist of 14-3-3 proteins (Wang et al., 1999). Difopein is composed of two R18 coding sequences separated by a sequence coding for a short peptide linker in an EYFP fusion mammalian vector. Expressed Difopein is capable of disrupting 14-3-3/ligand binding (Masters and Fu, 2001). Difopein binds 14-3-3 without any isoform selectivity and thereby inhibits the interaction of all 14-3-3 isoforms with their physiological binding partners (Qiao et al., 2014). We transfected DIV14 hippocampal neurons with either control EYFP construct or EYFP-Difopein construct and then measured the levels of pSept7 in neurons fixed at DIV16 (**Figure 5A**). Quantification of pSept7 intensity in the soma of neurons expressing Difopein showed a significant

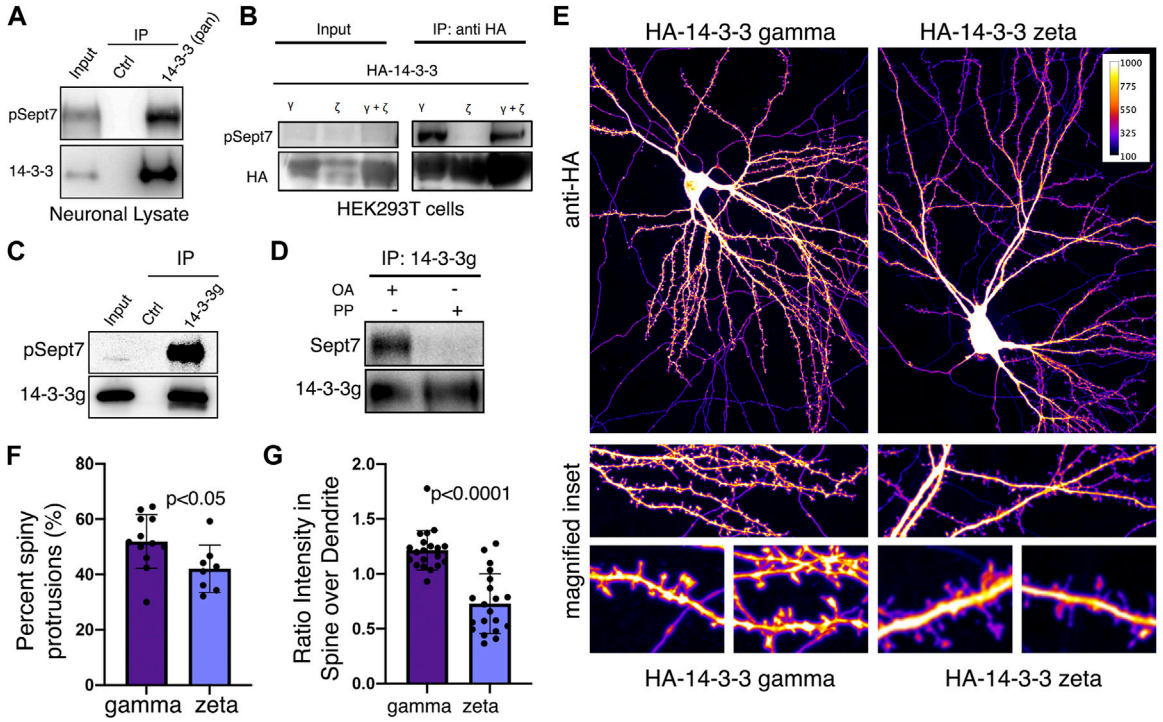

FIGURE 4 | 14-3-3γ associates with phosphorylated Sept7 and enhances dendritic spine maturation. **(A)** Western blot of endogenous 14-3-3 protein in DIV18 hippocampal neurons immunoprecipitated with 14-3-3 (pan) antibody and probed for 14-3-3 and phosphorylated Sept7 (pT426) ($n = 3$ experiments). **(B)** Western blot of HA-14-3-3γ, HA-14-3-3ζ, or both HA-tagged isoforms co-expressed along with GFP-Sept7 in HEK293T cells immunoprecipitated with HA antibody and probed for HA and phosphorylated Sept7 (pT426). Phosphorylated Sept7 co-immunoprecipitated with HA-14-3-3γ and HA-14-3-3(ζ+γ) but not HA-14-3-3ζ ($n = 3$ experiments). **(C)** Western blot shows coimmunoprecipitation of phosphorylated Sept7 with endogenous 14-3-3γ. Lysate from DIV18 hippocampal neurons immunoprecipitated with 14-3-3 (gamma) antibody and probed for 14-3-3γ and phosphorylated T426 Sept7 ($n = 3$ experiments). **(D)** Western blot shows phosphorylation dependent interaction of Sept7 with endogenous 14-3-3γ. DIV18 hippocampal neurons were treated with okadaic acid (OA) or DMSO, and lysate treated with or without lambda protein phosphatase (PP) were then immunoprecipitated with 14-3-3 (gamma) antibody and probed for 14-3-3γ and total Sept7 ($n = 3$ experiments). **(E)** Fixed images of DIV14 hippocampal neurons co-transfected with membrane marker myristoylated tdTomato and HA-14-3-3γ or HA-14-3-3ζ were immunostained for HA tag. Scale bar is 10μm, and image psuedocolored to represent fluorescence intensity. **(F)** Bar graph depicts percent of protrusions with mature, spiny morphology in DIV14 hippocampal neurons transfected with HA-14-3-3γ or HA-14-3-3ζ. HA-14-3-3γ expression results in significantly more spiny, mature protrusions ($p < 0.05$). Values indicate mean, error bars represent SEM and $n > 8$ neurons each. **(G)** Bar graph shows ratio of 14-3-3 fluorescent intensity in spines to intensity in corresponding dendritic shaft in DIV14 hippocampal neurons transfected with HA-14-3-3γ or HA-14-3-3ζ. Values indicate mean percent, error bars represent standard error of mean, and $n = 20$ spines from five neurons each.

decrease in the level of phosphorylated Sept7 compared to those expressing EYFP control, as detected by immunostaining using the pT426 Sept7 antibody (**Figure 5A**, yellow asterisk and 5B). Furthermore, neurons expressing Difopein had a dramatic decrease in density of mature mushroom spines compared to EYFP-Control transfected neurons (**Figure 5A**, middle row and 5C). These data suggest that interaction of the C-terminal tail of Sept7 with 14-3-3 proteins is protective of the phosphorylation status of Sept7 in neurons, revealing a mechanism for modulation of Sept7 function by association with 14-3-3 proteins (**Figure 5D**).

DISCUSSION

In this study, we utilize mass-spectrometry based discovery proteomics to identify binding partners that interact specifically with phosphorylated Sept7 in order to understand its role in dendritic spine development. Among the proteins we identified, we focus on the 14-3-3 family which are highly conserved phosphoprotein binding proteins that are important for brain development. We identify a specific interaction of pSept7 with 14-3-3γ (gamma) encoded by *YWHAG*. 14-3-3 gamma is highly expressed during brain development, and mainly in neurons. Our findings show that 14-3-3γ is specifically enriched in the dendritic spines, and that its expression in neurons leads to increased dendritic spine numbers.

14-3-3 proteins carry out a diverse array of functions in cellular processes, including in apoptosis (Masters and Fu, 2001), cell cycle progression (Peng et al., 1997), cytoskeletal rearrangements (Gohla and Bokoch, 2002), and neuronal growth (Cornell and Toyo-oka, 2017) that are mediated through the multitude of their phosphorylation dependent protein interactors. Accumulating evidence supports a profound role of 14-3-3 proteins in brain development. 14-3-3

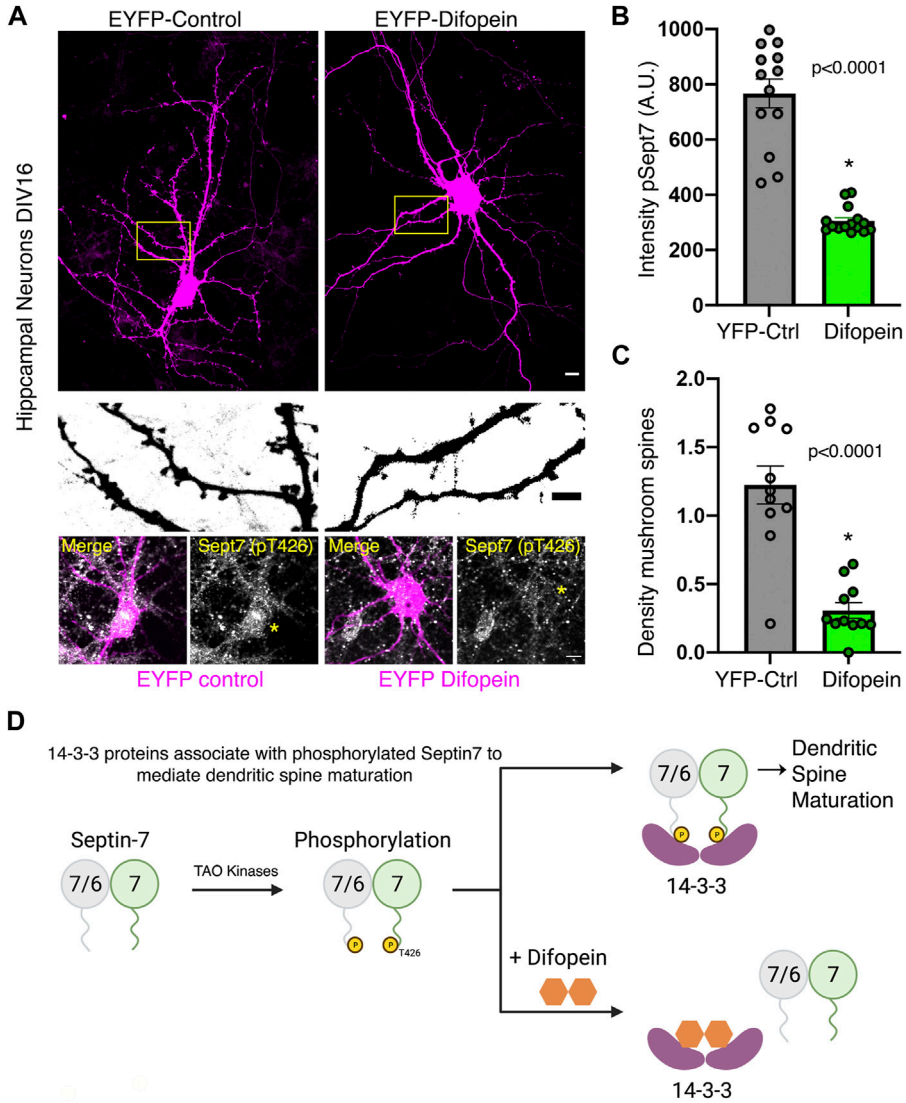

FIGURE 5 | Association with 14-3-3 protects phosphorylation state of Sept7. **(A)** Fixed images of DIV16 hippocampal neurons transfected at DIV14 with EYFP-control or EYFP-Difopein (magenta), scale bar is 10 μm. Yellow inset is magnified to highlight dendritic protrusions shown in inverted grayscale, scale bar is 5 μm. Bottom row shows levels of pSept7 immunostaining (gray) in the neuronal soma of control and difopein-transfected (magenta) neurons. Transfected neurons are depicted by yellow asterisk, and scale bar is 5 μm. **(B)** Quantification of phosphorylated Sept7 levels in the soma of DIV16 hippocampal neurons expressing YFP-control or YFP-Difopein. YFP-Difopein expression results in significantly decreased levels of phosphorylated Sept7 ($p < 0.0001$). Values indicate mean; error bars represent SEM; and $n = 13$ and 15 neurons, respectively, from three distinct experiments. **(C)** Density of mushroom spiny protrusions in DIV16 hippocampal neurons expressing YFP-control or YFP-Difopein. Values indicate mean, error bars represent SEM, and $n = 11$ neurons each from three distinct experiments. **(D)** Schematic summarizes findings of this study showing 14-3-3 protein association modulates Sept7 function in neurons through protection of its phosphorylation state.

proteins are important for neurogenesis, neuronal differentiation, and neuronal migration during cortical development (Cornell and Toyo-oka, 2017). Functional knockout of 14-3-3 proteins in mice brains with the dimeric 14-3-3 inhibitor Difopein results in reduced dendritic complexity and spine density accompanied by schizophrenia-related behaviors (Foote et al., 2015). 14-3-3 proteins are further required for hippocampal long term potentiation (LTP) and associative learning (Qiao et al., 2014), however, contribution of different 14-3-3 proteins in LTP was not ascertained. 14-3-3γ plays an important role in neuronal migration as either knockdown or overexpression of 14-3-3γ results in neuronal migration defects *in vivo* in mice (Wachi et al., 2015). Notably, 14-3-3γ expression is significantly reduced in human brain from Down Syndrome patients (Peyrl et al., 2002), indicating that perturbation of 14-3-3γ levels could contribute to disorders in human brain development. Furthermore, deletion of the *YWHAG* gene encoding 14-3-3γ is also associated with epilepsy and autistic traits in patients with atypical Williams Beuren syndrome due to deletions in 7q11.23 locus (Fusco et al., 2014).

Septins are important regulator of several aspects of neuronal development including dendrite growth, axon development and

dendritic spine maturation. Our data show that phosphorylated Sept7 associates with 14-3-3 proteins. While our mass spectrometry data indicates that isoforms gamma and zeta bind specifically with phosphorylated Sept7 C-terminal tail, we only were able to biochemically validate the interaction with 14-3-3 gamma. It remains unknown whether different isoforms can heterodimerize to associate with phosphorylated Sept7. Using peptide inhibitor Difopein, we found that blocking interaction of Sept7 with 14-3-3 led to a decrease in the level of phosphorylated Sept7, highlighting the importance of the interaction. Since Difopein quenches the blocking site for phosphoproteins in all 14-3-3 proteins, our study did not directly test isoform specific effect of blocking Sept7 interaction with 14-3-3. Contribution of phosphorylated Sept7 and hence its protection by 14-3-3 proteins in these diverse neuronal contexts will be an important area of study. Dysfunction in both 14-3-3 and septins have been associated with various diseases including neurodegenerative diseases (Ide and Lewis, 2010) (Foote and Zhou, 2012) (Marttinen et al., 2015). In addition to the 14-3-3 proteins, several actin binding proteins were also identified in our proteomic study. Cofilin, an actin binding protein important for dendritic spine maturation was identified as a phosphorylation dependent Sept7 interacting protein (Gu et al., 2010; Pyronneau et al., 2017). Notably, phosphorylated cofilin also associates with 14-3-3 proteins (Gohla and Bokoch, 2002). Further understanding the interplay of septins, actin binding proteins, and 14-3-3 proteins in dendritic spine development may provide important insights into neurodevelopment and pathophysiology underlying neurological disorders.

DATA AVAILABILITY STATEMENT

The original contributions presented in the study are included in the article/**Supplementary Material**, further inquiries can be directed to the corresponding author.

ETHICS STATEMENT

The animal study was reviewed and approved by IACUC UW.

AUTHOR CONTRIBUTIONS

SB and BW contributed equally to the work including neuronal studies, biochemical assays, data analyses, and manuscript preparation. RF performed neuronal experiments, biochemical assays, and molecular biology experiments. KD and CS performed peptide pulldown and mass spectrometry experiments. SEO supervised the mass spectrometry and MS data analyses. SY designed and supervised all experiments, obtained funding, and wrote the manuscript.

FUNDING

We are grateful for research funding provided by the National Institute of Mental Health, R00MH108648 and R01MH121674 to SY. Mass spectrometry was supported by instrumentation and funding to SEO by R01GM129090.

ACKNOWLEDGMENTS

We thank Yi Zhou (Florida State University) for generously sharing the EYFP-Difopein and its negative control expression constructs.

SUPPLEMENTARY MATERIAL

The Supplementary Material for this article can be found online at: https://www.frontiersin.org/articles/10.3389/fcell.2022.836746/full#supplementary-material

REFERENCES

Ageta-Ishihara, N., Miyata, T., Ohshima, C., Watanabe, M., Sato, Y., Hamamura, Y., et al. (2013). Septins Promote Dendrite and Axon Development by Negatively Regulating Microtubule Stability via HDAC6-Mediated Deacetylation. *Nat. Commun.* 4, 2532. doi:10.1038/ncomms3532

Aitken, A. (1996). 14-3-3 and Its Possible Role in Co-Ordinating Multiple Signalling Pathways. *Trends Cell Biol.* 6 (9), 341–347. doi:10.1016/0962-8924(96)10029-5

Almeida Marques, I., Valadares, N. F., Garcia, W., Damalio, J. C. P., Macedo, J. N. A., Araújo, A. P. U., et al. (2012). Septin C-Terminal Domain Interactions: Implications for Filament Stability and Assembly. *Cell Biochem. Biophys.* 62, 317–328. doi:10.1007/s12013-011-9307-0

Berg, D., Holzmann, C., and Riess, O. (2003). 14-3-3 Proteins in the Nervous System. *Nat. Rev. Neurosci.* 4, 752–762. doi:10.1038/nrn1197

Boston, P. F., Jackson, P., and Thompson, R. J. (1982). Human 14-3-3 Protein: Radioimmunoassay, Tissue Distribution, and Cerebrospinal Fluid Levels in Patients with Neurological Disorders. *J. Neurochem.* 38, 1475–1482. doi:10.1111/j.1471-4159.1982.tb07928.x

Cornell, B., and Toyo-oka, K. (2017). 14-3-3 Proteins in Brain Development: Neurogenesis, Neuronal Migration and Neuromorphogenesis. *Front. Mol. Neurosci.* 10, 318. doi:10.3389/fnmol.2017.00318

Cox, J., Neuhauser, N., Michalski, A., Scheltema, R. A., Olsen, J. V., and Mann, M. (2011). Andromeda: A Peptide Search Engine Integrated into the MaxQuant Environment. *J. Proteome Res.* 10 (4), 1794–1805. doi:10.1021/pr101065j

de Anda, F. C., Rosario, A. L., Durak, O., Tran, T., Gräff, J., Meletis, K., et al. (2012). Autism Spectrum Disorder Susceptibility Gene TAOK2 Affects Basal Dendrite Formation in the Neocortex. *Nat. Neurosci.* 15, 1022–1031. doi:10.1038/nn.3141

Dulovic-Mahlow, M., Trinh, J., Kandaswamy, K. K., Braathen, G. J., Di Donato, N., Rahikkala, E., et al. (2019). De Novo Variants in TAOK1 Cause Neurodevelopmental Disorders. *Am. J. Hum. Genet.* 105, 213–220. doi:10.1016/j.ajhg.2019.05.005

Ewers, H., Tada, T., Petersen, J. D., Racz, B., Sheng, M., and Choquet, D. (2014). A Septin-dependent Diffusion Barrier at Dendritic Spine Necks. *PLoS ONE* 9, e113916. doi:10.1371/journal.pone.0113916

Ferl, R. J., Manak, M. S., and Reyes, M. F. (2002). The 14-3-3s. *Genome Biol.* 3 (7), REVIEWS3010. doi:10.1186/gb-2002-3-7-reviews3010

Finnigan, G. C., Booth, E. A., Duvalyan, A., Liao, E. N., and Thorner, J. (2015). The Carboxy-Terminal Tails of Septins Cdc11 and Shs1 Recruit Myosin-II Binding Factor Bni5 to the Bud Neck in Saccharomyces cerevisiae. *Genetics* 200, 843–862. doi:10.1534/genetics.115.176503

Finnigan, G. C., Duvalyan, A., Liao, E. N., Sargsyan, A., and Thorner, J. (2016). Detection of Protein-Protein Interactions at the Septin Collar inSaccharomyces Cerevisiaeusing a Tripartite Split-GFP System. *MBoC* 27, 2708–2725. doi:10.1091/mbc.e16-05-0337

Foote, M., and Zhou, Y. (2012). 14-3-3 Proteins in Neurological Disorders. *Int. J. Biochem. Mol. Biol.* 3 (2), 152–164.

Foote, M., Qiao, H., Graham, K., Wu, Y., and Zhou, Y. (2015). Inhibition of 14-3-3 Proteins Leads to Schizophrenia-Related Behavioral Phenotypes and Synaptic Defects in Mice. *Biol. Psychiatry* 78, 386–395. doi:10.1016/j.biopsych.2015.02.015

Fu, H., Subramanian, R. R., and Masters, S. C. (2000). 14-3-3 Proteins: Structure, Function, and Regulation. *Ann. Rev. Pharmacol. Toxicol.* 40, 617–647. doi:10.1146/annurev.pharmtox.40.1.617

Fusco, C., Micale, L., Augello, B., Teresa Pellico, M., Menghini, D., Alfieri, P., et al. (2014). Smaller and Larger Deletions of the Williams Beuren Syndrome Region Implicate Genes Involved in Mild Facial Phenotype, Epilepsy and Autistic Traits. *Eur. J. Hum. Genet.* 22, 64–70. doi:10.1038/ejhg.2013.101

Gardino, A. K., Smerdon, S. J., and Yaffe, M. B. (2006). Structural Determinants of 14-3-3 Binding Specificities and Regulation of Subcellular Localization of 14-3-3-Ligand Complexes: A Comparison of the X-Ray Crystal Structures of All Human 14-3-3 Isoforms. *Semin. Cancer Biol.* 16 (3), 173–182. doi:10.1016/j.semcancer.2006.03.007

Gohla, A., and Bokoch, G. M. (2002). 14-3-3 Regulates Actin Dynamics by Stabilizing Phosphorylated Cofilin. *Curr. Biol.* 12, 1704–1710. doi:10.1016/s0960-9822(02)01184-3

Gu, J., Lee, C. W., Fan, Y., Komlos, D., Tang, X., Sun, C., et al. (2010). ADF/Cofilin-Mediated Actin Dynamics Regulate AMPA Receptor Trafficking during Synaptic Plasticity. *Nat. Neurosci.* 13, 1208–1215. doi:10.1038/nn.2634

Hu, C., Feng, P., Yang, Q., and Xiao, L. (2021). Clinical and Neurobiological Aspects of TAO Kinase Family in Neurodevelopmental Disorders. *Front. Mol. Neurosci.* 14, 655037. doi:10.3389/fnmol.2021.655037

Hu, J., Bai, X., Bowen, J. R., Dolat, L., Korobova, F., Yu, W., et al. (2012). Septin-driven Coordination of Actin and Microtubule Remodeling Regulates the Collateral Branching of Axons. *Curr. Biol.* 22, 1109–1115. doi:10.1016/j.cub.2012.04.019

Ide, M., and Lewis, D. A. (2010). Altered Cortical CDC42 Signaling Pathways in Schizophrenia: Implications for Dendritic Spine Deficits. *Biol. Psychiatry* 68, 25–32. doi:10.1016/j.biopsych.2010.02.016

Kinoshita, M. (2003b). Assembly of Mammalian Septins. *J. Biochem.* 134, 491–496. doi:10.1093/jb/mvg182

Kinoshita, M. (2003a). The Septins. *Genome Biol.* 4, 236. doi:10.1186/gb-2003-4-11-236

Marttinen, M., Kurkinen, K. M., Soininen, H., Haapasalo, A., and Hiltunen, M. (2015). Synaptic Dysfunction and Septin Protein Family Members in Neurodegenerative Diseases. *Mol. Neurodegeneration* 10, 16. doi:10.1186/s13024-015-0013-z

Masters, S. C., and Fu, H. (2001). 14-3-3 Proteins Mediate an Essential Anti-apoptotic Signal. *J. Biol. Chem.* 276, 45193–45200. doi:10.1074/jbc.m105971200

Mendonça, D. C., Guimarães, S. L., Pereira, H. D., Pinto, A. A., de Farias, M. A., de Godoy, A. S., et al. (2021). An Atomic Model for the Human Septin Hexamer by Cryo-EM. *J. Mol. Biol.* 433, 167096. doi:10.1016/j.jmb.2021.167096

Mostowy, S., and Cossart, P. (2012). Septins: the Fourth Component of the Cytoskeleton. *Nat. Rev. Mol. Cel Biol.* 13, 183–194. doi:10.1038/nrm3284

Nourbakhsh, K., Ferreccio, A. A., Bernard, M. J., and Yadav, S. (2021). TAOK2 Is an ER-Localized Kinase that Catalyzes the Dynamic Tethering of ER to Microtubules. *Dev. Cell* 56 (24), 3321–3333.e5. doi:10.1016/j.devcel.2021.11.015

Peng, C.-Y., Graves, P. R., Thoma, R. S., Wu, Z., Shaw, A. S., and Piwnica-Worms, H. (1997). Mitotic and G 2 Checkpoint Control: Regulation of 14-3-3 Protein Binding by Phosphorylation of Cdc25C on Serine-216. *Science* 277, 1501–1505. doi:10.1126/science.277.5331.1501

Peyrl, A., Weitzdoerfer, R., Gulesserian, T., Fountoulakis, M., and Lubec, G. (2002). Aberrant Expression of Signaling-Related Proteins 14-3-3 Gamma and RACK1 in Fetal Down Syndrome Brain (Trisomy 21). *Electrophoresis* 23, 152–157. doi:10.1002/1522-2683(200201)23:1<152::aid-elps152>3.0.co;2-t

Pyronneau, A., He, Q., Hwang, J. Y., Porch, M., Contractor, A., and Zukin, R. S. (2017). Aberrant Rac1-Cofilin Signaling Mediates Defects in Dendritic Spines, Synaptic Function, and Sensory Perception in Fragile X Syndrome. *Sci. Signal.* 10, eaan0852. doi:10.1126/scisignal.aan0852

Qiao, H., Foote, M., Graham, K., Wu, Y., and Zhou, Y. (2014). 14-3-3 Proteins Are Required for Hippocampal Long-Term Potentiation and Associative Learning and Memory. *J. Neurosci.* 34, 4801–4808. doi:10.1523/jneurosci.4393-13.2014

Richter, M., Murtaza, N., Scharrenberg, R., White, S. H., Johanns, O., Walker, S., et al. (2018). Altered TAOK2 Activity Causes Autism-Related Neurodevelopmental and Cognitive Abnormalities through RhoA Signaling. *Mol. Psychiatry* 20, 1237. doi:10.1038/s41380-018-0025-5

Sirajuddin, M., Farkasovsky, M., Hauer, F., Kühlmann, D., Macara, I. G., Weyand, M., et al. (2007). Structural Insight into Filament Formation by Mammalian Septins. *Nature* 449, 311–315. doi:10.1038/nature06052

Tada, T., Simonetta, A., Batterton, M., Kinoshita, M., Edbauer, D., and Sheng, M. (2007). Role of Septin Cytoskeleton in Spine Morphogenesis and Dendrite Development in Neurons. *Curr. Biol.* 17, 1752–1758. doi:10.1016/j.cub.2007.09.039

Uhart, M., and Bustos, D. M. (2013). Human 14-3-3 Paralogs Differences Uncovered by Cross-Talk of Phosphorylation and Lysine Acetylation. *PLoS One* 8 (2), e55703. doi:10.1371/journal.pone.0055703

Ultanir, S. K., Yadav, S., Hertz, N. T., Oses-Prieto, J. A., Claxton, S., Burlingame, A. L., et al. (2014). MST3 Kinase Phosphorylates TAO1/2 to Enable Myosin Va Function in Promoting Spine Synapse Development. *Neuron* 84, 968–982. doi:10.1016/j.neuron.2014.10.025

van Woerden, G. M., Bos, M., de Konink, C., Distel, B., Trezza, R. A., Shur, N. E., et al. (2021). TAOK1 Is Associated with Neurodevelopmental Disorder and Essential for Neuronal Maturation and Cortical Development. *Hum. Mutat.* 42 (4), 445–459. doi:10.1002/humu.24176

Wachi, T., Cornell, B., Marshall, C., Zhukarev, V., Baas, P. W., and Toyo-oka, K. (2015). Ablation of the 14-3-3gamma Protein Results in Neuronal Migration Delay and Morphological Defects in the Developing Cerebral Cortex. *Devel Neurobio* 76, 600–614. doi:10.1002/dneu.22335

Walikonis, R. S., Jensen, O. N., Mann, M., Provance, D. W., Mercer, J. A., and Kennedy, M. B. (2000). Identification of Proteins in the Postsynaptic Density Fraction by Mass Spectrometry. *J. Neurosci.* 20, 4069–4080. doi:10.1523/jneurosci.20-11-04069.2000

Wang, B., Yang, H., Liu, Y.-C., Jelinek, T., Zhang, L., Ruoslahti, E., et al. (1999). Isolation of High-Affinity Peptide Antagonists of 14-3-3 Proteins by Phage Display. *Biochemistry* 38, 12499–12504. doi:10.1021/bi991353h

Xie, Y., Vessey, J. P., Konecna, A., Dahm, R., Macchi, P., and Kiebler, M. A. (2007). The GTP-Binding Protein Septin 7 Is Critical for Dendrite Branching and Dendritic-Spine Morphology. *Curr. Biol.* 17, 1746–1751. doi:10.1016/j.cub.2007.08.042

Yadav, S., Oses-Prieto, J. A., Peters, C. J., Zhou, J., Pleasure, S. J., Burlingame, A. L., et al. (2017). TAOK2 Kinase Mediates PSD95 Stability and Dendritic Spine Maturation through Septin7 Phosphorylation. *Neuron* 93, 379–393. doi:10.1016/j.neuron.2016.12.006

Yasuda, S., Tanaka, H., Sugiura, H., Okamura, K., Sakaguchi, T., Tran, U., et al. (2007). Activity-Induced Protocadherin Arcadlin Regulates Dendritic Spine Number by Triggering N-Cadherin Endocytosis via TAO2β and P38 MAP Kinases. *Neuron* 56, 456–471. doi:10.1016/j.neuron.2007.08.020

Conflict of Interest: The authors declare that the research was conducted in the absence of any commercial or financial relationships that could be construed as a potential conflict of interest.

Publisher's Note: All claims expressed in this article are solely those of the authors and do not necessarily represent those of their affiliated organizations, or those of the publisher, the editors, and the reviewers. Any product that may be evaluated in this article, or claim that may be made by its manufacturer, is not guaranteed or endorsed by the publisher.

Advantages of publishing in Frontiers

OPEN ACCESS
Articles are free to read for greatest visibility and readership

FAST PUBLICATION
Around 90 days from submission to decision

HIGH QUALITY PEER-REVIEW
Rigorous, collaborative, and constructive peer-review

TRANSPARENT PEER-REVIEW
Editors and reviewers acknowledged by name on published articles

Frontiers
Avenue du Tribunal-Fédéral 34
1005 Lausanne | Switzerland

Visit us: www.frontiersin.org
Contact us: frontiersin.org/about/contact

REPRODUCIBILITY OF RESEARCH
Support open data and methods to enhance research reproducibility

DIGITAL PUBLISHING
Articles designed for optimal readership across devices

FOLLOW US
@frontiersin

IMPACT METRICS
Advanced article metrics track visibility across digital media

EXTENSIVE PROMOTION
Marketing and promotion of impactful research

LOOP RESEARCH NETWORK
Our network increases your article's readership